



Dublin City University
Ollscoil Chathair Bhaile Átha Cliath

**Synthetic and computational investigations into
reaction pathways towards complex
heterocyclic ring systems**

Sarah Kebbell B.Sc. (Hons)

Thesis submitted for the Degree of Doctor of
Philosophy (Ph.D)

Supervisors:

Dr. Dermot Brougham

Dr. Paraic James

School of Chemical Sciences

July 2011

I hereby certify that this material, which I now submit for assessment on the programme of study leading to the award of doctor of philosophy is entirely my own work, that I have exercised reasonable care to ensure that the work is original, and does not to the best of my knowledge breach any copyright, and has not been taken from the work of others save and to the extent that such work has been cited and acknowledged within the text of my work.

Signed: _____ (Candidate) ID No.: _____

Date: _____

In loving memory of my grandfather, Jack Carruthers.

Acknowledgements

First and foremost I would like to express my gratitude to my supervisor, Dr. Dermot Brougham who introduced me to the area of computational chemistry during my undergraduate project and for encouraging me to undertake a PhD in this area. I sincerely appreciate your support and guidance over the years and admire your integrity in your approach to science. Many thanks also to my second supervisor, Dr. Paraic James for his guidance and expertise in the area of organic chemistry. I will always remember your support at the ACS meeting in Washington! I appreciate the ‘quantum leap’ made by both to undertake a project such as this, working outside of their comfort zones at times, to understand each other’s area of expertise.

I sincerely wish to thank Prof. Anthony Stone at Cambridge for mentoring me in his GDMA suite of programs in order to perform the Distributed Multipole Analyses work in my thesis. A most respected computational scientist and a true gentleman. I also wish to extend my thanks to Dr. Michael Oelgemoeller and Dr. Fadi Hatoum for providing me with the equipment and guidance to perform the photochemistry experiments. To Dr. Helge Müller-Bunz at UCD for performing the X-Ray crystallography work, many thanks. I would also like to thank Mr. Alin Elena at the Irish Centre for High Performance Computing (IChec) for assisting me while using the facilities at IChec.

I would like to thank all the past and present postgrads and postdocs of the DB group for all their friendship and support over the years: Drs. Eoin Murray, Swanpankumar Ghosh (Calcutta’s favourite son), Jacek Stolarczyk, Carla Meledandri, Darren Carty, Galya Ivanova and Tsedev Ninjebadgar; Sarah Clarke and Eoin Fox. Many thanks also to the past and present postgrads who I’ve had many interesting discussions/enjoyed a pint with over the years: Drs. Stephen Carey, Lynda Hughes, Martina O’Toole, Benjamin Schazmann, Fadi Hatoum, Robert Groarke, Gerard Mc. Dermott, Noel O’Boyle, Thomas Mc Evoy, Elena Lestini, Saibh Morrissey, Pauline Griffin, Debbie Coleman, Neil O’Halloran, Shane O’Malley, Sonia Gallagher, Emma Coyle, Jamie Walsh, Nicola Boyle, Tony Coleman, Brian Moran, Elaine Spain; Kieran Joyce, Will Butler, Andy Harry, Sharon Murphy, Brian Murphy, Pavle Močilac, Emma Harvey, Irene Hughes, Rachel Nic Ardghail, Paula Kelly.

Many thanks to the wonderful technical staff here at DCU: Damien Mc Guirk, John Mc Loughlin, Vincent Hooper, Ambrose May, Dr. Brendan Twamley, Veronica Dobbyn, and Mary Ross. It was a great pleasure to work with you and I am indebted to you all for your help and guidance over the years.

I would like to extend my sincerest gratitude to Des and Ali Quigley at the National Hyperbaric Centre in Dublin for treating me for several months to recover from decompression illness; two fantastic applied physicists – may you continue in your quest in delivering Hyperbaric Oxygen Therapy (HBOT) to all and continue to provide the best level of healthcare this country has to offer. Your support has been a constant source of inspiration.

To all the people who've helped me retain my sanity through various activities: Steve Mc Carthy, Mark White, Mark Delaney and all the ten-pin bowlers at ALSAA; Harry Leech (coach Lee), Shane Mc Quillan, Stephen Travers (Hugh), Stephen Mc Donnell, Stephen Brennan, Neil Mc Cormick and Fergus Concannon at the Olympic weightlifting club in DCU. Much appreciation goes to Noel Walsh and Fran Bermingham for their I.T. and programming assistance, interview preparations and squash games!

I would like to say a sincere heartfelt thanks to my family- my parents, Don and Rita, who have always supported me in every possible way throughout my academic endeavours, thank you for your love and support; my brother Stephen, for encouraging me to study science and for his linguistic skills in translating several literature papers from German to English – putting your degree in Chemistry with German to some use! To my late grandfather, Jack Carruthers, who gave my brother and me a fantastic thirst for knowledge: 'One word a day; three hundred and sixty five words a year.' To my two adorable nieces, Megan and Fiona Kebbell, may you grow to be fantastic scientists of the future!

Last, and by no means least, I would like to thank my boyfriend, Philip Kirwan, my rock throughout this journey. Without your love and support I may not have completed this journey. I am indebted to you for your patience and encouragement at all times. Thank you to your own family (Jim, Ursula and Selig) for their support also.

Table of Contents

Abstract.....	9
List of Abbreviations	10
Chapter 1 Overview of Thesis and Literature Survey.....	11
1.1 The synthesis of dihydrazones/osazones.....	12
1.1.1 Preface.....	12
1.1.2 Mechanism of osazone formation	13
1.1.3 Dihydrazones from diketones	15
1.1.4 Dihydrazones from diazonium salts.....	19
1.1.5 Dihydrazones from α -substituted ketones.....	21
1.1.6 Dihydrazones via oxidation of a monohydrazone.....	25
1.1.7 The use of catalysts to form hydrazone groups.....	25
1.2 Computational Methods used in this Thesis	27
1.2.1 Molecular Mechanics/Force Field methods	28
1.2.2 Quantum Mechanical calculations – Electronic Structure Methods	29
1.2.3 Density Functional Theory.....	40
Chapter 2.....	47
2.1 Introduction.....	48
2.2 Synthesis of dihydrazones from diketones.....	50
2.3 Synthesis of dihydrazones by oxidation of monohydrazones	59
2.4 Dihydrazones from diazonium salts.....	60
2.5 Synthesis of dihydrazones from α -substituted ketones	61
2.6 Synthesis of azo compounds.....	64
2.7 Conclusion	66
2.8 Experimental details.....	66
2.8.1 Synthesis of monohydrazones.....	66
2.8.2 Synthesis of alternative dihydrazone precursors (formazans and azo-alkenes)....	70
2.8.3 Synthesis of dihydrazones.....	71

2.8.4 Synthesis of azo compounds	74
Chapter 3	77
3.1 Introduction	78
3.1.1 Osazones and dihydrazones	78
3.1.2 Methods for visualising charge distribution in a molecule	80
3.1.3 (<i>E</i>)/(<i>Z</i>) isomers	87
3.2 Computational methods	89
3.3 Results	90
3.3.1 Thermodynamics and Kinetics	90
3.3.2 Point charges	97
3.3.3 Multipole analyses of phenylhydrazine and monohydrazones 13(a)-(d)	99
3.4 Discussion	106
3.5 Conclusions	112
Chapter 4 Photochemical transformations of pyrrolo-1,2,3-triazoles	113
4.1 Introduction	114
4.1.1 Pericyclic Reactions	114
4.1.2 Photochemical excitation of pyrrolo-[2,3- <i>d</i>]-1,2,3-triazoles	116
4.2 Results	120
4.2.1 Photochemical excitation of hexahydro-pyrrolo-[2,3- <i>d</i>]-1,2,3-triazoles (42)	120
4.2.2 Photochemical excitation of tetrahydropyrrolo-[2,3- <i>d</i>]-1,2,3-triazoles (44)	127
4.3 Discussion	131
4.4 Conclusion	134
4.5 Experimental	135
4.5.1 Synthesis of hexahydropyrrolo[2,3- <i>d</i>]-1,2,3-triazoles	135
4.5.2 Synthesis of tetrahydropyrrolo[2,3- <i>d</i>]-1,2,3-triazoles	136
4.5.3 Synthesis of 1,2,3,5-tetrazocines	137
4.5.4. Synthesis of imidazo-pyrazoles	138
Chapter 5 <i>Ab initio</i> studies of 1,2,3,5-tetrazocines and related compounds	140

5.1 Introduction.....	141
5.2 Computational methods	144
5.3 Results and Discussion	145
5.3.1 Conformations of cyclooctane	145
5.3.2 Conformations of dihydro-1,2,3,5-tetrazocine.....	147
5.3.3 Conformations of bicyclic species (44),(46),(47)	151
5.3.4 Bond lengths of dihydro-1,2,3,5-tetrazocine (45)	154
5.3.5 Bond angles of dihydro-1,2,3,5-tetrazocine (45)	156
5.3.6 Dihedral angles of dihydro-1,2,3,5-tetrazocine (45)	158
5.3.7 Thermodynamics.....	160
5.3.8 Kinetics	168
5.4 Conclusions.....	173
Chapter 6.....	174
Conclusions and Future Work.....	174
6.1 Thesis Conclusions	175
6.2 Future Work	177
Appendix A.1	178
Molecular structure for 13(c): 1-phenyl-2-(phenylhydrazone)propan-1-one.....	178
References.....	187

Abstract

Tetrazocines are eight-membered rings possessing four nitrogen atoms. The development of new synthetic routes to novel heterocyclic systems has remained a critical branch of synthetic organic chemistry due to potential applications in biomimetics and pharmaceuticals, such as dyes and explosives. 1,2,3,5-tetrazocines were originally proposed as an intermediate in the formation of 1,3a,6,6a-tetrahydroimidazo[4,5-*c*]pyrazole (a promising anti-fungal agent) from the irradiation of 2,3a,4,6a-tetraphenyl-3,3a,4,5,6,6a-hexahydropyrrolo-[2,3-*d*]-1,2,3-triazole.

One of our main aims was to synthesise novel 1,2,3,5-tetrazocines that possessed three phenyl and one methyl group(s) attached to the eight-membered ring, as previously synthesised 1,2,3,5-tetrazocines are of the tetra-phenyl variety. Adopting the established synthetic route in the pursuit of novel 1,2,3,5-tetrazocines proved difficult however, as the asymmetric nature of the 1,2,3,5-tetrazocine precursors (dihydrazones) resulted in altered reactivity as compared with their symmetric equivalents, this finding was rationalised using distributed multipole analysis.

Ab initio calculations (B3LYP/6-31G(d)) indicate that for an underivatised 1,2,3,5-tetrazocine, the planar (aromatic) structure is the most stable, though this is not observed experimentally, presumably due to steric repulsions between the large aromatic substituents often used to stabilise these molecules. Excluding the planar geometry, we found that there is a significant thermodynamic stabilisation of 1,2,3,5-tetrazocine over the 1,3a,6,6a-tetrahydroimidazo[4,5-*c*]pyrazole, providing a novel route to heterocyclic systems.

List of Abbreviations

AM1	Austin Model No.1
B3LYP	Becke three parameter method (Lee-Yang-Parr)
CNDO	Complete Neglect of Differential Overlap
DFT	Density Functional Theory
DMA	Distributed Multipole Analysis
DZ	Double Zeta (Basis Set)
ESP	Electrostatic Potential
GGA	Generalised Gradient Approximation
GTO	Gaussian Type Orbitals
HF	Hartree Fock
LCAO	Linear Combination of Atomic Orbitals
LDA	Local Density Approximation
LSDA	Local Spin Density Approximation
MESP	Molecular Electrostatic Potential
MINDO	Modified Intermediate Neglect of Differential Overlap
MNDO	Modified Neglect of Diatomic Overlap
MO	Molecular Orbitals
NDDO	Neglect of Diatomic Differential Overlap
NPA	Natural Population Analysis
PES	Potential Energy Surface
PM3	Parametric Method No.3
SAM1	Semi-ab initio Method 1
SCF	Self-Consistent Field
SD	Slater Determinants
STO	Slater Type Orbitals
ZDO	Zero Differential Overlap

Chapter 1

Overview of Thesis and Literature Survey

1.1 The synthesis of dihydrazones/osazones

1.1.1 Preface

The focus of this work is the synthesis and computational investigation into reaction pathways towards complex heterocyclic ring systems, namely 1,2,3,5-tetrazocines and imidazo-[4,5-*c*]pyrazoles. Tetrazocines are eight membered rings possessing four nitrogen atoms. The most cited tetrazocine is 1,3,5,7-tetranitro-1,2,3,5-tetrazocine, (HMX) a high energy explosive material, but it is the nitro groups attached to the ring which confer its explosive properties, analogous to TNT, and not any physical property of the ring structure itself.¹ The tetrazocine of interest here however, is a 1,2,3,5-tetrazocine. 1,2,3,5-tetrazocines were originally proposed by Butler *et al* to be a reactive intermediate in the photochemical transformation of a pyrrolo-triazole to an imidazo-[4,5-*c*]pyrazole.² There was great interest in imidazo-[4,5-*c*]pyrazoles at the time as they had displayed promising antifungal activity.³⁻⁵ James later isolated a stable 1,2,3,5-tetrazocine itself, with the criteria for isolation being: an electron withdrawing group attached to C-7 of the ring and a saturated C-6 carbon.⁶ 1,2,3,5-tetrazocines are novel eight-membered rings and do not occur in nature. Therefore it would be desirable to exploit this synthetic route to develop a library of these compounds as they may possess interesting biological activity. Consequently, some of the aims of this work are as follows:

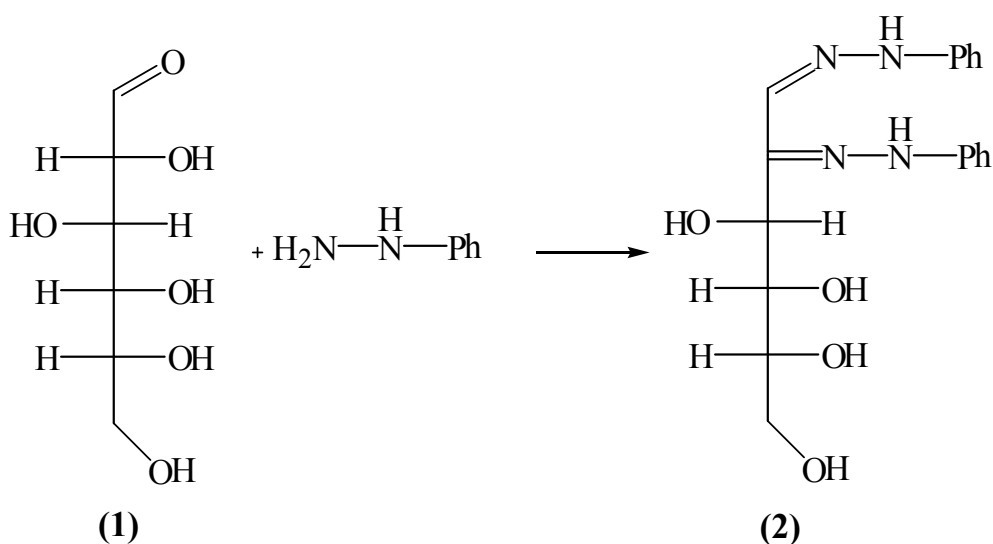
- To extend the library of compounds for 1,2,3,5-tetrazocines with four phenyl groups attached to the eight-membered ring
- To synthesise imidazo-[4,5-*c*]pyrazoles *via* a 1,2,3,5-tetrazocine intermediate (with four phenyl rings attached to the bicyclic species)
- Investigate the intermediacy of the 1,2,3,5-tetrazocine in this synthetic route using DFT calculations (B3LYP/6-31G(d))
- Previous attempts to synthesise a 1,2,3,5-tetrazocine with two methyl and two phenyl groups attached to the eight-membered ring were not successful. Therefore, it would be desirable to investigate if 1,2,3,5-tetrazocines with three phenyls and one methyl group attached to the ring can be isolated,

hence determining the minimum number of phenyl groups that need to be attached to isolate an eight-membered ring.

As the first step in the synthesis of these compounds will be the conversion of a diketone to a dihydrazone, this is the first synthetic step that will be presented in detail.

1.1.2 Mechanism of osazone formation

The terms osazone and dihydrazone are often used interchangeably in the literature, however an osazone is derived from a sugar substrate whereas a dihydrazone is derived from a non-sugar substrate. Osazone synthesis was originally a classification reaction for reducing sugars in biochemistry since aldehydes and ketones are readily transformed by a condensation reaction into osazones (dihydrazones) upon reaction with three molar equivalents of phenylhydrazine.

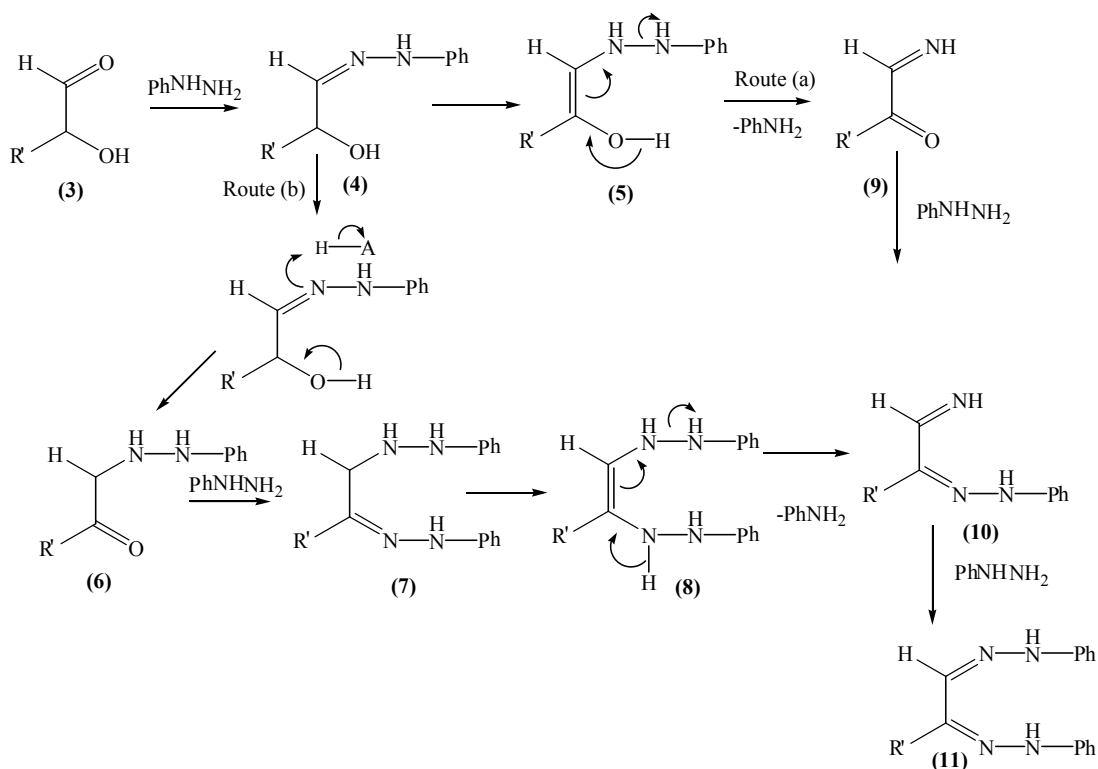


Scheme 1.1 Formation of an osazone **(2)** (glucose osazone) from a reducing sugar **(1)** (glucose) by the action of excess phenylhydrazine.

Fischer pioneered the work in this area in 1884 by converting reducing sugars into osazones; thus enabling him to determine the relative configuration of the reducing sugar about the carbon centres.⁷ Fischer noted that aniline (PhNH_2) and ammonia (NH_3) were by-products in the reaction.

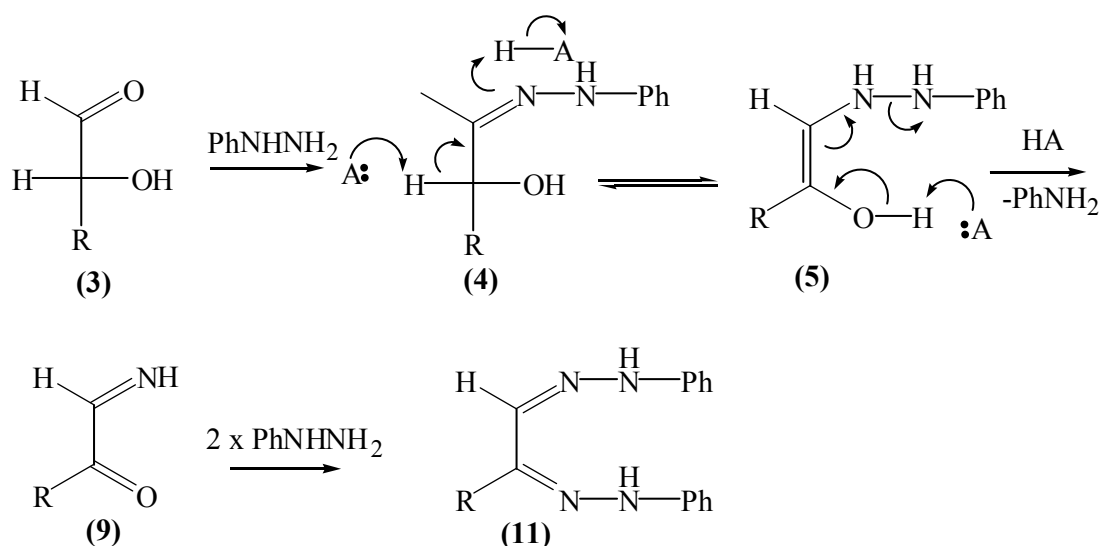
There was controversy in the literature as to the exact mechanism of osazone formation, although most authors agree that it involves three equivalents of phenylhydrazine to complete the transformation. In 1918, Garard and Sherman determined the optimum conditions required for the maximum yield of phenylosazone.⁸ These workers reported that the reaction should proceed under acidic conditions, with the optimum pH lying between 4-6.

Weygand proposed two routes, as in **Scheme 1.2**,⁹ and there is evidence in favour of each pathway.¹⁰⁻¹⁴ The difference between the proposed routes is whether aniline is lost from the enol amine (**5**) or from the ene diamine (**8**). Neither of these routes can explain the role of acid in the mechanism.



Scheme 1.2 Two possible routes to osazone formation proposed by Weygand.⁹

The mechanism of osazone formation is more likely to be Weygand's route (a), which depends on a series of reactions in which the C=N behaves very much like C=O in giving a nitrogen version of an enol, and is susceptible to nucleophilic attack from phenylhydrazine. The role of an acid HA, is also illustrated in **Scheme 1.3**.

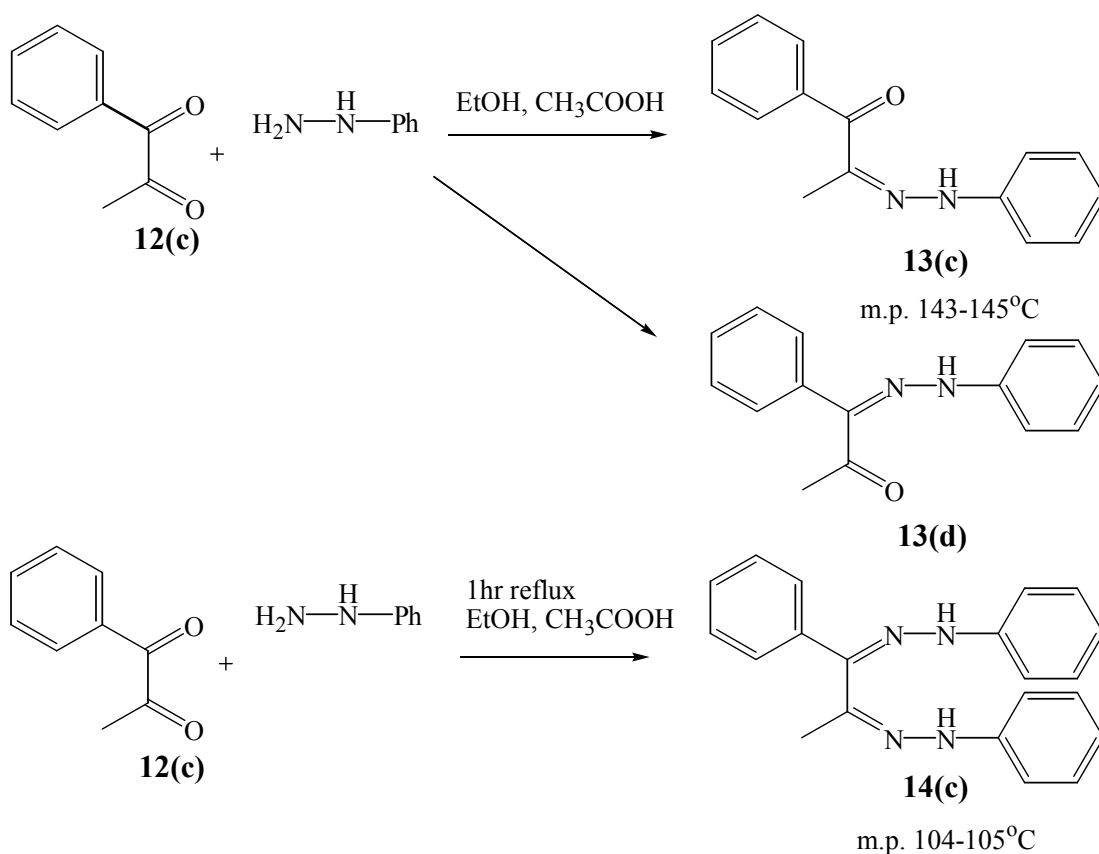


Scheme 1.3 Most likely mechanism for osazone formation including the role of an acid.

The osazone mechanism is much more complex than dihydrazone formation. For instance, osazones require the reaction of three equivalents of phenylhydrazine with the reducing sugar, whereas dihydrazones only require the addition of two molar equivalents.

1.1.3 Dihydrazones from diketones

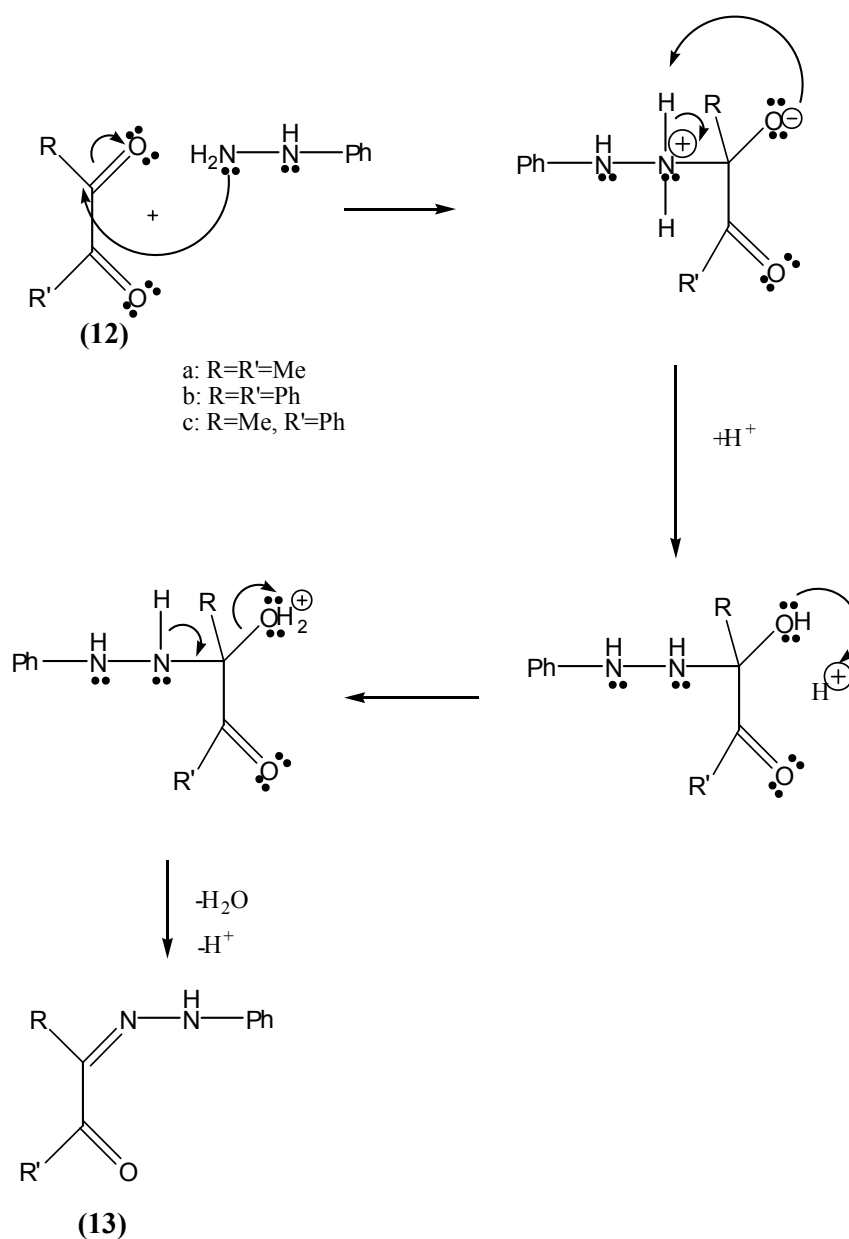
In 1889 Müller and von Pechmann reported that if 1-phenyl-propan-1,2-dione **12(c)** is reacted with an excess of phenylhydrazine in the presence of ethanol and a few drops of glacial acetic acid, a keto-monohydrazone is formed **13(c)/(d)**, (see **Scheme 1.4**) although the workers made no attempt to determine the relative position of the hydrazone group, *i.e.* **13(c)** or **13(d)**.¹⁵ They also reported on the purported synthesis of the dihydrazone **14(c)** by adding excess phenylhydrazine to the diketone **12(c)** in the presence of ethanol and acetic acid, by heating the mixture to reflux.



Scheme 1.4 Synthesis of the keto-monohydrazone **13(c)/(d)** and the purported synthesis of the dihydrazone **14(c)**.¹⁵

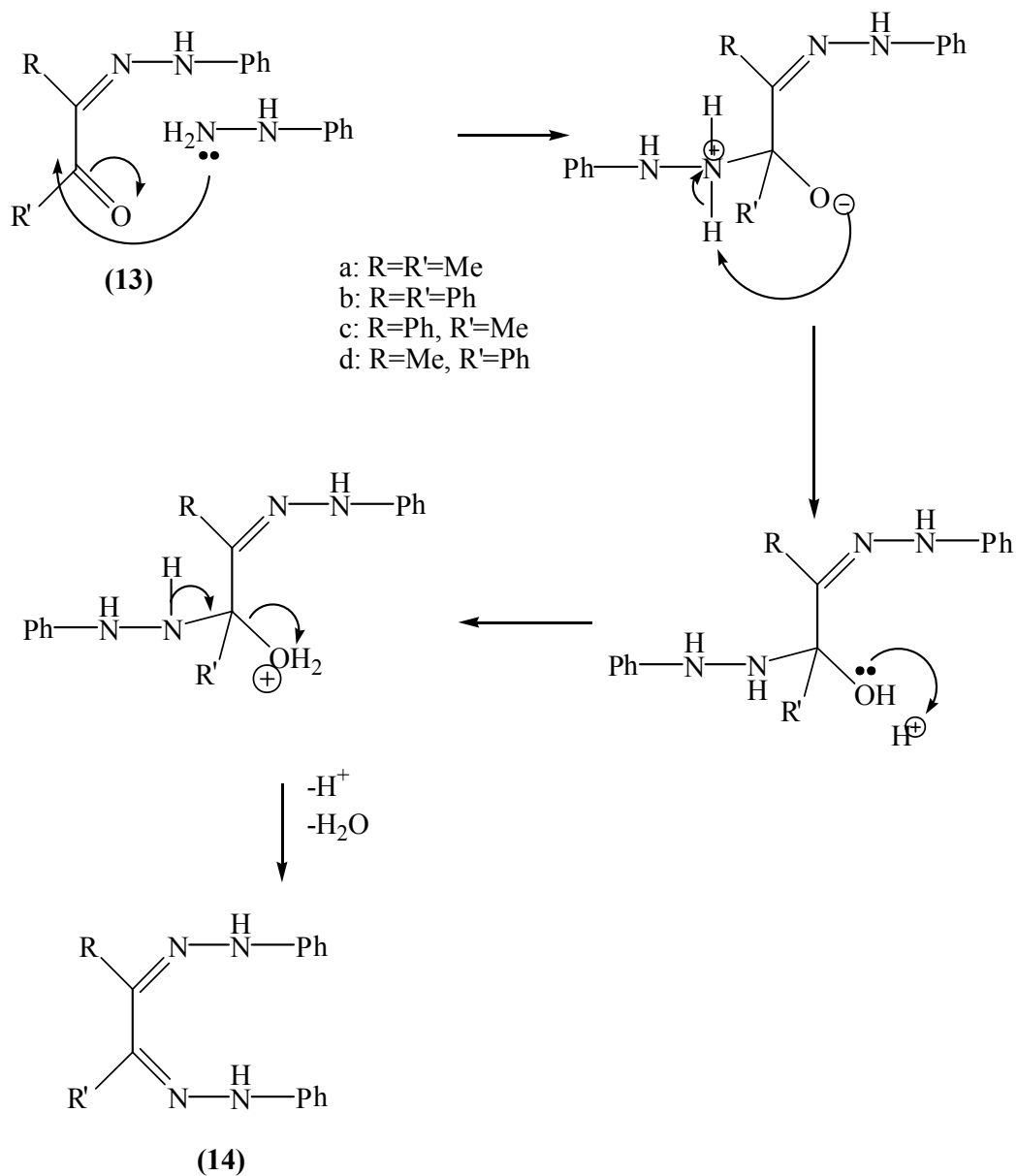
In the reported synthesis of the 1-phenyl-1,2-diphenylhydrazone **14(c)** the authors note that the melting point of the dihydrazone **14(c)** is $104-105^\circ\text{C}$, which is lower than that of the monohydrazone ($143-145^\circ\text{C}$). This is unusual, given that dihydrazones should have a higher melting point than that of their corresponding monohydrazones. Monohydrazones typically have a melting point in the range $133-152^\circ\text{C}$,¹⁶⁻¹⁹ whereas dihydrazones melt in the region of $169-293^\circ\text{C}$.²⁰⁻²³ These findings cast doubt over Müller and von Pechmann's synthesis of 1-phenyl-1,2-diphenylhydrazone **14(c)**, as no spectroscopic proof was available at the time.

The mechanism for the dihydrazone formation is a two-step process with the first step involving the addition of one molecule of phenylhydrazine to form the keto-monohydrazone (**13**). When phenylhydrazine initially attacks the diketone (**12**) a zwitterionic species is generated. A proton is transferred to the oxygen atom, consequently forming a keto-alcohol. The hydroxyl group subsequently attacks a proton, generating a hydronium ion. Finally, the pair of electrons in the N-H bond move in to form a carbon-nitrogen double bond, expelling a water molecule in the process.



Scheme 1.5 Mechanism for the formation of the keto-monohydrazone (**13**) from a diketone (**12**).

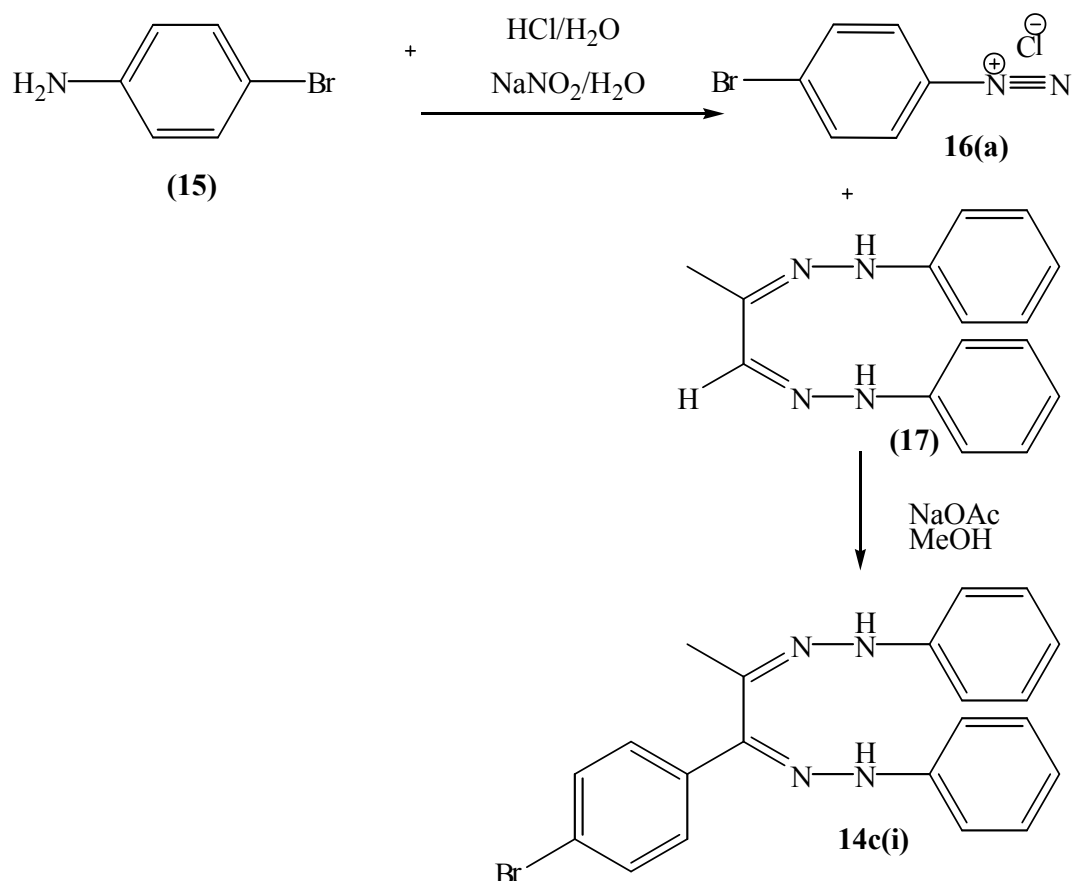
To form the dihydrazone (**14**) from the keto-monohydrazone (**13**) requires the addition of a second molar equivalent of phenylhydrazine to (**13**), following a similar mechanism as for the formation of a keto-monohydrazone (**13**) as in *Scheme 1.5*.



Scheme 1.6 Formation of a dihydrazone (**14**) from a keto-monohydrazone (**13**).

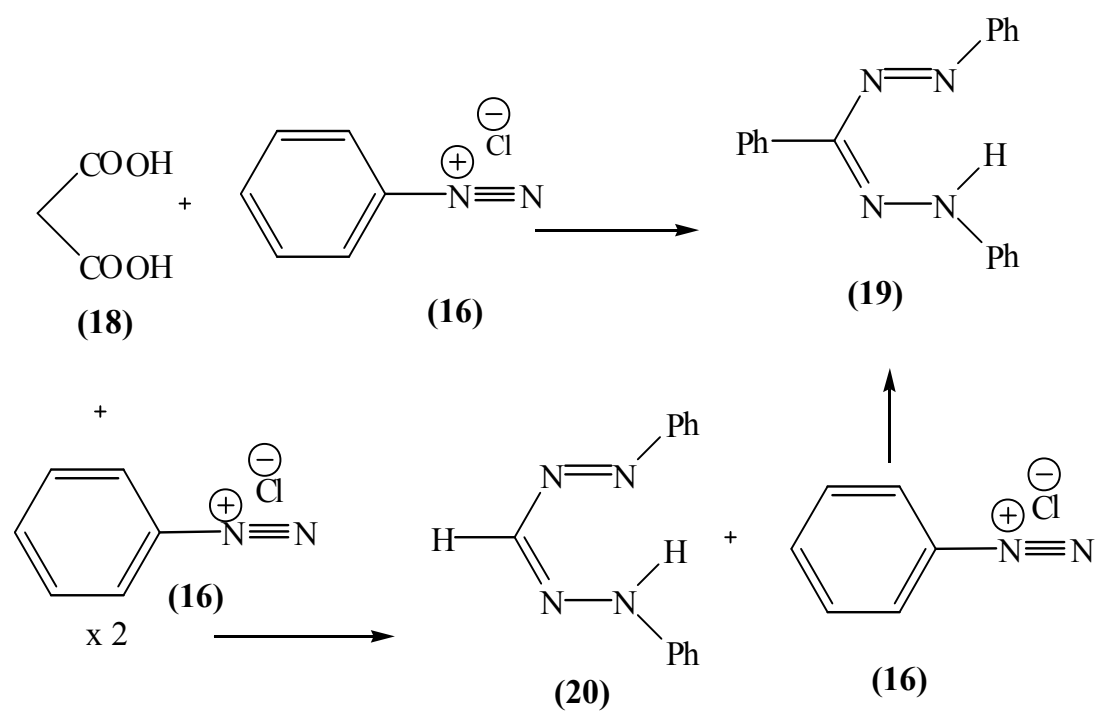
1.1.4 Dihydrazones from diazonium salts

An alternative route to dihydrazones is *via* the addition of a diazonium salt to a less substituted dihydrazone, to yield a dihydrazone. In 1958, Ried and Sommer synthesised the asymmetric dihydrazone **14c(i)** by adding a diazonium salt to methyl glyoxal phenylosazone (**17**),²⁴ see *Scheme 1.7*. The yield of the dihydrazone was modest (~31%).



Scheme 1.7 Synthesis of a dihydrazone **14c(i)** from methyl glyoxal phenylosazone (**17**).²⁴

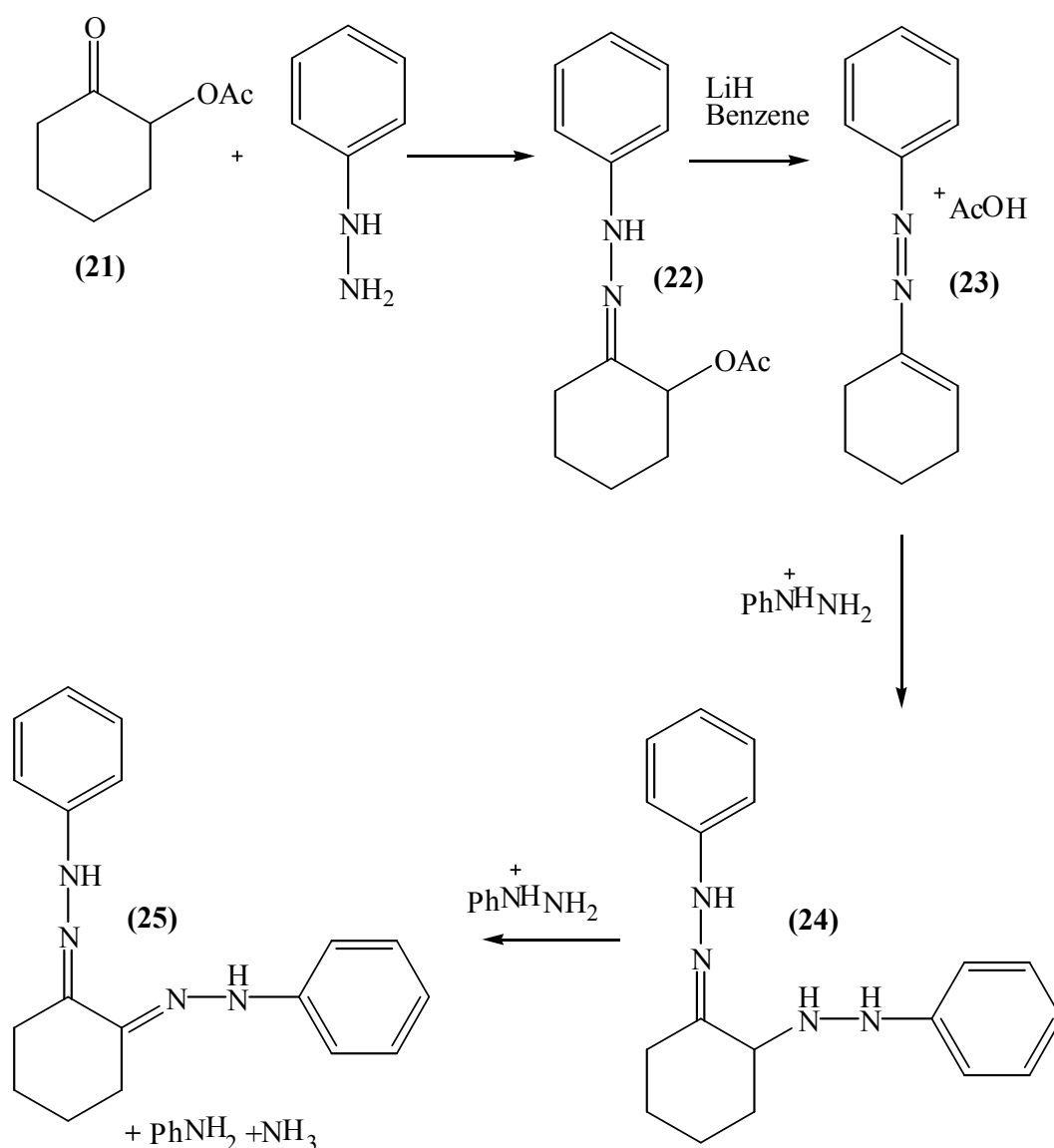
Interestingly, in a review at the time Mester reported that “sugar osazones yield osazone formazans, while non-sugar osazones react with substitution of the phenyl ring of the aniline on C-1 or do not react at all.”²⁵ Neugebauer and Küchler also reported similar findings in that a triaryl formazan (**19**) could be constructed from a biformazan (**20**) with replacement of the hydrogen for a phenyl group.²⁶



Scheme 1.8 Synthesis of a triaryl formazan (19) from malonic acid (18).²⁶

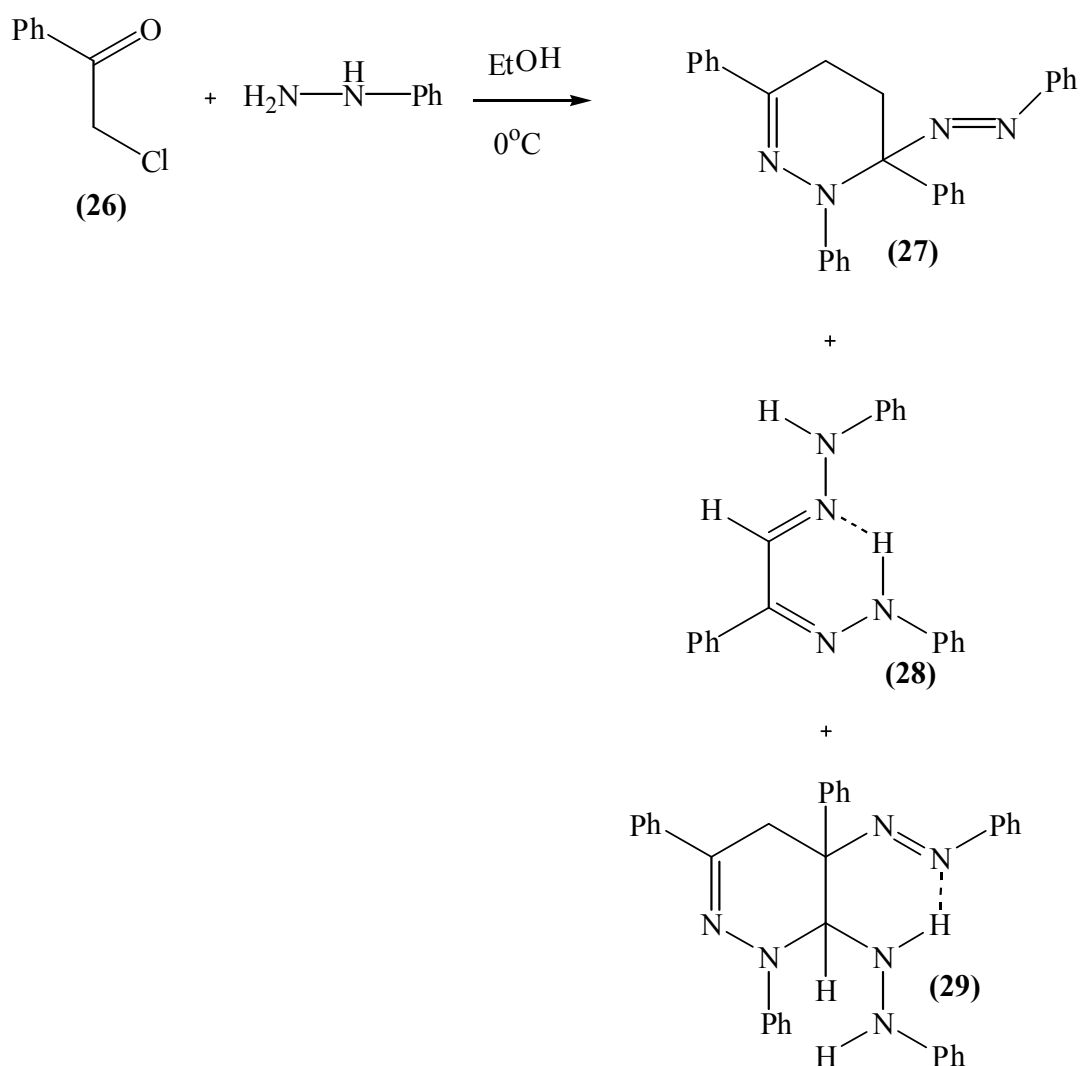
1.1.5 Dihydrazones from α -substituted ketones

An alternative method of synthesising a dihydrazone is to add three molecular equivalents of phenylhydrazine to an α -substituted hydrazone. In 1966 Caglioti *et al* reported on the formation of a dihydrazone (**25**) from an α -acetoxy ketone (**21**).²⁷ According to these workers if phenylhydrazine is added to α -acetoxycyclohexanone (**21**) in the presence of LiH and warm benzene, it should yield 1-(phenylazo)cyclohexene (**23**) in quantitative yield. 1-(Phenylazo)cyclohexene (**23**), forms from (**22**) rapidly and if treated with another two equivalents of phenylhydrazine, then converts to the dihydrazone (**25**).



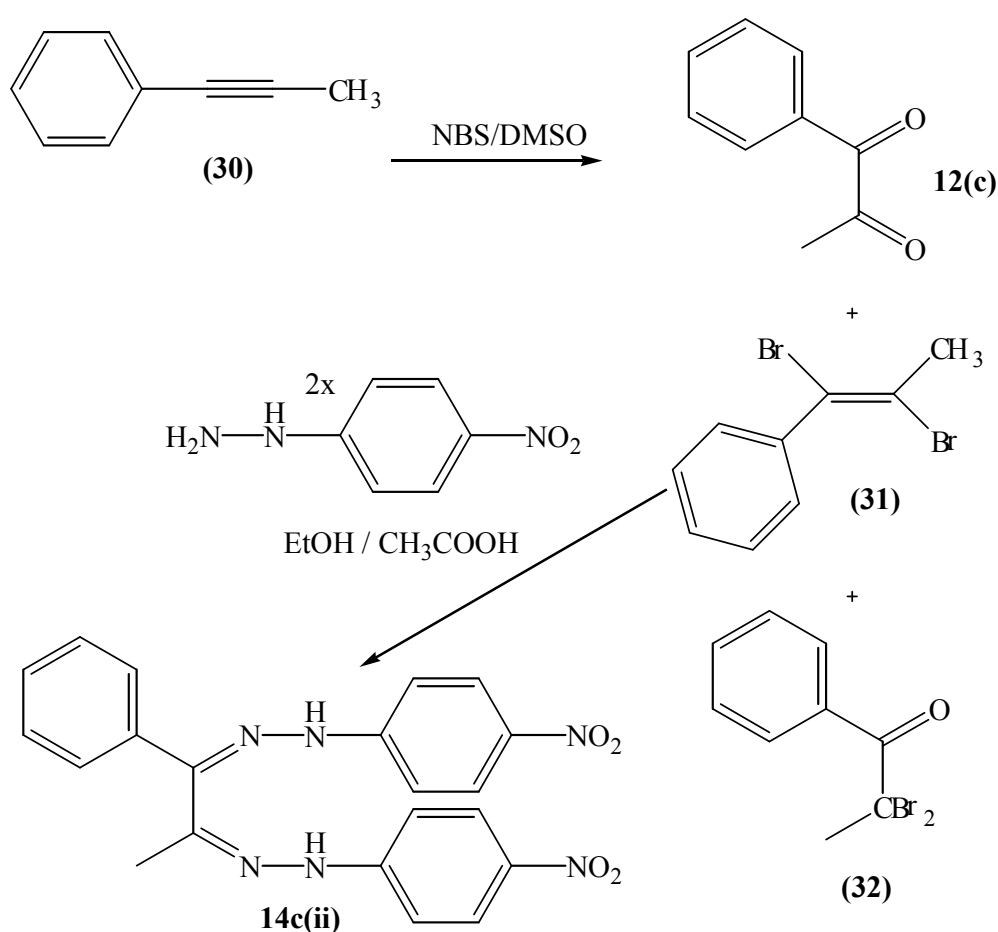
Scheme 1.9 Formation of a dihydrazone (**25**) from α -acetoxycyclohexanone (**21**) via 1-(phenylazo)cyclohexene (**23**) according to Caglioti *et al.*²⁷

An alternative route to dihydrazones from α -substituted hydrazones was developed by Stickler and Hoffman in 1970. These workers reported that phenyl glyoxal phenylosazone (**28**) was synthesised from phenacyl chloride (**26**), an α -haloketone.²⁸ The authors reported that if phenacyl chloride (**26**) is reacted with phenylhydrazine in cold ethanolic solutions, a yellow crystalline product, identified as 6-benzeneazo-1,3,6-triphenyl-1,4,5,6-tetrahydropyridazine (**27**) is isolated. This six-membered ring structure (**27**) forms very quickly, and reaches a maximum concentration after about 30 minutes, and the dihydrazone (**28**) forms gradually, reaching a maximum concentration after about 24 hours. A third yellow substance, (**29**), with a m.p. of 194-196°C, is detected after several days. This is illustrative of a pathway we adopt in the synthesis of an asymmetric dihydrazone **14(c)** as will be described in *Chapter 2*.



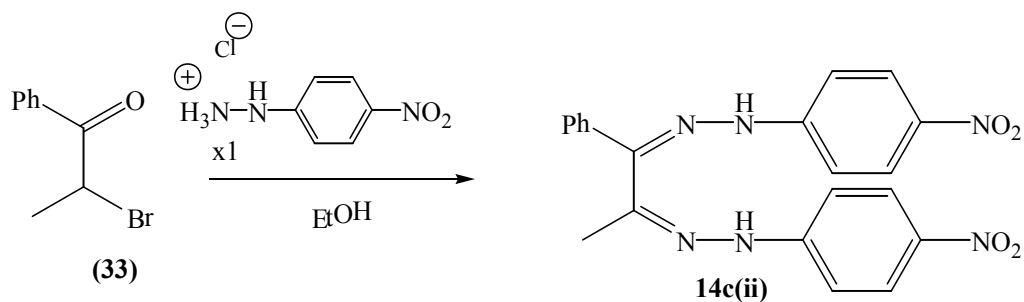
Scheme 1.10 Synthesis of a dihydrazone according to Stickler and Hoffman.²⁸

In the same year (1970), Wolfe *et al* reported on the synthesis of 1-phenyl-propanedione di-*p*-nitrophenylhydrazone **14c(ii)** from an oxidation product of 1-phenylprop-1-yne (**30**). Oxidising 1-phenyl-prop-1-yne (**30**) with *N*-bromosuccinimide in DMSO yields three products: 1-phenyl-propanedione **12(c)**, 1,2-dibromo-1-phenyl-prop-1-ene (**31**) and 2,2-dibromo-1-phenyl-propan-1-one (**32**). The authors reported that they isolated ‘an oil’ from the oxidation mixture and treated it with *p*-nitrophenylhydrazine to yield 1-phenyl-propanedione di-*p*-nitrophenylhydrazone **14c(ii)**. The authors believed that this substance was 1-phenyl-propanedione **12(c)**, however we believe that the dihydrazone **14c(ii)** was in fact formed from 1,2-dibromo-1-phenyl-prop-1-ene (**31**), for reasons that will be discussed in **Chapter 2**. The NMR spectra of these two compounds **12(c)**/**(31)** would be very similar, but as our findings show, 1-phenyl-propanedione **12(c)** does not readily convert to the dihydrazone but α -halo-ketones can be transformed to dihydrazones (**14**).



Scheme 1.11 Synthesis of 1-phenyl-propan-1,2-bis(4'-nitro-phenylhydrazone) **14c(ii)** from 1-phenyl-propyne (**30**).²⁹

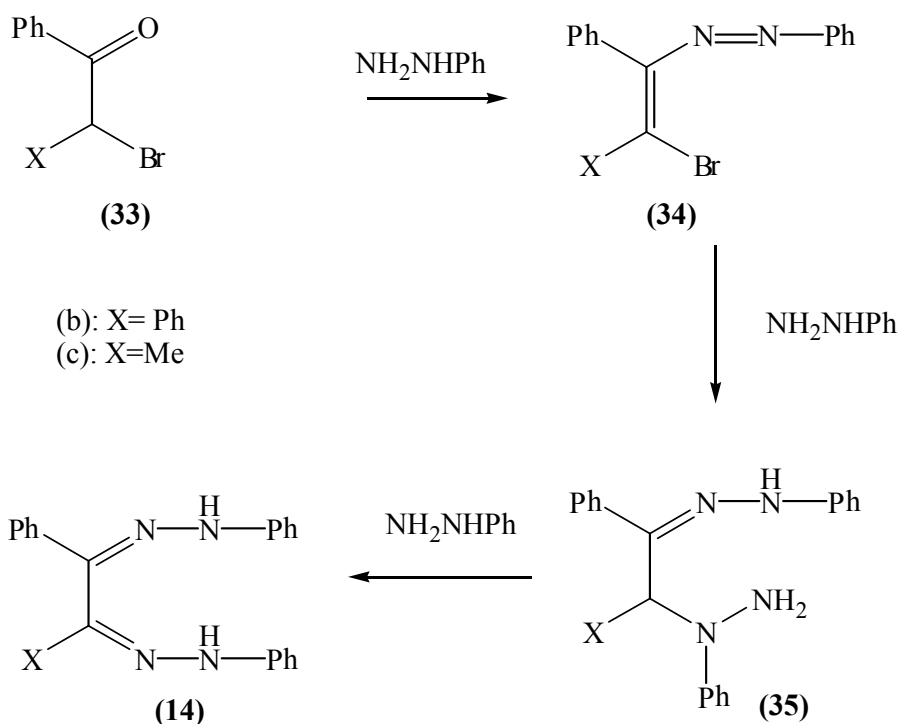
Interestingly von Auwers reported on the synthesis of 1-phenyl-propanedione di-*p*-nitrophenylhydrazone **14c(ii)** from α -bromo propiophenone (**33**) by the addition of three molecular equivalents of *p*-nitrophenylhydrazine. This may be significant given our claim that Wolfe *et al* may have synthesised the dihydrazone **14c(ii)** from a di-bromo compound (**31**) rather than from the diketone **12(c)**.



Scheme 1.12 Synthesis of 1-phenyl-propan-1,2-(4'-bromo)diphenylhydrazone **14c(ii)** from α -bromo-propiophenone (**33**).

Furthermore Schantl *et al* also reported on the synthesis of a similar compound, 1-phenyl-propan-1,2-diphenylhydrazone **14(c)**, from α -bromo propiophenone (**33**).³⁰

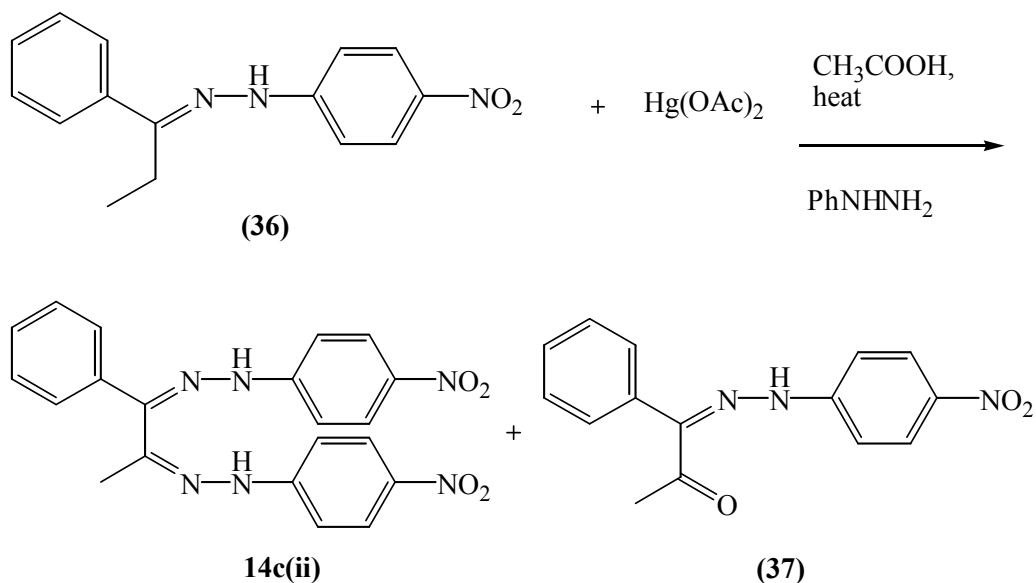
The mechanism that Schantl proposed is very similar to that of Caglioti *et al* as in **Scheme 1.9** as it involves the route to the dihydrazone *via* an azo-alkene intermediate (**34**).²⁷



Scheme 1.13 Synthesis of 1-phenyl-propan-1,2-(bis)phenylhydrazone **14(c)** via an azo alkene compound (**34**).³⁰

1.1.6 Dihydrazones via oxidation of a monohydrazone

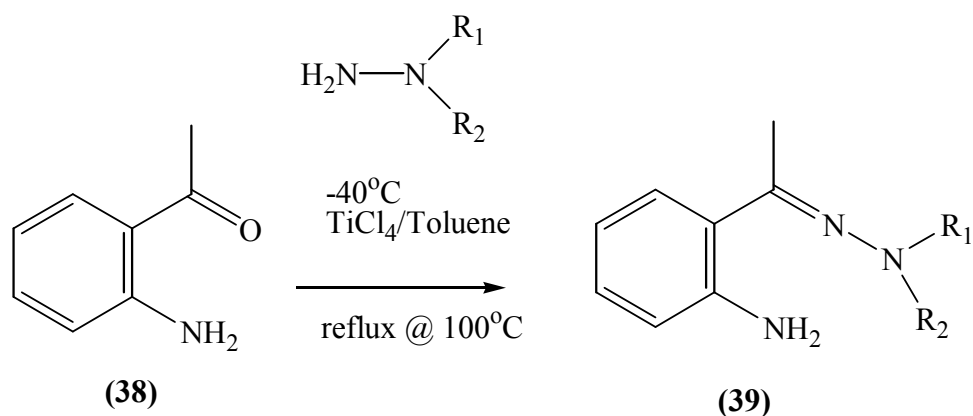
In 1980, Butler and co-workers developed a route to dihydrazones which involved the oxidation of the methylene group adjacent to the phenylhydrazone in compound **(36)** and the consequent addition of phenylhydrazine to yield a dihydrazone **14c(ii)**. However this oxidation step provides only a modest yield of the dihydrazone, **14c(ii)** at just 10%.



Scheme 1.14 The synthesis of 1-phenyl-propanedione di-*p*-nitrophenylhydrazone **14c(ii)** via the oxidation of 1-phenyl-1-*p*-nitrophenylhydrazone-propane (**36**).

1.1.7 The use of catalysts to form hydrazone groups

It was reported by Tita and Kornet that *o*-aminoacetophenone (**38**) can undergo a condensation reaction with an appropriate hydrazine to give the corresponding hydrazone (**39**).³¹ This reaction was catalysed by titanium tetrachloride in toluene at -40°C . The mixture was allowed to warm to room temperature and then refluxed for five hours.



Scheme 1.15 Synthesis of a hydrazone (39) from a ketone (38) using titanium tetrachloride as a catalyst.

One of the main aims of this thesis was to determine if a 1,2,3,5-tetrazocine with three phenyl groups and one methyl group attached to the ring could be synthesised. 1,2,3,5-tetrazocines with four phenyl groups attached to the ring were synthesised previously by the group by converting benzil **12(b)**, a diketone, to its corresponding dihydrazone **14(b)** and the subsequent reactions that follow. The mechanism for this reaction was provided previously in *Section 1.1.2*, in that each phenylhydrazine molecule attacks a subsequent carbonyl group in the diketone, to form the dihydrazone. The dimethyl dihydrazone **14(a)**, was also successfully synthesised by this same route, therefore it would be a trivial task to convert the methyl-phenyl diketone **12(c)** to its dihydrazone **14(c)**, by the same method. This however, was not the case, the reaction did not proceed past the monohydrazone stage **13(c)**. The second carbonyl group would not undergo a nucleophilic attack from phenylhydrazine, irrespective of the conditions employed. Consequently, other synthetic routes, such as those provided in *Sections 1.1.3-1.1.6* were adopted, in an attempt to synthesise the asymmetric dihydrazone **14(c)**. The experimental details of this study are provided in *Chapter 2*.

1.2 Computational Methods used in this Thesis

In computational chemistry, there are two different approaches; molecular mechanics and related methods, and quantum mechanical methods. The latter can be further sub-divided into three main categories: semi-empirical, *ab initio* and density functional theory (see **Figure 1.1**). The progress of computational chemistry has historically been linked to the development of the microelectronics industry, whereby the speed and power of the microprocessor is proportional to the number of transistors per integrated circuit. Since the development of the first integrated circuit in 1961, the number of transistors per circuit has increased exponentially as predicted by Gordon Moore.³² By extrapolation transistor size will eventually reach the atomic scale, and given the fact that transistors have recently been synthesised at nanoscale proportions, this limit may very well be approaching soon. The benefit of more powerful and faster processors is that it reduces the computational effort required (both cost and speed), and for calculations that are extremely complex, this is a major benefit to computational chemistry.

There is increasing interest in the use of computers to predict the conformations of molecules and to calculate physical properties (e.g. determine energies, molecular orbitals, I.R. and Raman spectra) and even to predict transition states and to perform reaction path simulations. The different types of calculations that are available to the computational chemist will be described here.

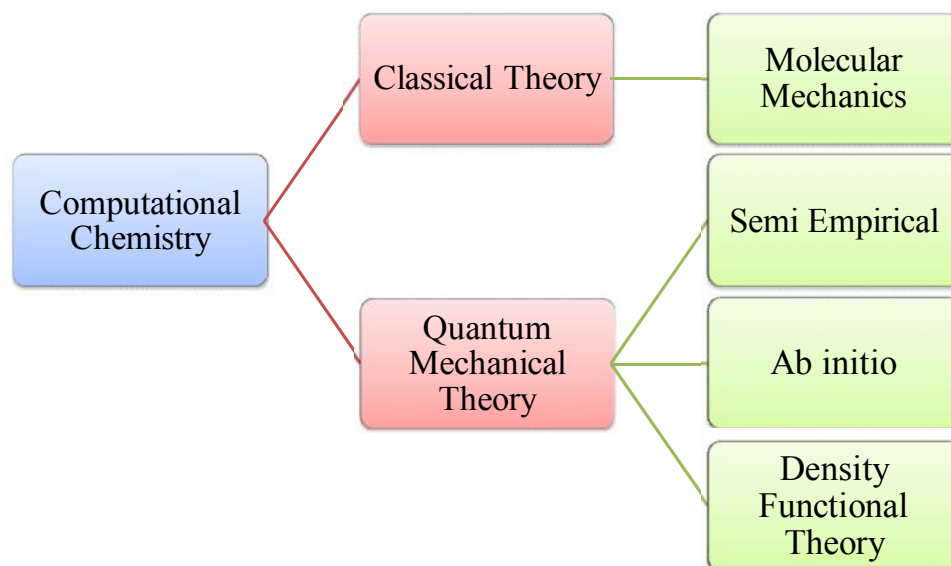


Figure 1.1 Organisational chart of different methods which have evolved within computational chemistry

1.2.1 Molecular Mechanics/Force Field methods

The steric energy for fixed geometric conformations of a molecule can be calculated as the sum of various strain-producing interactions which are functionally dependent on bond lengths (r), bond angles (θ), torsional angles (φ) and non-bonded interatomic distances (d):

$$E_{steric} = E(r) + E(\theta) + E(\varphi) + E(d) \quad (1.1)$$

The pioneering work of Westheimer in 1946 investigated the rate of racemisation of optically active diphenyls such as 2,2'-dibromo-4,4'-dicarboxydiphenyl.³³ Hendrickson later extended this work to calculate the energies of medium-sized rings such as cyclooctane.³⁴⁻³⁵ Wiberg later went on to develop an energy minimisation method,³⁶ so that all the internal coordinates could be optimised to locate an energetic minimum on the potential energy surface, using the method of steepest descent.

The credibility of force field models is based on their successful application to a wide variety of structural types, *e.g.* acyclic, cyclic and polycyclic structures that were parameterised against a large body of experimental data. Allinger developed a molecular mechanics force field MM1³⁷⁻³⁸ with which it is possible to determine the conformations and energies of hydrocarbons. This has since been extended to include a wide range of functional groups/atom types such as

ketones and olefins,³⁹⁻⁴⁰ and aromatic molecules such as benzene and naphthalene, generating the MM2/MM3/MM4 forcefields.^{38,41-43}

1.2.2 Quantum Mechanical calculations – Electronic Structure

Methods

Within quantum mechanical theory the electron is characterised by a wavefunction, as described by the Schrödinger equation:

$$H\Psi = E\Psi \quad (1.2)$$

where H is the Hamiltonian operator and E is the energy of the system. Ψ is called an eigenfunction whereby the Hamiltonian operator is multiplied by Ψ and the product of this calculation is E, a new eigenvalue, times the original eigenfunction, Ψ . The Hamilton operator includes a series of attractive and repulsive terms, corresponding to the potential and kinetic contributions to the energy of the system:

$$H = -\sum_i \frac{\hbar^2}{2m_e} \nabla_i^2 - \sum_k \frac{\hbar^2}{2m_k} \nabla_k^2 - \sum_i \sum_k \frac{e^2 Z_k}{r_{ik}} + \sum_{i < j} \frac{e^2}{r_{ij}} + \sum_{k < l} \frac{e^2 Z_k Z_l}{r_{kl}} \quad (1.3)$$

In this equation, i and j are the subscripts for electrons, k and l the subscripts for nuclei. \hbar is Planck's constant divided by 2π , m_e and m_k are the masses of the electrons and nuclei respectively; ∇^2 is known as the Laplacian operator which is the sum of the second derivatives of the wavefunction in three dimensions $\frac{\partial^2}{\partial x^2} + \frac{\partial^2}{\partial y^2} + \frac{\partial^2}{\partial z^2}$. e is the charge of an electron and r is the distance between particles i and k. Z is the atomic number of the nuclei in question for an atom/molecule. There are five individual terms, the first and second are the kinetic energies of the electrons and nuclei respectively. The third term is the electrostatic attraction of the electrons and nuclei, and the last two terms consider the repulsion between electrons and nuclei respectively.

In order to obtain a solution for multi-electron/particle systems, a number of approximations have to be made. Firstly, the Hamilton operator can be simplified if the Born-Oppenheimer approximation is applied. The Born-Oppenheimer approximation takes note of the fact that there is a large difference

in the masses of electrons and nuclei (an electron has a mass of 1/1836 a.m.u. compared with 1 a.m.u. for a proton/neutron) and therefore the nuclei can be considered to be stationary particles with respect to the electrons. Therefore the Schrödinger equation can be solved for the electrons in a static potential arising from the nuclei fixed in a particular location. The Hamiltonian can thus be separated into a nuclear part and an electronic part. The notion of a fixed nuclear position gives rise to the generation of a potential energy surface (PES) and the coordinates are variables, which reduce the Hamiltonian to the following:

$$= -\frac{\hbar^2}{2m_e} \sum_i \nabla_i^2 - \sum_i \sum_k \frac{Z_k}{4\pi\epsilon_0 r_{ik}} + \frac{1}{2} \sum_{i < j} \frac{e^2}{4\pi\epsilon_0 r_{ij}} \quad (1.4)$$

Quantum mechanical calculations generally make use of this form (1.4) of the Hamilton operator and hence utilise the electronic Schrödinger equation (1.5):

$$\hat{H} \Psi(r; R) = E(R) \Psi(r; R) \quad (1.5)$$

where r is a function of the electrons and R is a function of the fixed nuclear coordinates.

In *ab initio* calculations, a model is chosen for the electronic wavefunction and equations (1.4) and (1.5) are solved by inputting the values of the fundamental constants, the internuclear separations, the atomic numbers of the atoms and the overall charge. For large molecules, accurate *ab initio* calculations become computationally expensive as the computing power is scaled to n^4 where n is related to the number of atoms. Semiempirical methods have been developed in an attempt to treat a wider variety of chemical species and are not as computationally expensive as *ab initio* methods. A semiempirical calculation makes use of a simplified form for the Hamiltonian as well as adjustable parameters with values obtained from experiment.

1.2.2.1 Potential Energy Surface

When studying a chemical reaction/system, it is very important to understand the different geometries that a molecule can adopt and how much energy is required to interconvert between these geometries. One way to observe the effect of different geometries on energy is to calculate a potential surface.

A potential energy surface (PES) may possess distinct stationary points corresponding to chemically important configurations. Local minima are points on the PES that have the lowest energy value in that particular region, whereas the global minimum is the point on the PES that has the lowest energy value over the entire surface. Saddle points are other stationary points of interest as they are a maximum in one direction only (transition state) and are minima in the other. Minima on the PES can often correspond to different conformations or structural isomers of the same molecule, including reactant, intermediate and product configurations.

1.2.2.2 Geometry optimisation

The purpose of a geometry optimisation is to locate minima on a potential energy surface; initially stationary points are located, where the forces (i.e. the first derivatives with respect to energy) are equal to zero. Programs that perform geometry optimisations require an input geometry either in internal coordinates (known as a Z-matrix) or Cartesian coordinates. A basis set (which will be described later) is also specified and the program calculates the energy and the gradient at that point, and decides if the forces are sufficiently low. The geometry of the molecule will be altered with new integrals calculated, new self-consistent field calculations (also explained later), new energy and gradient calculated until convergence has been achieved.

A variety of different algorithms that have been developed to locate minima such as Berny, method of steepest-descent, quasi-Newton and Fletcher-Powell. Most of these methods calculate the second derivative of the energy with respect to the coordinates, also known as the Hessian. The Hessian provides information about the curvature of the PES, and hence allows the program to determine how to vary the geometry in the next step.

1.2.2.3 Variational theorem

It is only possible to solve the Schrödinger equation (1.5) exactly for one electron systems, i.e. the hydrogen atom, He^+ , Li^{2+} , H_2^+ . In order to solve the Schrödinger equation for multielectron systems, one has to rely on approximate numerical methods. The variational theorem provides one such method. In the variational approach, a guess ψ_{trial} is generated, the energy of which ϵ , is always greater than E_0 .

$$E_0 \leq \epsilon = \frac{\int \psi_{\text{trial}}^* H \psi_{\text{trial}} d\tau}{\int \psi_{\text{trial}}^* d\tau} \quad (1.6)$$

The energy of the trial wavefunction ϵ , is always greater than the true E_0 for any ψ_{trial} . This process makes possible an iterative procedure for minimising the energy by varying the coefficients of the trial wavefunction.

1.2.2.4 Self-consistent field theory

To calculate a potential energy surface, as mentioned in **Section 1.4.2.1**, the electronic Schrödinger equation must first be solved for a system with n electrons and N nuclei, with a given set of nuclear coordinates. *Ab initio* methods attempt to do this from ‘first principles’.

In the SCF technique it is assumed that each electron moves in a potential which is a spherical average of the entire field due to all the other electrons and nuclei.

The electronic Hamiltonian operator is normally written as

$$H_e = T_e + V_{ne} + V_{ee} + V_{nn} \quad (1.7)$$

where T_e is the kinetic energy of the electrons, V_{ne} is the potential energy between the nuclei and electrons, V_{ee} is repulsive energy between electrons and V_{nn} is the energy of repulsion between nuclei. This equation neglects relativistic effects. Every electron possesses a spin of $\pm \frac{1}{2}$, but if two electrons occupy the same orbital, they must be spin paired. The corresponding spin functions are denoted α and β , and obey the following orthonormality conditions.

$$\begin{aligned}\langle \alpha | \alpha \rangle &= \langle \beta | \beta \rangle = 1 \\ \langle \alpha | \beta \rangle &= \langle \beta | \alpha \rangle = 0\end{aligned}\quad (1.8)$$

The *Pauli Exclusion Principle* states that the total wavefunction must be antisymmetric with respect to exchange and hence no two electrons can possess the same set of four quantum numbers (i.e. if two electrons reside in the same orbital one must be spin up, the other spin down). The concept of the spinorbital $\phi_a(i)$ was introduced, as the product of an orbital wavefunction and a spin function. The antisymmetry of the resulting wave function is then ensured by employing *Slater Determinants*.

$$\Phi_{SD} = \frac{1}{\sqrt{N!}} \begin{vmatrix} \phi_1(1) & \phi_2(1) & \dots & \phi_N(1) \\ \phi_1(2) & \phi_2(2) & \dots & \phi_N(2) \\ \dots & \dots & \dots & \dots \\ \phi_1(N) & \phi_2(N) & \dots & \phi_N(N) \end{vmatrix}, \quad \langle \phi_i | \phi_j \rangle = \delta_{ij} \quad (1.9)$$

The self consistent field method is a computational procedure for identifying numerical solutions to the Schrodinger equation to describe atomic orbitals. It achieves this using an iterative procedure that involves selecting an approximate Hamiltonian, solving the Schrödinger equation to obtain a more accurate set of orbitals (corresponding to a lower total electronic energy), and then solving the Schrödinger equation again until convergence has been achieved.

1.2.2.5 Linear variation method

A method that can be used in the study of multielectron systems is that of the linear variation function. Linear combinations of n linearly independent functions $\psi_1, \psi_2, \dots, \psi_n$ (atomic orbitals) are functions that satisfy the boundary conditions of the problem, i.e. $\phi = \sum_i c_i \psi_i$. The coefficients c_i are parameters to be determined by minimising the variational integral (1.6). Therefore:

$$\begin{aligned}\langle \phi | H | \phi \rangle &= \langle \sum_i c_i \psi_i | H | \sum_j c_j \psi_j \rangle \\ &= \sum_i \sum_j c_i^* c_j \langle \psi_i | H | \psi_j \rangle \\ &= \sum_i \sum_j c_i^* c_j H_{ij}\end{aligned}\quad (1.10)$$

$$\begin{aligned}
\langle \psi | \psi \rangle &= \langle \sum_i \sum_j c_i c_j^* \psi_i | \psi_j \rangle \\
&= \sum_i \sum_j c_i c_j^* \langle \psi_i | \psi_j \rangle \\
&= \sum_i \sum_j c_i c_j^* S_{ij}
\end{aligned} \tag{1.11}$$

where H_{ij} is the Hamiltonian matrix element and S_{ij} is the overlap matrix element.

The variational energy can then be calculated from:

$$E = \frac{\sum_i \sum_j c_i c_j^* H_{ij}}{\sum_i \sum_j c_i c_j^* S_{ij}} \tag{1.12}$$

Rearranging this equation to give

$$E \sum_i \sum_j c_i c_j^* S_{ij} = \sum_i \sum_j c_i c_j^* H_{ij} \tag{1.13}$$

To minimise the energy with respect to linear coefficients c_i , one would require

$$\frac{\partial E}{\partial c_k} = 0 \text{ for all } i.$$

Differentiating both sides gives

$$\begin{aligned}
\frac{\partial E}{\partial c_k} \sum_i \sum_j c_i c_j^* S_{ij} + E \sum_i \sum_j \left[\frac{\partial c_i^*}{\partial c_k} c_j + \frac{\partial c_i}{\partial c_k} c_j^* \right] S_{ij} \\
= \sum_i \sum_j \left[\frac{\partial c_i^*}{\partial c_k} c_j + \frac{\partial c_j}{\partial c_k} c_i^* \right] H_{ij}
\end{aligned} \tag{1.14}$$

Given that $\frac{\partial c_i^*}{\partial c_k} = \delta_{ik}$ and $S_{ij} = S_{ji}$, $H_{ij} = H_{ji}$, we obtain

$$\frac{\partial E}{\partial c_k} = \sum_i \sum_j c_i c_j^* S_{ij} + 2E \sum_i S_{ik} = 2 \sum_i c_i H_{ik} \tag{1.15}$$

When $\frac{\partial E}{\partial c_k} = 0$, the equation becomes

$$\sum_i c_i (H_{ij} - E S_{ik}) = 0 \tag{1.16}$$

for all k . Equation (1.15) is known as a secular equation and there are k associated simultaneous linear equations in k unknowns. These equations can also be written in matrix form, and linear dependence demands that the secular

determinant be equal to zero.

$$|H_{ik} - ES_{ik}| = 0 \quad (1.17)$$

Solving the determinant gives the energies E . If arranged in order, this will provide the approximate energies of the first k states. In order to obtain the corresponding wavefunction for a particular state, one can substitute the appropriate energy into the secular equations and solve for the coefficients c_i .

1.2.2.6 Hartree-Fock approach

One of the primary objectives of a quantum mechanical calculation is to solve the time-independent Schrödinger equation for atoms and molecules. The Hartree-Fock method attempts to solve this equation by assuming that the wavefunction can be approximated by a single Slater determinant comprised of one spin orbital per electron. Recalling equation (1.9)

$$\Phi_{SD} = \frac{1}{\sqrt{N!}} \begin{vmatrix} \phi_1(1) & \phi_2(1) & \dots & \phi_N(1) \\ \phi_1(2) & \phi_2(2) & \dots & \phi_N(2) \\ \dots & \dots & \dots & \dots \\ \phi_1(N) & \phi_2(N) & \dots & \phi_N(N) \end{vmatrix}, \quad \langle \phi_i | \phi_j \rangle = \delta_{ij} \quad (1.9)$$

The Hartree-Fock method determines the set of spin orbitals that minimise the energy that provides the ‘best single determinant’. To achieve this, some initial guesses are made for the orbitals while the variational theorem as in equation (1.6) is solved iteratively. The Hartree-Fock equation for the spin-orbital becomes

$$f_1 \phi_i(1) = \varepsilon_a \phi_i(1) \quad (1.18)$$

where ε_a is the orbital energy of the spin-orbital and f_1 is the Fock operator:

$$f_1 = h_1 + \sum_u \{J_u(1) - K_u(1)\} \quad (1.19)$$

Here J_j and K_j refer to the coulomb and exchange operators respectively.

$$J_j(1)\phi_i(1) = \left\{ \phi_j^*(2) \left(\frac{e^2}{4\pi\epsilon_0 r_{12}} \right) \phi_j(2) d\mathbf{x}_2 \right\} \phi_i(1) \quad (1.20)$$

$$\hat{K}^j(\mathbf{r}_1)\phi_i(\mathbf{r}_1) = \left\{ \phi_j^*(\mathbf{r}_2) \left(\frac{e^2}{4\pi\epsilon_0 r_{12}} \right) \phi_i(\mathbf{r}_2) d\mathbf{x}^2 \right\} \phi_j(\mathbf{r}_1) \quad (1.21)$$

The Coulomb operator **(1.20)** gives the Coulombic interaction of an electron in a spin orbital ϕ_i with the average charge distribution of the other electrons. Therefore one can see how Hartree-Fock is a ‘mean field’ theory. The Coulomb operator also gives the average local potential at point \mathbf{x}_1 due to the charge distribution from the electron in orbital ϕ_j .

The exchange term **(1.21)** arises from the antisymmetry requirements of the wavefunction. It looks very similar to the Coulomb term **(1.24)**, with the exception that it switches or ‘exchanges’ spin orbitals, ϕ_i and ϕ_j . The exchange energy only involves electrons of the same spin.

The main drawback in applying this mean field approximation in Hartree-Fock theory is that correlation between electrons of the same spin is ignored. As a consequence on this, neglecting electron correlation can lead to large deviations from experimental results. A number of approaches which try and overcome this problem, known collectively as post-Hartree-Fock methods, have been devised to include electron correlation to multi-electron wave function. Such approaches include Møller-Plesset perturbation theory,⁴⁴⁻⁵¹ configuration interaction (CI)⁵²⁻⁵⁴ and coupled-cluster theory (CC).⁵⁵⁻⁵⁶ In the Møller-Plesset perturbation theory for example, electron correlation is treated as a perturbation of the Fock operator **(1.19)**. It improves the Hartree-Fock method by adding electron-correlation effects by means of Rayleigh-Schrödinger perturbation theory (RS-PT), usually to second (MP2), third (MP3) or fourth (MP4) order. Scaling to higher orders does improve the accuracy of the calculation however, although the main disadvantage is that it also scales the computational cost dramatically.

In recent years density functional theory has largely replaced Hartree-Fock calculations as it includes both the exchange and correlation energies, while still maintaining a similar computational cost to that of Hartree-Fock. Density functional theory or DFT will be discussed in more detail in **Section 1.2.3**.

1.2.2.7 Basis Sets

Basis sets are mathematical functions that represent atomic orbitals. Effectively they are the set of linearly independent functions which can be used to generate an orbital descriptor of the wavefunction. Basis sets are usually comprised of either slater-type functions or gaussians. The slater-type basis set is not used in *ab initio* calculations as the integrals are very difficult to calculate, particularly if the orbitals are centred on different nuclei.

There are a large number of basis sets that use gaussians used in quantum mechanical calculations, such as STO-3G, STO-4G, 3-21G, 3-21G+, 4-31G, 6-31G, 6-31G* and 6-311++G**. The notation used to describe the basis sets describes the type of functions used to accommodate all the filled orbitals in every atom.

The STO-3G basis set, has the prefix STO – meaning ‘Slater Type Orbital’ and has three gaussian functions. Gaussian type functions are of the form $\exp(-\alpha r^2)$ and *ab initio* Gaussian functions are generally of the following form:

$$f(n) = x^a y^b z^c \exp(-\alpha r^2) \quad (1.22)$$

where the summation of x,y and z gives the order of the equation, i.e. $x+y+z=1$ is a first order function. ‘ α ’ is a value that determines the ‘radial extent’ of the gaussian; a small value of α gives a large extent of the gaussian function and vice-versa.

When adding two Gaussian functions together, the product is just one Gaussian function, centred between the two original Gaussians.

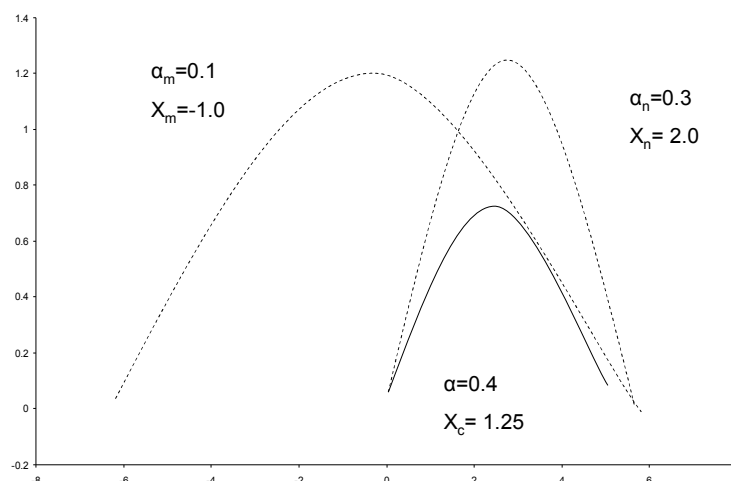


Figure 1.2 The summation of two Gaussian functions results in a single gaussian, centred between the original two functions

Once a type of function is selected (STO/GTO) the most important factor that needs to be considered is the number of functions that needs to be used. The smallest number of functions possible that describe an atom/molecule is referred to as a *minimum basis set*. In this case, sufficient functions are employed to represent all the electrons of the neutral species. For example, the minimum basis set for hydrogen and helium would be a single s-function.

The next step up in basis set would be to double all basis functions, giving rise to a *Double Zeta* (DZ) type basis set. The term zeta arises from the greek letter ζ , which is used to denote the exponent of STO basis functions. For example, a DZ basis set would utilise two s-functions for the hydrogen or helium atom(s) (1s and 1s'). The advantage of using a DZ basis set over a minimal basis set is that it allows for a better description of electronic distribution around a particular nucleus, which will vary depending on the electronic environment.

Triple-Zeta and Quadruple-Zeta basis sets also exist, where by the name suggests three and four Gaussians are used respectively, as for the Double-Zeta basis sets.

Adding more functions improves the representation but makes the calculation more time consuming. Since it is mainly the valence electrons, and not the core electrons that participate in bonding *split valence basis sets* have been developed to divide the atomic orbitals into: the inner, more compact orbitals and the outer, valence orbitals. In split valence basis sets it is common to use a double, triple or quadruple-zeta for the valence orbitals only, and to describe the core electrons with a single Slater type orbital. For example, the 3-21G basis set has three gaussian functions summed to describe the core orbitals, two Gaussian functions that comprise the first STO of the double zeta and one Gaussian function summed in the second STO.

Another extension to a basis set is to include *polarisation effects*. If different atoms are brought into contact with each other, then when a p-orbital approaches an s-orbital, for example, the s electron density is polarised in a non spherically symmetrical way. For example, in the molecule HCN, the C-H bond consists predominantly of the hydrogen s-orbital and the p_z orbital on carbon, whereas the π bond between C and N consists of the p_x and the p_y orbitals of C and N. Therefore polarisation functions take into account the fact that the electron distribution about atoms in molecules is anisotropic by providing the possibility of altering the symmetry of the electron distribution. One asterisk (*) at the end of a basis set will denote that polarisation has been taken into account in the 'p' orbitals.

The last basis set convention to note is the use of *diffuse* functions. In basis sets, the main energy of an atom or molecule is calculated from the core electrons. In an actual chemical reaction however, an atom is often in an excited or anionic state, which means that the electron density is significantly further from the nucleus than would otherwise be the case. To allow the basis set accommodate this situation, diffuse functions can be added which use small positive exponents to optimise the properties of the tail. Diffuse functions are represented by the '+' sign. One '+' means that a diffuse function on a p-orbital is being accounted for, whereas '++' means that both 'p' and 's' orbitals are being taken into account.

1.2.3 Density Functional Theory

Density functional theory, is based on the fact that the ground-state electronic energy is determined completely from the electron density, ρ . This theorem was proven by Hohenberg and Kohn⁵⁷. A functional is essentially a function of a function. A wavefunction and the electron density can be considered to be functions whereas as energy depending on a wavefunction or an electron density is a functional. The objective of the DFT method is to design functionals connecting the electron density with the energy.⁵⁸

In DFT methods, the energy functional is divided into three parts – the kinetic energy $T[\rho]$, the attraction between the nuclei and electrons, $E_{ne}[\rho]$ and the electron-electron repulsion, $E_e[\rho]$.

$$E_{ne}[\rho] = \sum_a \int \frac{Z_a \rho(r)}{|R_a - r|} dr \quad (1.23)$$

$$J[\rho] = \frac{1}{2} \iint \frac{\rho(r)\rho(r')}{|r - r'|} dr dr' \quad (1.24)$$

Early DFT work focused on the development of functionals for the kinetic and exchange energies, treated a molecule as a collection of atoms that behaved like a non-interacting uniform electron gas. For these systems the kinetic energy, $T[\rho]$ and the exchange energy, $K[\rho]$ can be described as

$$T_{TF}(\rho) = C_F \int \rho^{2/3}(\mathbf{r}) d\mathbf{r} \quad (1.25)$$

$$C_F = \frac{3}{10} (3\pi^2)^{2/3}$$

$$C_x = \frac{3}{4} \left(\frac{3}{\pi} \right)^{1/3}$$

The subscript *TF* in equation (1.25) refers to the fact that this is Thomas-Fermi theory, and C_F and C_x are constants.⁵⁹⁻⁶⁰ Under the Thomas-Fermi theory the energy functional is thus defined as

$$E_{TF}[\rho] = T_{TF}[\rho] + E_{ne}[\rho] + J[\rho] \quad (1.26)$$

The Thomas-Fermi energy can be quite inaccurate in calculating the electronic energy of a molecule (± 15 -50%). It is not surprising therefore that the idea of treating a molecule as a non-interacting uniform electron gas is flawed.

Block and Dirac attempted to improve the results by including an exchange term, $K_D[\rho]$.⁶¹⁻⁶² There are some similarities to Hartree-Fock theory in that the E_{ee} term may be separated into a Coulomb and an exchange part, $J[\rho]$ and $K[\rho]$, similar to equations (1.20) and (1.21) that were introduced earlier. The energy under the Thomas-Fermi-Dirac (TFD) model is

$$E_{TFD}[\rho] = T_{TFD}[\rho] + E_{ne}[\rho] + J[\rho] + K_D[\rho] \quad (1.27)$$

$$\text{where } K_D[\rho] = -C_x \int \left(\rho_\alpha^{\frac{4}{3}}(\mathbf{r}) + \rho_\beta^{\frac{4}{3}}(\mathbf{r}) \right) d\mathbf{r} \quad (1.28)$$

The accuracy in DFT methods improved dramatically with the introduction of an orbital based approach by Kohn and Sham.⁶³ Kohn and Sham progressed on the work previously completed by Hohenberg and Kohn in that a set of self-consistent equations were included, which incorporated in an approximate way, exchange and correlation effects.

$$E_{DFT}[\rho] = T_S[\rho] + E_{ne}[\rho] + J[\rho] + E_{XC}[\rho] \quad (1.29)$$

Here $T_S[\rho]$ refers to the kinetic energy of the system calculated from a Slater determinant and in addition the exchange energy may be taken to be

$$E_{XC}[\rho] = (T[\rho] - T_S[\rho]) + (E_{ee}[\rho] - J[\rho]) \quad (1.30)$$

The first bracket in equation (1.30) represents the kinetic correlation energy, and the second contains both the exchange and potential correlation energy. The largest contributor to E_{XC} is in fact the exchange energy and most modern methods have evolved to calculate this term more accurately. DFT methods are now classified by the functional form of the exchange-correlation energy.

1.2.3.1 Local Density Methods

In the local density approximation (LDA), the exchange-correlation energy $\epsilon_{XC}[\rho(\mathbf{r})]$ per electron in a uniform gaseous electric field is given by:

$$E_{XC} = \int \rho(\mathbf{r}) \epsilon_{XC}[\rho(\mathbf{r})] d\mathbf{r} \quad (1.31)$$

Each electron is treated as being in a homogenous electric field of infinite volume, with the approximation of a continuous distribution of positive charge to retain electroneutrality. To account for the inhomogeneity, gradient corrections are often included to the exchange-correlation energy E_{XC} .

The exchange energy is normally given as the sum of contributions from the α and β spin densities, as exchange energy only involves electrons of the same spin. The total density of the system should therefore be $\rho = \rho_\alpha + \rho_\beta$.

In the Dirac formula, the local density approximation is given by

$$E_X^{LDA}[\rho] = -C_X \int \rho^{4/3}(\mathbf{r}) d\mathbf{r} \quad (1.32)$$

$$\epsilon_X^{LDA}[\rho] = -C_X \rho^{1/3}$$

When the α and β densities are not equal, the local spin density approximation (LSDA) is a better way to represent the system.

$$E_X^{LSDA}[\rho] = -2^{1/3} C_X \int [\rho_\alpha^{4/3} + \rho_\beta^{4/3}] d\mathbf{r} \quad (1.33)$$

$$\epsilon_X^{LSDA}[\rho] = -2^{1/3} C_X [\rho_\alpha^{1/3} + \rho_\beta^{1/3}]$$

The LSDA is essentially an extension of LDA, but it also accounts for spin polarisation, in other words open-shell systems. LSDA may be written in terms of the total density and the spin polarisation as follows:

$$\begin{aligned}\epsilon_x^{LSDA}[\rho] &= -\frac{1}{2} c_x \rho^{1/3} \left[(\frac{1}{2} + \zeta)^{4/3} + (\frac{1}{2} - \zeta)^{4/3} \right] \\ \zeta &= \frac{\rho^\alpha - \rho^\beta}{\rho^\alpha + \rho^\beta}, \frac{4}{3} \pi r_s^3 = \rho^{-1}\end{aligned}\quad (1.34)$$

where r_s refers to the radius of the effective volume.

For closed shell systems, LSDA would actually be the same as LDA, and since closed shell system calculations are more common, the terms LDA and LSDA are often used interchangeably.

The LSDA approximation underestimates the exchange energy by $\sim 10\%$, thereby creating errors which are greater than the entire correlation energy. In addition, electron correlation is overestimated, often by a factor of up to 2. As a result bond lengths are overestimated. LSDA methods provide similar accuracy to HF methods at only a fraction of the computational cost.

1.2.3.2 Gradient Corrected Methods

In order to improve upon the LSDA approach, one has to consider a non-uniform electron gas. To account for this, the exchange and correlation energies need to be dependent not just the electron density but also on the derivatives of the electron density. Such methods or thus known as Gradient corrected or Generalised Gradient Approximation (GGA) methods.

Perdew and Wang (PW86) suggested modifying the LSDA exchange expression to the following, where x is a dimensionless gradient variable:

$$\epsilon_x^{PW86} = \epsilon_x^{LDA} (1 + ax^2 + bx^4 + cx^6)^{1/15}, \quad x = \frac{|\nabla \rho|}{\rho^{4/3}} \quad (1.35)$$

Becke later proposed a widely used correction (B88) to the LSDA exchange energy:⁶⁴

$$\epsilon_x^{\sim\sim} = \epsilon_x^{LDA} + \Delta_x^{B88}$$

$$\Delta_x^{B88} = -\beta \rho^{1/3} \frac{x^2}{1 + 6\beta x \sinh^{-1} x} \quad (1.36)$$

β is a parameter that is determined by fitting to known atomic data and x was defined in equation (1.35).

The GGA methods give a substantial improvement over LDA, although further improvements proved possible using hybrid methods.

1.2.3.3 Hybrid Methods

Hybrid functionals are a class of approximations to the exchange-correlation energy functional in DFT that incorporate the exact exchange from Hartree-Fock theory with the exchange and correlation treated differently (LDA/empirical). A hybrid approach was constructed by Becke where the exchange-correlation functional was constructed as a linear combination of the Hartree-Fock exact exchange functional (E_x^{HF}) and any number of exchange and correlation explicit density functionals. For example, the B3LYP method is a hybrid of the B88 exchange developed by Becke⁶⁴ and the LYP correlation of Lee, Yang and Parr.⁵⁵

$$E_{EX}^{B3LYP} = E_{XC}^{LDA} - a_o(E_x^{HF} - E_x^{LDA}) + a_x(E_x^{GGA} - E_x^{LDA}) + a_c(E_c^{GGA} - E_c^{LDA}) \quad (1.37)$$

Where $a_o=0.20$, $a_x=0.72$ and $a_c=0.81$ are the three empirical parameters determined by fitting the predicted values to a set of atomisation energies, ionisation potentials, proton affinities, and total atomic energies.⁶⁶

The advantage of DFT is that only the total density needs to be considered. To calculate the kinetic energy of the electrons with reasonable accuracy, however, orbitals need to be introduced. This makes the level of computational power required for DFT calculations similar to that of HF, although it has been established that the results are far more accurate than for Hartree Fock.

A practical advantage with DFT methods is that the scaling of the computational effort with increasing molecular size is much smaller when compared with other ab initio methods. If N is the number of basis functions, the scaling behaviour is N^3 for B3LYP, but increases to N^4 for HF and up to N^{10} for MP7, CISDTQ and CCSDTQ.

A study performed by Riley *et al* benchmarked the performance of DFT methods against different ab initio methods.⁶⁷ Some of these findings are presented in **Table 1.1** below. It can be seen from this table that the geometries calculated at the HF level are quite good compared with the more sophisticated levels of theory (MP2/B3LYP). When comparing other physical parameters however (vibrational frequencies/heats of formation/conformational energies/reaction barrier heights) B3LYP performs consistently better than the ab initio methods (HF/MP2). Interestingly, using the 6-31G basis set with B3LYP functional provides better accuracy for vibrational frequencies to those of the more computationally expensive Dunning-type basis set (aug-cc-pVDZ or aug-cc-pVTZ). The thermochemistry is generally more accurate for the Dunning-type basis sets, although the computational expense is often too great to warrant the employment of such a large basis set. A good compromise is to employ a DFT method (B3LYP) using a medium sized basis set (6-31G*), which gives an excellent computational cost to accuracy ratio. This is the approach which we have adopted in this thesis as given the size of the systems under study, > 20 atoms, it would be very difficult to perform geometry optimisations with an extremely large basis set. B3LYP/6-31G* is still very much the theory of choice for studying organic reactions, and a recent review reported B3LYP as the most commonly employed DFT functional.⁶⁸

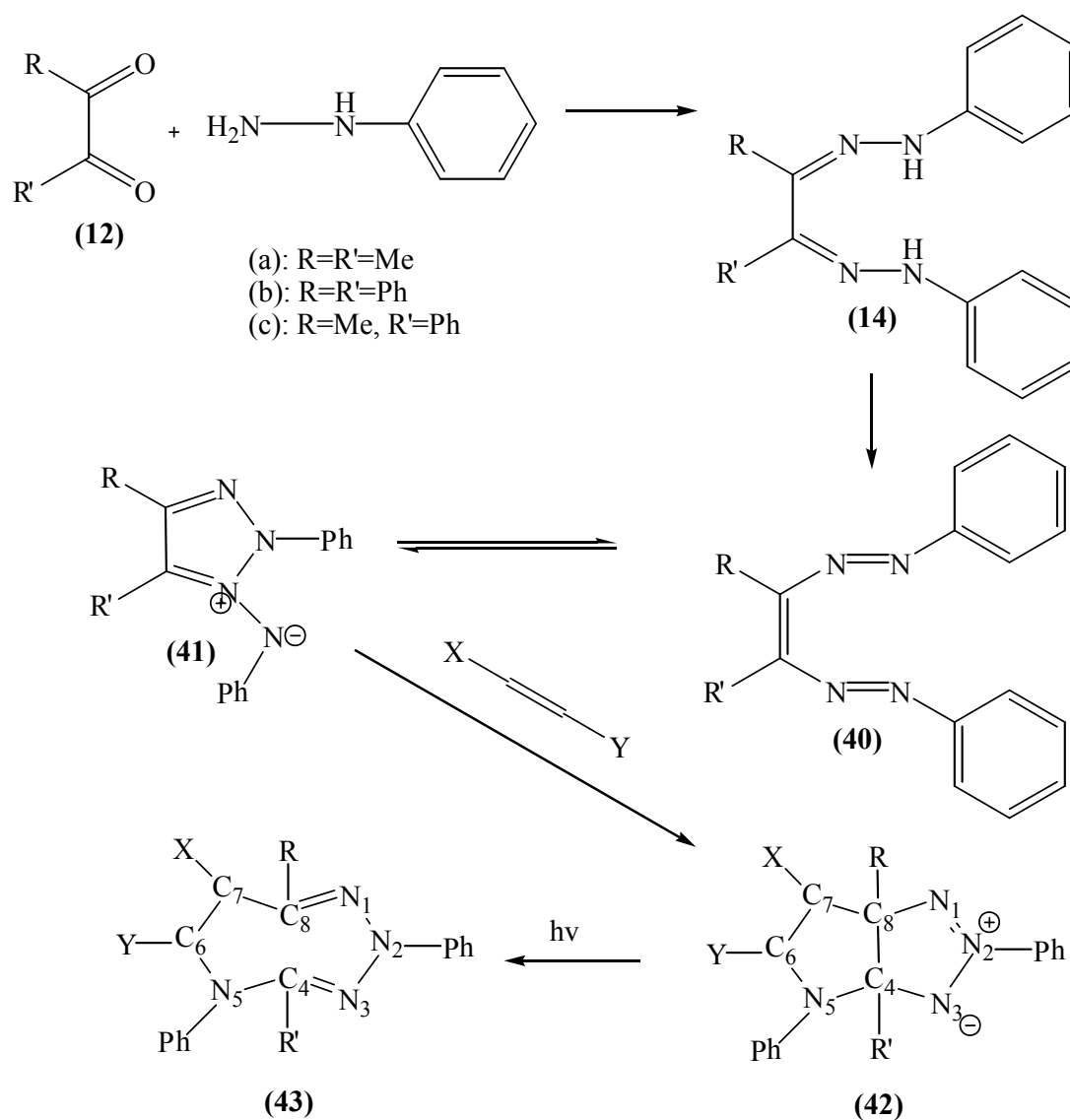
Table 1.1 Comparison of performance of ab initio and DFT methods using different basis sets ⁶⁷					
Bond Lengths: Average signed errors (Å)					
Theory/Basis Set	3-21G*	6-31G*			
HF	0.00	0.01			
MP2	-0.02	-0.01			
B3LYP	-0.02	-0.01			
Bond Angles: Average signed errors (°)					
HF	-0.83	-0.03			
MP2	0.43	0.75			
B3LYP	0.32	0.71			
Vibrational frequencies: Average signed errors (cm ⁻¹)					
Theory/Basis Set	3-21G	6-31G	6-31++G	Aug-cc-pvdz	Aug-cc-pvtz
HF	162	186	216	184	188
MP2	82	94	106	76	89
B3LYP	29	39	60	40	50
Heats of formation: Average signed errors (kcal/mol)					
Theory/ Basis Set	3-21G*	6-31G*			
HF	289.94	252.94			
MP2	49.93	-83.07			
B3LYP	24.04	6.90			
Conformational energies: Average signed errors (kcal/mol)					
Theory/Basis Set	3-21G	6-31G	6-31++G	Aug-cc-pvdz	Aug-cc-pvtz
HF	0.86	-17.21	-14.21	-12.23	-9.30
MP2	-6.77	-18.32	-12.12	-4.39	-2.05
B3LYP	-3.95	-15.83	-10.93	-4.58	-3.14
Reaction barrier heights: (kcal/mol)					
HF	-7.79	-13.93	-13.89	-13.39	-14.39
MP2	5.68	4.51	5.18	8.80	-
B3LYP	7.15	3.40	3.33	4.12	3.06

Chapter 2

Synthesis of Dihydrazone and Azo Compounds

2.1 Introduction

In *Chapter 1* synthetic routes to dihydrazones (**14**) - 1,2,3,5-tetrazocine precursors, were discussed. The sequence of reactions commences with the synthesis of a dihydrazone (**14**) from a diketone (**12**). One of our main aims was to synthesise a 1,2,3,5-tetrazocine of the type **43(c)**, hence the first step towards making the eight-membered ring would be the conversion of the diketone **12(c)** to its dihydrazone **14(c)**, and the subsequent reactions. In this chapter reactions corresponding to the first two steps of this reaction scheme, namely the synthesis of dihydrazone (**14**) and azo compounds (**40**) are discussed.



Scheme 2.1 Synthesis of a 1,2,3,5-tetrazocine (**43**) from a 1,2-diketone (**12**).

In **Section 2.2**, a number of experiments will be presented that document the attempts made to synthesise the dihydrazone **14(c)** from the diketone **12(c)**. Both the dimethyl **12(a)** and diphenyl **12(b)** diketone derivatives convert readily to the equivalent dihydrazones **14(a)/(b)** at room and reflux temperatures, respectively. Therefore it was expected that the conversion of the methyl-phenyl diketone **12(c)** to form its dihydrazone **14(c)** would be possible, given that the most sterically hindered diketone **12(b)** can react successfully. This however proved not to be the case, the reaction consistently faltered at the monohydrazone stage for the methyl-phenyl derivative, **13(c)**.

Given the difficulty in synthesising the dihydrazone **14(c)** from the diketone **12(c)**, alternative routes to dihydrazones were investigated by adapting reported procedures. In **Section 2.3** an alternative route to dihydrazones that was reported by Butler *et al* is explored.⁶⁹ Here the authors formed a methyl-phenyl dihydrazone **14c(ii)** by oxidising the methylene position adjacent to a monohydrazone (**36**) with the addition of phenylhydrazine. The yield of this reported reaction was quite low (10%) however, which is not ideal as this would be the first reaction of a multi-step sequence.

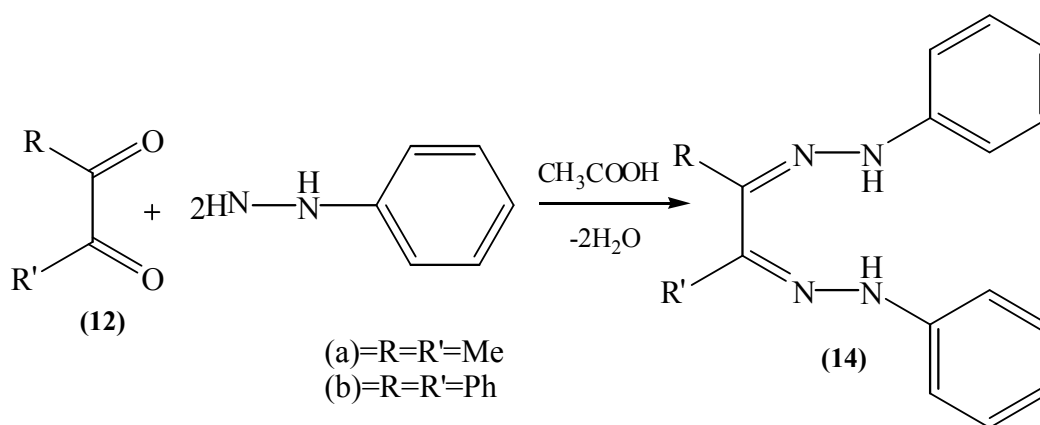
A different route to the desired dihydrazone **14(c)** was shown in **Section 2.4**. In a report that follows this pathway, Ried and Sommer described the alteration of side chains of dihydrazones by replacement with diazonium salts.²⁴ Interestingly, they claimed to have synthesised a 4'-bromo-derivative of the dihydrazone **14(c)**, by adding a diazonium salt to methyl phenylosazone (**17**). The purported yield of this reaction was 31%, however trace quantities could only be reproduced in this work.

An alternative high-yield dihydrazone route is described in **Section 2.5**; whereby α -substituted ketones are converted to dihydrazones.³⁰ Schantl *et al* claimed to have synthesised the exact dihydrazone **14(c)** through the addition of three molecular equivalents of phenylhydrazine to α -bromopropiophenone (**33**). We found that the reaction faltered after the addition of the second molecular equivalent of phenylhydrazine, producing α -(phenylhydrazino)-phenylhydrazone **35(c)**. A report by von Auwers describes the transformation of α -bromopropiophenone **33(c)** to a 1-phenyl-1,2-bis-(4'-nitro-phenylhydrazone)propane **14c(ii)** by the addition of three molecular equivalents of 4'-nitrophenylhydrazine hydrochloride.⁷⁰ By altering the

molar ratio of the phenylhydrazine salt to diketone from 3:1 to phenylhydrazine salt:phenylhydrazine: diketone to 1:2:1 for this reported procedure, we were able to generate a high yield entry route (78%) to the desired dihydrazone **14c(ii)**. This allowed us to proceed to the next step in the multistep reaction.

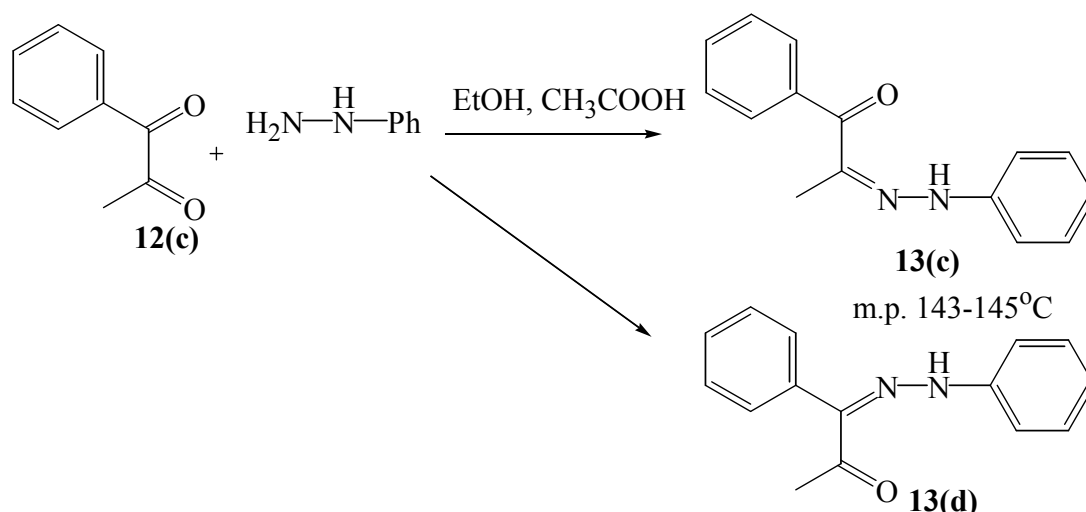
Consequently, **Section 2.6** describes the reaction that formed the azo compound, **40(c)**, which is the product generated from the second step in the multistep reaction in **Scheme 2.1**. The azo compound proved difficult to purify however, which made it difficult to proceed through the final steps of the reaction in this scheme.

2.2 Synthesis of dihydrazones from diketones



Scheme 2.2 Synthesis of a dihydrazone (**14**) from a diketone (**12**) by the addition of phenylhydrazine.

The dihydrazone 2,3-bis-(phenylhydrazone)butane **14(a)** was synthesised by dissolving butane-2,3-dione **12(a)** in glacial acetic acid with two molar equivalents of phenylhydrazine and stirring the reaction mixture gently at room temperature. This reaction gave a maximum yield of 89% after 45 minutes. Furthermore, the corresponding diphenyl derivative **14(b)**, can be synthesised by heating the reaction mixture to reflux (118°C) for a duration of one hour. Therefore, it was expected that it should be possible to convert the methyl-phenyl diketone derivative **12(c)**, *i.e.* R=Me, R'=Ph to its dihydrazone **14(c)** using similar conditions. This however, was not found to be the case; the reaction stalled at the monohydrazone stage (*see Scheme 2.3*).



Scheme 2.3 Addition of two molar equivalents of phenylhydrazine to 1-phenylpropane-1,2-dione **12(c)** yielding a monohydrazone (**13**). The authors made no attempts to ascertain which isomer is formed in the reaction **13(c)/(d)**.

Table 2.1 provides a comprehensive list of the physical parameters that were varied in the reaction between diketone **12(c)** and phenylhydrazine. The first experimental parameter to be varied was the temperature of the reaction. The generation of the dimethyl phenylhydrazone 1,2-bis(phenylhydrazone)butane **14(a)** required the diketone **12(a)** to be stirred in glacial acetic acid with phenylhydrazine at room temperature, whereas the diphenyl dihydrazone 1,2-bis(phenylhydrazone)stilbene **14(b)** required the reaction mixture to be heated to reflux temperatures (118°C). The temperature dependence presumably arises due to kinetic limitations as the diphenyl species is the most sterically hindered diketone **12(b)** and the dimethyl diketone **12(a)** is the least sterically hindered diketone. Therefore, it is possible that the even more sterically hindered dihydrazone **14(b)** could be made to react by further raising the temperature. Success would indicate that this is a kinetic issue. It is expected that the methyl-phenyl diketone **12(c)** should also react to the dihydrazone **14(c)** by this argument, by heating the reaction mixture to an intermediate temperature.

Table 2.1 Experimental parameters varied (temperature, molar ratio, solvent, nucleophile) in an attempt to synthesise the dihydrazone **14(c)** from the diketone **12(c)**.

Expt Type	Expt	Results	Yield	Solvent/Conditions	Temp	Molar ratio
Temp	SK195	Monohydrazone	46.0%	Ethanol	-40°C	1:2
Temp	SK161	Monohydrazone	32.3%	Glacial Acetic Acid	RT	1:2
Temp	SK165	Monohydrazone	48.7%	Glacial Acetic Acid	45°C	1:2
Temp	SK166	Red resin	-	Glacial Acetic Acid	48°C	1:2
Temp	SK169	Red resin	-	Glacial Acetic Acid	50°C	1:2
Temp	SK166a	Red resin	-	Glacial Acetic Acid	55°C	1:2
Temp	SK167	Red resin	-	Glacial Acetic Acid	65°C	1:2
Temp	SK164	Red resin	-	Glacial Acetic Acid	70°C	1:2
Molar ratio	SK161	Monohydrazone	32.3%	Glacial Acetic Acid	RT	1:1
Molar ratio	SK200	Monohydrazone	64.0%	Glacial Acetic Acid	RT	1:2
Molar ratio	SK213	Monohydrazone	30.4%	Glacial Acetic Acid	RT	1:3
Molar ratio	SK193	Monohydrazone	29.0%	Glacial Acetic Acid	RT	1:4
Molar ratio	SK208	Monohydrazone	27.0%	Glacial Acetic Acid	RT	1:5
Molar ratio	SK263	Monohydrazone	60.0%	Glacial Acetic Acid	45°C	1:1
Molar ratio	SK165	Monohydrazone	48.7%	Glacial Acetic Acid	45°C	1:2
Molar ratio	SK213b	Red resin	-	Glacial Acetic Acid	45°C	1:3
Molar ratio	SK193b	Red resin	-	Glacial Acetic Acid	45°C	1:4
Molar ratio	SK208b	Red resin	-	Glacial Acetic Acid	45°C	1:5
Solvent	SK193a	Monohydrazone	29%	Toluene	<45°C	1:2
Solvent	SK207	Monohydrazone	34.0%	Toluene + few drops of Acetic Acid	<45°C	1:2
Solvent	SK169	Red resin	-	Chloroform	45°C	1:2
Solvent	SK191	Red resin	-	Acetonitrile + 2% TFA	45°C	1:2
Solvent	SK211	Monohydrazone	49.0%	Glacial Acetic Acid	45°C	1:2
Solvent	SK168	Monohydrazone	48.0%	Ethanol	45°C	1:2
Solvent	SK263	Monohydrazone	60.0%	Ethanol + few drops of acetic acid	45°C	1:2
Solvent	SK200	Monohydrazone	64.0%	Ethanol + few drops of TEA	45°C	1:2

Nucleophile	SK263	2'nitro-monohydrazone	60.0%	Ethanol + few drops of acetic acid	Reflux	1:2
Nucleophile	SK266	4'nitro-monohydrazone	60.2%	Glacial acetic acid	Reflux	1:2
Nucleophile	SK211	2',4'-dinitro-monohydrazone	79.0%	Glacial acetic acid	Reflux	1:2
Nucleophile	SK265	4'fluoro-monohydrazone	68.4%	Ethanol and 3 drops of acetic acid	Reflux	1:2
Dean Stark	SK206	Monohydrazone	8.0%	Toluene /Dean Stark apparatus	Reflux	1:2
Dean Stark	SK207	Monohydrazone	24.0%	Toluene + few drops of acetic acid/ Dean Stark apparatus	Reflux	1:2

As can be seen from **Table 2.1**, when the reaction was heated above 45°C, the reaction mixture did not yield neither the mono- nor the dihydrazone, but a red resin, from which no recognisable product could be isolated.

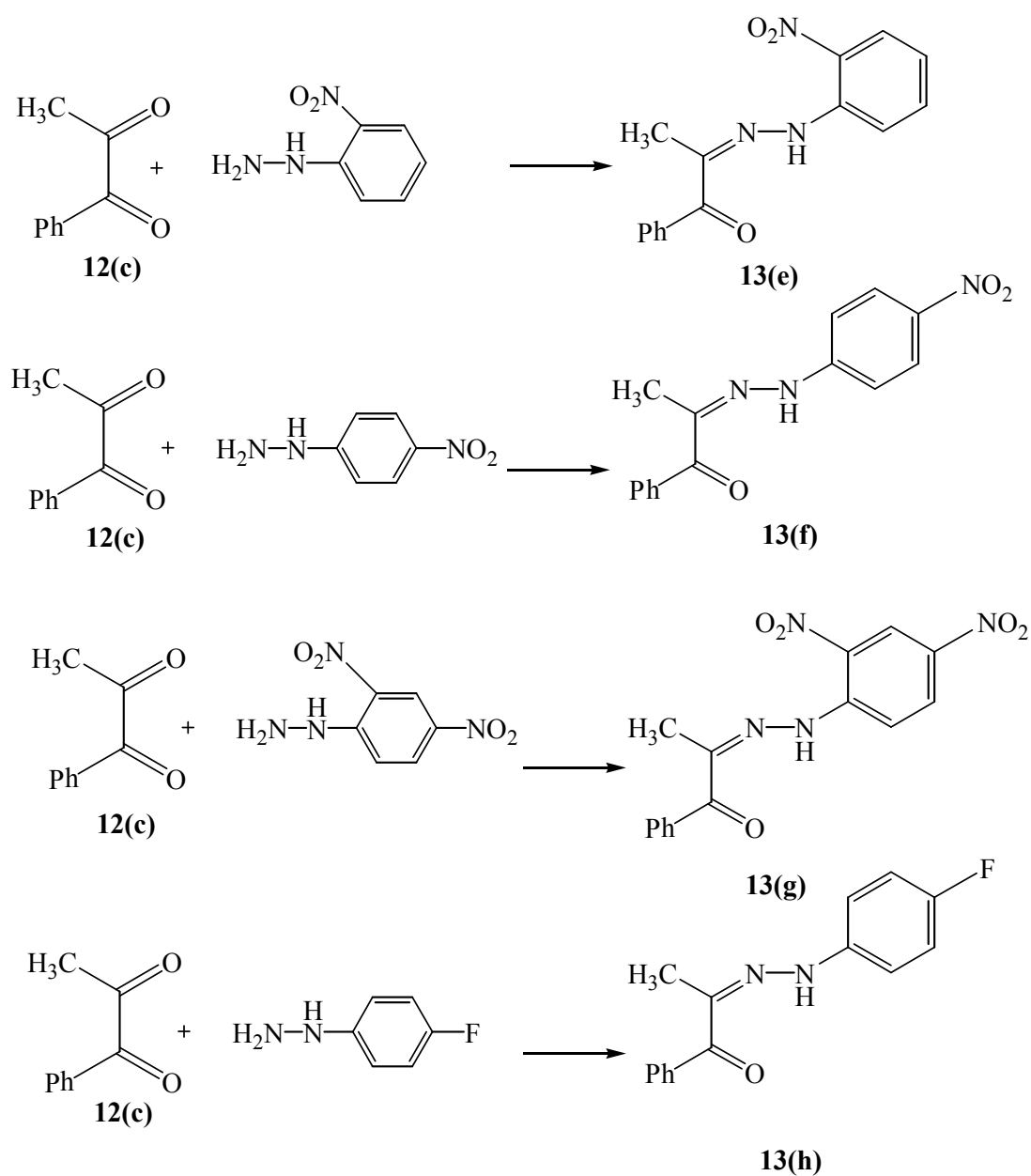
The next parameter that was varied was the molar ratio. A number of experiments involving different molar ratios of diketone to phenylhydrazine were investigated, however the monohydrazone, **13(c)**, was the only product obtained at room temperature (64% yield). The dihydrazone **14(c)** could be not formed either when the reaction mixture was heated, with the ratio of diketone **12(c)** to phenylhydrazine increased up to a maximum molar ratio of 1:5.

A variety of non-polar (toluene, chloroform), polar aprotic (acetonitrile) and polar protic solvents (glacial acetic acid, ethanol) were utilised in the reaction between the diketone **12(c)** and phenylhydrazine. Regardless of the solvent employed however, the monohydrazone was the only product obtained in the reaction.

Table 2.2 Dielectric constants of non-polar, polar aprotic and polar protic solvents

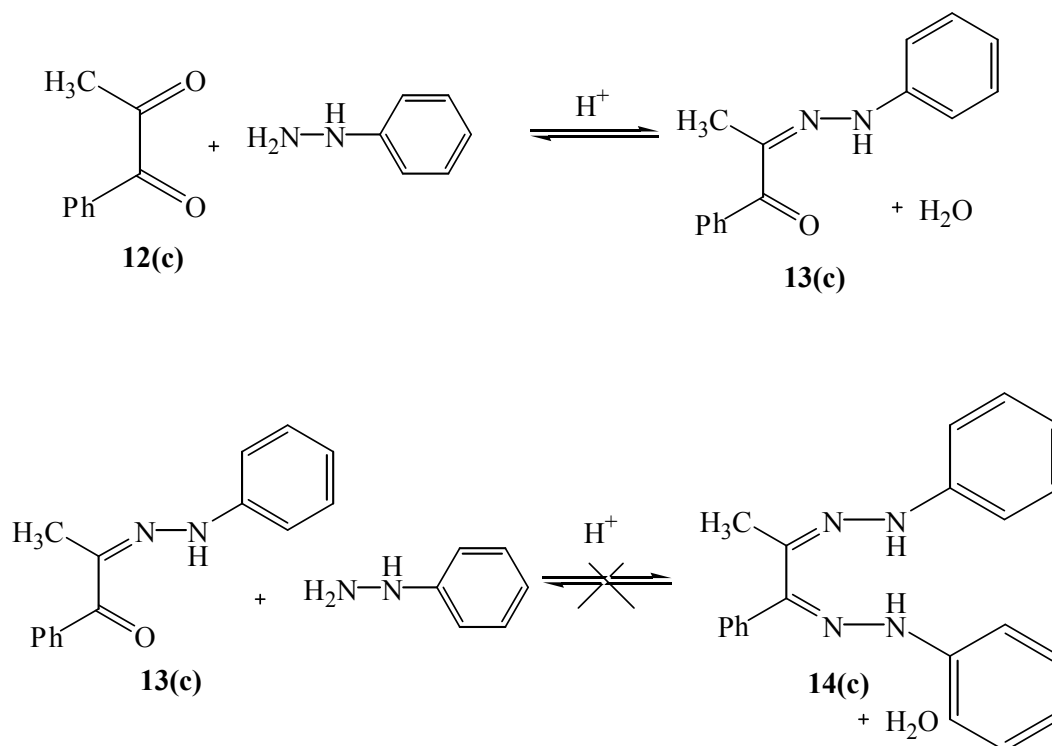
Solvent type	Solvent	Dielectric constant
Non-polar	Toluene	2.4
Non-polar	Chloroform	4.8
Polar aprotic	Acetonitrile	37
Polar protic	Glacial Acetic Acid	6.2
Polar protic	Ethanol	30

The next set of experiments investigated the effect of altering the nucleophile in the reaction. Phenylhydrazine derivatives (2'-nitro-phenylhydrazine, 4'-nitro-phenylhydrazine, 2',4'-dinitro-phenylhydrazine and 4'-fluoro-phenylhydrazine) were used in a 1:2 molar ratio. Unfortunately, these reactions faltered at the monohydrazone stage yet again. These monohydrazone derivatives **13(e-h)** are novel compounds however, not previously reported in the literature.



Scheme 2.4 Monohydrazone derivatives **13(e-h)** obtained in the experiments that were designed to alter the nucleophile in an attempt to form the dihydrazone **14(c)**

The addition of phenylhydrazine to a carbonyl group is a condensation reaction, therefore if the monohydrazone has been generated; water will be present in the reaction mixture. As the water may affect the kinetics of the reaction, (see **Scheme 2.5**) a Dean Stark trap was attached to the reflux condenser to isolate any water generated. Two experiments, SK206 and SK207 are documented in **Table 2.1** with the results of these showing that the removal of any water generated does not aid in the formation of the dihydrazone **14(c)**.

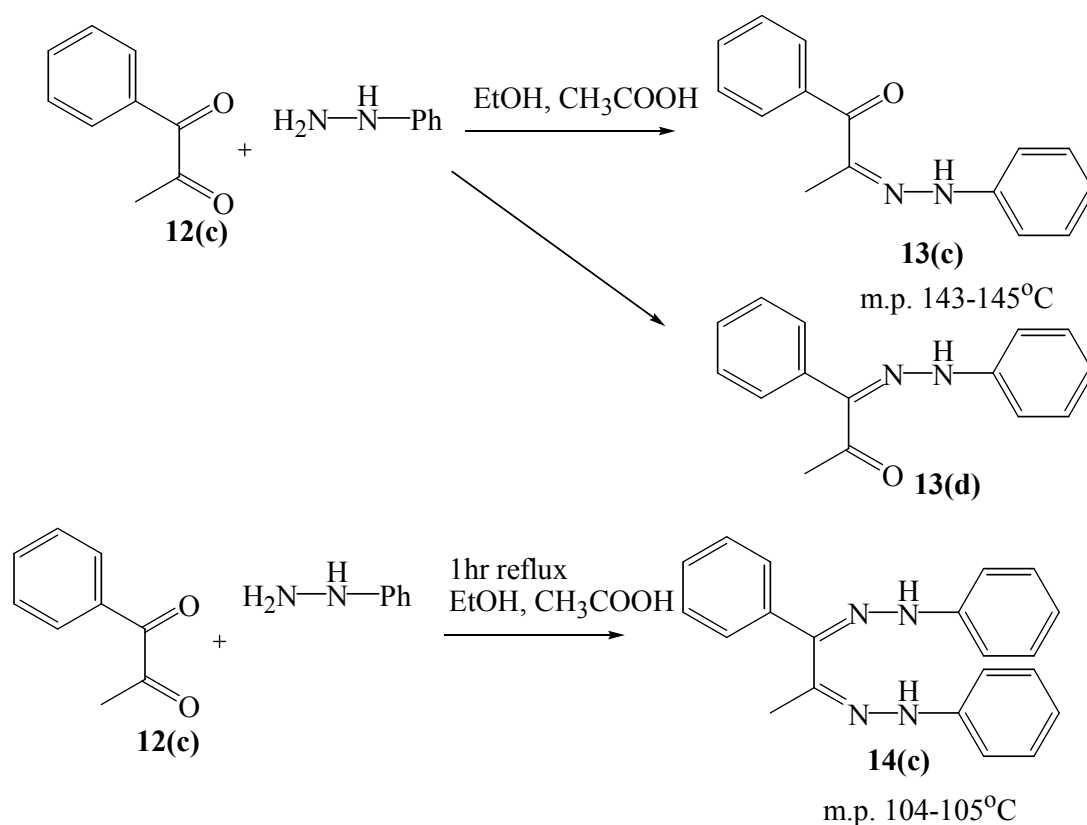


Scheme 2.5 Reaction mechanism of the two-step process to dihydrazone formation **14(c)**

The role of a proton (acid) was previously highlighted in **Scheme 1.5** of **Chapter 1**, whereby the hydroxyl group in the intermediate picks up a proton to form the hydronium ion, yielding the next intermediate. This contains a good leaving group, so there should be a driving force for $\text{C}=\text{N}$ formation, leading to the monohydrazone (**13**).

This reaction was also found to be base catalysed, which is interesting, given that the reaction (SK200) which produced the highest yield of monohydrazone (64%), contained a few drops of triethylamine (TEA) in the solvent mixture.

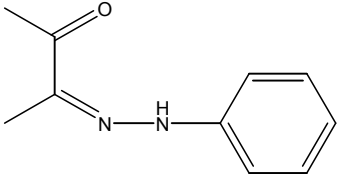
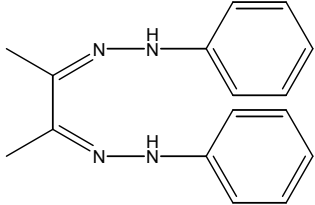
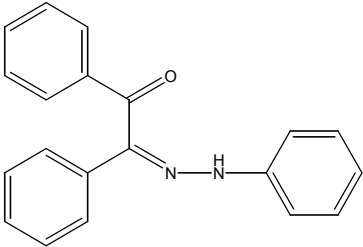
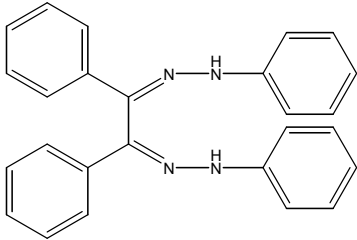
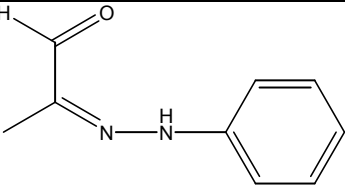
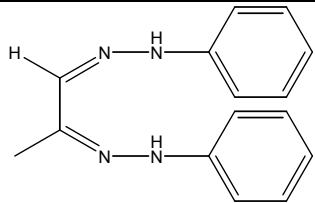
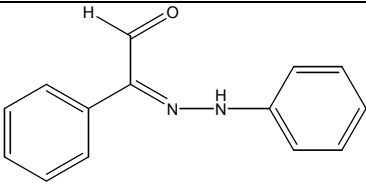
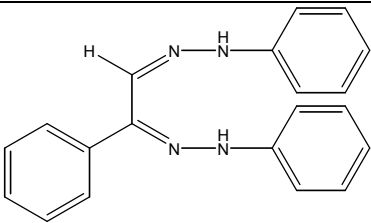
Despite a variety of efforts to synthesise the dihydrazone **14(c)** from the diketone **12(c)**, the synthesis consistently falters at the monohydrazone stage **13(c)**. Interestingly, in 1889, Müller and von Pechmann had previously reported¹⁵ that the monohydrazone **13(c)** was formed (m.p. 143-145°C) when the diketone **12(c)** was added to phenylhydrazine and stirred at room temperature. In addition, they purportedly synthesised the dihydrazone **14(c)** by heating the reaction mixture to reflux temperature; the reported melting point of the dihydrazone **14(c)** was 104-105°C (**Scheme 2.3**). This is unusual however, given that dihydrazones generally have melting points that are *higher* than that of their corresponding monohydrazones. (see **Table 2.3**).



Scheme 2.6 Synthesis of the methyl phenyl monohydrazone **13(c)** by Müller and von Pechmann and the purported synthesis of the dihydrazone **14(c)**.¹⁵

The melting points for other mono- and dihydrazone derivatives are presented in **Table 2.3**. In all cases, the dihydrazone has a significantly higher melting point than that of the corresponding monohydrazone. Therefore, it seems unlikely that Müller and von Pechmann had actually synthesised the dihydrazone, but perhaps an alternative product.

Table 2.3 Melting points of some mono- and dihydrazones. The dihydrazones generally display much higher melting points than that of their corresponding monohydrazones.

	Monohydrazone	Dihydrazone
		
m.p.	134-135°C ¹⁷	246-247°C ²¹
		
m.p.	133-135°C ¹⁶	234°C ²⁰
		
m.p.	152°C ¹⁸	291-293°C ²²
		
m.p.	138°C ¹⁹	169-170°C ²³

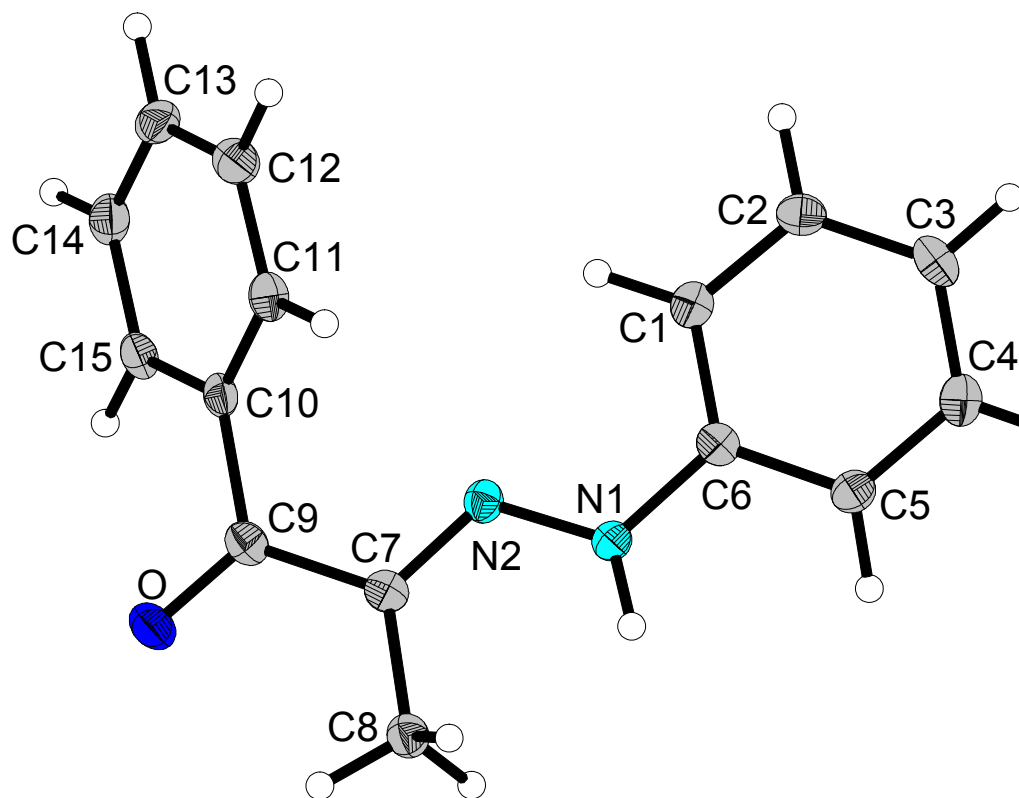


Figure 2.1 X-ray structure of 1-phenyl-2-(phenylhydrazone)propan-1-one, **13(c)**.

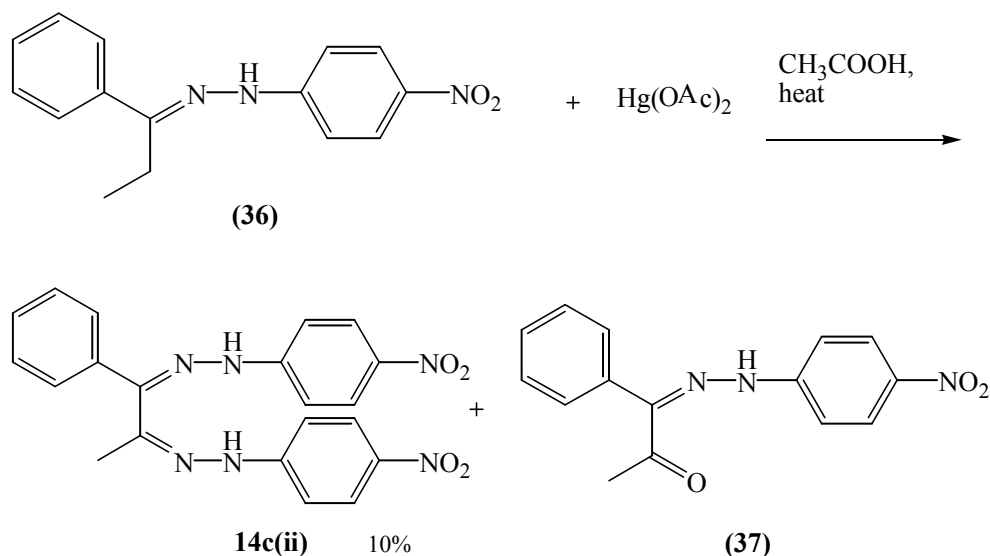
To ascertain the exact isomeric form of the monohydrazone formed, *i.e.* **13(c)/(d)**, **Scheme 2.3**, crystals of the product were grown. It was found from the X-ray structure (*see Figure 2.1*) that the monohydrazone formed is of the type **13(c)**. The fact that the other isomer **13(d)**, has never been observed by this route suggests that phenylhydrazine consistently attacks the carbonyl group adjacent to the methyl group. Interestingly the conformation of the monohydrazone **13(c)** in the crystal structure is an open chain (*E*) isomeric form. The conformation of the different monohydrazone derivatives are discussed in **Chapter 3**. Full details of this crystal structure are provided in **Appendix (a)**. In **Table A.3** of the appendix, the N₁-C₆ distance in the molecular structure is given as 1.39 Å, which is slightly shorter than a typical C-N bond length (1.47 Å), but may be due to the fact that a phenyl ring is attached to this nitrogen atom. In addition, the N₁-N₂ distance is 1.33 Å, which is slightly shorter than normal for a N-N bond (1.45 Å). The N₂-C₇ bond distance is given as 1.29 Å, which is also slightly shorter than a typical C-N bond length (1.47 Å), although this may be attributed to the fact that crystal packing forces may also be

present. The C₉-O (C=O) carbonyl distance is 1.228 Å, which is typical of a C=O bond length (~1.23 Å).

As the dihydrazone 1-phenyl-1,2-bis(phenylhydrazone)propane, **14(c)**, is required for our selected route to the 1,2,3,5-tetrazocine **43(c)**, other routes to this compound were then explored.

2.3 Synthesis of dihydrazones by oxidation of monohydrazones

The synthesis of a dihydrazone by the oxidation of a monohydrazone was mentioned earlier in *Chapter 1*, as reported by Butler *et al.*⁶⁹ The treatment of *p*-nitrophenylhydrazone with an aliphatic hydrazone (**36**) with one molar equivalent of mercuric acetate in hot acetic acid resulted in a mixture of dimeric products; 1-phenyl-1,2-bis-(4'-nitro-phenylhydrazone)propane **14c(ii)**, and 1-phenyl-1-(4'-nitrophenylhydrazono)propan-2-one (**37**). The dihydrazone is only formed in 10% yield, which poses a problem if the dihydrazone is to be carried through a number of steps. In addition, when this procedure was repeated a number of times, the dihydrazone **14c(ii)** was formed in only one instance and the quantity was not sufficient to be carried through to the tetrazocine stage.



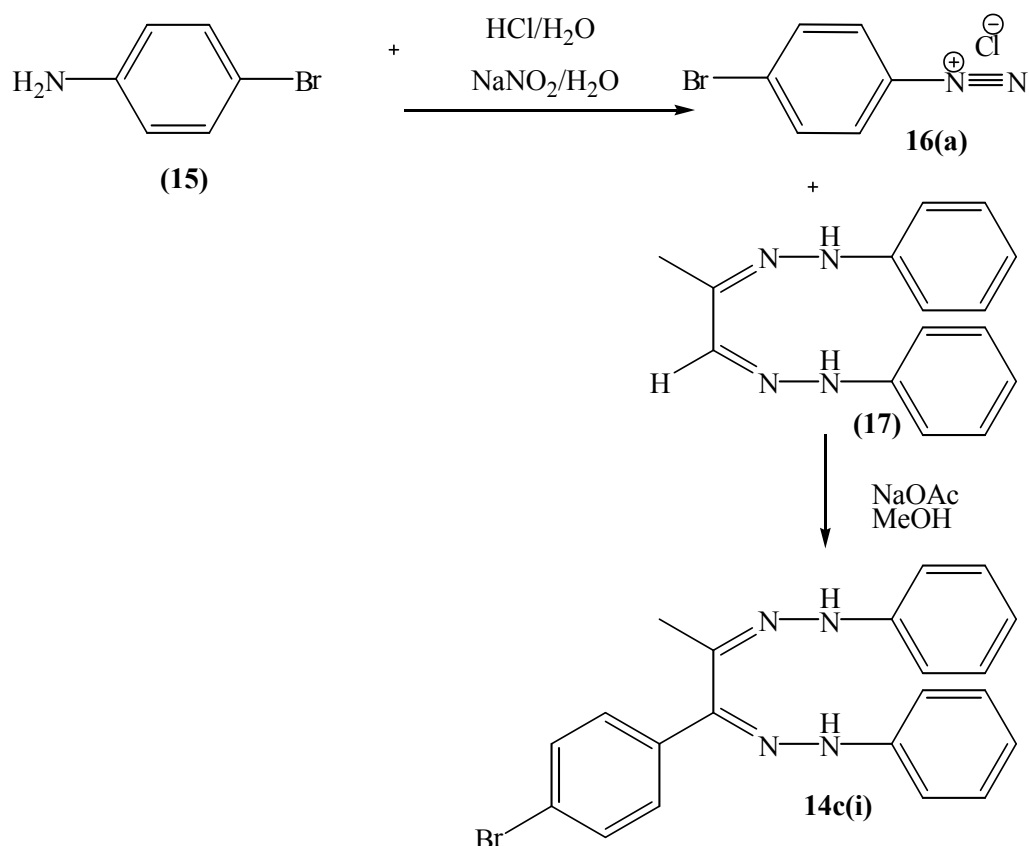
Scheme 2.7 A dihydrazone **14c(ii)** formed by the oxidation of 1-phenyl-1-(4'-nitrophenylhydrazone)propane (**36**)

It is interesting though, that the second dimeric product formed is 1-phenyl-1-(4'-nitro-phenylhydrazono) propane (**37**), which is the alternative isomer to the one formed from the addition of phenylhydrazine to the diketone **12(c)**, 1-phenyl-2-(phenylhydrazono)propane **13(c)**. Interestingly, it was reported⁶⁹ that this monohydrazone (**37**) was successfully converted to the dihydrazone **14c(ii)** by addition of 1 molar equivalent of 4-nitrophenylhydrazine.

2.4 Dihydrazones from diazonium salts

There are alternative ways of synthesising dihydrazones, one of which involves transforming the hydrogen atom of the dihydrazone (*see*

Scheme 2.8). 1,2-*bis*-(phenylhydrazone)propane (**17**) can be converted into 1-(4'-bromophenyl)-1,2-*bis*-phenylhydrazonopropane **14c(i)** via the addition of a diazonium salt.²⁴ The diazonium salt, **16(a)** replaces the hydrogen with the aromatic side chain, 4-bromo-phenylhydrazine, to form 1-(4'-bromo-phenyl)-1,2-*bis*-phenylhydrazone propane, **14c(i)**. This exact procedure reported by Ried and Sommer²⁴ was repeated several times, however it only produced trace quantities of the dihydrazone **14c(i)**. Ried and Sommer reported a 31% yield.



Scheme 2.8 Altering the side-chain of a dihydrazone using a diazonium salt

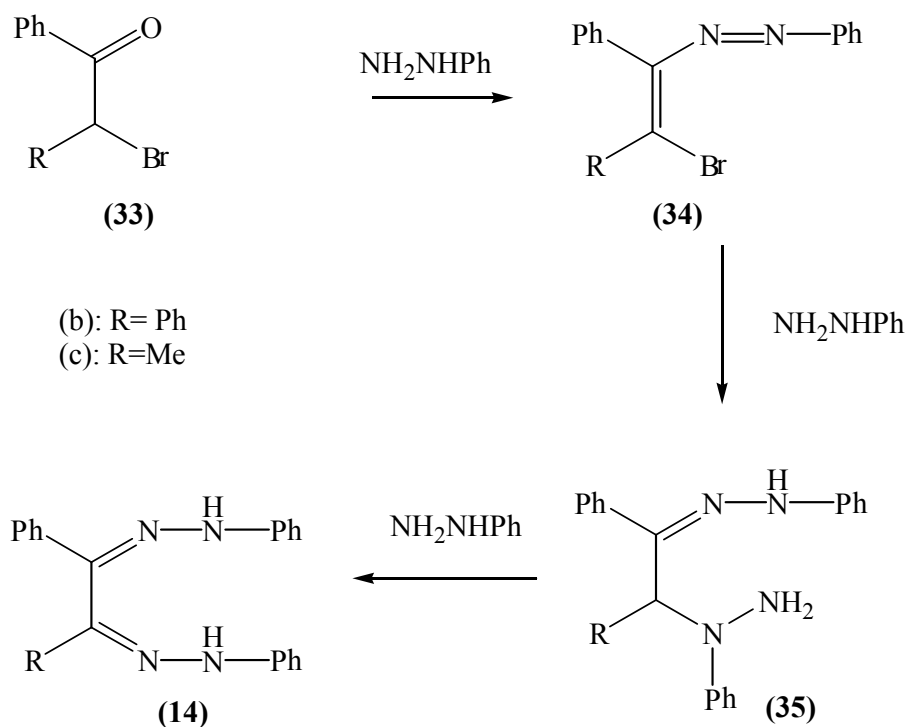
2.5 Synthesis of dihydrazones from α -substituted ketones

An alternative synthetic route to dihydrazones from α -bromo ketones (**33**) was reported by Schantl *et al.*³⁰ In this account, the authors report a 14% yield of 1,2-bis(phenylhydrazone)stilbene **14(b)** from the action of phenylhydrazine on α -bromo ketone **33(b)**. According to their proposed mechanism, an azo alkene (**34**) is initially generated (see **Scheme 2.9**) before conversion to the α -(phenylhydrazino)-phenylhydrazone (**35**), which in turn can be converted to the dihydrazone **14(c)**. It was inferred from this reaction scheme that 1,2-bis(phenylhydrazone)propane **14(c)** could also be synthesised in the same way, although no characterisation data was provided by the authors.

Further investigation into the experimental details revealed that the dihydrazone formation **14(b)** was not a ‘one-pot’ synthesis, but a two-stage reaction in which the azo-alkene **34(b)** was formed from the α -bromo ketone **33(b)**. The azo-alkene **34(b)** was isolated and subsequently transformed to the dihydrazone **14(b)**, through the

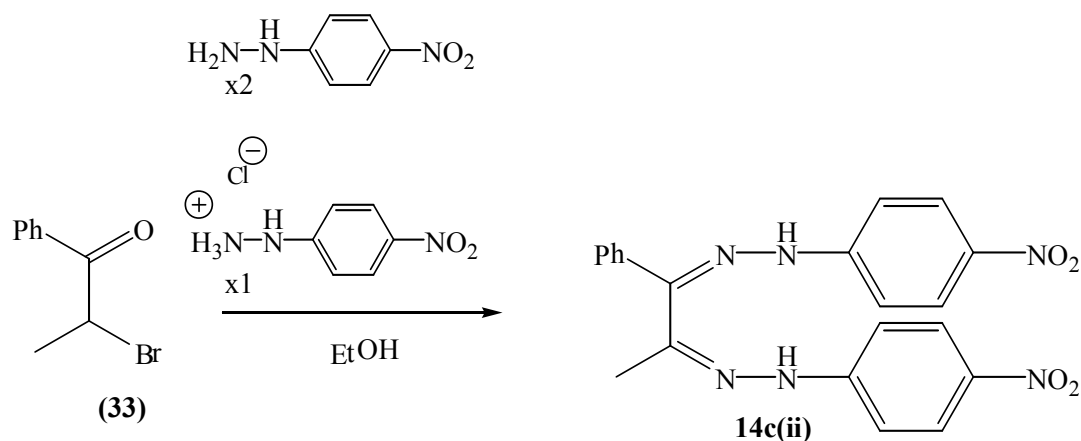
addition of two molar equivalents of phenylhydrazine. Interestingly, the α -(phenylhydrazino)-phenylhydrazone **35(b)** was not isolated in the second stage of the reaction. We repeated this procedure for the methyl-phenyl derivative **33(c)** in an attempt to transform the α -bromo ketone **33(c)** to 1,2-bis(phenylhydrazone)propane **14(c)**, although it was only possible to form the α -(phenylhydrazino)-phenylhydrazone **35(c)** from the α -bromo ketone **33(c)**. It was not possible to convert α -(phenylhydrazino)phenylhydrazone **35(c)** to the dihydrazone **14(c)**. Furthermore the azo-alkene **34(c)** was never isolated.

There may exist therefore, competing reactions between phenylhydrazine and the α -bromo ketone **33(b)/(c)**. In the case of the diphenyl species **33(b)**, the azo alkene may be the favoured product when reacted with phenylhydrazine, whereas when the methylphenyl α -bromo ketone reacts with phenylhydrazine **33(c)**, the α -(phenylhydrazino)phenylhydrazone **35(c)** is the favoured product. These are not sequential reactions therefore, as the α -(phenylhydrazino)phenylhydrazone **35(c)** does not proceed to form the dihydrazone **14(c)**, regardless of the quantity of phenylhydrazine added.



Scheme 2.9 Synthesis of a dihydrazone (**14**) via an azo alkene (**34**) from an alpha bromo ketone (**33**) according to Schantl *et al.*³⁰

There are reports in the literature of different α -substituted products that were transformed into dihydrazones such as α -acetoxy epoxides and α -halo ketones.^{28,70-71} Interestingly, the report by von Auwers (*see Scheme 2.10*) describes the transformation of α -bromopropiophenone **33(c)** to a 1-phenyl-1,2-bis-(4'-nitro-phenylhydrazone) propane **14c(ii)** by the addition of three molecular equivalents of *p*-nitrophenylhydrazine hydrochloride. Upon repeating this procedure, we found that by reacting two equivalents of 4'-nitro-phenylhydrazine and one equivalent of the salt with α -bromopropiophenone **33(c)** a maximum yield of 78% of the dihydrazone **14c(ii)** was obtained. Therefore, we have developed a good synthetic route to the dihydrazone **14c(ii)** in sufficient yield to proceed with the next reaction in the sequence to form the 1,2,3,5-tetrazocine **43(c)**, that is the formation of the azo compound **40c(ii)**.



Scheme 2.10 The formation of 1-phenyl-1,2-bis-(4'-nitro-phenylhydrazone)propane **14c(ii)**.³⁰

2.6 Synthesis of azo compounds

Recalling the synthetic route to 1,2,3,5-tetrazocines (**43**), see *Scheme 2.1*, the next step in the formation of this compound is the oxidation of the dihydrazone **14c(ii)** to the azo compound **40c(ii)** by treating the dihydrazone with two molecular equivalents of lead tetraacetate, $\text{Pb}(\text{OAc})_4$.

The absence of the N-H peaks in the ^1H NMR spectrum indicated that the azo compound **40c(ii)** had been formed and furthermore the solid material changed colour from a deep red to a dark purple, characteristic of the oxidation step. Despite extensive efforts to purify by recrystallisations/column chromatography, an unknown impurity is always observed in the ^1H NMR spectrum (see *Figure 2.2*)

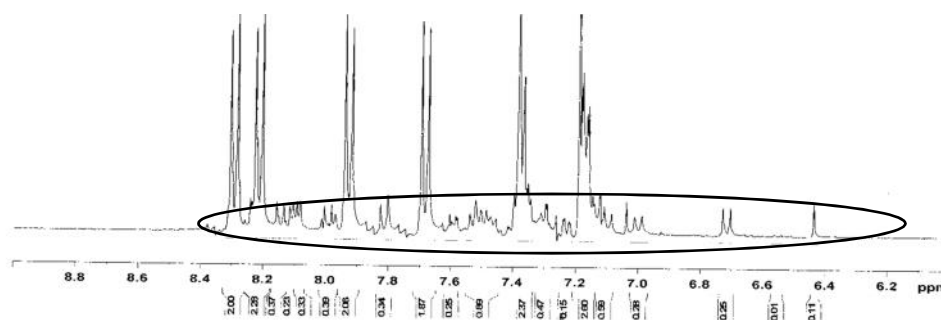


Figure 2.2 ^1H NMR spectrum of the azo compound **40c(ii)** containing some form of impurity, at approximately 5%.

To investigate if the azo compound **40c(ii)** establishes an equilibrium with another substance in solution, the azo compound was heated from 30 °C up to 100 °C in increments of ten degrees, and cooled back down again. The doublet at around 6.9 ppm and the broad singlet at 6.4 ppm are characteristic of the impurity, but not of the azo compound. It was found that the relative integrals of the major product and impurity did not change with temperature up to 100 °C, suggesting that there is no equilibrium between these two species. The fact that the azo compound cannot be obtainable readily pure made it difficult to proceed with the sequence of reactions to the 1,2,3,5-tetrazocine **43(c)** however.

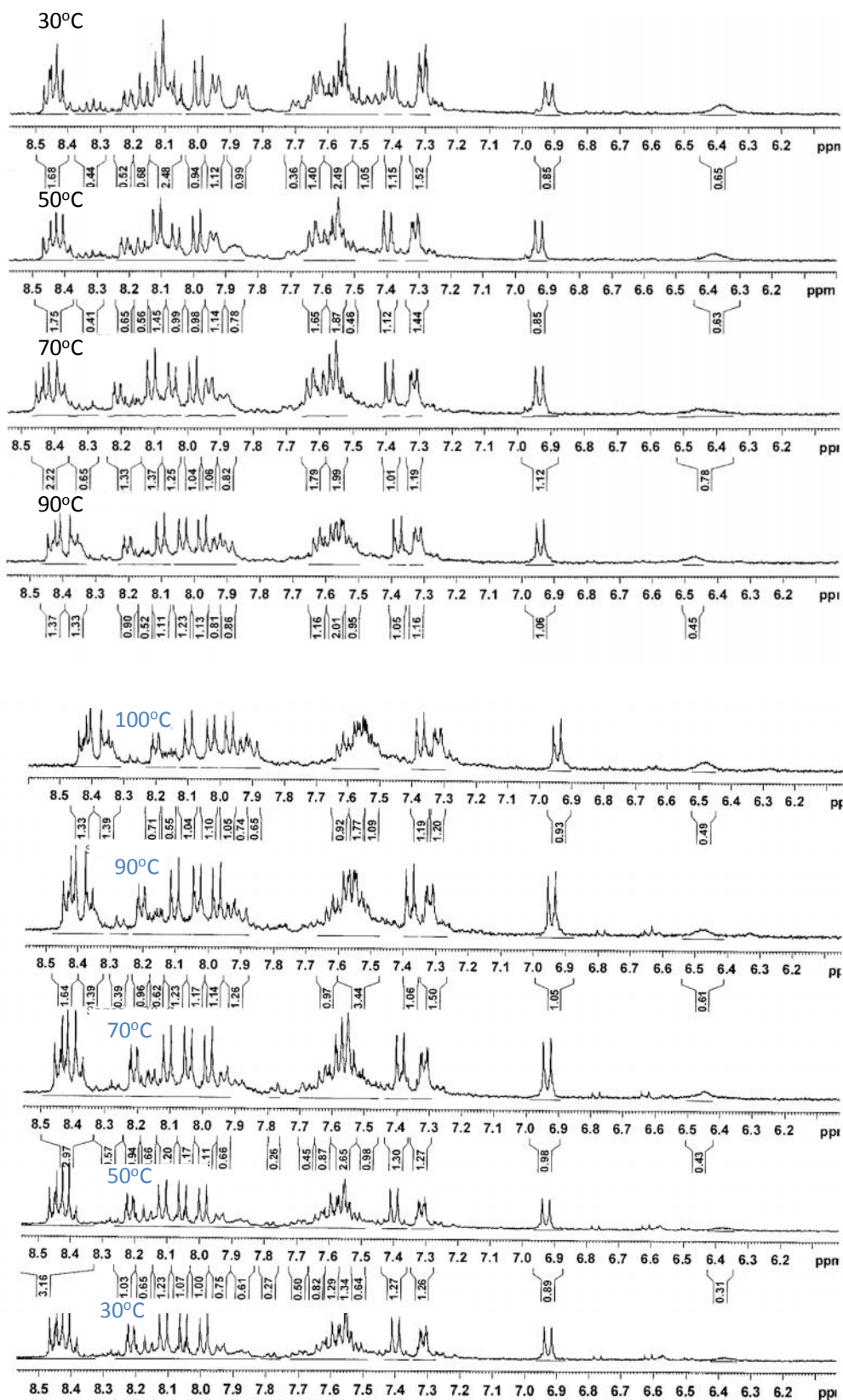


Figure 2.3 Variable temperature ^1H NMR spectra of the azo compound **40c(ii)**, showing the heating and cooling sequence in the order the spectra were recorded, reading from the top down.

2.7 Conclusion

The original route to the dihydrazones from the synthetic scheme was not a viable route to 1,2,3,5-tetrazocines (**43**) as the reaction consistently falters at the monohydrazone **13(c)** stage. As a result of this, synthetic efforts were redirected towards developing novel 1,2,3,5-tetrazocines that possess four phenyl rings **43(a)**, but with novel side chains, this work is presented in *Chapter 4*.

2.8 Experimental details

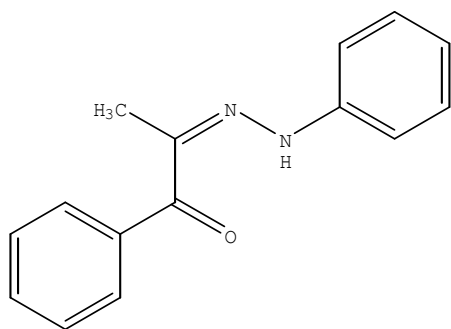
Infra-Red spectra were recorded on a Perkin-Elmer System 2000 FT-IR spectrometer. NMR spectra were recorded on a Bruker 400 MHz spectrometer unless otherwise stated.

Microanalytical and Crystallographic data were recorded by the Chemistry Department in University College Dublin, Belfield, Dublin 4.

Melting points were recorded on a Griffin Melting Point Apparatus.

2.8.1 Synthesis of monohydrazones

Synthesis of 1-phenyl-2-(phenylhydrazone)propan-1-one: 13(c)



Method 1: 1-phenyl-1,2-propanedione (1.3 mLs, 0.010 moles) and phenylhydrazine (1.9 mLs, 0.020 moles) were dissolved in 15 mLs of glacial acetic acid and stirred at room temperature for 0.5 hrs. The solution was subsequently filtered and washed with

petroleum ether 40-60, yielding 0.8 g of a yellow solid (0.0031 moles, **31% yield**). It was determined that this compound was the monohydrazone, 1-phenyl-2-(phenylhydrazone)propan-1-one.

Method 2: 1-phenyl-1,2-propanedione (2 mLs, 0.013 moles) and phenylhydrazine (2.5 mLs, 0.026 moles) were dissolved in 20 mLs of glacial acetic acid and allowed to reflux at 45 °C for 1 h. The solution was filtered and washed with pet ether 40-60 and 1.92 g of a pale yellow solid remained as the residue (0.0073 moles, **56% yield**).

Method 3: A solution of 1-phenyl-1,2-propane-dione (2 mLs, 0.013 moles) and phenylhydrazine (2.5 mLs, 0.026 moles) in 25 mLs of ethanol were stirred in the presence of triethylamine (3.6 mLs, 0.030 moles). This solution was allowed to stir overnight, yielding 2.18 g of the monohydrazone (0.0083 moles, **64% yield**).

Method 4: A solution of 1.93 mLs (0.013 moles) of 1-phenyl-1,2-propanedione in 26 mLs of toluene was cooled to -40 °C (slurry of acetone/liquid nitrogen). To this stirred solution 5.11 mLs (0.052 moles) of phenylhydrazine were added drop wise. The solution was allowed to stir for 3 h, after which time the mixture was filtered, yielding 1.56 g of the pale yellow solid, 1-phenyl-2-(phenylhydrazone)propan-1-one (0.006 moles, **46% yield**).

M.p. 138-140 °C

IR: ν_{\max} 3,280 cm^{-1} (N-H), 1630 cm^{-1} (C=O) and 1600 cm^{-1} (C=N)

^1H NMR (DMSO- d_6) (ppm): 2.15 (3H, CH₃, s), 6.88 (1H, Ar, t, J= 7.2 Hz), 7.15 (4H, Ar, m), 7.46 (3H, Ar, m), 7.78 (2H, Ar, d, J= 9.6 Hz), 10.20 (1H, s) (N-H)

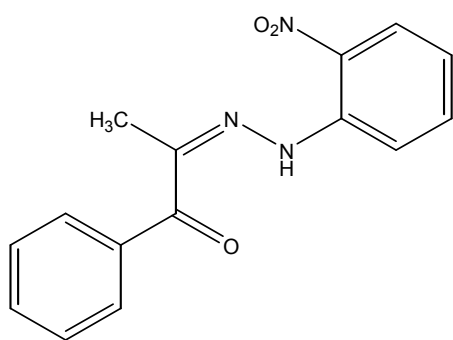
^{13}C NMR (DMSO- d_6) (ppm): 10.25, 114.00, 121.41, 127.56, 129.16, 129.92, 131.06, 138.36, 139.92, 144.04, 191.60 (C=O)

Microanalysis: Theory C 75.61%, H 5.92%, N 11.76%

Found C 75.39%, H 5.93%, N 11.40%

Crytallographic data for this compound can be found in *Appendix A.1*

Synthesis of 1-phenyl-2-(2'-nitro-phenylhydrazone) propan-1-one: 13(e)



0.4 mLs (0.003moles) of 1-phenyl-propane-1,2-dione was treated with a solution of 2'-nitro phenyl hydrazine (0.6 g = 0.004 moles) and glacial acetic acid (2 drops) in ethanol (15 mLs). The resulting solution was refluxed for 0.5 h. Upon cooling, the solution was consequently filtered and a brown solid was obtained (0.51 g; 0.0018

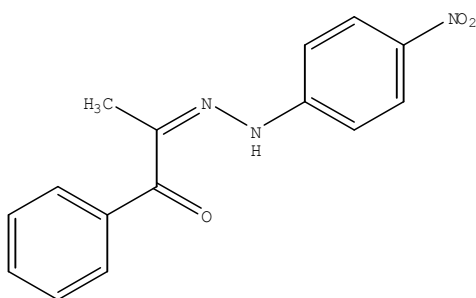
moles; **59.94%**).

M.p. 204-206 °C

¹H NMR (CDCl₃) (ppm): 2.07 (3H, CH₃, s), 7.46 (5H, Ar, m), 7.79 (2H, Ar, d, J=7.6 Hz), 8.09 (2H, Ar, d, J=7.2 Hz), 10.60 (1H, s) (N-H).

¹³C NMR (CDCl₃) (ppm): 26.44, 118.52, 128.87, 130.34, 134.64, 136.21, 137.03, 138.21, 148.54, 152.08, 192.84.

Synthesis of 1-phenyl-2-(4'-nitro-phenylhydrazone)propan-1-one: 13(f)



Method 1: To a solution of 1-phenylpropane-1,2-dione (0.67 mLs= 0.005 moles) in 25 mLs of glacial acetic acid, 1.56 g (0.011 moles) of 4-nitrophenylhydrazine were added, and the solution was heated gradually to

reflux temperature. When the solution reached boiling temperature it was allowed to reflux for a total of 4 h. The solution was allowed to cool to room temperature, after which time an orange/red precipitate formed and was filtered. The product was washed with a little cold ethanol and was dried, yielding 0.86 g of product (0.003 moles; **60.19% yield**).

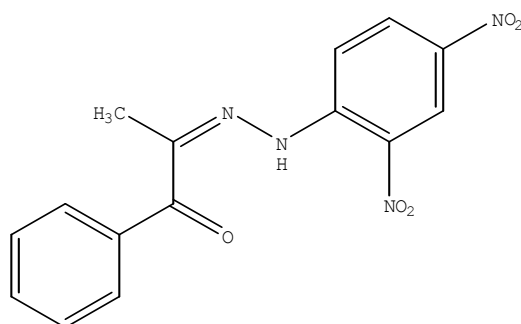
Method 2: A mixture of the hydrazone (**46**), 200 mg (7.5 mmol) in acetic acid (15 mLs) was treated with mercuric acetate (1mol equivalent: 0.24 g) dissolved in 10 mLs of acetic acid and stirred at ambient temperatures for 2.5 h. The mixture was consequently heated to between 64-68 °C and held in this temperature range for a total of 3.5 h. The solution was allowed to stand overnight, after which time a deep red precipitate had formed in **3.2% yield** (25.2 mg).

M.p. 207-209 °C

¹H NMR (DMSO-d₆) (ppm): 2.22 (3H, CH₃, s), 7.28 (2H, Ar, d, J=12 Hz), 7.52 (2H, Ar, t, J=8 Hz), 7.61 (1H, Ar, t, J=6.4 Hz), 7.85 (2H, Ar, d, J=7.2 Hz), 8.17 (2H, Ar, d, J=12 Hz), 10.76 (1H, s) (N-H).

¹³C NMR (DMSO-d₆) (ppm): 26.41, 128.52, 128.74, 128.87, 130.65, 133.87, 134.64, 172.58, 191.45 (C=O).

Synthesis of 1-phenyl-2-(2',4'-dinitro-phenylhydrazone)propan-1-one: 13(g)



A solution of 1-phenyl-1,2-propanedione (2 mLs, 0.013 moles) in 25 mLs of glacial acetic acid was set to reflux. To this solution 5.15 g (0.026 moles) of 2,4-dinitrophenylhydrazine were added, and the solution was allowed to reflux for 2 h, after which

time the solution was cooled and recrystallised in ethanol, yielding 3.8 g of a deep red solid. This proved to be the monohydrazone, 1-phenyl-2-(2,4-dinitrophenylhydrazone)propan-1-one. (0.012 moles, **92% yield**).

M.p. 235-239 °C

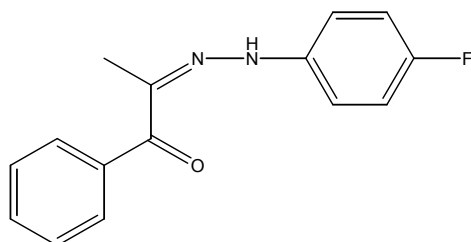
¹H NMR (DMSO-d₆) (ppm): 2.34, (3H, CH₃, s), 7.55 (5H, Ar, m), 7.91 (1H, Ar, d, J=9.6 Hz), 8.48 (1H, Ar, d, J=9.6 Hz), 8.90, (1H, Ar, s), 11.04 (1H, s) (N-H).

¹³C NMR (DMSO-d₆) (ppm): 11.19, 116.73, 122.70, 128.16, 130.24, 130.55, 131.86, 132.57, 136.33, 139.06, 143.56, 150.27, 191.33 (C=O).

Microanalysis:	Theory	C 54.88%, H 3.68%, N 17.07%
-----------------------	--------	-----------------------------

	Found	C 53.97%, H 3.67%, N 16.87%
--	-------	-----------------------------

Synthesis of 1-phenyl-2-(4'-fluoro-phenylhydrazone)propan-1-one: 13(h)



0.4 mLs (0.003 moles) of 1-phenyl-propane-1,2-dione were treated with a solution of 4-fluoro-phenylhydrazine hydrochloride (0.65 g; 0.004 moles) and glacial acetic acid (2 drops) in ethanol (15 mLs). The resulting

solution was refluxed for 0.5 h, after which time the solution was cooled to room temperature, yielding 0.53 g (0.002 moles; **68.44% yield**).

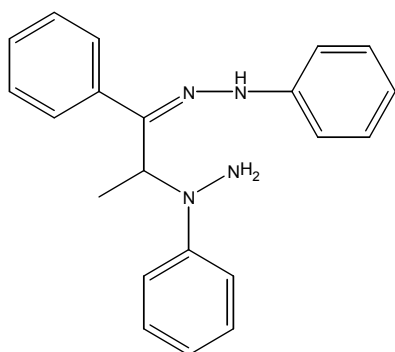
M.p. 190-192 °C

¹H NMR (DMSO-d₆) (ppm): 2.15 (3H, CH₃, s), 7.23 (5H, Ar, m), 7.48 (2H, Ar, d, J=9.6 Hz), 7.80 (2H, Ar, d, J=9.6 Hz), 10.22 (1H, s) (N-H).

¹³C NMR (DMSO-d₆) (ppm): 10.34 (CH₃), 115.47 (C=N), 127.56, 128.62, 129.40, 129.89, 131.01, 138.40, 139.97, 158.42, 191.46 (C=O).

2.8.2 Synthesis of alternative dihydrazone precursors (formazans and azo-alkenes)

Synthesis of 1-phenyl-2-(1-phenylhydrazino)-1-propanone-phenylhydrazone (35)



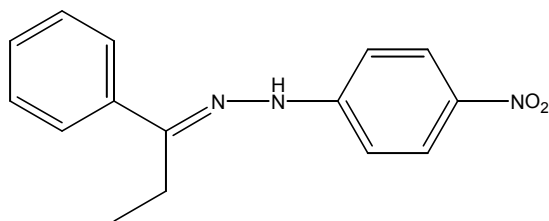
0.6 mLs of 2-bromo-propiophenone (4 mmoles) were dissolved in 20 mLs of methanol. To this solution, 1.6 mLs (16 mmoles) of phenylhydrazine were added and allowed to stir overnight. After filtering the resultant solution, 926 mg (2.8 mmoles) of the hydrazino-hydrazone were obtained (**70% yield**).

M.p. 114-116 °C

¹H NMR (DMSO-d₆) (ppm): 1.37 (3H, CH₃, d, J=6.4 Hz), 3.36 (2H, s) (NH₂), 5.06 (1H, (CH₃-C-H-), q, J=6.4Hz), 6.64 (1H, Ar, t, J=6.4Hz), 6.71 (1H, Ar, t, J=6.4Hz), 7.06 (4H, Ar, m), 7.15 (4H, Ar, m), 7.48 (5H, Ar, m), 8.55 (1H, s) (N-H).

¹³C NMR (DMSO-d₆) (ppm): 18.48, 56.05, 113.26, 119.07, 121.83, 126.05, 127.36, 127.68, 128.25, 128.48, 128.53, 128.70, 128.77, 128.91, 129.01, 134.10, 145.78, 151.57.

Synthesis of 1,2-bis(phenylhydrazone)stilbene (**36**)



Propiophenone (6.65 mLs, 0.05 moles) and 4'-nitrophenylhydrazine (0.046 moles, 5 g) were stirred in 100 mLs ethanol and 20 drops of acetic acid and refluxed for 1.5 h.

After this time, the reaction mixture was allowed to cool. The solvent was removed by rotary evaporation under reduced pressure (300mBar). The resulting solid was recrystallised in hot ethanol, yielding an orange-mustard coloured solid in 56% yield. (6.9 g, 0.0258 moles).

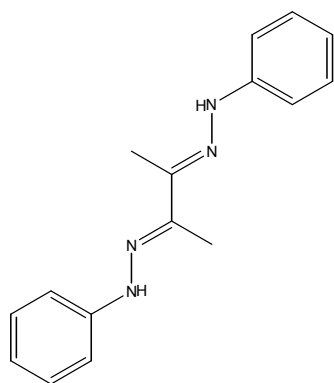
M.p. 150-152 °C

¹H NMR (DMSO-d₆) (ppm): 1.12 (3H, CH₃, t, J=7.6 Hz) (CH₃), 2.88 (2H, (CH₃-CH₂) q, J=7.6 Hz), 7.45 (5H, Ar, m), 7.85 (2H, Ar, d, J=7.2 Hz), 8.15 (2H, Ar, d, J=9.6 Hz), 10.35 (1H, s) (N-H)

¹³C NMR (DMSO-d₆) (ppm): 10.81 (CH₃), 18.92 (CH₂), 117.03 (C=N), 125.78, 125.88, 128.50, 128.54, 137.11, 138.47, 150.29, 150.39 (aromatic Cs).

2.8.3 Synthesis of dihydrazones

Synthesis of 1,2-bis(phenylhydrazone)butane **14(a)**



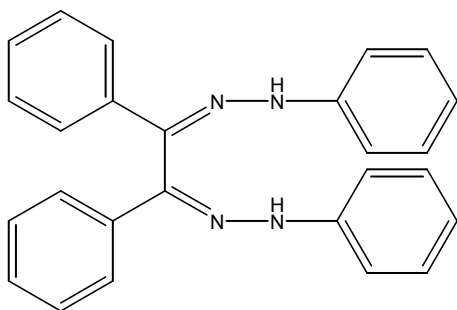
2,3-Butanedione (3.5 mLs, 0.04 mol) and phenylhydrazine (10 mLs, 0.10 mol) were stirred in glacial acetic acid (30 mLs) at room temperature for 45 min. The resulting mustard yellow crystals were removed by filtration and washed with petroleum ether 40-60, yielding 9.45 g (0.035 mol, 89%) of 1,2-bis-(phenylhydrazone)butane.

M.p. 242-244 °C (lit 245 °C)

¹H NMR (DMSO-d₆) (ppm): 2.20 (6H, 2xCH₃, s) (CH₃), 6.75 (2H, Ar, t, J=4Hz), 7.215 (8H, Ar, d, J=4Hz), 9.25 (2H, s) (N-H)

^{13}C NMR (DMSO- d_6) (ppm): 10.94 (CH_3), 113.03, 119.18, 129.23, 143.09, (all phenyl C and CH), 146.18 ($\text{C}=\text{N}$)

Synthesis of 1,2-bis(phenylhydrazone)stilbene 14(b)



Benzil (5 g, 0.024 moles) and phenylhydrazine (5 mLs, 0.05 moles) were stirred under reflux in glacial acetic acid (50 mLs) for 1 h. The solution was cooled in ice, and a yellow solid formed. This was removed by filtration and washed with petroleum ether 40-60, yielding 1,2-bis(phenylhydrazone) stilbene, 6.04 g (0.0209 moles, **87.3% yield**).

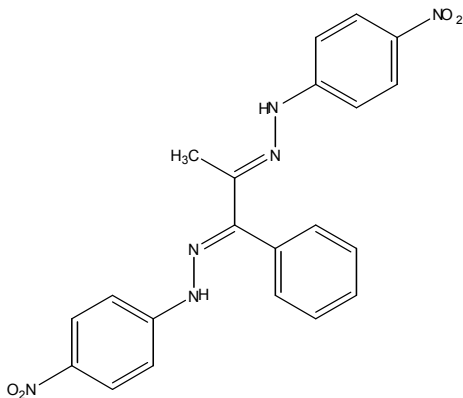
M.p. 218-221 °C (lit. 234 °C)²⁰

IR: ν_{max} 3,323 cm^{-1} (N-H), 3051 cm^{-1} (N-H), 1599 cm^{-1} ($\text{C}=\text{N}$), 1543 cm^{-1} ($\text{C}=\text{N}$).

^1H NMR (DMSO- d_6) (ppm): 6.79 (2H, H=8 Hz), 7.20 (4H, t, J=8 Hz), 7.27 (2H, t, J=8 Hz), 7.32-7.37 (8H, m), 7.60 (4H, d, J=8 Hz) (all phenyl CH), 9.62 (2H, s) (N-H)

^{13}C NMR (DMSO- d_6) (ppm): 113.77, 120.02, 125.7, 128.16, 128.99, 129.14, 135.87, 135.94 (all phenyl C and CH), 145.52 ($\text{C}=\text{N}$)

Synthesis of 1,2-bis(4'-nitro-phenylhydrazone)propane 14c(ii)



Method 1: A mixture of hydrazone (**36**) 200 mg in acetic acid (15 mLs) was treated with mercuric acetate 0.24 g (1 mol equivalent) dissolved in 10 mLs of acetic acid and stirred at ambient temperatures for 2.5 h followed by heating between 64-68 °C for a further 3.5 h. The solution was allowed to stand overnight and a red precipitate formed in **3.2% yield** (25.2 mg, 95.5 μmoles).

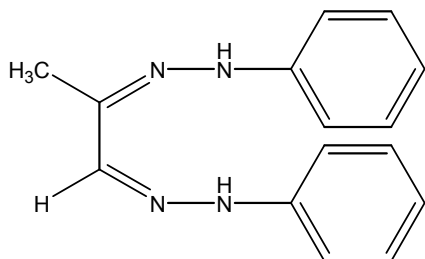
Method 2: To a solution of 4-nitrophenylhydrazine hydrochloride (1.5 g, 8 mmoles) in 50 mLs of ethanol and 4-5 drops of acetic acid, 0.58 g of 2-bromopropiophenone (0.0027 moles) were added dropwise. The reaction mixture was set to reflux for 3.5 h. The solution was allowed to cool overnight and on standing a reddish/brown solid precipitated. This was removed by filtration and washed with hexane, yielding 0.87 g (2.1 mmoles, **78% yield**) of 1,2-bis(4'-nitro-phenylhydrazone)propane.

M.p. 248-251 °C

¹H (DMSO-d₆) (ppm): 2.41 (3H, s), 6.90 (2H, d, J=8.4 Hz), 7.30 (2H, d, J=7.6 Hz), 7.39 (2H, d, J=9.6 Hz), 7.56 (3H, m), 7.99 (2H, d, J=9.2 Hz), 8.11 (2H, d, J=9.2 Hz), 9.97 (1H, s)(N-H), 10.40 (1H, s)(N-H).

¹³C (DMSO-d₆) (ppm): 30.66, 111.94, 112.64, 125.64, 128.38, 128.78, 128.34, 131.93, 132.64, 138.16, 138.80, 139.03, 147.08, 148.71, 150.50, 150.69.

Synthesis of 1,2-bis(phenylhydrazone)propane; (methyl glyoxal phenyl osazone)



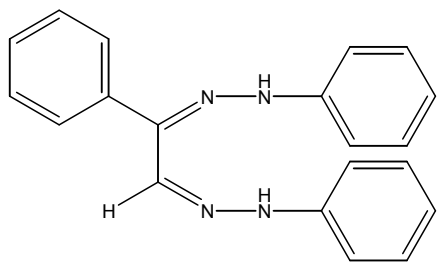
8.15 mLs of a 40% methyl glyoxal solution (3.6 g, 0.05 moles) were stirred in 50 mLs of ethanol. To this, 10 mLs of phenylhydrazine were added (0.01 moles) and the solution was allowed to reflux for 1 h. After this time the reaction is allowed to cool in an ice bath.

Upon filtration, a mustard yellow solid was obtained and washed several times with hot ethanol to remove impurities, yielding 12.6 g of product. (0.49 moles, **98% yield**).

M.p. 124-126 °C

Microanalysis:	Theory	C 71.41%, H 6.39%, N 22.20%
	Found	C 71.43%, H 6.25%, N 22.53%

Synthesis of 1-phenyl-1,2-bis(phenylhydrazone)ethane; phenyl glyoxal phenyl osazone



3.67 g of phenyl glyoxal monohydrate (0.024 moles) were dissolved in 50 mLs of glacial acetic acid and to this 5 mLs of phenylhydrazine were added (0.05 moles). The solution was allowed to reflux for 1.5 h, after which time the solution was allowed to cool to 0 °C in an ice bath. The solution was

then filtered and the residue obtained was a sandy brown solid. (5.8 g, 0.018 moles, 77% yield).

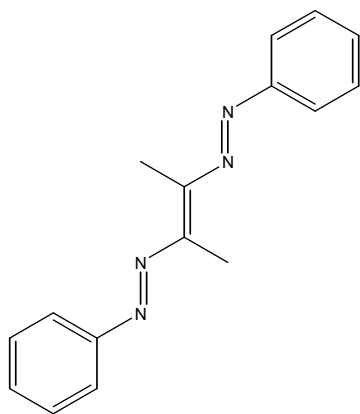
M.p. 139-141 °C

¹H (DMSO-d₆) (ppm): 2.5 (1H, s), 6.91 (2H, Ar, dd, J=7.2 Hz), 7.07 (2H, Ar, d, H=7.2 Hz), 7.27 (2H, Ar, d, J=7.2 Hz), 7.40 (5H, Ar, m), 7.42 (2H, Ar, t, J=7.2 Hz), 7.72 (2H, Ar, d, J=7.2 Hz), 10.82 (N-H), 12.68 (N-H).

¹³C (DMSO-d₆) (ppm): 112.06 (C=N), 113.19 (C=N), 120.11, 120.80, 125.57, 127.43, 128.51, 129.51, 129.61, 132.96, 133.06, 138.13, 143.71, 144.18.

2.8.4 Synthesis of azo compounds

Synthesis of 2,3-bis(phenylazo)butene 40(a)



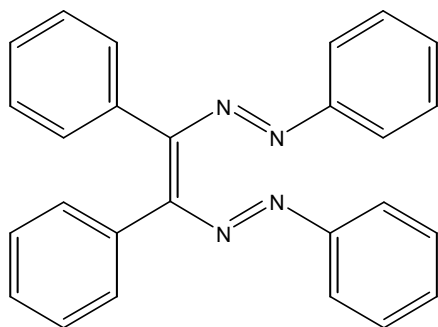
1,2-Bis(phenylhydrazone)butane (2.0 g, 0.0075 mol) was stirred in 25 mLs of glacial acetic acid. Lead tetraacetate (6.0 g, 0.013 mol) was added and the mixture stirred for 0.5 h., after which time 1.59 g (0.006 mol, 80%) of the brown 1,2-bis(phenylazo)butene was removed by filtration and washed with petroleum ether 40-60.

M.p. 158-159 °C (lit. 159 °C)⁷²

¹H NMR (DMSO-d₆) (ppm): 1.25 (6H, s) (CH₃), 7.27 (4H, d, J=4 Hz), 7.64-7.70 (2H, m), 7.99 (4H, d) (all phenyl CH).

¹³C NMR (DMSO-d₆) (ppm): 11.34 (CH₃), 123.62, 129.53, 131.58, 153.95, 157.48.

Synthesis of 1,2-bis(phenylazo)stilbene 40(b)



1,2-Bis(phenylhydrazone)stilbene (2.0 g, 0.005 mol) was stirred in 25 mLs glacial acetic acid. Lead tetraacetate (4.5 g, 0.01 mol) was added and the mixture stirred for 0.5 h, after which time the brown 1.68 g (0.004 mol, 90%) 1,2-bis-(phenylazo)stilbene was removed by filtration and washed with petroleum ether 40-60.

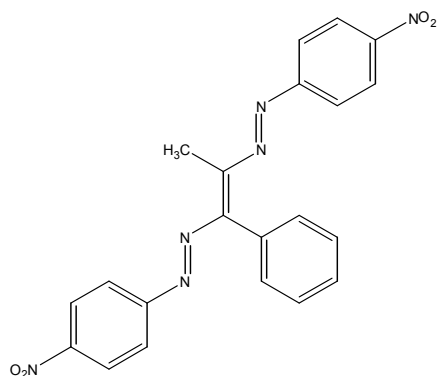
M.p. 165-167 °C (lit. 179 °C)⁷³

IR: ν_{\max} 1480 cm⁻¹ (C=C), 770 cm⁻¹ (C-H bend, mono), 763 cm⁻¹ (C-H bend).

¹H NMR (DMSO-d₆) (ppm): 6.95 (2H, t, J=7.2 Hz), 7.12 (4H, dd, J=7.2 Hz), 7.23 (2H, t, J=7.2 Hz), 7.41 (4H, dd, J=7.2 Hz), 7.48 (2H, d, J=7.2 Hz) 7.58 (2H, d, J=7.2 Hz) (all aromatic CH).

¹³C NMR (DMSO-d₆) (ppm): 119.10 (C=C), 123.88, 127.50, 128.84, 129.26, 129.32, 130.37, 131.80, 132.75.

Synthesis of 1-phenyl-1,2-bis(phenylazo)propene 40(c)



0.8 g of 1-phenyl-1,2-(4'-nitro-phenylhydrazine)propane (0.002 moles) were dissolved in 50 mLs of glacial acetic acid. To this stirred solution 1.8 g (0.004 moles) of lead tetraacetate were added and allowed to stir for 0.5 h yielding 0.74 g (0.0017 moles; **88.7% yield**).

M.p. 165-167 °C

¹H NMR (DMSO-d₆) (ppm): 2.67 (3H, CH₃, s), 6.91 (1H, t, J=4.8Hz), 7.12 (2H, dd, J=4.8 Hz), 7.35 (2H, d, J=4.8 Hz), 7.64 (2H, d, J=4.8 Hz), 7.68 (2H, d, J=4.8 Hz), 8.11 (2H, d, J=4.8 Hz), 8.31 (2H, d, J=4.8 Hz).

¹³C NMR (CDCl₃) (ppm): 20.91, 112.38, 112.69, 123.70, 125.41, 126.05, 126.19, 126.36, 128.23, 128.28, 128.41, 128.65, 128.71, 129.05, 149.09.

Chapter 3

Synthesis of Dihydrazones:

A Theoretical Investigation into the

Reactivity of

Keto-monohydrazones

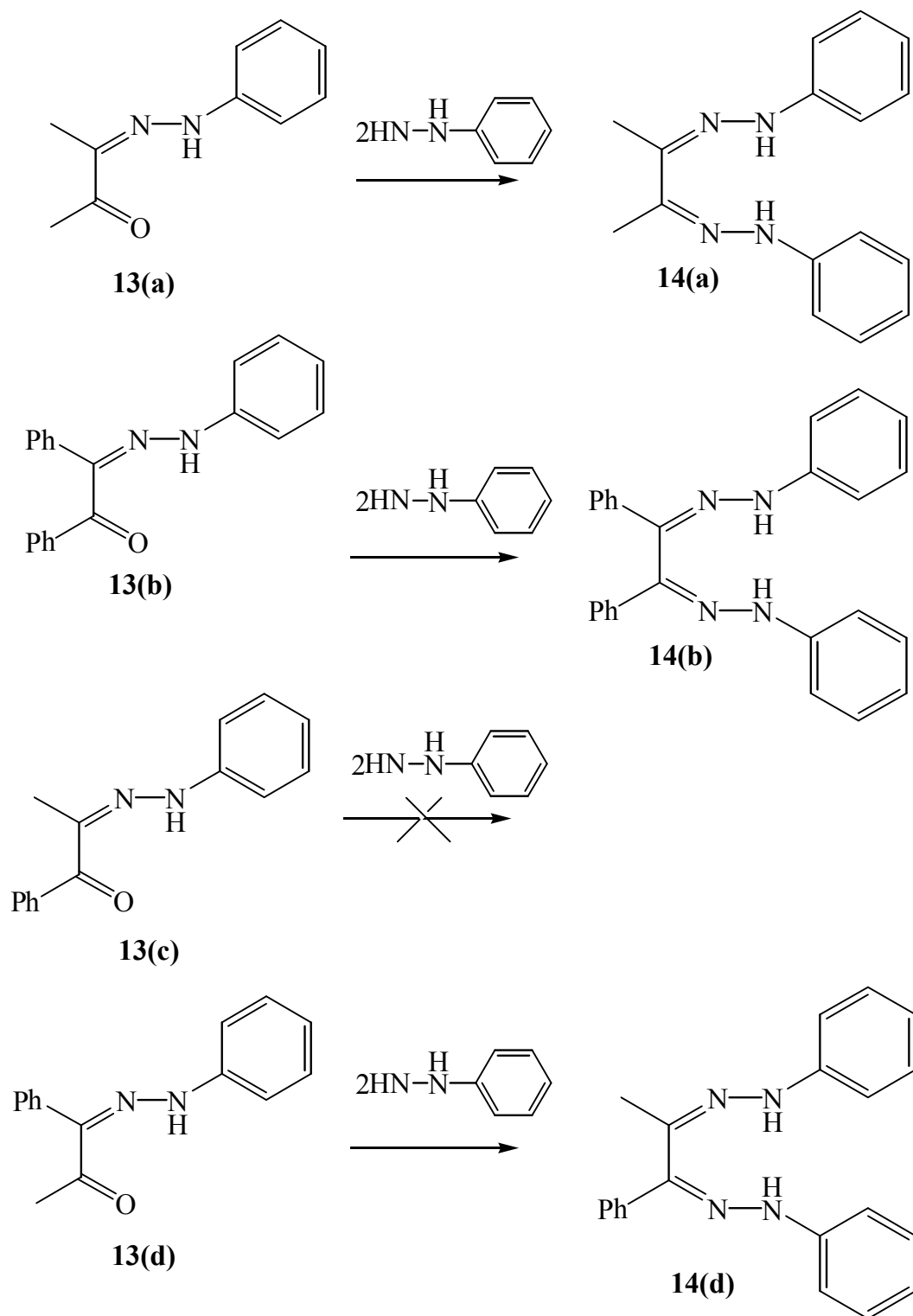
3.1 Introduction

3.1.1 Osazones and dihydrazones

One of the major synthetic obstacles described in *Chapter 2* was the synthesis of the asymmetric dihydrazone, 1-phenyl-1,2-bis(phenylhydrazone)propane **14(c)** via the two step mechanism illustrated in both *Scheme 1.5* and *Scheme 1.6*. The established mechanism for dihydrazone formation is that the diketone **12(c)** is subject to nucleophilic attack from phenylhydrazine at the carbonyl group, to form the keto-monohydrazone **13(c)**, see *Scheme 1.5*. The second step in this mechanism is then anticipated to be the conversion of the keto-monohydrazone **13(c)** to the dihydrazone **14(c)**, *Scheme 1.6*. However no reaction was observed for the methyl-phenyl derivative as **13(c)** is inert towards further nucleophilic attack, irrespective of the reaction conditions used; altering the solvent, the molar ratios, addition of catalysts, or temperatures.

While the methyl-phenyl monohydrazone **13(c)** does not react, the dimethyl and diphenyl monohydrazones **13(a)/(b)** can be converted into their respective dihydrazones **14(a)/(b)** by reacting with phenylhydrazine (see *Scheme 3.1*). The alternative methyl-phenyl monohydrazone **13(d)**, an isomer of **13(c)**, is expected to convert to its dihydrazone. This is known as Butler *et al* have synthesised a 4'-nitro-dihydrazone derivative **14c(ii)** from a 4'-nitro-monohydrazone **13c(ii)**.⁶⁹ The non-reactivity of the carbonyl group in **13(c)** cannot be rationalised on steric grounds since the most sterically crowded monohydrazone **13(b)**, can react to form its dihydrazone **14(b)**. (see *Scheme 3.1*).

The purpose of the computational study presented here is to rationalise the observed reactivity of monohydrazones by investigating their electronic structure through quantum mechanical calculations. Specifically we will attempt to correlate calculated properties and parameters *e.g.* point charges and multipole analyses. If the physical parameters vary dramatically between the reactive and non-reactive monohydrazones then it may be possible to predict reactivity on the basis of calculations, which is desirable for cost and environmental reasons.



Scheme 3.1 Summary of the reactivity of the keto-monohydrazones (**13**).

3.1.2 Methods for visualising charge distribution in a molecule

In *Chapter 1*, quantum mechanical methods for calculating electronic structure were discussed. Several methods to produce approximate solutions to the Schrödinger equation were described. What is interesting however, is the *solution* to the Schrödinger equation, as it provides a starting point for calculating different properties (point charges/multipole analyses) of molecules.

3.1.2.1 Point charges

Many computational chemistry software packages can calculate the partial atomic charges from calculations, these indicate how the electronic charge is distributed within a molecule. The point charge methods available within the Gaussian software package include⁷⁴:

1) Mulliken charges

The Mulliken population analysis was the first system devised to gain insight into the LCAO (Linear Combination of Atomic Orbitals) MO (Molecular orbitals) wavefunctions.⁷⁵ The probability of finding an electron at a certain position r , from a single molecular orbital containing one electron is the square of the molecular orbital (MO).

$$\rho_i(r) = \phi_i^2 \quad (3.1)$$

If that molecular orbital is to be expanded for a set of normalised basis functions, then this can also be written as

$$\begin{aligned} \phi_i &= \sum_{\alpha}^{AU} c_{\alpha i} \chi_{\alpha} \\ \phi_i^2 &= \sum_{\alpha\beta}^{AU} c_{\alpha i} c_{\beta i} \chi_{\alpha} \chi_{\beta} \end{aligned} \quad (3.2)$$

By integrating and summing over all occupied molecular orbitals one can determine the total number of electrons, N , where $S_{\alpha\beta}$ is the overlap integral.

$$\sum_i^{MO} \int \phi_i^2 d\tau = \sum_i^{MO} \sum_{\alpha\beta}^{AO} c_{\alpha i} c_{\beta i} \int \chi_{\alpha} \chi_{\beta} d\tau = \sum_i^{MO} \sum_{\alpha\beta}^{AO} c_{\alpha i} c_{\beta i} S_{\alpha\beta} = N \quad (3.3)$$

This expression can be generalised by introducing the number of electrons, n , for each molecular orbital. This figure will be 0, 1 or 2, for a single determinant wave function.

$$\sum_i^{MO} n_i \int \phi_i^2 d\tau = \sum_{\alpha\beta}^{AO} \left(\sum_i^{MO} n_i c_{\alpha i} c_{\beta i} \right) S_{\alpha\beta} = \sum_{\alpha\beta}^{AO} D_{\alpha\beta} S_{\alpha\beta} = N \quad (3.4)$$

Thus, the number of electrons is the sum of the product of the density and overlap matrix elements. The Mulliken population analysis uses the density matrix for distributing the electrons into atomic contributions. The Mulliken electron population is hence defined as

$$\rho_A = \sum_{\alpha \in A}^{AO} \sum_{\beta}^{AO} D_{\alpha\beta} S_{\alpha\beta} \quad (3.5)$$

Consequently, the gross charge on atom A is the sum of the nuclear and electronic contributions.

$$Q_A = Z_A - \rho_A \quad (3.6)$$

In summary, the Mulliken population analysis provides a count of the number of electrons that are assigned to each atom and thus can provide information about the nature of the bonding within a molecule.

The Mulliken population analysis, however, sometimes fails to give a useful and reliable characterisation of the charge distribution. The three main drawbacks are:

- a. Mulliken populations can in some cases have negative values. For example, in a study performed by Weinhold *et al* on the molecule SF₆, one of the sulphur s orbitals had a Mulliken population of -0.7e,

despite the fact that fluorine is the most electronegative of all the elements.⁷⁶

- b. Mulliken populations are not stable with respect to changes in the basis set. A study performed on ferrocene using basis sets of better than triple zeta quality demonstrated that the charge on the iron atom varied between +0.59 and +1.38, depending on the basis set employed.⁷⁷
- c. Mulliken populations can sometimes provide an unphysical picture of the charge distribution in compounds which have a significant ionic character. Studies on lithium compounds have shown that in some instances lithium possesses a charge opposite in sign to that expected from electronegativity values.⁷⁸

2) Natural Population Analysis

The NPA method is based on the construction of a set of ‘natural atomic orbitals’ (NAO) for a particular molecule in an arbitrary atomic orbital basis set. The natural population analysis represents the occupancies of these NAOs in the molecule of interest. NAOs form an orthonormal set, completely spanning the space of basis orbitals and, hence, the natural populations are inherently positive, and sum to the total number of electrons in the molecule. In addition, the NAOs are intrinsic to the wave function, as opposed to a particular choice of basis set.

The natural population analysis is a type of population analysis that uses Löwdin partitioning.⁷⁹ The DS matrix product is consequently written as:

$$\begin{aligned}
 \sum D\vec{s} &= \vec{v} \\
 \sum S^{1/2}P(S^{1/2}S^{1/2}) &= S^{1/2}N \\
 \sum S^{1/2}DS^{1/2}(S^{1/2}S^{-1/2}) &= S^{1/2}NS^{-1/2} \\
 \sum S^{1/2}DS^{1/2} &= N
 \end{aligned}
 \tag{3.7}$$

The Löwdin method uses the $S^{1/2}DS^{1/2}$ matrix for analysis and corresponds to the population analysis of the density matrix in the orthogonalised basis set, constructed by transforming the original set of functions by $S^{-1/2}$. Thus

$$\chi' = S^{-1/2}\chi \quad (3.8)$$

The Mulliken and NPA methods differ in the predicted atomic charge, but there is nothing in the mathematical treatment to indicate which of these partitioning methods gives the ‘correct’ result. There are some issues with Mulliken population analyses based on partitioning the wave function in terms of basis functions such as:

- a. If the value of the diagonal elements exceeds a value of 2, it would exceed the Pauli principle.
- b. The off-diagonal elements may become negative, which would imply a negative number of electrons, which is non-physical.
- c. The off-diagonal contributions are divided equally between two orbitals. A more electronegative element should intuitively receive the major share of electrons in a bond.

A natural population analysis is an alternative to a conventional Mulliken population analysis in that it provides a better description of the electronic distribution in compounds of high ionic character, such as those containing metal atoms.⁸⁰ The natural populations are found to give a satisfactory description for molecules that are at the covalent and ionic limits at a modest computational cost.

3) Merz Kollman Singh method

The MKS method is an electrostatic potential method devised by Merz, Kollman and Singh⁸¹. Out of the different non-bonded interactions that can take place between molecules (van der Waals forces/dipole-dipole forces, *etc.*), a significant portion of these interactions involve electrostatic interactions between fragments having an internal asymmetry in the electron

distribution. The intrinsic interaction here is between the electrostatic potential (ESP) of one molecule and the charged particles of another. The ESP is described mathematically as:

$$V_{ESP}(r) = \sum_A^{nu^{C_{ei}}} \frac{Z_A}{|r - R_A|} - \int \frac{|\Psi(r_i)|^2}{|r - r_i|} dr_i \quad (3.9)$$

The first term in this expression is deduced from the nuclear charges, whereas the second term (the electronic contribution) is based primarily on the wavefunction, $\Psi(r_i)^2$. In order to interpret the potential, a force field method is used to calculate the van der Waals surface of the molecule. In practise the potential is then sampled by producing a grid of points around each nucleus at 1.4, 1.6, 1.8 and 2.0 times the van der Waals surface.

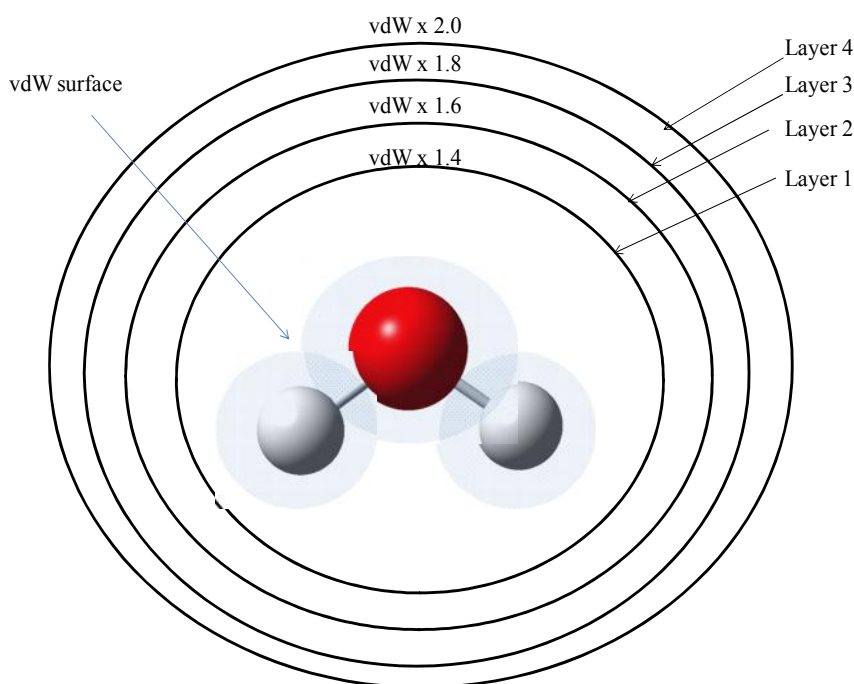


Figure 3.1 Gridpoints surrounding a water molecule to reproduce the molecular electrostatic potential (MEP). The default MKS scheme adds layers that have scaling factors of 1.4, 1.6, 1.8 and 2.0 respectively.

The atomic charges are subsequently determined as those parameters which reproduce the ESP as closely as possible at these points. The only constraint in the fitting is that the sum of the point charges are equal to the sum of the total molecular charge (in most cases this will equal zero).

4) CHelpG method

The CHelpG method (Charges from Electrostatic potentials using a Grid based method) is an atomic charge calculation system that was devised by Breneman and Wiberg⁸². In this scheme, atomic charges are fitted to reproduce the molecular electrostatic potential (MESP) at a number of points around the molecule, similar to that of the MKS method.

The potential is evaluated on a grid of points surrounding the molecule, and a least-squares fitting procedure is used to obtain a set of atomic charges that can reproduce the potential at the grid points as closely as possible. The charges are constrained so that the total charge on the molecule is correct. It is important to choose grid points that lie outside the molecular charge distribution, otherwise the potential contains penetration effects which cannot be represented by any multipolar description. Usually, the grid points are chosen so that they lie at least an angstrom outside the van der Waals surface of the molecule.

ESP schemes for deriving atomic charges differ in the number and location of points used in the fitting, and whether additional constraints are implemented, besides that of preserving the charge of the molecule.

3.1.2.2. Distributed Multipole analysis

The shortfall of these ESP methods is that in medium or large systems it is difficult to accurately represent the atomic charge of the innermost atoms, since they are 'buried' and the ESP experienced outside the molecule is largely determined by the atoms near the surface.

Another problem with all ESP methods is related to the absolute accuracy, which makes comparison of calculated properties of atoms between molecules difficult. Although the inclusion of charges on all atoms does not significantly improve the results over those determined from a reduced set of parameters, the absolute deviation between the true and fitted electrostatic potentials can be quite large. Interaction energies, as calculated by an atom centred charge model in a force field, may possess errors of several kJ/mol per atom, which is one or two times the energy of the van der Waals interaction.

In order to improve the description of the electrostatic interaction, additional sites may be added that are not necessarily centred on nuclei. Furthermore, dipole, quadrupole, octapole and even hexadecapole moments may be added at these sites. This now brings us to the next alternative mode of describing charge distribution in a molecule, that of a distributed multipole analysis.

In recent times, computational chemistry has progressed towards the use of distributed multipole analysis (DMA) when looking at the electron density of a molecule in preference to point charges.⁸³ The charge distribution derived from *ab initio* wavefunctions is described in terms of charges, dipoles, quadrupoles and so on located at a number of sites on the molecule. The basis for a distributed multipole analysis (DMA) is a one-electron density matrix over a basis of gaussian-type orbitals (GTOs), together with a specification of the basis set and the nuclear charge and positions. Any type of *ab initio* wavefunction can be analysed, since the method works directly from the density matrix. This density matrix is given by

$$\rho(r) = \sum_{tu} \rho_{tu} \phi_t^A(\mathbf{r}) \phi_u^B(\mathbf{r}) \quad (3.10)$$

where ϕ_t^A is a gaussian primitive function centred at A. The distributed multipole analysis developed by Stone is based on the fact that the ESP arising from the charge overlap between two basis functions can be written in terms of a multipole expansion around a point between the two nuclei.⁸⁴

$$\phi_t^A = f_t(\mathbf{r} - \mathbf{A}) \exp[-\alpha(\mathbf{r} - \mathbf{A})^2] \quad (3.11)$$

The product of two such functions ϕ_t^A and ϕ_u^B with exponents α and β is itself a gaussian function, where the overlap centre, P is given by

$$P = \frac{\alpha A + \beta B}{\alpha + \beta} \quad (3.12)$$

Initially the multipoles were calculated using force field or semi-empirical methods.⁸⁴ The problem with force field or semi-empirical methods however, is that they do not separate the individual interactions (dispersion, repulsion, electrostatic, induction) properly. The advancement of DMAs has progressed in parallel with computational chemistry since current *ab initio* methods can calculate numerical

values for each of these individual interactions and can be described using analytical formulae in an appropriate way.⁸⁵

The DMA approach is very precise, in the sense that it accurately reproduces the overall multipole moments of the charge distribution as they are built from the distributed moments of the molecule. When DMAs were first developed, they were not very stable with respect to changes of the basis set, however, recently a procedure has been devised to overcome this problem.⁸⁶

3.1.3 (*E*)/(*Z*) isomers

In this chapter, reference will be made to different (*E*) and (*Z*) isomers of nitrogen containing compounds. In **Figure 3.2**, a pair of (*E*) and (*Z*) isomers are illustrated.

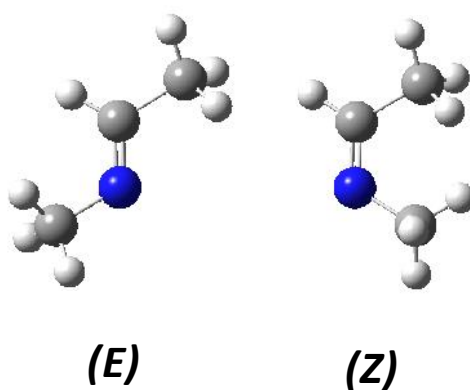


Figure 3.2 (*E*) and (*Z*) isomers of a dimethyl imine

The acid-catalysed (*E*)/(*Z*) isomerisation of compounds containing a carbon-nitrogen double bond has received a lot of attention as this is a very common structural motif in a broad range of reactions and there is controversy as to the exact mechanism.⁸⁷⁻⁹⁹ Early accounts suggest that the only structural factors affecting the isomerisation are steric effects.¹⁰⁰ However, subsequent studies have shown that both steric and polar effects can have an effect on the first-order rate constants.⁸⁹ Two mechanisms for uni-molecular inter-conversion have been proposed; rotation about the C=N bond, and planar inversion about nitrogen, *see Figure 3.3*.

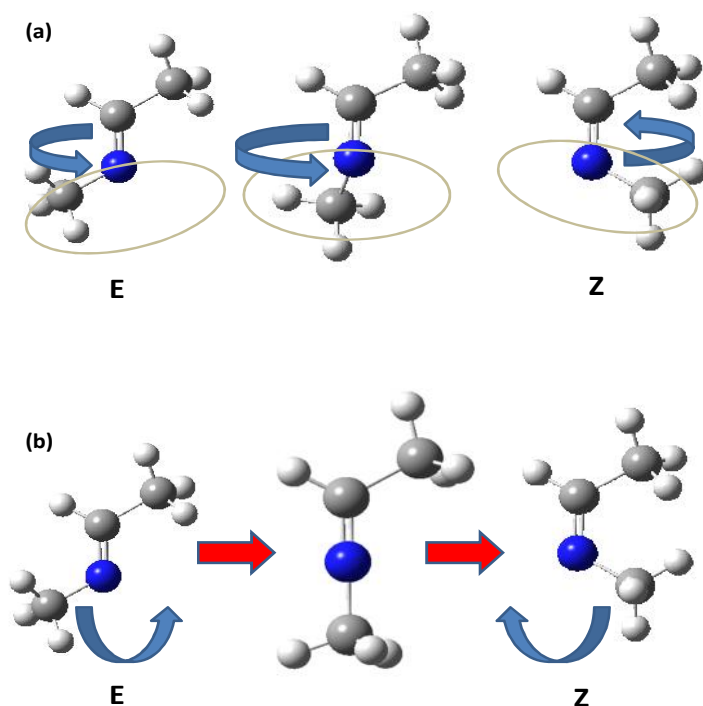


Figure 3.3 (*E*) to (*Z*) isomerisation in a dimethyl imine. Route (a) involves the rotation about a dihedral angle to interconvert between the (*E*) and (*Z*) isomers. Route (b) involves a linear transition state, whereby the C=N-CH₃ bond angle is 180°.

In the case of simple alkyl or aryl substituted imines, experimental evidence and MO calculations suggest that the nitrogen inversion or route ‘b’ as illustrated in **Figure 3.3**, usually provides the lower energy path for isomerisation.⁹⁰ Route ‘a’ is likely to be a higher energy process since the thermal isomerisation barrier will be related to the π -bond energy.¹⁰¹

A low energy acid-catalysed (*E*)/(*Z*) interconversion pathway for imines was recently reported.¹⁰² In this mechanism, a proton attaches to the nitrogen of the double bond which adopts an sp³-like configuration, consequently the internal re-orientation can take place with a very low barrier. In this scheme, once the isomerisation is complete, the proton is detached, reforming a neutral (*E*) or (*Z*) isomer. This process is illustrated in **Figure 3.4**.

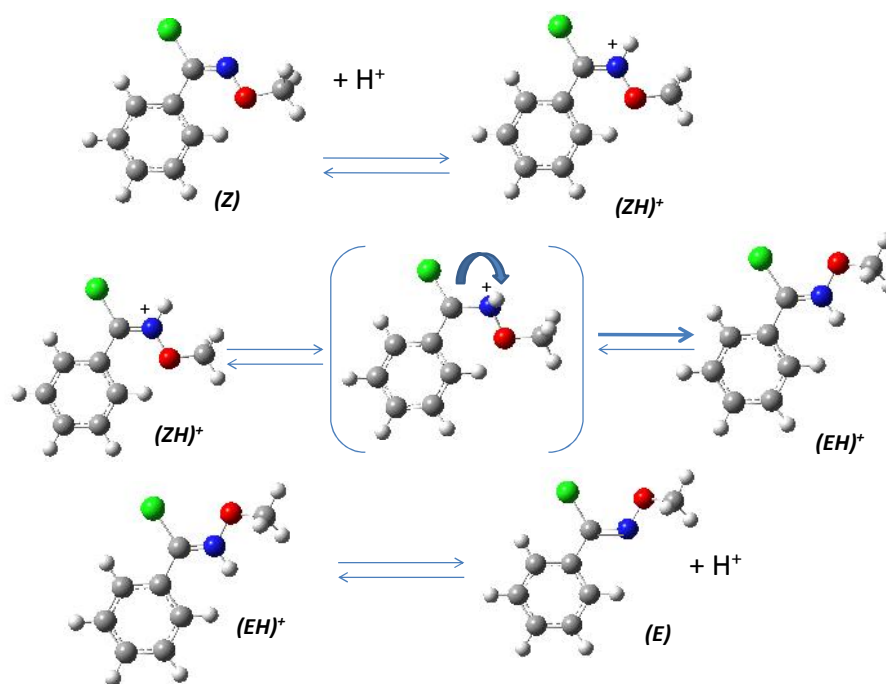


Figure 3.4 Protonation-rotation mechanism to *(E)/(Z)* isomerisation in an imine species as reported by Johnson et al¹⁰²

The actual pathway of *(E)/(Z)* isomerisation will correspond to that of lowest energy. Therefore the energetics of all plausible routes must be explored in order to determine the most likely pathway in any individual reaction sequence.

3.2 Computational methods

Optimisations, frequency analyses and point charges of all species presented in this chapter were performed using Gaussian 09⁷⁴ at the B3LYP/6-31G (d) level of theory. Minima were identified by vibrational analyses and the zero point vibrational energies were calculated for all species. The conformational space of all linear molecules was explored by performing relaxed scans over the full conformational space. The final optimised structures of all the species obtained were characterised as either absolute minima or transition states using Hessian calculations for vibrational frequency analysis. All frequencies obtained for minima were real where as the transition states possessed one imaginary frequency in the infrared spectrum. Distributed multipole analyses were performed by taking the Gaussian checkpoint files and using these in tandem with the GDMA program (version 2.2.04) developed by A.J.Stone.¹⁰³ Orient version 4.6.11 was used to generate the distributed multipoles^{86,103}.

3.3 Results

3.3.1 Thermodynamics and Kinetics

The diketones (**12**), keto-monohydrazones (**13**) and dihydrazones (**14**) illustrated in *Scheme 1.5* and *Scheme 1.6* were chosen for this study as three of the four keto-monohydrazones **13(a)**, **13(b)**, **13(d)** react with phenylhydrazine to yield dihydrazones (**14**), whereas the monohydrazone derivative **13(c)** is inert towards further nucleophilic attack, irrespective of the experimental conditions employed.

There are two possible isomers for the dimethyl keto-monohydrazone species **13(a)**, (*E*) and (*Z*), and three possible isomers for its corresponding dihydrazone **14(a)**, (*EE*), (*EZ*) and (*ZZ*) as seen in *Figure 3.5*. The ΔE of the reaction is based on the following equation, which is corrected for the zero-point energy of each species:

$$E_{\text{products}} - \sum E_{\text{reactants}} = \sum (E_{13a(Z)} + E_{H_2O}) - \sum (E_{12a} + E_{\text{phenylhydrazine}}) = (274.9 - 314.0) = -39.0 \text{ kJ/mol}. \quad (3.1)$$

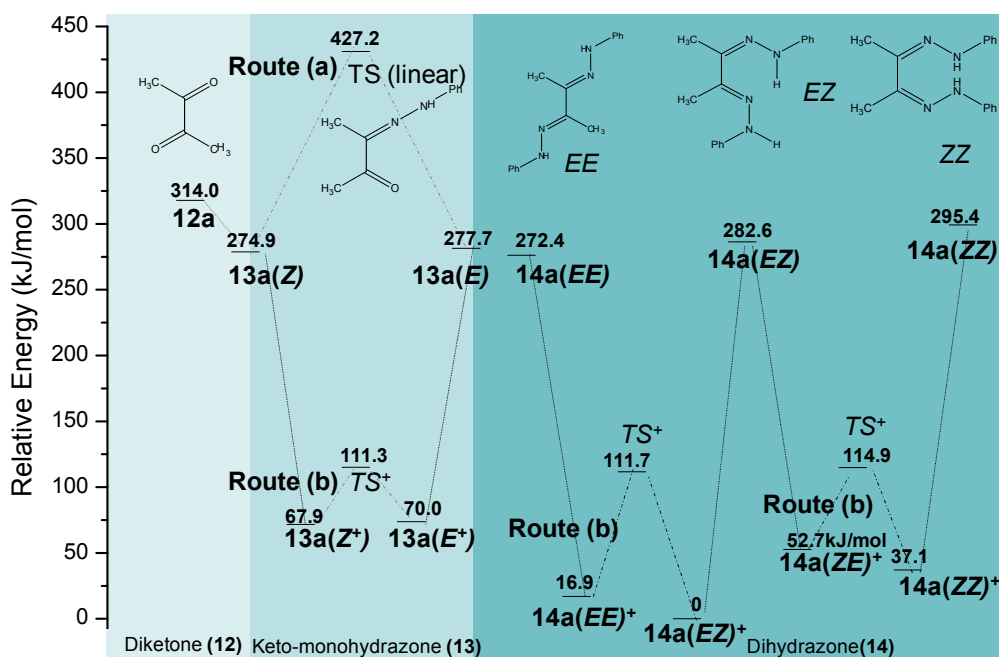


Figure 3.5 Energy diagram for the conversion of the dimethyl diketone **12(a)** to the keto-monohydrazone **13(a)**, moving from left to right and the subsequent conversion to the dihydrazone **14(a)** calculated at the B3LYP/6-31G(d) level. Routes (a) and (b) indicated in this figure refer to two possible modes of (*E*)/(*Z*) interconversion.

Two different pathways to inter-conversion between the (*E*) and (*Z*) isomers of **13(a)** are presented in **Figure 3.5**, route (a) is via a linear transition state, where the C=N-N bond angle and the C-C=N-N dihedral angles in the (*E*) isomer would change from 120° and 0°, to -120° and 180° respectively, in the (*Z*) isomer. Therefore, the transition state connecting these two on the potential energy surface should possess a bond angle of 180° and a dihedral angle of 90°. A transition state with these exact geometric requirements was located on the B3LYP/6-31G(d) potential energy surface and an IRC following was performed to confirm that it did connect the two minima of interest, **13(a)** (*E*) and **13(a)** (*Z*).¹⁰⁴ A more detailed diagram of this pathway is illustrated in **Figure 3.6**, substitution is observed to make little difference to the reaction energetics.

Route (b) however, is based on the mechanism proposed by Johnson *et al*¹⁰² (see **Figure 3.4**), which involves protonation of the isomer followed by a rotation. The protonated (*E*⁺) and (*Z*⁺) isomer of **13(a)** were located at the B3LYP/6-31G(d) level and a transition state corresponding to the protonated species was also located on the same surface. Subsequently an IRC following was performed for this species, proving that this transition state geometry links the (*E*⁺) and (*Z*⁺) isomers¹⁰⁴. The protonation of **13(a)** is a highly exothermic reaction, with the ΔE for the transformation of the (*E*) and (*Z*) isomers to (*E*⁺) and (*Z*⁺) being -207.7 and -207.0 kJmol⁻¹, respectively. Therefore this route is a highly feasible one given its exothermicity. Furthermore, this pathway has a lower barrier to interconversion (43.3 kJ/mol) compared with route (a) which requires 152.3 kJ/mol to interconvert via the linear transition state. Therefore the actual mechanism for (*E*)/(*Z*) interconversion is probably route (b).

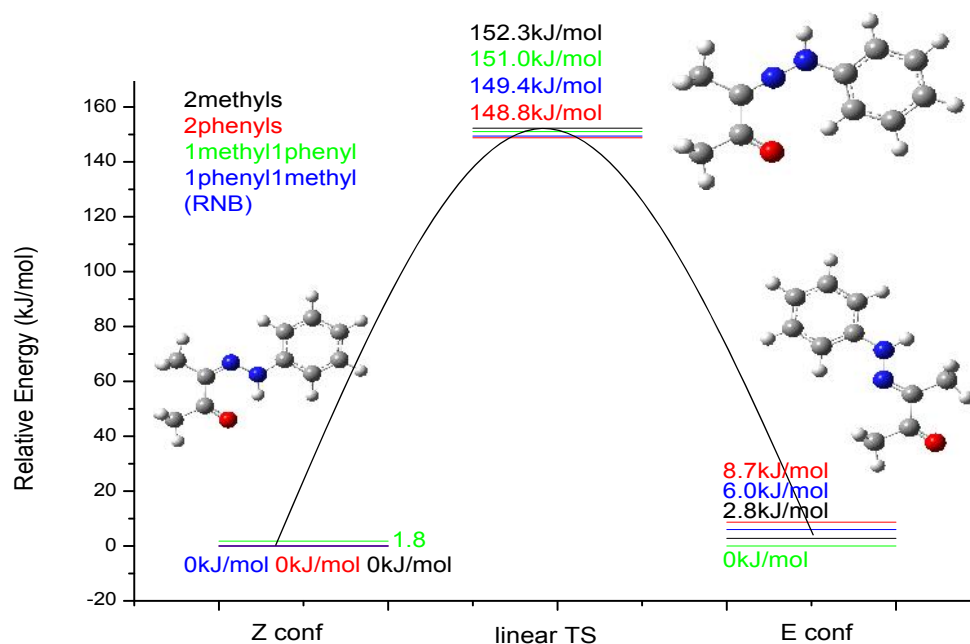


Figure 3.6 Inter-conversion between the (*E*) and (*Z*) isomers in the keto-monohydrazone (**13**) via a linear TS state (route (a) **Figure 3.5**). Calculated at the B3LYP/6-31G(d) level.

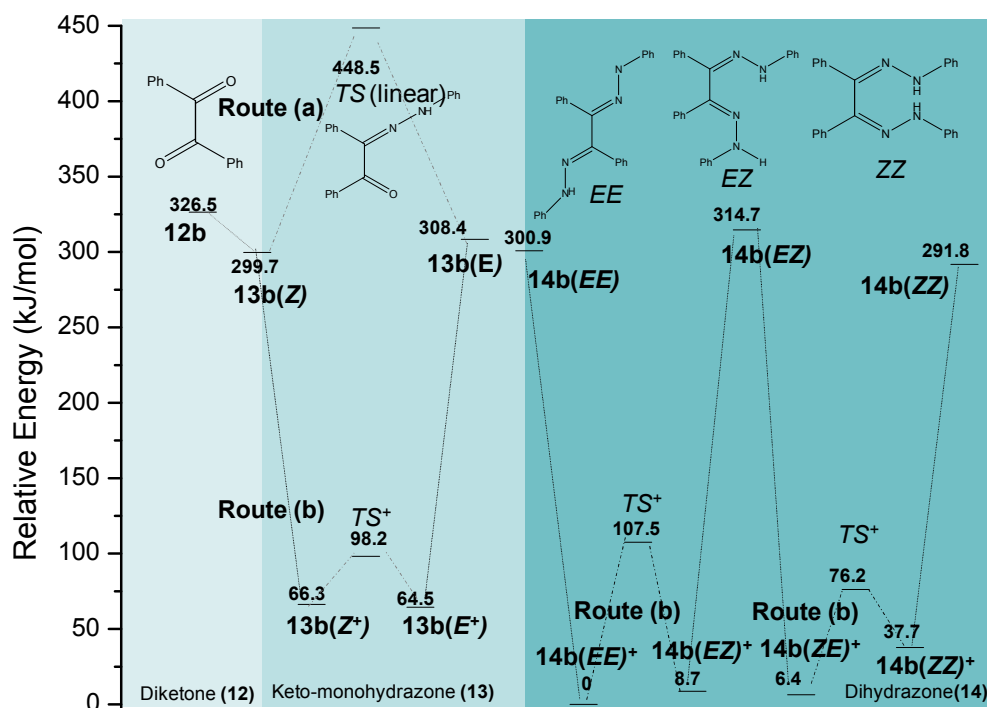


Figure 3.7 Energy diagram for the conversion of the diphenyl ketone **12(b)** to its monohydrazone **13(b)** and subsequent conversion to the dihydrazone **14(b)**. Calculated at the B3LYP/6-31G (d) level.

Based on the formula provided in equation (3.1), the ΔE for the conversion of the diphenyl diketone, benzil **12(b)** to its monohydrazone is exothermic (299.7-326.5= -26.8 kJ/mol), see **Figure 3.7**. There are three possible dihydrazone isomers, (*EE*), (*EZ*) and (*ZZ*), that can be formed, the most stable of which is the (*ZZ*) isomer. There is a thermodynamic driving force, to form the dihydrazone from the monohydrazone for the diphenyl derivative (291.8-299.7=-7.9 kJ/mol), albeit a modest driving force, but the dihydrazone is isolated experimentally.

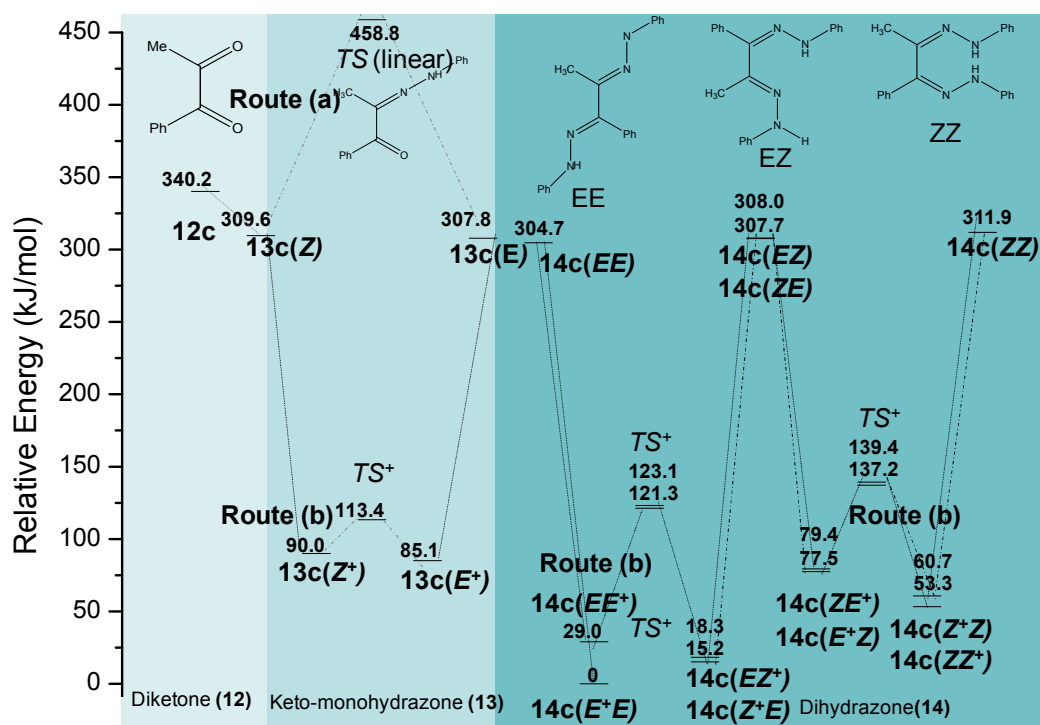


Figure 3.8 Energy diagram for the conversion of the methyl-phenyl diketone **12(c)** to its monohydrazone **13(c)** and the hypothetical conversion of the monohydrazone to the dihydrazone **14(c)** calculated at the B3LYP/6-31G(d) level.

For the methyl-phenyl derivative (see **Figure 3.8**), the conversion of the diketone **12(c)** to its monohydrazone **13(c)** is exothermic (=307.8-320.2=-32.4 kJ/mol). There are four possible dihydrazone isomers for the methyl-phenyl derivative **14(c)**, (*EE*), (*ZE*), (*EZ*) and (*ZZ*), given the asymmetric nature of the starting diketone **12(c)**. This step should be thermodynamically favourable (=304.7-307.8=-3.1 kJ/mol). This is not observed experimentally, the reaction falters at the second stage of the reaction. As there is nothing in the calculated thermodynamics to suggest a reason for the non-reactivity, the problem may be kinetic in origin.

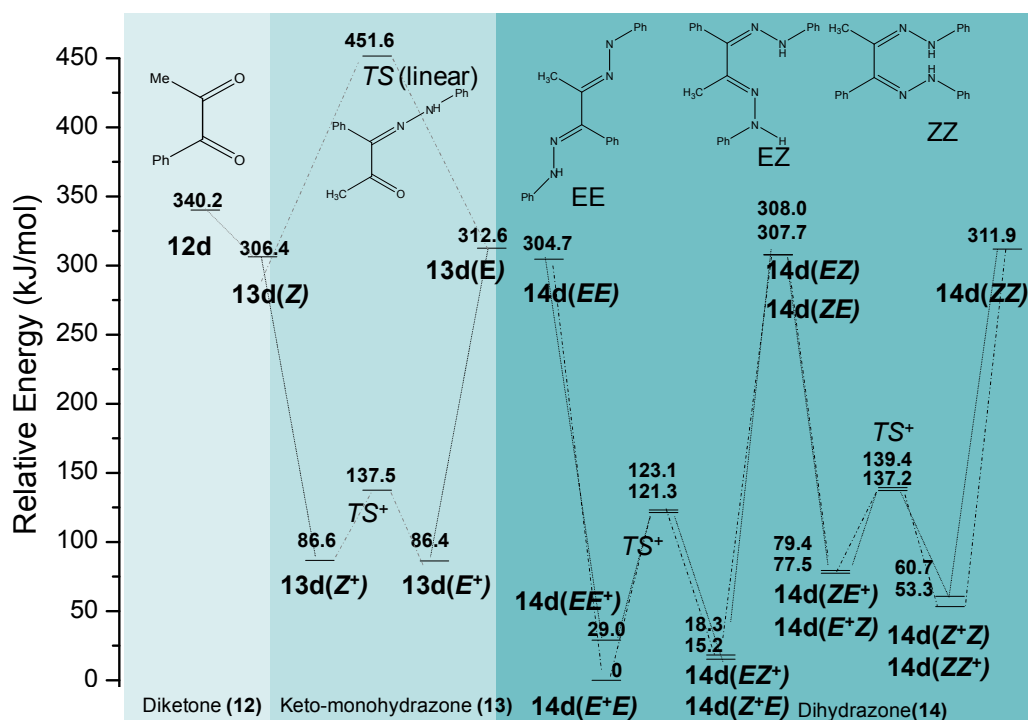


Figure 3.9 Energy diagram for the conversion of the phenyl-methyl ketone **12(d)** to its monohydrazone **13(d)** and the hypothetical conversion of the monohydrazone to the dihydrazone **14(d)** calculated at the B3LYP/6-31G(d) level.

Finally the energetics of the fourth species, the alternative methyl-phenyl derivative is presented here in **Figure 3.9**. The first step is a hypothetical one, as the reaction between the diketone **12(d)** and phenylhydrazine always yields the monohydrazone **13(c)** and not **13(d)** but the thermodynamics of the second step is what interests us here, so it is included for completeness. There are four possible dihydrazone isomers for the methyl-phenyl derivative **14(d)**, (*EE*), (*ZE*), (*EZ*) and (*ZZ*), given the asymmetric nature of the starting diketone **12(d)**. If the monohydrazone **13(d)** were formed in the first reaction step, it would be thermodynamically favourable to form the dihydrazone **14(d)** from **13(d)** ($=304.7-306.4=-1.7$ kJ/mol), which is interesting as R. N. Butler's reported formation of a similar dihydrazone derivative **14c(ii)** from a monohydrazone of this isomeric form **13(d)**.⁶⁹

The ΔE , ΔH , ΔS and ΔG values that were obtained from the PES analysis for reactions of the diketones **12(a)-(d)** are collected in **Table 3.1**. It should be noted that these values correspond to the energetics performed in the gas phase (*in vacuo*). The figures were calculated following the guidelines in the Gaussian white paper by Ochterski.¹⁰⁵ The ΔE_{solv} , ΔH_{solv} , ΔS_{solv} and ΔG_{solv} that are presented in **Table 3.1**

correspond to the energies, enthalpies, entropies and Gibbs free energies of solvation for the reaction, using the SMD solvent model.¹⁰⁶ The calculations were performed to simulate solvation in ethanol, as hydrazone synthesis generally proceeds best in this polar protic solvent.

Comparison of the ΔE with the ΔE_{solv} values for the reaction between the diketones (**12**) with phenylhydrazine, *i.e.* step 1, is shown in **Table 3.1**. This step is predicted to be slightly more exothermic when solvation is included. In three of the four (**Z**) forms **12(a-c)**, this difference is slight (≤ 2 kJ/mol). In the case of the conversion of the diketone (**12**) to the monohydrazone (**13**) in its (**E**) isomer, solvation makes a greater difference, with the average stability increasing by 14.4 kJ/mol. This may be due to the fact that the (**E**) isomer is an open-chain form of the molecule and can interact with the solvent more strongly as a result. The trend in the ΔG values is similar to that of the ΔE values in that the reaction in step 1 is predicted to be feasible for all four derivatives.

In the second step of the reaction (**Table 3.1**), not all isomeric conversions were predicted to be feasible. For example, in the conversion of the dimethyl monohydrazone **13(a)** to its dihydrazone **14(a)** only the (**E**) isomer conversion to its (**EE**) dihydrazone is predicted to be spontaneous ($\Delta G_{\text{solv}} = -1.29$ kJ/mol). For the diphenyl derivative (**Figure 3.7**), the (**Z**) to (**ZZ**) conversion is the most likely reaction to take place ($\Delta G_{\text{solv}} = -11.18$ kJ/mol). Surprisingly, for the non-reactive monohydrazone **13(c)** a few isomeric forms were predicted to be convertible to the dihydrazone **14(c)**. This is not observed experimentally, suggesting that there are kinetic limitations in this case. For the alternative methyl-phenyl derivative **13(d)**, the conversion of the monohydrazone to its dihydrazone **14(d)** is most likely to take place when the monohydrazone adopts the (**E**) conformation, $\Delta G_{\text{solv}} = -8.27$ kJ/mol for conversion to the (**EE**) dihydrazone.

Table 3.1 Enthalpic and entropic contributions to the Gibbs Free Energy for the two individual steps involved in the formation of a dihydrazone (**14**): conversion of the diketone (**12**) to the monohydrazone (**13**): Step 1 and the conversion of the monohydrazone (**13**) to the dihydrazone (**14**): Step 2. ΔG_{solv} represents the Gibbs Free Energy with the reaction solvated in ethanol using the SMD solvent model.

		Step 1							
		ΔE	ΔE_{solv}	ΔH	ΔH_{solv}	ΔS	ΔS_{solv}	ΔG	ΔG_{solv}
(12) to (13)		kJ/mol						kJ/mol	
Me-Me	diketone to Z	-39.15	-40.70	-23.32	-33.99	-0.017	-0.010	-18.13	-30.91
	diketone to E	-36.38	-49.80	-26.39	-42.02	-0.028	0.006	-18.01	-43.93
Ph-Ph	diketone to Z	-26.73	-28.90	-16.65	-24.58	-0.037	-0.033	-5.69	-14.87
	diketone to E	-18.03	-32.11	-7.03	-27.23	-0.025	-0.025	0.56	-19.85
Me-Ph	diketone to Z	-30.66	-30.57	-18.41	-27.26	-0.042	-0.038	-5.85	-15.95
	diketone to E	-32.42	-46.97	-19.17	-42.82	-0.034	-0.029	-8.93	-34.17
Ph-Me	diketone to Z	-33.87	-38.29	-24.16	-34.89	-0.040	-0.033	-12.33	-24.66
	diketone to E	-27.64	-43.18	-17.16	-38.78	-0.031	-0.028	-7.95	-30.35

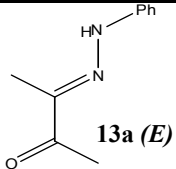
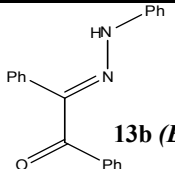
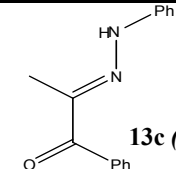
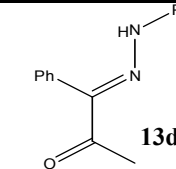
		Step 2							
		ΔE	ΔE_{solv}	ΔH	ΔH_{solv}	ΔS	ΔS_{solv}	ΔG	ΔG_{solv}
(13) to (14)		kJ/mol						kJ/mol	
Me-Me	Z to ZZ	20.48	7.19	25.72	13.77	-0.033	0.003	35.58	13.01
	E to EE	-5.24	-11.87	6.15	-6.62	-0.017	-0.018	11.17	-1.29
	Z to EZ	7.70	-8.89	11.78	-3.78	-0.045	-0.017	25.31	1.17
	E to EZ	4.93	0.21	14.85	1.01	-0.035	-0.033	25.19	14.19
Ph-Ph	Z to ZZ	-7.93	-20.11	4.61	-13.82	-0.007	-0.009	6.84	-11.18
	E to EE	-7.95	-14.27	4.71	-9.98	-0.019	-0.032	7.55	-0.39
	Z to EZ	14.97	-4.88	27.80	1.35	-0.002	-0.016	28.39	5.98
	E to EZ	6.27	-1.67	18.18	4.00	-0.013	-0.023	22.14	10.96
Me-Ph	Z to ZZ	2.34	-13.75	11.97	-7.44	-0.011	-0.015	15.19	-2.88
	E to EE	-3.16	-10.98	6.02	-4.68	-0.011	-0.001	9.33	-4.46
	Z to EZ	-1.58	-21.78	7.70	-16.01	-0.013	-0.022	11.57	-9.34
	Z to ZE	-1.90	-18.29	7.57	-11.79	-0.008	-0.007	10.09	-9.71
	E to EZ	0.18	-5.37	8.46	-0.45	-0.021	-0.031	14.65	8.88
	E to ZE	-0.14	-1.89	8.34	3.78	-0.016	-0.016	13.17	8.51
Ph-Me	Z to ZZ	5.55	-6.03	17.72	-0.22	-0.013	-0.020	21.67	5.82
	E to EE	-7.94	-14.76	4.01	-8.72	-0.015	0.028	8.35	-8.27
	Z to EZ	1.63	-14.05	13.45	-8.79	-0.015	0.002	18.05	-0.64
	Z to ZE	1.31	-10.57	13.33	-4.56	-0.011	0.003	16.57	-1.01
	E to EZ	-4.60	-9.16	6.44	-4.49	-0.024	-0.017	13.67	5.06
	E to ZE	-4.92	-5.67	6.32	-0.27	-0.020	-0.016	12.19	4.69

3.3.2 Point charges

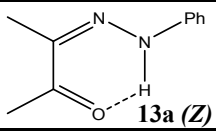
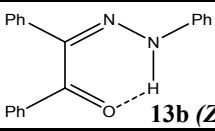
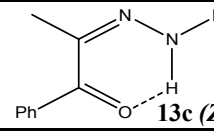
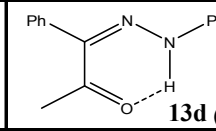
To investigate whether the electronic distribution differs across the monohydrazone series of molecules **13(a)-(d)**, the point charges of both the (*E*) and (*Z*) isomers for all species were extracted from the B3LYP/6-31G(d) calculations. As the **13(c)** derivative is not reactive towards further nucleophilic attack, then one would expect the carbonyl carbon atom to carry a lesser positive charge compared with its more reactive counterparts, **13(a)**, **13(b)** and **13(d)**. The point charges of these aforementioned species are presented in *Table 3.2* below.

Table 3.2 Point charges of the carbonyl carbon atom for the (*E*) and (*Z*) conformations of the keto-monohydrazones (**13**) optimised at the B3LYP/6-31G(d) level

E conformations

				
	C O	C O	C O	C O
Mulliken	0.416 -0.456	0.374 -0.471	0.350 -0.476	0.439 -0.451
NPA	0.538 -0.549	0.548 -0.560	0.523 -0.554	0.532 -0.536
CHelpG	0.436 -0.462	0.288 -0.417	0.271 -0.422	0.438 -0.451
MKS	0.487 -0.468	0.323 -0.418	0.312 -0.423	0.517 -0.471

Z conformations

				
	C O	C O	C O	C O
Mulliken	0.436 -0.514	0.363 -0.530	0.357 -0.537	0.444 -0.518
NPA	0.507 -0.598	0.503 -0.601	0.491 -0.604	0.516 -0.602
CHelpG	0.499 -0.498	0.431 -0.498	0.371 -0.482	0.571 -0.526
MKS	0.532 -0.498	0.456 -0.479	0.360 -0.469	0.621 0.515

The dimethyl keto-monohydrazone species **13(a)** converts most readily to its dihydrazone **14(a)**, whereas the diphenyl keto-monohydrazone species **13(b)** requires reflux temperatures to enable the conversion over to the dihydrazone **14(b)**. Therefore, the least reactive keto-monohydrazone **13(b)**, will be compared with the non-reactive monohydrazone **13(c)** to see if a limit for the calculated charge that corresponds to the experimental reactivity for the keto-monohydrazones (**13**).

Table 3.3 Comparison of the positive charge on the carbonyl carbon atoms between the reactive diphenyl monohydrazone species **13(b)** and the non-reactive methyl-phenyl species **13(c)**

	13b (E)	13c (E)	Diff	%Diff
Mulliken	0.374	0.350	0.024	6.4
NPA	0.548	0.523	0.025	4.6
CHelpG	0.288	0.271	0.017	5.9
MKS	0.323	0.312	0.011	3.4

	13b (Z)	13c (Z)	Diff	%Diff
Mulliken	0.363	0.357	0.006	1.7
NPA	0.503	0.491	0.012	2.4
CHelpG	0.431	0.371	0.060	13.9
MKS	0.456	0.360	0.096	21.1

Considering the Mulliken charges presented in **Table 3.3** for the reactive **13(b)(E)** compared with non-reactive **13(c)(E)**, there is a modest decrease of 6.4% in the positive charge on the carbonyl carbon atom of **13(c)(E)** compared with the more reactive diphenyl species **13(b)(E)**. There is a moderate 1.7% reduction in electrophilicity of the same carbon atom between **13(c)(Z)** with **13(b)(Z)**, the alternate isomer. The NPA point charge method also illustrates a similar decrease of 4.6 and 2.4% on the same carbon atom for the **(E)** and **(Z)** isomers respectively.

The two electrostatic potential methods however, (CHelpG and MKS) predict a more substantial difference in the electrophilicity of the reactive carbonyl carbon atoms. The point charges in **13(b)(Z)** and **13(c)(Z)** differ by 13.9 and 21.1% decrease respectively under the CHelpG and MKS methods. The trend across the four methods suggests that qualitatively the carbonyl carbon atom is less positive in **13(c)** compared with **13(b)**, however the values vary from method to method. Therefore

one cannot ‘pick and choose’ the result to explain the reactivity of the monohydrazones (**13**). A more representative method for viewing the distribution of electronic charge about a molecule is the distributed multipole analysis (DMA), developed by Stone and co-workers.⁸⁴ Hence, the next section will look at the DMAs for phenylhydrazine and the monohydrazones **13(a)-(d)**.

3.3.3. Multipole analyses of phenylhydrazine and monohydrazones **13(a)-(d)**

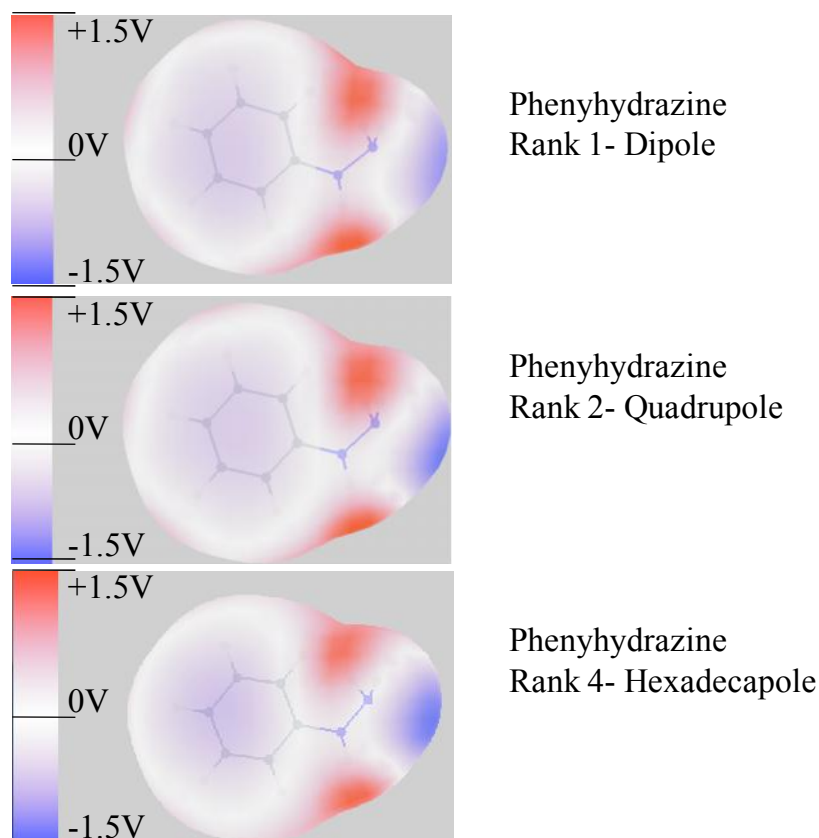


Figure 3.10 Dipole, quadrupole and hexadecapole of phenylhydrazine, generated at a scale of 1.5 times the van de Waals radius.

The multipole analysis for phenylhydrazine is shown in **Figure 3.10** (dipole/quadrupole/hexadecapole), all surfaces show a similar negative potential (blue region) located on the terminal nitrogen atom. This suggests that this region of the phenylhydrazine moiety is highly nucleophilic in character and consequently would be expected to attack a region of positive potential in the monohydrazones (**13**).

Multipole analyses of both the (*E*) and (*Z*) isomers were performed for all four monohydrazone derivatives **13(a)-(d)**. In **Figure 3.11**, the dipoles, quadrupoles and hexadecapoles are presented for the dimethyl monohydrazone **13(a)**. The multipoles

for the (**Z**) conformation are displayed in panels (**a-c**) and the multipoles for the (**E**) conformation are displayed in panels (**d-f**). The global minimum for the (**E**) conformation however, does not display any positive potential for the same region. If one of the soft modes of the (**E**) conformation is adopted, (**E'**), then a positive potential is generated near the carbonyl site (**g-i**), making it a ‘reactive’ conformation which could be attacked by phenylhydrazine. The barrier to interconversion between the soft modes was calculated to be 52.2 kJ.mol⁻¹ for the gas phase or 46.5 kJmol⁻¹ in solution using the SMD model at the B3LYP/6-31G(d) level (see **Figure 3.12**).

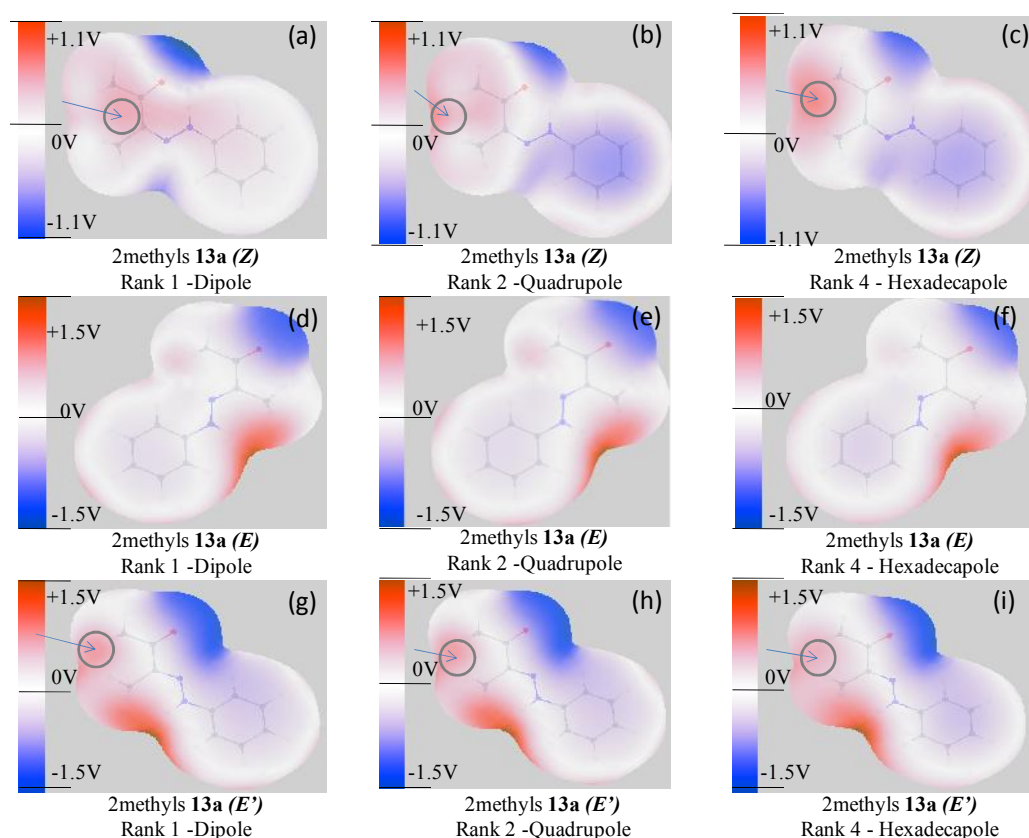


Figure 3.11 Dipoles, quadrupoles and hexadecapoles generated for the dimethyl monohydrazone **13(a)** for both the (**E**) and (**Z**) isomers at a scale of 1.5 times that of the van der Waals radius (x1.5vdW). A positive potential exists adjacent to the carbonyl group when 1-phenylhydrazone-propan-2-one **13(a)** exists in the (**Z**) isomer.

Distributed multipoles for the diphenyl monohydrazone species **13(b)** are illustrated in **Figure 3.13**. Similar potentials exist in the (*E*) and (*Z*) isomers of this monohydrazone **13(b)** compared with **13(a)** in that a positive potential exists near the carbonyl group in the (*Z*) conformation. In the (*E*) conformation the only positive potential present is located near the N-H group. This suggests that collisions between phenylhydrazine and **13(b)** are unlikely to result in the formation of a dihydrazone **14(b)**. The (*Z*) conformation can therefore be considered to be the reactive isomer of the diphenyl monohydrazone **13(b)**.

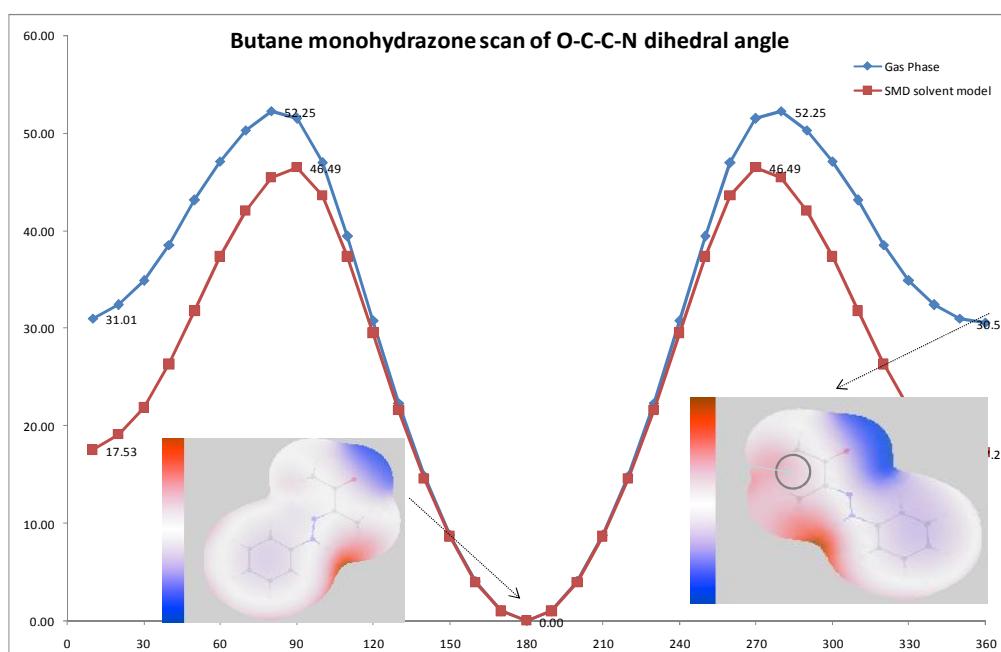


Figure 3.12 Rotational barrier in the (*E*) isomer for dimethyl-monohydrazone **13(a)** for both the gas phase and in solution, using the SMD solvent model (ethanol).¹⁰⁷

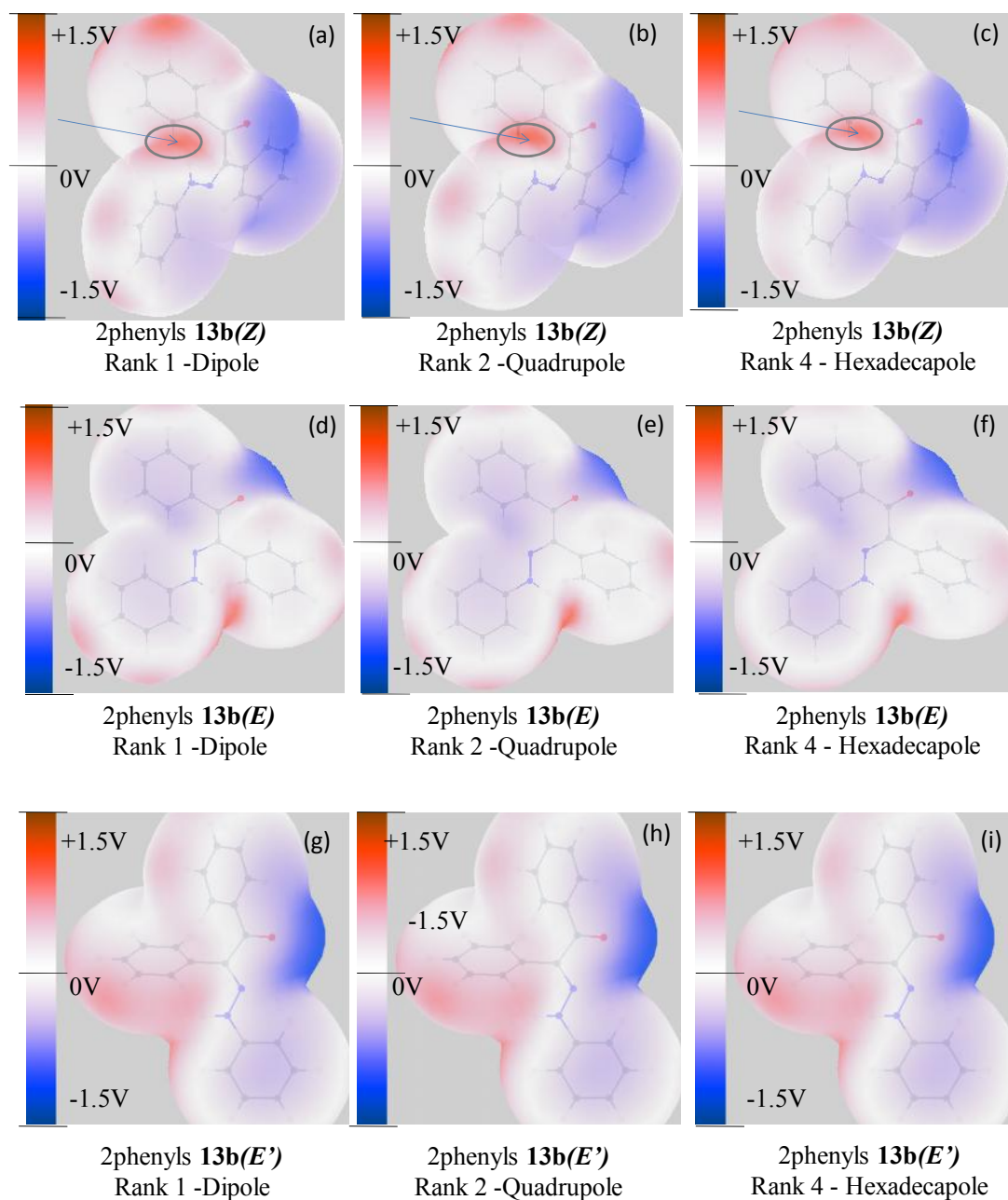


Figure 3.13 Dipoles, quadrupoles and hexadecapoles generated for the diphenyl monohydrazone **13(b)** for both the (*E*) and (*Z*) isomers at a scale of 1.5 times that of the van der Waals radius (x1.5vdW). A positive potential is apparent adjacent to the carbonyl group while in the (*Z*) conformation only making this the ‘reactive’ isomer. A soft mode of one of the (*E*) conformers is also illustrated, (*E'*), demonstrating that is also not a reactive conformer.

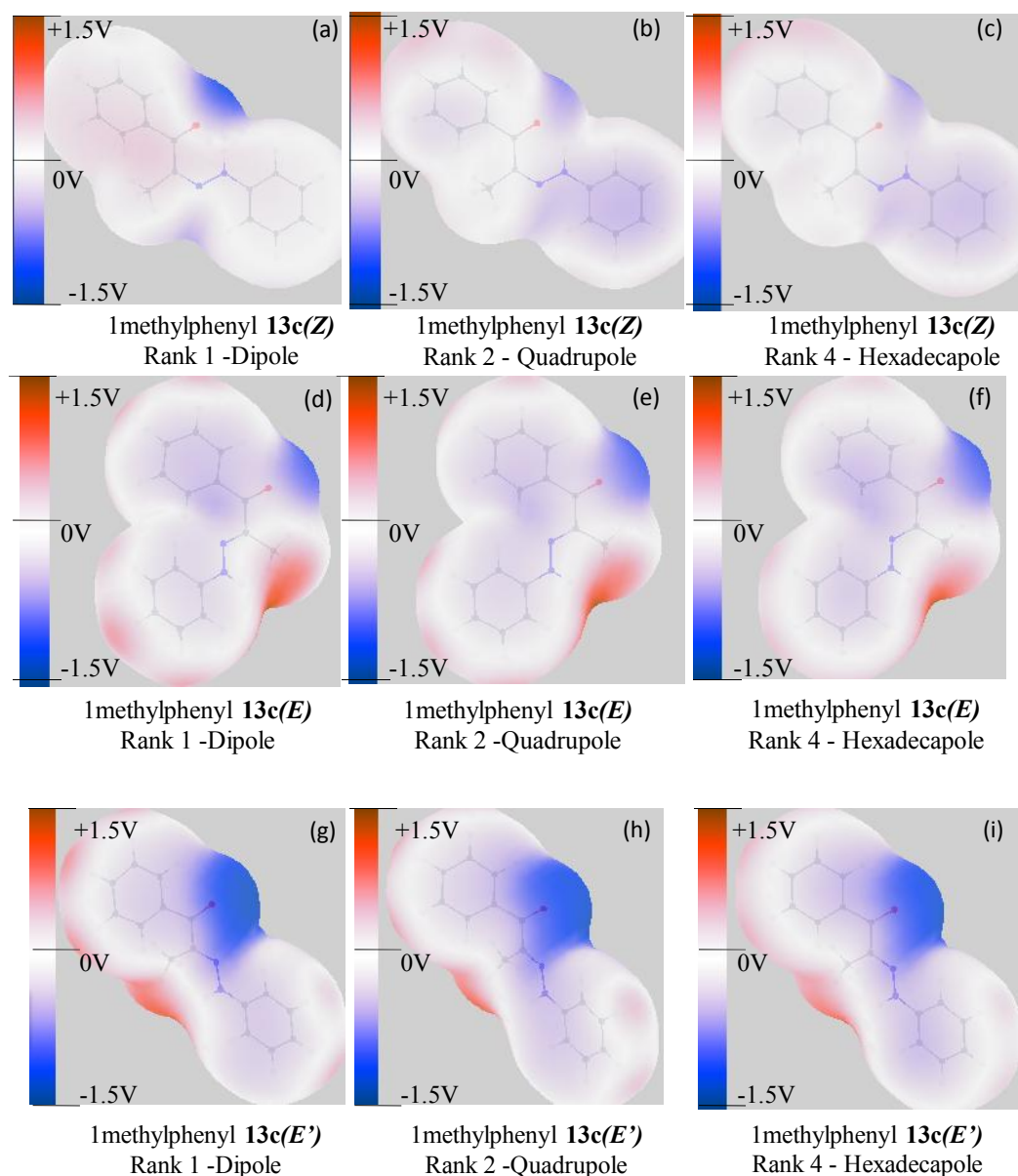


Figure 3.14 Dipoles, quadrupoles and hexadecapoles generated for the methyl-phenyl monohydrazone **13(c)** for both was the (*E*) and (*Z*) isomers at a scale of 1.5 times that of the van der Waals radius (x1.5vdW).

Interestingly, a slightly different picture emerges for the unreactive methyl-phenyl monohydrazone derivative **13(c)** (see **Figure 3.14**). In both isomers (*E*) and (*Z*), no positive potential exists in close proximity to the carbonyl group. Therefore it is difficult to envisage an orientation of **13(c)** that could be attacked by phenylhydrazine, if there are no electron/nucleophilic centres associated with the two molecules.

Multipoles were also generated for one of the soft modes of the **13(c)** (*E*) isomer, (*E'*) as the conversion of the (*E*) isomer to the (*EE*) dihydrazone would be the most energetically favourable reactions (see **Figure 3.14**). The absence of a positive centre adjacent to the carbonyl group for this conformation (*E'*) suggests that this is the reason why it is not possible for phenylhydrazine to react with the methyl-phenyl-monohydrazone **13(c)**, regardless of the isomeric or conformational form.

Considering the monohydrazone **13(d)**, multipole analyses were performed for the (*E*) or (*Z*) isomers of this derivative, see **Figure 3.15**. For example, in the (*Z*) conformation, a region of positive potential exists in close proximity to the carbonyl group, whereas in the (*E*) conformation, the only positive potential is predicted to be over the N-H hydrogen. Therefore, the reactive form of this molecule is predicted to be the (*Z*) isomer.

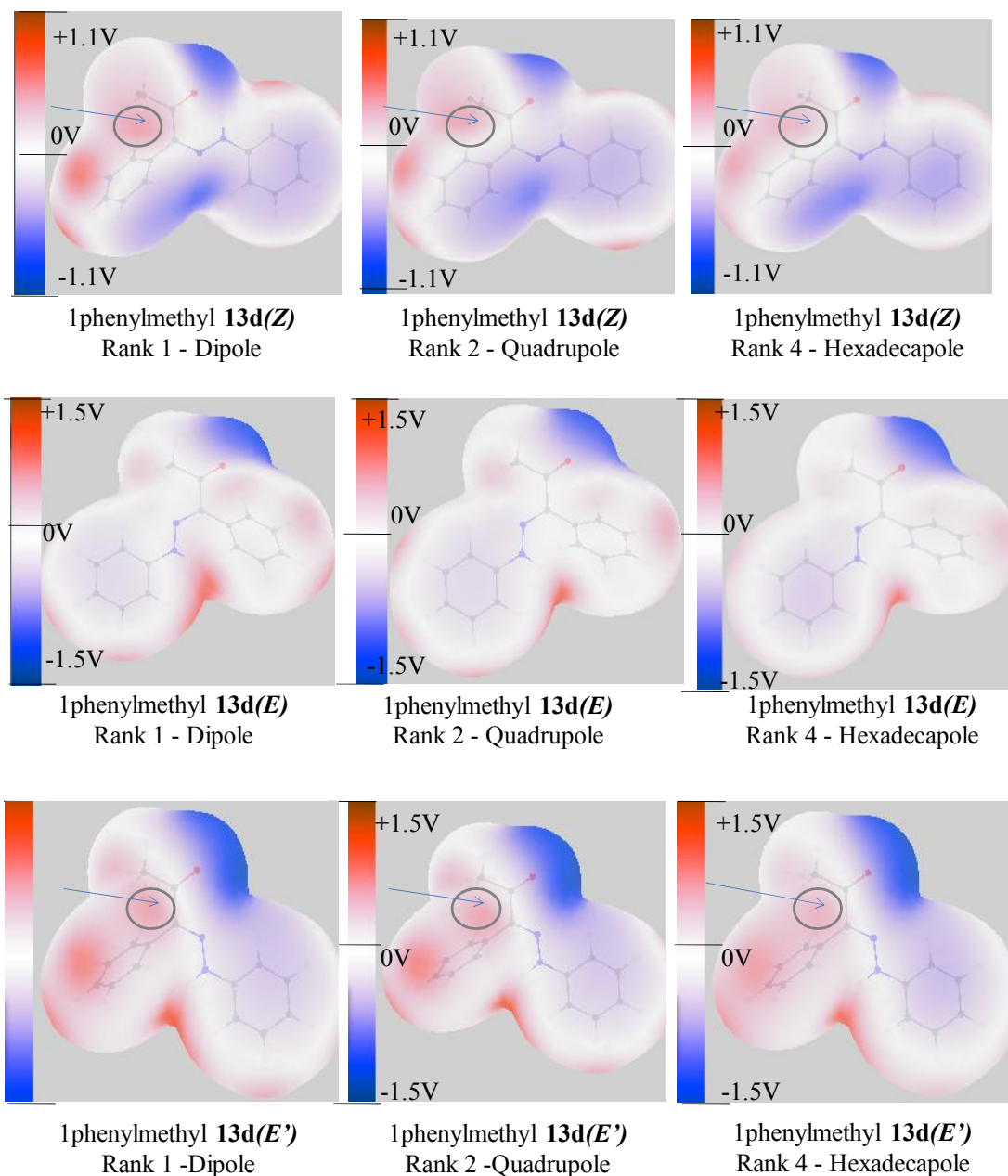


Figure 3.15 Dipoles, quadrupoles and hexadecapoles generated for the methyl-phenyl monohydrazone **13(d)** for both the (*E*) and (*Z*) isomers at a scale of 1.5 times that of the van der Waals radius (x1.5vdW).

3.4 Discussion

Figure 3.5 shows that calculations suggest the presence of an energetic driving force to form the dimethyl-monohydrazone **13(a)(Z)** in the reaction between butane-2,3-dione **12(a)** and phenylhydrazine ($39.1 \text{ kJ/mol} = 314.0 - 274.9 \text{ kJ/mol}$). There are two possible isomers of the keto-monohydrazone (**13**) that may be formed; a (**Z**) or an (**E**) isomer, but they differ very little in terms of stability; 2.8 kJ/mol ($= 274.9 - 277.7 \text{ kJ/mol}$). The slight stabilisation of the (**Z**) isomer over the (**E**) may be attributed to the fact that hydrogen bonding can exist in the (**Z**) isomer, but not in the (**E**). The strength of a hydrogen bond can vary broadly from 0.8 - 167 kJ/mol and this interaction can operate up to an inter-nuclear distance of 3.2 \AA .¹⁰⁸ In the (**Z**) conformation there is potential for a hydrogen bonding interaction as the N-H hydrogen and the oxygen of the carbonyl group are only 1.8 \AA apart (*see Figure 3.16*).

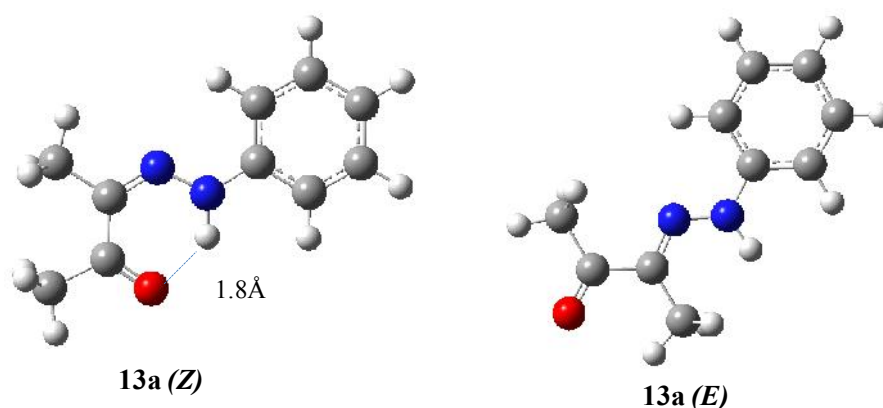


Figure 3.16 Only the (**Z**) isomer of **13(a)** possesses intramolecular hydrogen bonding.

The energetic driving force for the second stage of the reaction (conversion of the dimethyl monohydrazone **13(a)** to its dihydrazone **14(a)**) is also illustrated in **Figure 3.5**. Comparing the *non*-protonated dihydrazone isomers in this figure, (**EE**), (**EZ**) and (**ZZ**), the (**EE**) dihydrazone is the most stable dihydrazone isomer by 10.2 kJ/mol ($= 272.4 - 282.6$) and 23.0 kJ/mol ($= 272.4 - 295.4$) over the (**EZ**) and (**ZZ**) isomers, respectively.

The protonation-rotation mechanism as in **Figure 3.4** for the (**E**)/(**Z**) isomerisation in the dihydrazones (**14**) is worth mentioning here. In the case of the dimethyl species

14(a), the barrier to interconversion along this pathway is substantially higher (see **Figure 3.5**) for the dihydrazones ($\Delta E = c.100$ kJ/mol) compared with the monohydrazones ($\Delta E = c.40$ kJ/mol). This is as expected, the molecule has become more sterically hindered upon addition of the second phenylhydrazine moiety in the dihydrazone **14(a)**, making the interconversion more costly in terms of energy compared with the less sterically hindered monohydrazone **13(a)**. Therefore, interconversion may not always be possible in the dihydrazones (**14**).

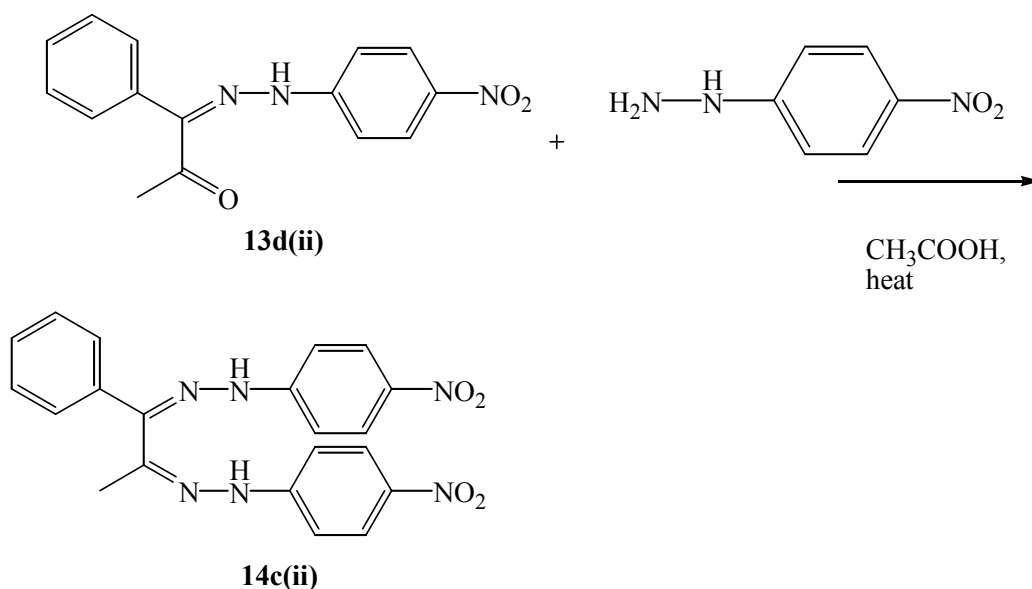
The energy diagram for the diphenyl species shown in **Figure 3.7** suggests that the formation of the monohydrazone **13(b)** from benzil **12(b)** is an energetically favourable process; $\Delta E = 26.8$ kJ/mol (299.7-326.5 kJ/mol). As with the dimethyl monohydrazones **13(a)**, there is a stabilisation of the (*Z*) isomer over the (*E*) isomer, but by an even greater margin in the diphenyl series ($\Delta E = 8.7$ kJ/mol = 299.7 - 308.4 kJ/mol). The most energetically favourable route for (*E*) to (*Z*) isomerisation is also via the protonation-rotation route with a calculated barrier to inter-conversion of 33.7 kJ/mol ($\Delta E = 98.2 - 64.5$ kJ/mol), route (b) (**Figure 3.7**).

The order of stability of the (*E*) or (*Z*) isomers of **13(b)** is reversed upon protonation, in that the (*E*⁺) isomer is more stable than the (*Z*⁺) isomer. This is by the smallest of margins however (1.8 kJ/mol; 66.3 - 64.5 kJ/mol). The melting point and NMR spectra of the benzil dihydrazone **14(b)** as presented in **Chapter 2** correspond to the (*ZZ*) isomer however, as reported by Mirifico *et al.*¹⁰⁹ This suggests that for our work the dihydrazone **14(b)** was synthesised from the (*Z*) monohydrazone **13(b)** as the barriers to interconversion between dihydrazones (**14**) are much higher than for the monohydrazones (107.5 kJ/mol compared with 33.7 kJ/mol).

Considering the *non*-protonated forms the most stable dihydrazone isomer in the diphenyl species, **14(b)** is the (*ZZ*) isomer, with this isomer being 9.1 and 22.9 kJ/mol more stable than the (*EE*) and (*EZ*) isomers respectively. This is also in accordance with the findings of Mirifico *et al.*, who report the order of decreasing total energy as (*EZ*) > (*EE*) > (*ZZ*) and the total energy differs by 20.9 kJ/mol. These calculations¹⁰⁹ were performed at a lower level of theory (PM3) than is presented here. The (*Z*) to (*ZZ*) transformation of **13(b)** to **14(b)** was also correctly predicted from the figures presented in **Table 3.1**.

The reaction of the diketone **12(c)** and phenylhydrazine to form **13(c)** should be energetically favourable, $\Delta E = -32.4$ kJ/mol; 307.8 - 340.2). The (*E*) to (*Z*) protonation-rotation isomerisation can also take place for the methyl-phenyl species, with the barrier for this process being the lowest for all four derivatives (28.3 kJ/mol for route b). Interestingly, the open-chain (*E*) isomer is the most stable monohydrazone **13(c)** for this series of compounds, albeit marginally, by 1.8 kJ/mol, over the (*Z*) isomer.

The energy level diagram for the reaction of the alternate methyl-phenyl series of compounds **12(d)/13(d)/14(d)** is illustrated in **Figure 3.9**. Although **13(d)** was not synthesised by the route illustrated in **Scheme 1.5**, R.N. Butler *et al* reported the synthesis of 1-phenyl-1,2-bis(4'-nitro-phenylhydrazone)propane **14c(ii)** from 1-phenyl-1-(4'-nitrophenylhydrazono)propan-2-one **13d(ii)**, see **Scheme 3.2**. Hence a derivative of **13(d)** can be converted to **14(c/d)**, which is interesting given the non-reactivity of its isomer **13(c)**.⁶⁹



Scheme 3.2 Synthesis of 1-phenyl-1,2-bis(4'-nitrophenylhydrazone)propane **14c(ii)** from 1-phenyl-1-(4'-nitrophenylhydrazono)propan-2-one **13d(ii)** according to Butler *et al*⁶⁹

Therefore the data represented in **Figure 3.9** is for a hypothetical reaction for the diketone **12(d)** converting to the monohydrazone **13(d)**. The subsequent conversion of the monohydrazone **13(d)** to its dihydrazone **14(d)** is the reaction of interest here for rationalising the experimentally observed reactivities.

Synthesis of the monohydrazone **13(d)** by the route shown in **Figure 3.9** is problematic because phenylhydrazine consistently attacks the carbonyl group adjacent to the methyl position in the diketone **12(c)/(d)**, as described in **Chapter 2**. If the monohydrazone **13(d)** could be formed via an alternative route then the calculations suggest that the (*Z*) conformation would be the most stable form of this monohydrazone, by 6.2 kJ/mol, over the open-chain (*E*) form. As noted earlier, the most energetically favourable route to (*E*)/(*Z*) isomerisation is probably through the protonation-rotation route as this barrier to inter-conversion is 51.1 kJ/mol compared with 145.2 kJ/mol for the linear ‘nitrogen inversion’ transition state. The dihydrazones are expected to have the same order of stability as the methyl-phenyl derivatives, illustrated in **Figure 3.8**, as the products formed (dihydrazone and water) are the same as for the methyl-phenyl derivative **14(c)**.

It is worth revisiting the figures presented in **Table 3.1** to compare the results with experimental observations. For the conversion of the diketone **12(a)** to the keto-monohydrazone **13(a)**, in the dimethyl series of compounds, the most favourable reaction is the formation of the (*Z*) isomer ($\Delta E = -39.15$ kJ/mol) over the (*E*) ($\Delta E = -36.38$ kJ/mol). Taking solvation effects into account however, the order of stability is actually reversed. The ΔE_{solv} predicts the (*E*) isomer ($\Delta E_{\text{solv}} = -49.80$ kJ/mol) to be favoured over the (*Z*) ($\Delta E_{\text{solv}} = -40.70$ kJ/mol). Hence the ΔE_{solv} values match the experimental observation of the (*E*) form in the molecular structure for the dimethyl species, whereas (*Z*) is predicted to be favoured by the gas phase calculations.¹¹⁰ A trend emerges in that the solvation energies (ΔE_{solv}) suggest greater stability for the (*E*) isomer over the (*Z*). This may be due to the fact that the open-chain (*E*) isomer would have a greater capacity to participate in hydrogen bonding with solvent molecules than in the (*Z*) form. The (*E*) isomer is stabilised by an average of 14.40 kJ/mol, whereas the (*Z*) isomer is only stabilised by 2.06 kJ/mol. In fact the ΔE_{solv} values predict that the (*E*) isomer would be the most stable form of keto-monohydrazone (**13**) across the whole series of compounds **13(a)-(d)**, which is also

in accordance with the enthalpy predictions (ΔH_{solv}). All reactions are predicted to be exothermic, and all combinations are predicted to be spontaneous (negative ΔG values).

Table 3.1 Enthalpic and entropic contributions to the Gibbs Free Energy for the two individual steps involved in the formation of a dihydrazone (**14**): conversion of the diketone (**12**) to the monohydrazone (**13**): Step 1 and the conversion of the monohydrazone (**13**) to the dihydrazone (**14**): Step 2. The figures highlighted in grey mirror that of experimental observations.

		Step 1							
		ΔE	ΔE_{solv}	ΔH	ΔH_{solv}	ΔS	ΔS_{solv}	ΔG	ΔG_{solv}
(12) to (13)		kJ/mol						kJ/mol	
Me-Me	diketone to Z	-39.15	-40.70	-23.32	-33.99	-0.017	-0.010	-18.13	-30.91
	diketone to E	-36.38	-49.80	-26.39	-42.02	-0.028	0.006	-18.01	-43.93
Ph-Ph	diketone to Z	-26.73	-28.90	-16.65	-24.58	-0.037	-0.033	-5.69	-14.87
	diketone to E	-18.03	-32.11	-7.03	-27.23	-0.025	-0.025	0.56	-19.85
Me-Ph	diketone to Z	-30.66	-30.57	-18.41	-27.26	-0.042	-0.038	-5.85	-15.95
	diketone to E	-32.42	-46.97	-19.17	-42.82	-0.034	-0.029	-8.93	-34.17
Ph-Me	diketone to Z	-33.87	-38.29	-24.16	-34.89	-0.040	-0.033	-12.33	-24.66
	diketone to E	-27.64	-43.18	-17.16	-38.78	-0.031	-0.028	-7.95	-30.35

		Step 2							
		ΔE	ΔE_{solv}	ΔH	ΔH_{solv}	ΔS	ΔS_{solv}	ΔG	ΔG_{solv}
(13) to (14)		kJ/mol						kJ/mol	
Me-Me	Z to ZZ	20.48	7.19	25.72	13.77	-0.033	0.003	35.58	13.01
	E to EE	-5.24	-11.87	6.15	-6.62	-0.017	-0.018	11.17	-1.29
	Z to EZ	7.70	-8.89	11.78	-3.78	-0.045	-0.017	25.31	1.17
	E to EZ	4.93	0.21	14.85	1.01	-0.035	-0.033	25.19	14.19
Ph-Ph	Z to ZZ	-7.93	-20.11	4.61	-13.82	-0.007	-0.009	6.84	-11.18
	E to EE	-7.95	-14.27	4.71	-9.98	-0.019	-0.032	7.55	-0.39
	Z to EZ	14.97	-4.88	27.80	1.35	-0.002	-0.016	28.39	5.98
	E to EZ	6.27	-1.67	18.18	4.00	-0.013	-0.023	22.14	10.96
Me-Ph	Z to ZZ	2.34	-13.75	11.97	-7.44	-0.011	-0.015	15.19	-2.88
	E to EE	-3.16	-10.98	6.02	-4.68	-0.011	-0.001	9.33	-4.46
	Z to EZ	-1.58	-21.78	7.70	-16.01	-0.013	-0.022	11.57	-9.34
	Z to ZE	-1.90	-18.29	7.57	-11.79	-0.008	-0.007	10.09	-9.71
	E to EZ	0.18	-5.37	8.46	-0.45	-0.021	-0.031	14.65	8.88
	E to ZE	-0.14	-1.89	8.34	3.78	-0.016	-0.016	13.17	8.51
Ph-Me	Z to ZZ	5.55	-6.03	17.72	-0.22	-0.013	-0.020	21.67	5.82
	E to EE	-7.94	-14.76	4.01	-8.72	-0.015	0.028	8.35	-8.27
	Z to EZ	1.63	-14.05	13.45	-8.79	-0.015	0.002	18.05	-0.64
	Z to ZE	1.31	-10.57	13.33	-4.56	-0.011	0.003	16.57	-1.01
	E to EZ	-4.60	-9.16	6.44	-4.49	-0.024	-0.017	13.67	5.06
	E to ZE	-4.92	-5.67	6.32	-0.27	-0.020	-0.016	12.19	4.69

It appears therefore that the difference in reactivity lies in the dihydrazone (**14**) formation, **Table 3.1**, **step 2**. The ΔG_{solv} values predict the formation of the (*EE*) isomer from the (*E*) in the dimethyl species **14(a)**, and the (*ZZ*) from the (*Z*) for the diphenyl **14(b)**. This is mirrored by the experimental observations in **Chapter 2**. However, the calculated thermodynamics are similarly favourable for the ‘unreactive’ molecule **13(c)**. This suggests that the non-reactivity is kinetic in origin.

Table 3.4 (*E*) to (*Z*) isomerisation barrier for all four monohydrazone derivatives

Derivative	(<i>E</i>)/(<i>Z</i>) isomerisation barrier kJ/mol
Me-Me 13(a)	43.3
Ph-Ph 13(b)	33.7
Me-Ph 13(c)	28.3
Ph-Me 13(d)	51.1

Turning to the kinetics, firstly the (*E*)/(*Z*) isomerisation barrier for the ‘non-reactive’ monohydrazone species **13(c)** is the lowest of all four of these derivatives, (28.3, 33.7, 43.3 or 51.1 kJ/mol for **13(c)**, **13(b)**, **13(a)** and **13(d)** respectively), so there is no reason to suggest that monohydrazone **13(c)** is locked in one isomeric form (*E*)/(*Z*). However, as we have seen the multipole analysis for **13(c)** predicts the reaction to be non-favoured (see **Figure 3.14**). There is no positive potential in the vicinity of the carbonyl group; it seems that this make nucleophilic attack of **13(c)** impossible.

3.5 Conclusions

A detailed computational study into the non-reactivity of the keto-monohydrazone, 1-phenyl-2-phenylhydrazone propan-1-one **13(c)** compared with other ketomonohydrazones **13(a)/(b)/(d)** was completed. The calculated thermodynamics suggest no reason why the dihydrazone **14(c)** cannot be formed. In addition, the calculations reveal that the keto-monohydrazone **13(c)** can undergo a facile (*E*) to (*Z*) isomerisation and is therefore not locked in one particular conformation.

The trend within the point charges study however, suggests that the carbonyl carbon may not be sufficiently ‘electropositive’ to interact with a phenylhydrazine molecule and therefore any encounters between phenylhydrazine and the keto-monohydrazone **13(c)** are unlikely to result in a reaction. The distributed multipole analysis further strengthens this claim as, irrespective of which conformation the keto-monohydrazone **13(c)** adopts, a positive potential adjacent to the carbonyl carbon atom is not observed (see **Figure 3.14**). For all of the ‘reactive’ keto-monohydrazones **13(a)/(b)/(d)**, there is at least one conformation or nearby soft mode, whereby a region of positive potential can be identified adjacent to the carbonyl group.

A detailed kinetic study examining the path from the keto-monohydrazone (**13**) to the dihydrazone (**14**) for these compounds, would involve three intermediates and four unique transition states. Such a large study is beyond the scope of this work. Nonetheless this study has identified the principles behind the observed reactivity. It is clear from this project that detailed analysis of reaction pathways using realistic computational methods remains an arduous task.

Prediction of regioselectivity of nucleophilic attack of hydrazines in sugar chemistry remains a significant challenge. Our findings suggest that where the reactivity is kinetically determined that multipole analyses of the ground state and nearby soft modes may have predictive value.

Chapter 4

Photochemical transformations of pyrrolo- 1,2,3-triazoles

4.1 Introduction

4.1.1 Pericyclic Reactions

Photochemistry is a branch of chemistry involving the use of light to promote chemical transformations. One of the main features of photochemistry is the promotion of electron(s) from their ground state to excited states. The electronic excited state of a species can exhibit a significantly different reactivity to that of its ground state. This high energy species is thus capable of participating in a number of different reactions as a result of the new electronic configuration.

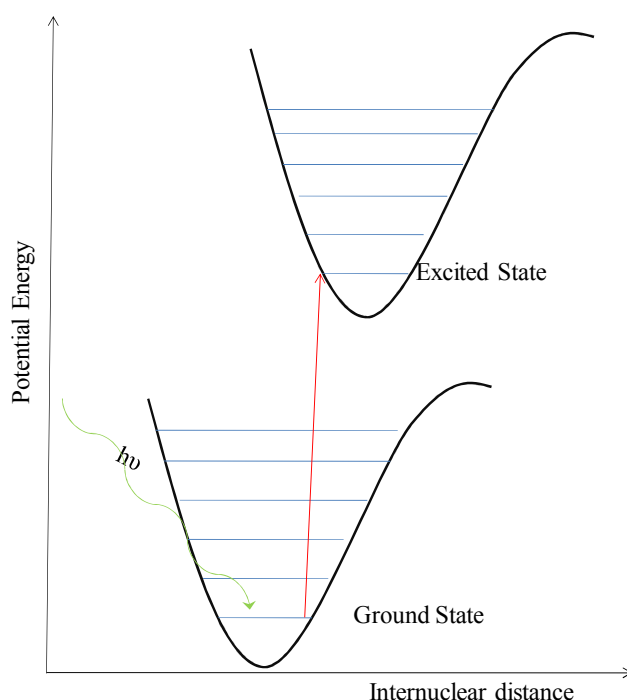


Figure 4.1 Promotion of an electron from its ground state to an excited state

There are a number of fates for the excited state species. Three of these are chemical routes; dissociation, electron transfer and isomerisation. Non-chemical routes of energy dissipation include luminescence and physical quenching. In the process of dissociation, a molecule AB is irradiated to form the excited state species, AB*, which then dissociates into two neutral fragments, A and B. Electron transfer differs in that the excited state species AB* can undergo a reaction that the ground state species (AB) could not. For example $AB^* + E \rightarrow AB^+ + E^-$. Although this example is of an *intermolecular* reaction involving two different species, it is possible to have an *intramolecular* reaction also, whereby a fragment of a molecule in the excited

state reacts with another part of the same molecule. The third possible chemical transformation afforded by light is an isomerisation reaction. Examples of this kind include **(E)-(Z)** (*cis-trans*) isomerisations e.g. the photochemical **(E)/(Z)** interconversion of stilbene.

In this chapter we are concerned with *intramolecular* rearrangements of bicyclic systems, or pericyclic reactions. Pericyclic reactions are defined by the IUPAC as ‘a chemical reaction in which concerted reorganisation of bonding takes place throughout a cyclic array of continuously bonded atoms.’ It may be viewed as a reaction proceeding through a fully conjugated cyclic transition state. In pericyclic reactions, orbital symmetry must be conserved during the reaction, as proposed by Woodward and Hoffman.¹¹¹

Taking buta-1,3-diene as an example to explain Woodward and Hoffman’s principle of conservation of orbital theory; if the terminal p_π orbitals have the positive phase lobes oriented in parallel with each other, then the cyclisation reaction will take place in such a manner that these lobes will overlap, also known as a ‘disrotatory’ ring closure. Alternatively, if the terminal p_π orbitals have the positive phase lobes oriented in opposite directions, the only way to attain a constructive overlap would be for the p orbitals to rotate in the same direction (conrotatory). The orientation of these lobes in the ground state is critical to the regioselectivity of both photochemical and thermochemical reactions.

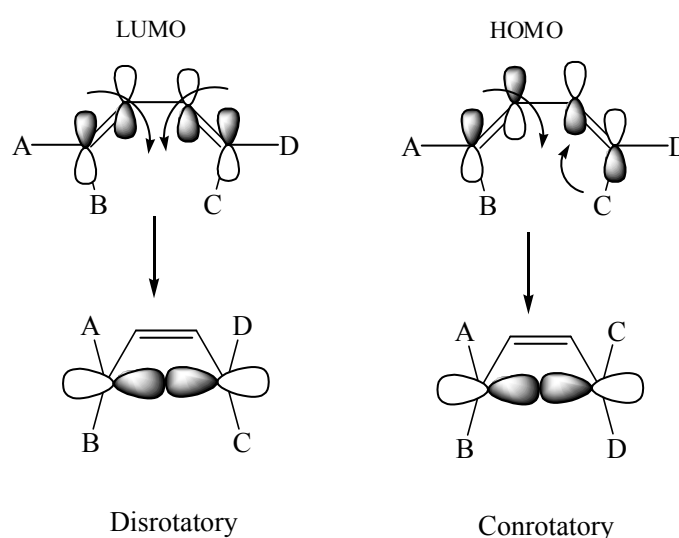
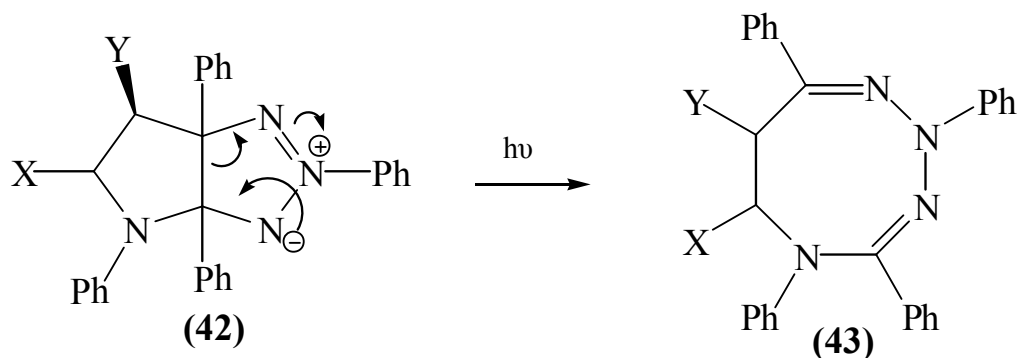


Figure 4.2 Disrotatory and conrotatory ring closure in buta-1,3-diene to form cyclobutene.

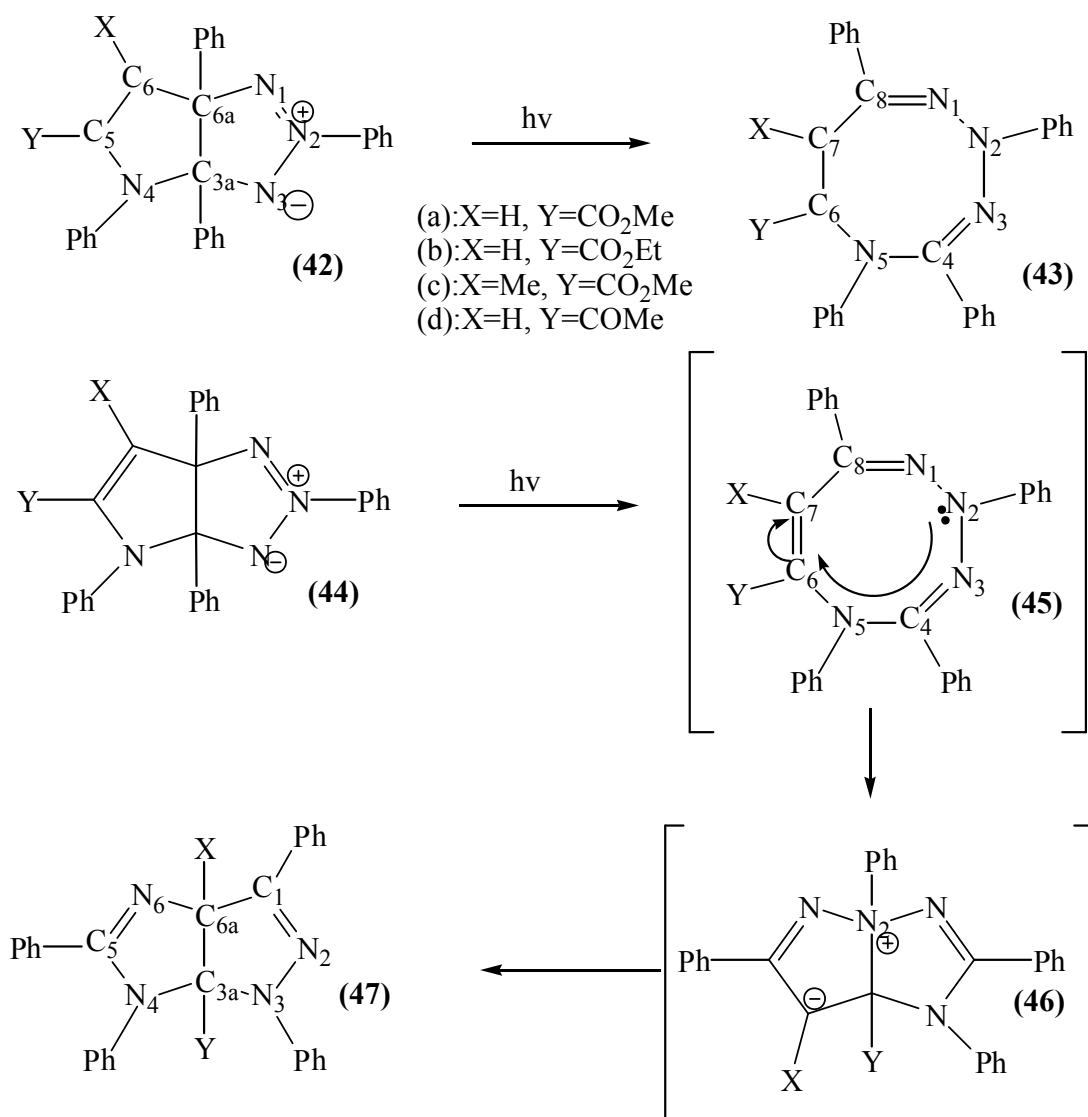
4.1.2 Photochemical excitation of pyrrolo-[2,3-*d*]-1,2,3-triazoles

In **Scheme 2.1**, the synthetic route to 2,5,6,7-tetrahydro-1,2,3,5-tetrazocines (**43**) was presented. The main step that is of interest in this chapter is the photochemical reaction where a pyrrolo[2,3-*d*]-1,2,3-triazole (**42**) is exposed to UV light causing a ring-opening reaction, to yield the 2,5,6,7-tetrahydro-1,2,3,5-tetrazocine (**43**).



Scheme 4.1 The transformation of a pyrrolo-[2,3-*d*]-1,2,3-triazole (**42**) into a 2,5,6,7-tetrahydro-1,2,3,5-tetrazocine (**43**).

The photochemical reaction presented in **Scheme 4.1** is an example of a disrotatory ‘ring opening’ reaction, involving the 4π electrons of the triazole ring. Irradiation of the hexahydro-pyrrolo-[2,3-*d*]-1,2,3-triazole (**42**) is our main entry route to the tetrahydro-1,2,3,5-tetrazocine (**43**).

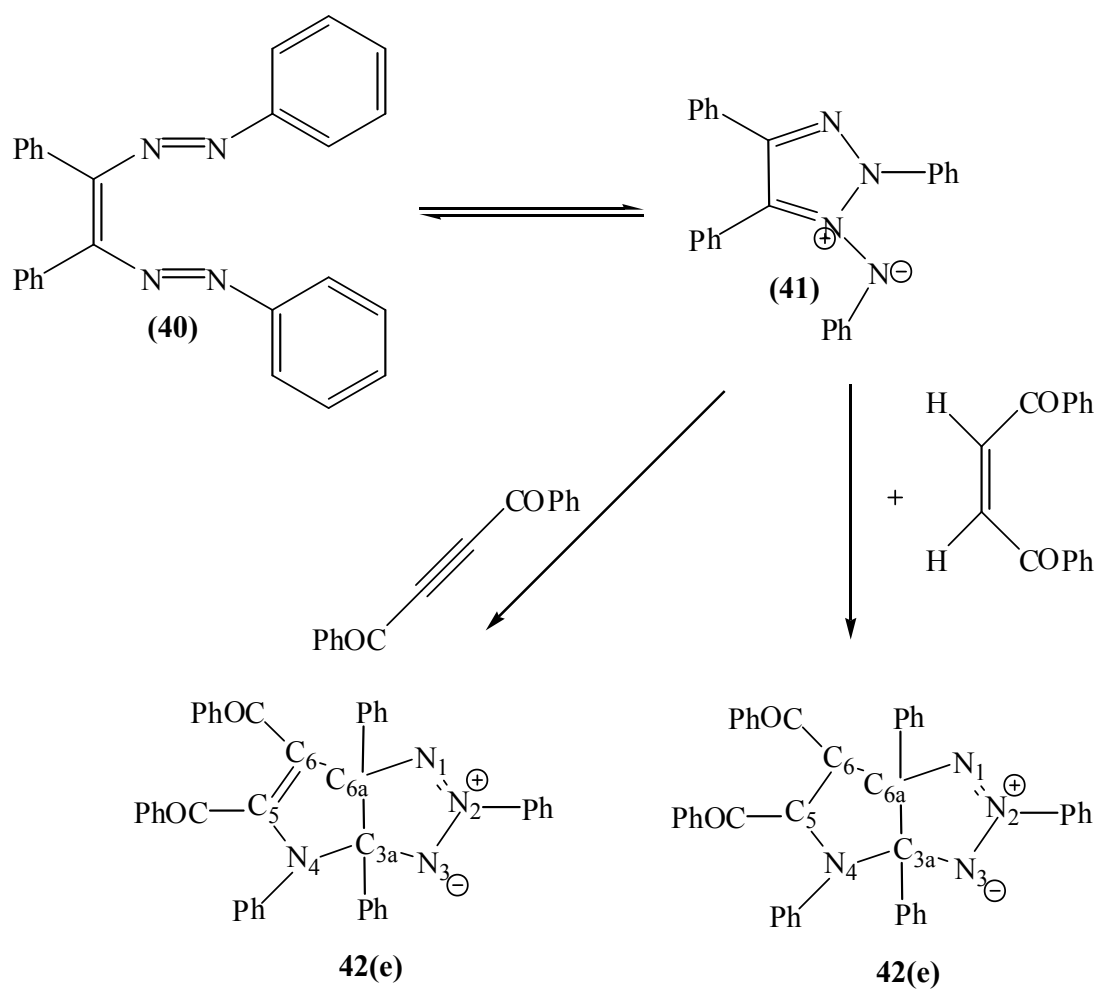


Scheme 4.2 2,5,6,7-tetrahydro-1,2,3,5-tetrazocine (**43**) formed by the irradiation of a pyrrolo-1,2,3-triazole (**42**) and an imidazo[4,5-*c*]pyrazole (**47**) formed *via* a 1,2,3,5-tetrazocine (**45**) intermediate.

A few examples of 2,5,6,7-tetrahydro-1,2,3,5-tetrazocines (**43**) have been prepared by James *et al*, with the substituents attached to C-7 of the eight-membered ring usually being ester or acyl functionalities **43(a)-(d)** (CO₂Me, CO₂Et, COMe).⁶ Our main aim for this chapter is to synthesise further novel 1,2,3,5-tetrazocine examples (**43**) to increase the library of these eight-membered ring compounds, by the routes indicated in **Scheme 4.2**. In addition, we wish to further explore the effect of substitution on the reactivity of the starting materials.

M.V.George *et al* reportedly synthesised the cycloadducts **42(e)** and **44(e)** by reacting different dipolarophiles with the 1,3-dipole (**41**) *see Scheme 4.3*.¹¹² One of our preliminary goals was to repeat this synthesis and subsequently transform the cycloadduct **42(e)** by photochemical means, into a novel 1,2,3,5-tetrazocine **43(e)**, using the methodology established by James *et al*,⁶ *Scheme 4.2*, which was shown to work for the substituent groups (**a**)-(d) indicated therein. The use of two electron withdrawing group will allow us to probe the effect of the frontier orbital electronic states on the ring-opening and subsequent stability of the products.

Specifically, according to the synthetic scheme provided in *Scheme 4.2*, if 5,6-dibenzoyl-2,3a,4,6a-tetraphenyl-3,3a,4,5,6,6a-hexahydro-pyrrolo-[2,3-*d*]-1,2,3-triazole **42(e)** were irradiated with UV light, the product of this reaction is expected to be 6,7-dibenzoyl-2,4,5,8,-tetraphenyl-2,5,6,7-tetrahydro-1,2,3,5-tetrazocine **43(e)**. On the other hand if the 5,6-dibenzoyl-2,3a,4,6a-tetraphenyl-3,3a,4,6a-tetrahydropyrrolo[2,3-*d*]-triazole **44(e)** were irradiated with UV light, the product of the reaction is expected to be an imidazo-[4,5-*c*]pyrazole (**47**), due to the additional unsaturation present in this cycloadduct **44(e)**.



Scheme 4.3 Synthesis of two cycloadducts **42(e)**/**44(e)** synthesised by M.V. George,¹¹² precursors to 1,2,3,5-tetrazocines.

4.2 Results

In the first section, **4.2.1**, the photochemical excitation of hexahydro-pyrrolo-[2,3-*d*]-1,2,3-triazoles (**42**) is described. In the second section, **4.2.2**, the photochemical excitation of tetraahydro-pyrrolo-[2,3-*d*]-1,2,3-triazoles (**44**) is described, *see Figure 4.2*.

4.2.1 Photochemical excitation of hexahydro-pyrrolo-[2,3-*d*]-1,2,3-triazoles (**42**)

To synthesise the novel eight-membered ring: 6,7-dibenzoyl-2,4,5,8,-tetraphenyl-2,5,6,7-tetrahydro-1,2,3,5-tetrazocine **43(e)**, the 5,6-dibenzoyl-2,3a,4,6a-tetraphenyl-3,3a,4,5,6,6a-hexahydro-pyrrolo-[2,3-*d*]-1,2,3-triazole **42(e)** was dissolved in dichloromethane and a UV spectrum was recorded, to ascertain the wavelength of max absorbance (λ_{max}). The λ_{max} for this compound was found to be 310 nm. Consequently the photoreactor was fitted with bulbs that emit in the region of 300-325 nm (*see Figure 4.3*), the details of this synthesis can be found in the experimental section.



Figure 4.3 Rayonet photochemical reactor (RPR-200) equipped with 16 RPR 3000Å lamps, used in the synthesis of 2,4,5,8,-tetraphenyl-2,5,6,7-tetrahydro-1,2,3,5-tetrazocines (**43**) and of imidazo-[4,5-*c*]pyrazoles(**47**).

The ^1H NMR spectrum of the starting material, 5,6-dibenzoyl-2,3a,4,6a-tetraphenyl-3,3a,4,5,6,6a-hexahydropyrrolo-[2,3-*d*]-1,2,3-triazole **42(e)** is presented in **Figure 4.4**. Thirty of the thirty-two protons are expected to appear in the aromatic region, the exception being the two aliphatic hydrogens, attached to C-5 and C-6. Apparently, only one of these resonances appears in the aliphatic region (4.9 ppm). Further analysis of the COSY spectrum (see **Figure 4.7**) reveals that this H is coupled with another at 6.7 ppm. Both H nuclei are adjacent to a benzoyl group (COPh), so both are expected to be shifted comparably downfield by this effect, however the ^1H attached to C-5 is neighbouring a nitrogen atom, which would have an additional shielding effect, so we assign this resonance to C-6.

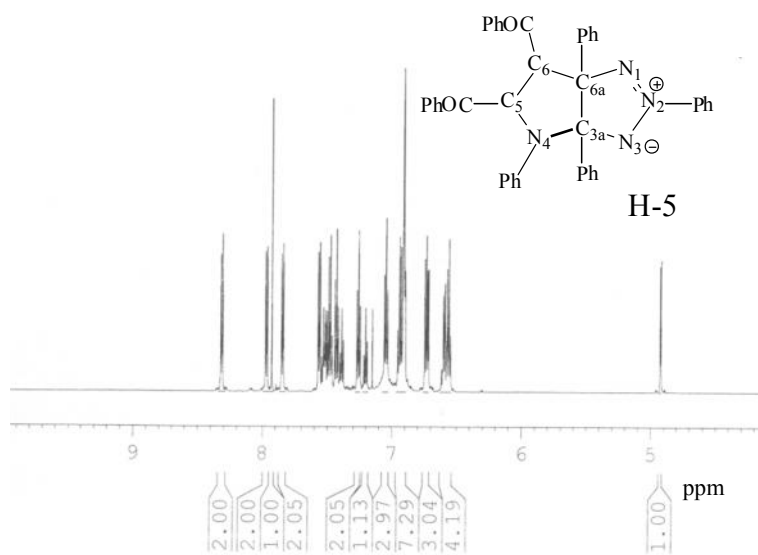


Figure 4.4 ^1H NMR spectrum of 5,6-dibenzoyl-2,3a,4,6a-tetraphenyl-3,3a,4,5,6,6a-hexahydropyrrolo[2,3-*d*]-1,2,3-triazole **42(e)**. All resonances are assigned; full details are in the experimental section.

The carbon spectrum for **42(e)** reveals two aliphatic resonances (61.53 and 65.52 /ppm) which are assigned to the C-5 and C-6 carbon atoms. The two signals at 89.50 and 102.49 ppm are assigned to the two bridgehead carbons (C3a/C6a). This is further verified by the fact that these two quaternary carbons are absent in the DEPT spectrum (see **Figure 4.6**). There are also two carbonyl carbon environments present at 189.10 and 198.74 ppm, which can be assigned to the two benzoyl groups attached to the ring.

The NMR analysis confirms the formation of 5,6-dibenzoyl-2,3a,4,6a-tetraphenyl-3,3a,4,5,6,6a-hexahydropyrrolo-[2,3-*d*]-1,2,3-triazole **42(e)**, with good purity. This is confirmed by the presence of a single spot in thin layer chromatography. This bicyclic system is our starting material for the photochemical step to the 1,2,3,5-tetrazocine (**43**).

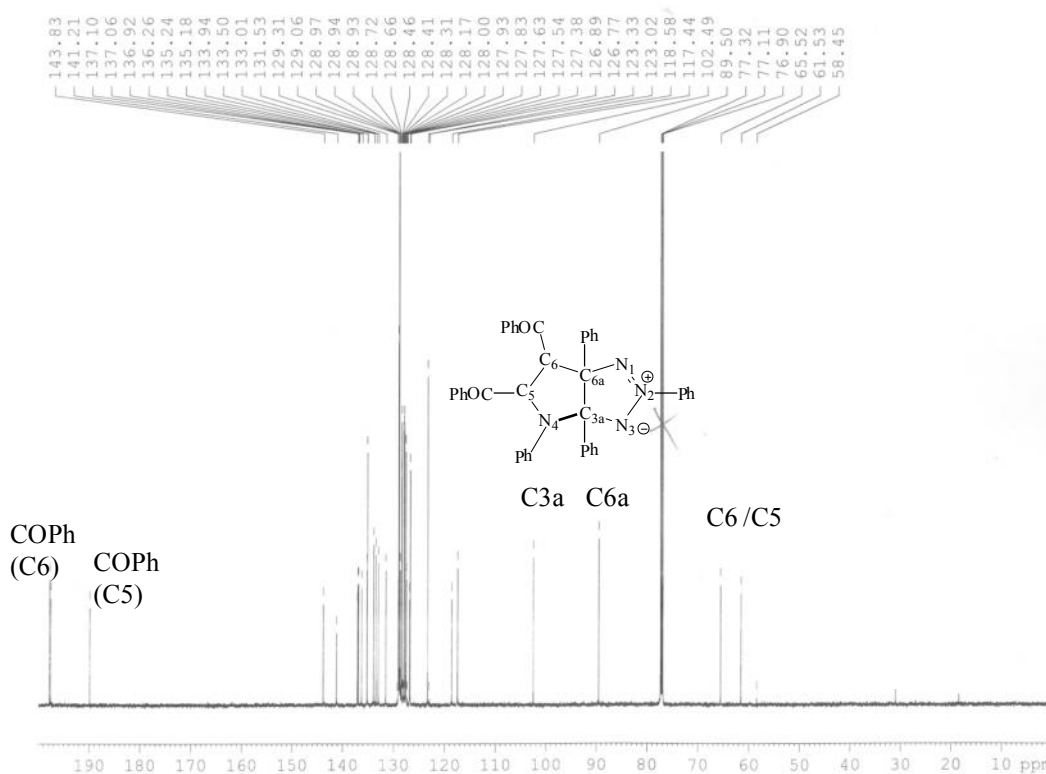
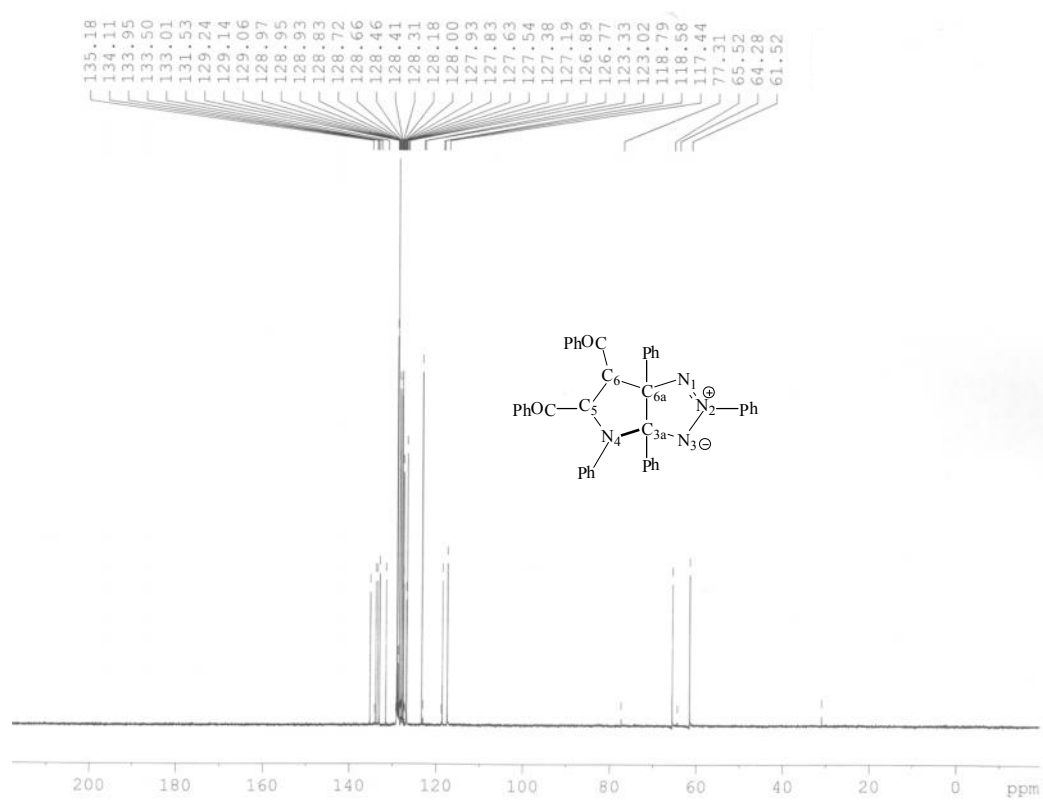


Figure 4.5 ^{13}C spectrum of 5,6-dibenzoyl-2,3a,4,6a-tetraphenyl-3,3a,4,5,6,6a-hexahydropyrrolo[2,3-*d*]-1,2,3-triazole **42(e)**.



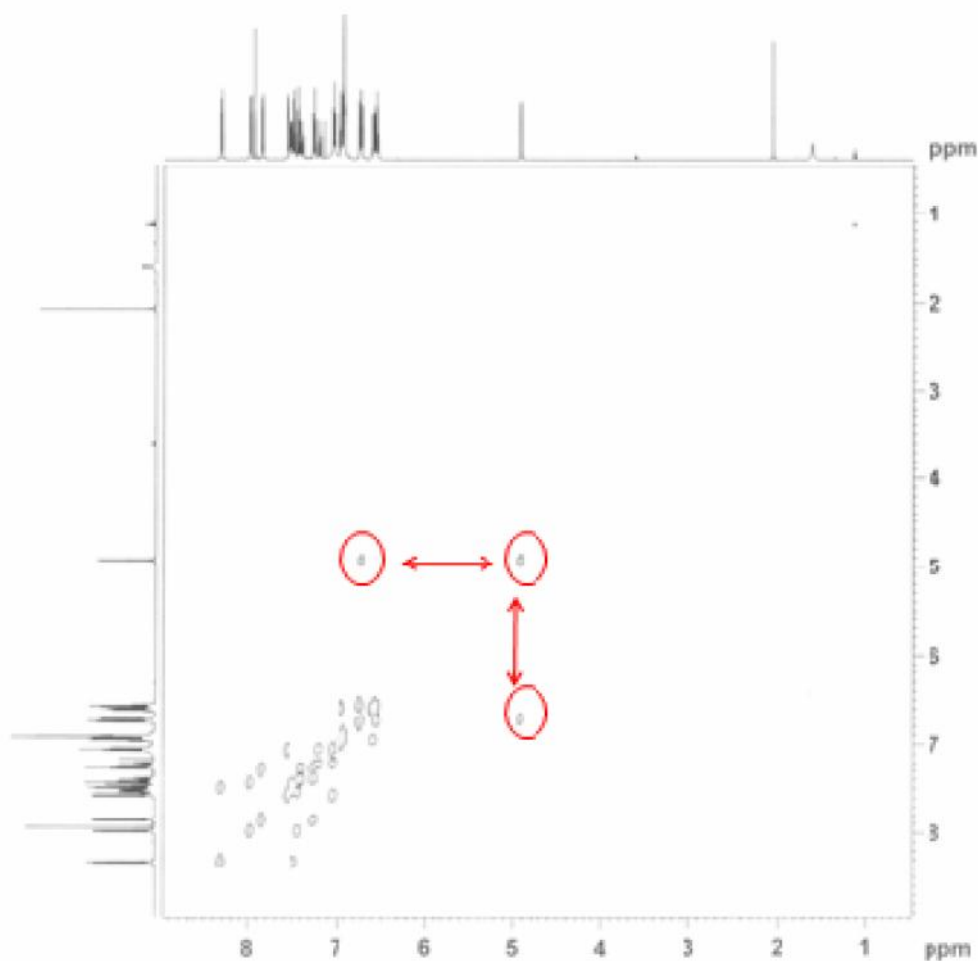


Figure 4.7 COSY spectrum of 5,6-dibenzoyl-2,3a,4,6a-tetraphenyl-3,3a,4,5,6,6a-hexahydropyrrolo[2,3-*d*]-1,2,3-triazole **42(e)**.

The next step was the photochemical irradiation of **42(e)**, in the hope of forming the eight-membered ring 1,2,3,5-tetrazocine, **43(e)**. The reaction was performed using the photoreactor in **Figure 4.3**. The expected product was formed, 6,7-dibenzoyl-2,4,5,8-tetraphenyl-2,3,6,7-tetrahydro-1,2,3,5-tetrazocine **43(e)**, as the NMR spectra reveal. In the ^1H NMR spectrum (**Figure 4.8**) some of the aromatic ^1H resonances appear slightly more upfield than normal for aromatics (6.5, 6.6 and 6.9 ppm). The aromatic protons are attached to the phenyl ring tethered to N(2) of the tetrazocine ring. In addition, this N(2) is neighbored by two nitrogen atoms, N(1) and N(3) and as a result, additional electron density is donated into the ring from the lone pair on nitrogen. This has an additional shielding effect for these nuclei, causing these resonances to appear more upfield than for normal aromatic ^1H nuclei. Examining the ^{13}C spectrum (**Figure 4.9**), the two ring carbons (C5 and C6) appear at 28 and 67

ppm respectively. The DEPT-135 spectrum (**Figure 4.10**) confirms the fact that these carbon resonances arise from methine groups. Mass spectrometry revealed a molecular ion at $M/z=624$, as expected, which further establishes this novel ring structure, demonstrating that the eight membered ring remains intact following the irradiation with UV light.

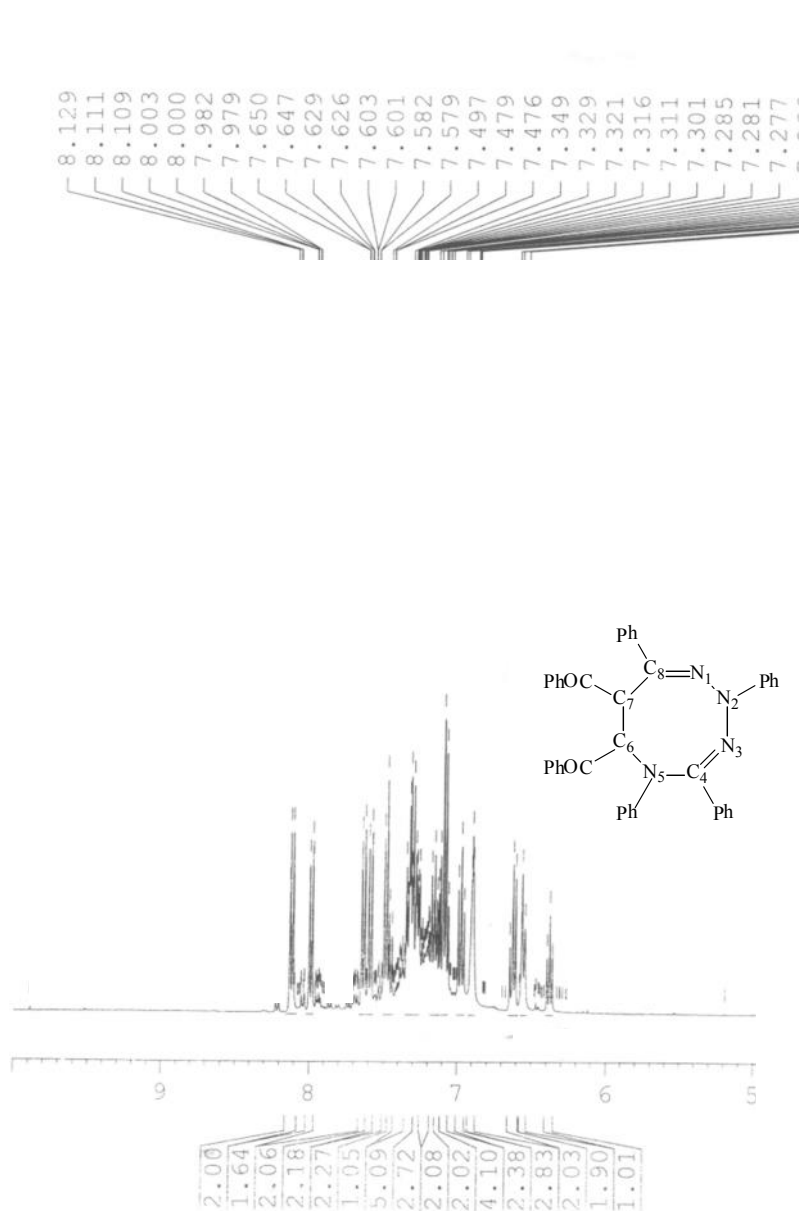


Figure 4.8 ^1H NMR spectrum of 6,7-dibenzoyl-2,4,5,8-tetraphenyl-2,3,6,7-tetrahydro-1,2,3,5-tetrazocine **43(e)**, indicating that only aromatic ^1H resonances are present.

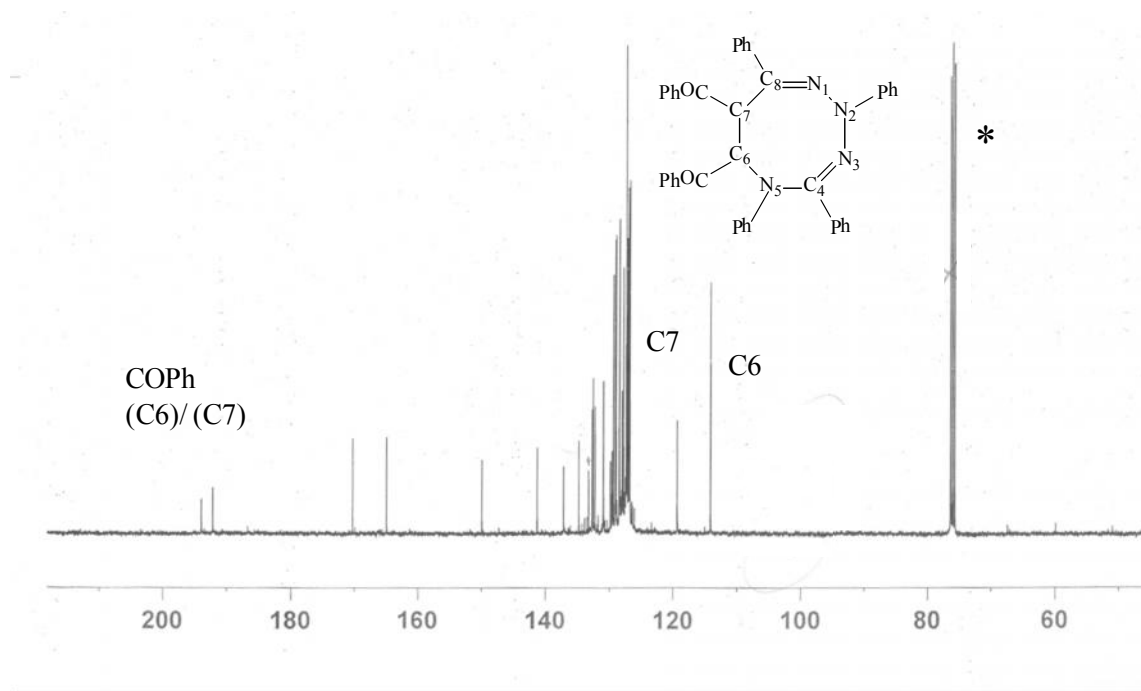


Figure 4.9 ^{13}C spectrum of 6,7-dibenzoyl-2,4,5,8-tetraphenyl-2,3,6,7-tetrahydro-1,2,3,5-tetrazocine **43(e)**

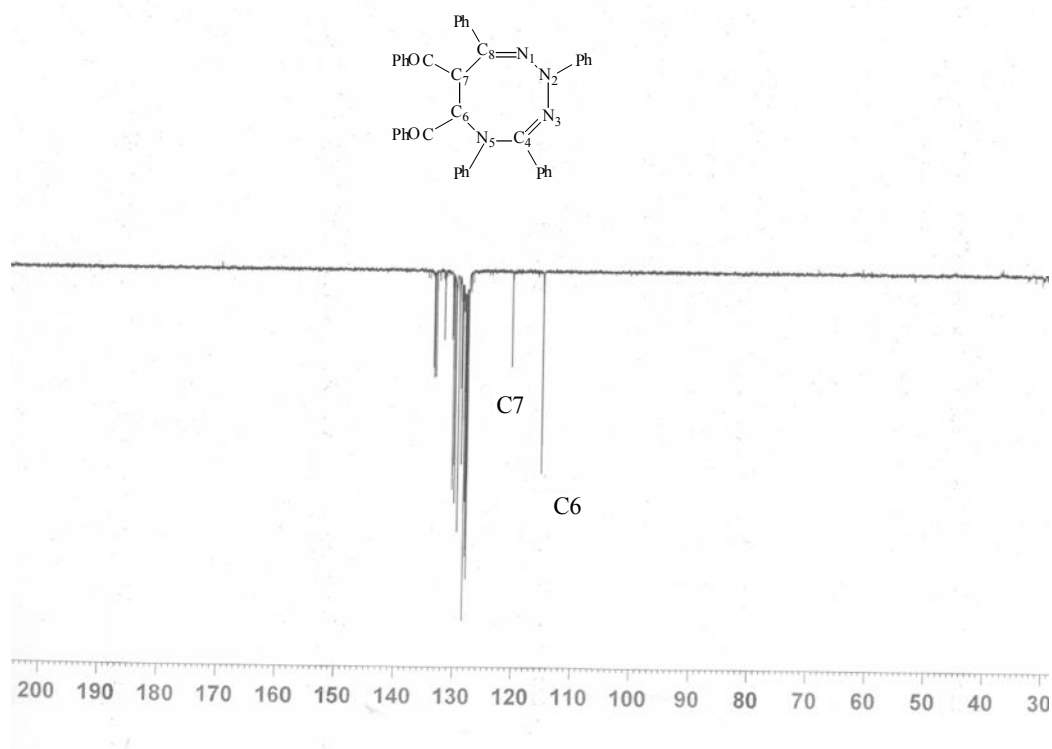


Figure 4.10 DEPT-135 spectrum of 6,7-dibenzoyl-2,4,5,8-tetraphenyl-2,3,6,7-tetrahydro-1,2,3,5-tetrazocine **43(e)**

As can be seen from the NMR spectra and from the singular spot in TLC, this material **43(e)**, is pure, stable and has a sharp melting point range in the range 112-114 °C. We found it was not possible to grow crystals for this material, however, although this may not be possible if the eight-membered ring is conformationally diverse, and can interconvert between conformations.

4.2.2 Photochemical excitation of tetrahydropyrrolo-[2,3-*d*]-1,2,3-triazoles (**44**)

Unlike (**42**), irradiation of tetrahydropyrrolo-[2,3-*d*]-1,2,3-triazoles (**44**) does not lead to the isolation of a 1,2,3,5-tetrazocine(**45**). An alternative product, 1,3a,6,6a-tetrahydroimidazo[4,5-*c*]-pyrazoles (**47**) was isolated, *see Scheme 4.2*. The imidazo-pyrazole species 3a,6a-dibenzoyl-1,3,5,6-tetraphenyl-1,3a,6,6a-tetrahydroimidazo[4,5-*c*]-pyrazole **47(e)** was synthesised using the same photo-reactor approach used for the 1,2,3,5-tetrazocine. Again, details of this synthesis are provided in the experimental section. The ¹H NMR spectrum of the imidazo-[4,5-*c*]-pyrazole is presented in *Figure 4.11*. In this spectrum, all the resonances are in the aromatic region, which is as expected, given that there are no ¹H attached directly to either ring of the bicyclic species **47(e)**. For this reason, full assignment is not possible from the ¹H spectrum alone.

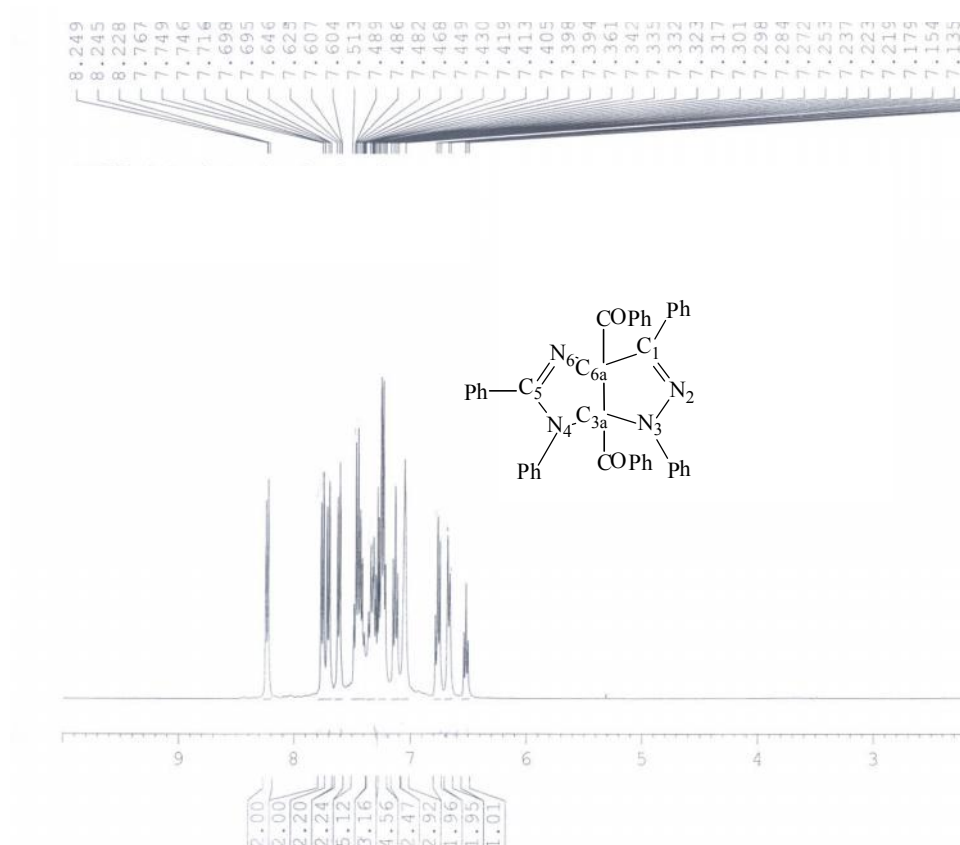


Figure 4.11 ¹H NMR spectrum (CDCl₃) of 3a,6a-dibenzoyl-1,3,5,6-tetraphenyl-1,3a,6,6a-tetrahydroimidazo[4,5-c]-pyrazole **47(e)**

In the ¹³C spectrum for 3a,6a-dibenzoyl-1,3,5,6-tetraphenyl-1,3a,6,6a-tetrahydroimidazo[4,5-c]-pyrazole **47(e)**, see **Figure 4.12**, two carbon resonances at 100.95 and 103.00 ppm can be observed, which are assigned to the two ring carbons C1 and C5 respectively. The signals at 115.13 and 120.36 ppm are the two bridgehead carbons, C3a and C6a, respectively. The absence of these resonances in the DEPT spectrum (**Figure 4.13**) confirms that they are quaternary carbons. The ¹³C resonances in the 121-142 ppm region are aromatic carbons. The two carbon signals that appear furthest downfield are the two carbonyl carbons at 193.48 and 195.27 ppm. These two quaternary carbons are also absent from the DEPT spectrum (**Figure 4.13**). Hence all the resonances (apart from the aromatic region) are assigned.

This material is of high purity, as can be seen by the presence of a single spot under TLC. The melting point of this compound is in a sharp range between 161-163 °C, which is in the expected melting point range for imidazo-[4,5-*c*]-pyrazoles.²

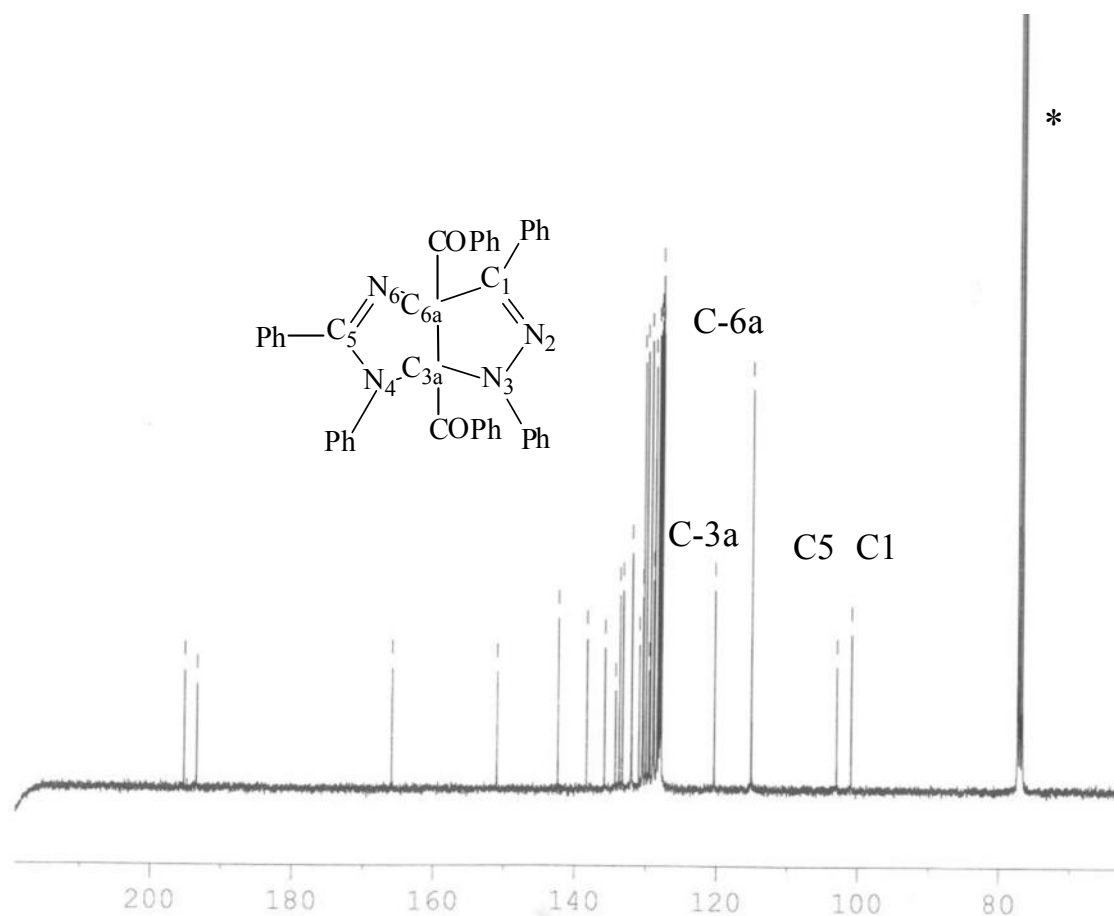


Figure 4.12 ¹³C spectrum (CDCl₃) of 3a,6a-dibenzoyl-1,3,5,6-tetraphenyl-1,3a,6,6a-tetrahydroimidazo[4,5-*c*]-pyrazole **47(e)**

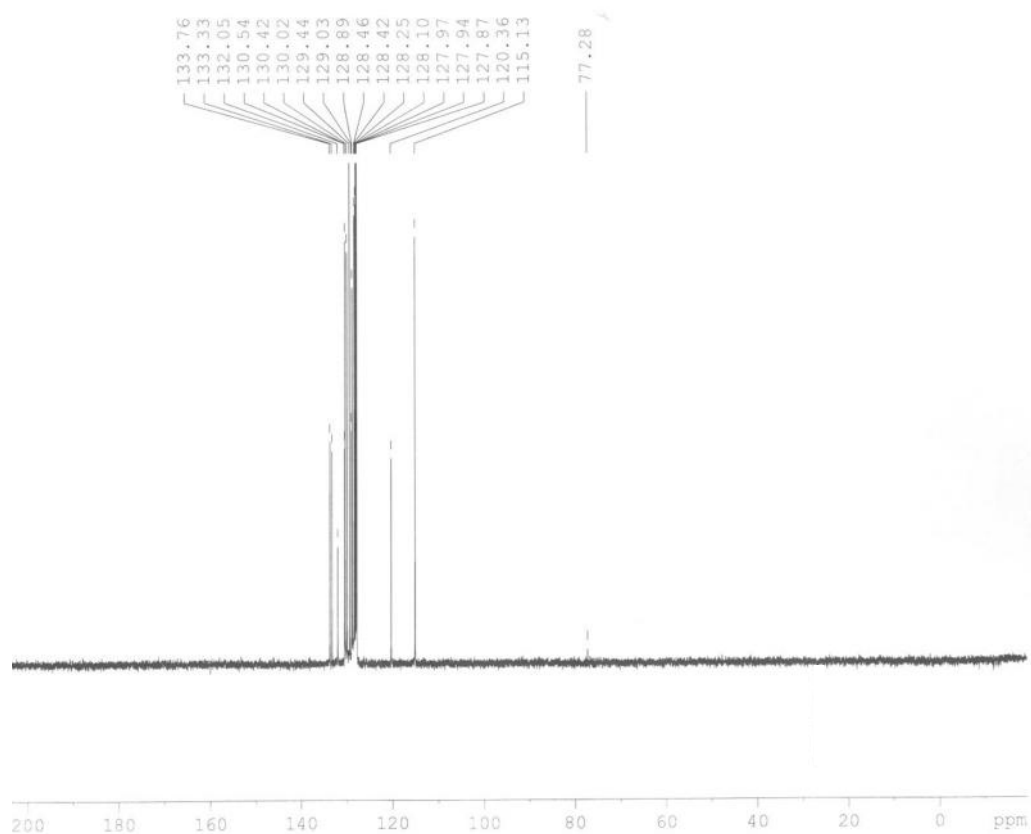


Figure 4.13 DEPT-135 spectrum (CDCl_3) of 3a,6a-dibenzoyl-1,3,5,6-tetraphenyl-1,3a,6,6a-tetrahydroimidazo[4,5-c]-pyrazole **47(e)**

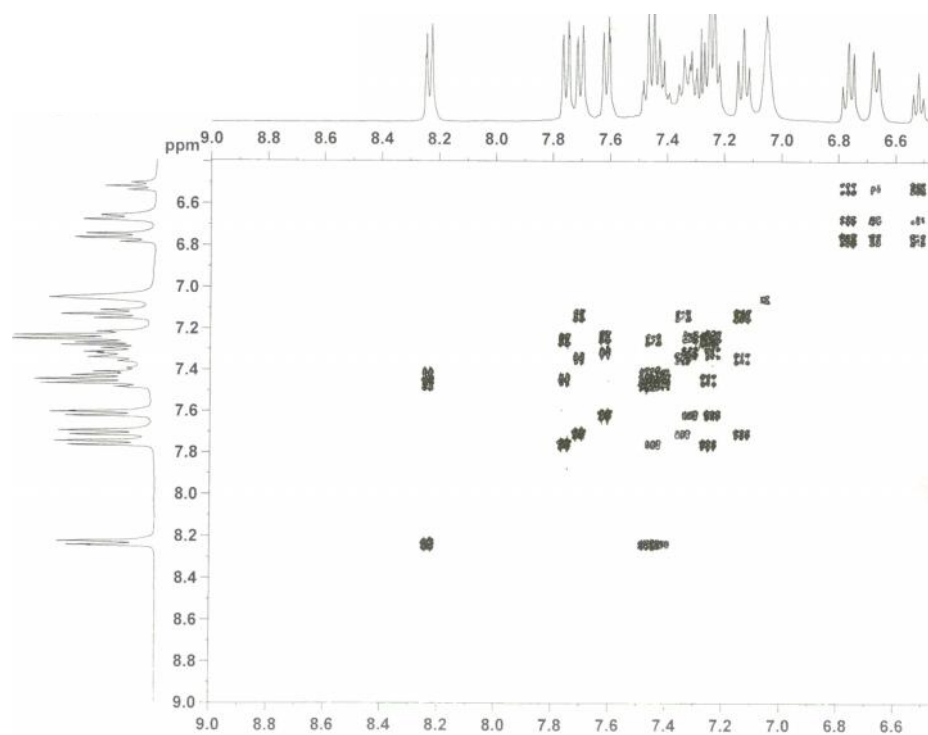


Figure 4.14 COSY spectrum (CDCl_3) of 3a,6a-dibenzoyl-1,3,5,6-tetraphenyl-1,3a,6,6a-tetrahydroimidazo[4,5-c]-pyrazole **47(e)**

4.3 Discussion

In the photochemical reaction of 5,6-dibenzoyl-2,3a,4,6a-tetraphenyl-3,3a,4,5,6,6a-hexahydro-pyrrolo-[2,3-*d*]-1,2,3-triazole **42(e)**, the main product was the novel 1,2,3,5-tetrazocine ring, **43(e)**, see *Scheme 4.2*. The 1,2,3,5-tetrazocine is accessed by a disrotatory ‘ring opening’ reaction, involving the 4π electrons of the triazole ring. In *Figure 4.15*, the p orbital arrangement for the ground state of the 1,2,3-triazole fragment of (**42**) is represented. If the 1,2,3,5-tetrazocine (**43**) could be accessed by thermal means, the bicyclic system (**42**) would need to undergo a conrotatory ring opening in order to generate the appropriate orbital orientation. This is not observed experimentally, as the phenyl rings would collide during the rotation of the ring opening mechanism.

Only the five p orbitals derived from the 1,2,3-triazole fragment are illustrated as these are the relevant frontier orbitals. As can be seen from this figure, irradiation of hexahydro-pyrrolo-[2,3-*d*]-1,2,3-triazole (**42**), promotes an electron from ψ_2 to ψ_3 . From ψ_3 , a disrotatory motion leads to the orientation of the p orbital lobes so that a bonding σ -interaction can occur.

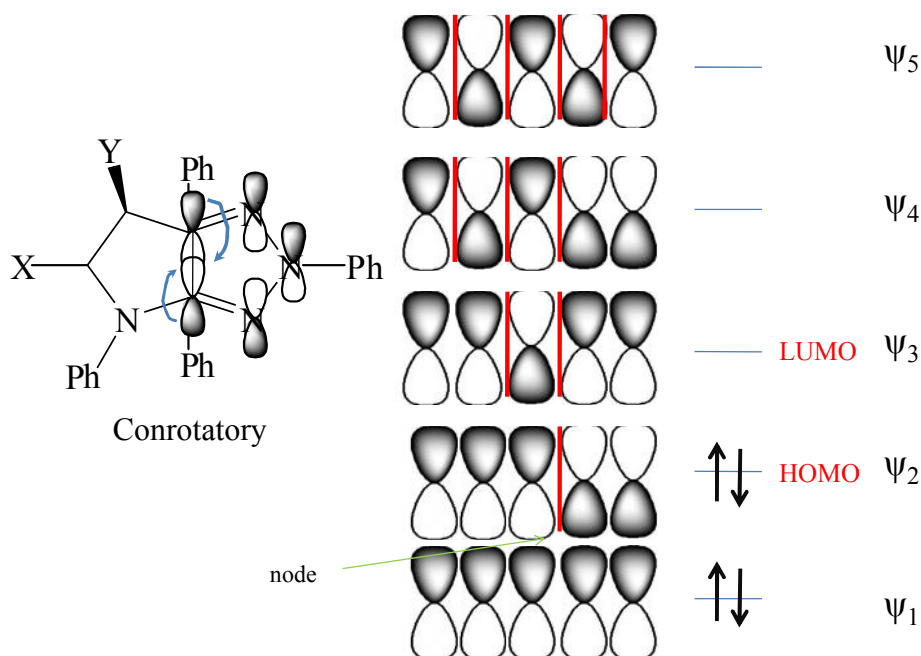


Figure 4.15 The five p orbitals that constitute the C=N-N-N=C fragment of the 1,2,3-triazole (**42**) in the ground state. If it were to undergo a ring-opening reaction to form the 1,2,3,5-tetrazocine (**43**) it would need to undergo a thermal conrotatory reaction.

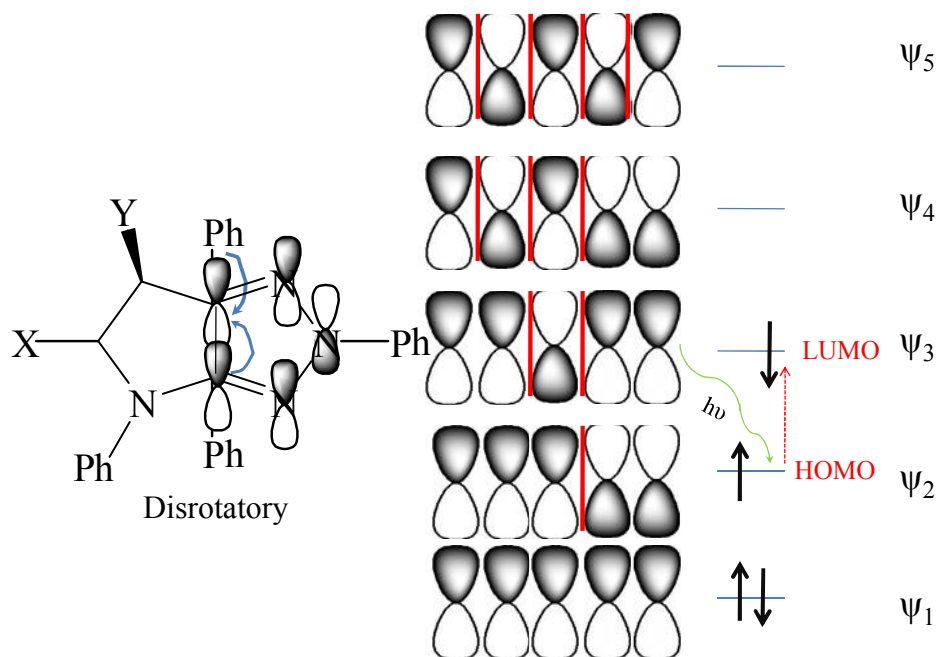


Figure 4.16 Five p orbitals that would constitute the C=N-N-N=C fragment of the 1,2,3-triazole of **(42)** in the excited state. If the 1,2,3,5-tetrazocine **(43)** is to be formed, a disrotatory ring opening reaction would need to take place.

The 1,2,3,5-tetrazocine **(43)** cannot be accessed by thermal means, as the bicyclic system **(42)** would need to undergo a conrotatory ring opening in order to generate the appropriate orbital orientation (see **Figure 4.16**). This is not possible however, as the phenyl rings would collide during such a rotation.

The 1,2,3,5-tetrazocine **(45)** was originally proposed by Butler *et al*² to be a reactive intermediate in the photorearrangement of substituted pyrrolo-[2,3-*d*]-1,2,3-triazoles **(44)** to substituted 1,3a,6,6a-tetrahydroimidazo-[4,5-*c*]pyrazoles **(47)**, see **Scheme 4.2**. James *et al* isolated a stable 1,2,3,5-tetrazocine itself, with the two criteria found for isolation being the presence of a saturated carbon at position C-6 of the eight-membered ring and an electron-withdrawing group present at position C-7 of the ring (substituent Y).⁶

In the photochemical rearrangement of the 5,6-dibenzoyl-1,3,5,6-tetraphenyl-3,3,4,6a-tetrahydropyrrolo-[2,3-*d*]-triazole **44(e)** it was only possible to form the imidazo-[4,5-*c*]pyrazole **47(e)**. James *et al* oxidised a 2,4,5,8-tetraphenyl-2,5,6,7-tetrahydro-1,2,3,5-tetrazocine **(42)**, see **Figure 4.17** which should initially form a

Chemical reaction scheme showing the synthesis of 1,2,4,5-tetraphenyl-1,2,4,5-tetrazine derivatives (47) from 1,2,4,5-tetraphenyl-1,2,4,5-tetrazine derivatives (42) via intermediate (43) and (44).

Structure (42) is a 1,2,4,5-tetraphenyl-1,2,4,5-tetrazine derivative with substituents X and Y. It is irradiated with UV light ($h\nu$) to form intermediate (43).

Structure (43) is a 1,2,4,5-tetraphenyl-1,2,4,5-tetrazine derivative with substituents X and Y. It is irradiated with UV light ($h\nu$) to form intermediate (44).

Structure (44) is a 1,2,4,5-tetraphenyl-1,2,4,5-tetrazine derivative with substituents X and Y. It is irradiated with UV light ($h\nu$) to form intermediate (45).

Structure (45) is a 1,2,4,5-tetraphenyl-1,2,4,5-tetrazine derivative with substituents X and Y. It is irradiated with UV light ($h\nu$) to form intermediate (46).

Structure (46) is a 1,2,4,5-tetraphenyl-1,2,4,5-tetrazine derivative with substituents X and Y. It is irradiated with UV light ($h\nu$) to form intermediate (47).

Structure (47) is a 1,2,4,5-tetraphenyl-1,2,4,5-tetrazine derivative with substituents X and Y.

Legend:

- (a): X=H, Y=CO₂Me
- (b): X=H, Y=CO₂Et
- (c): X=Me, Y=CO₂Me
- (d): X=H, Y=COMe

133

4.4 Conclusion

In keeping with previous experimental observations on photochemical excitations of pyrrolo-triazoles,⁶ if a hexahydropyrrolo-[2,3-*d*]-1,2,3-triazole (**42**) is irradiated, a tetrahydro-1,2,3,5-tetrazocine (**43**) is formed. George *et al* had previously reported the synthesis of 5,6-dibenzoyl-2,3a,4,6a-tetraphenyl-3,3a,4,5,6,6a-hexahydropyrrolo-[2,3-*d*]-1,2,3-triazole **42(e)**,¹¹² a novel cycloadduct and a precursor to a 1,2,3,5-tetrazocine. We have extended this work by photochemically transforming the cycloadduct into 6,7-dibenzoyl-2,4,5,8,-tetraphenyl-2,5,6,7-tetrahydro-1,2,3,5-tetrazocine **43(e)**, a novel eight-membered heterocycle. In the same work by George,¹¹² the formation of a cycloadduct with an additional unsaturation, 5,6-dibenzoyl-2,3a,4,6a-tetraphenyl-3,3a,4,6-tetrahydropyrrolo[2,3-*d*]-1,2,3-triazole **44(e)**, was reported. We formed the predicted photochemical product of this reaction also, a novel imidazo-pyrazole ring compound; 3a,6a-dibenzoyl-1,3,5,6-tetraphenyl-1,3a,6,6a-tetrahydroimidazo[4,5-*c*]-pyrazole **47(e)**.

In *Chapter 5*, a computational study on tetra-hydro-2,5,6,7-tetraphenyl-1,2,3,5-tetrazocines (**45**) and related compounds will be presented. The aim of that work is to assess the role, if any, of the tetrazocine in the synthetic route that leads to 1,3,5,6-tetraphenyl-1,3a,6,6a-tetrahydroimidazo-[4,5-*c*]-pyrazoles (**47**) and to investigate possible routes for the synthesis of stable eight-membered heterocycles.

4.5 Experimental

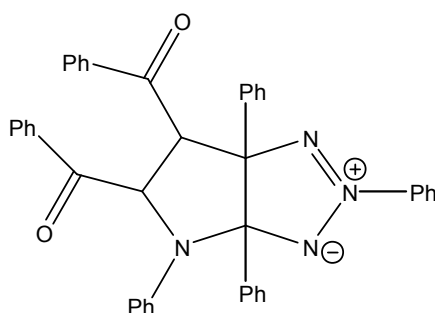
Infra-Red spectra were recorded on a Perkin-Elmer System 2000 FT-IR spectrometer. NMR spectra were recorded on a Bruker 400MHz spectrometer unless otherwise stated. Photoreactions were performed using a Rayonet Photochemical reactor (RP-200) equipped with 16xRPR 3000Å lamps.

Microanalytical and Crystallographic data were recorded by the Chemistry Department in University College Dublin, Belfield, Dublin 4.

Melting points were recorded on a Griffin Melting Point Apparatus.

4.5.1 Synthesis of hexahydropyrrolo[2,3-*d*]-1,2,3-triazoles

*Synthesis of 5,6-dibenzoyl-2,3a,4,6a-tetraphenyl-3,3a,4,5,6,6a-hexahydropyrrolo[2,3-*d*]-1,2,3-triazole 42(e)*



1.8 g of 1,2-bis(phenylazo)stilbene (0.0046 moles) were dissolved in 75 mLs of dry acetone. To this solution 1.1 g (0.0046 moles) of dibenzoyl ethene were added and the solution was allowed to reflux for 2 h. The solution was subsequently allowed to cool, after which time the solvent was removed by reduced pressure, yielding 2.4 g (0.0038 moles; **83% yield**) of the cycloadduct 5,6-dibenzoyl-2,3a,4,6a-tetraphenyl-3,3a,4,5,6-hexahydropyrrolo[2,3-*d*]-1,2,3-triazole.

M.p. 192-194 °C

MS: M_z 624

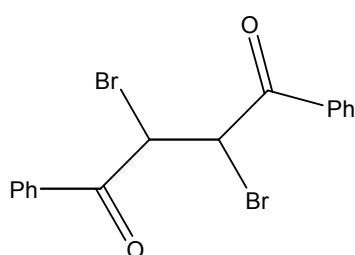
UV: λ_{\max} =318nm

^1H NMR (CDCl_3) (ppm): 4.93 (1H, d, $J=4\text{Hz}$), 6.60 (4H, m), 6.75 (3H, m), 6.94 (8H, m), 7.24 (1H, t, $J=5.2\text{Hz}$), 7.27 (2H, t, $J=5.2\text{Hz}$), 7.38 (1H, t, $J=5.2\text{Hz}$), 7.51 (3H, m), 7.57 (2H, d, $J=4.8\text{Hz}$), 7.59 (3H, m), 7.84, (2H, d, $J=8\text{Hz}$), 8.32 (2H, d, $J=8\text{Hz}$).

^{13}C NMR (CDCl_3) (ppm): 61.45 (C-H), 65.44 (C-H), 89.47, 102.42, 117.37, 118.53, 123.21, 126.73, 126.85, 127.51, 127.61, 127.90, 127.96, 128.39, 128.44, 128.67, 128.90, 128.93, 128.95, 129.04, 131.50, 132.98, 133.47, 133.94, 135.14, 135.18, 136.23, 136.88, 137.00, 137.06, 141.18, 143.76, 197.56 (C=O), 197.76 (C=O).

4.5.2 Synthesis of tetrahydropyrrolo[2,3-*d*]-1,2,3-triazoles

Synthesis of dibenzoyl-1,2-dibromoethane (precursor to dipolarophile)



1.18 g (5 mmol) of *trans*-dibenzoyl ethylene was dissolved in 20 mLs of acetic acid by warming the mixture slightly, and 0.8 g (5 mmol) of bromine was added to the solution dropwise. The mixture was stirred at room temperature for 1 h and consequently cooled to

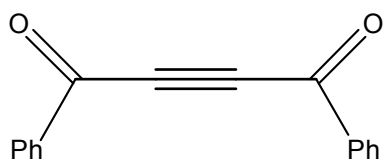
0° C. The resulting crystalline precipitate was filtered as a pale-yellow solid in quantitative yield.

M.p. 185-186 °C

^1H NMR (CDCl_3) (ppm): 5.98 (2H, s), 7.57 (4H, t, $J=7.2$ Hz), 7.69 (2H, t, $J=7.2$ Hz), 8.14 (4H, m, $J=7.2$ Hz).

^{13}C NMR (CDCl_3) (ppm): 41.17, 129.11, 133.96, 134.52, 190.64.

Synthesis of dibenzoylacetylene (dipolarophile)



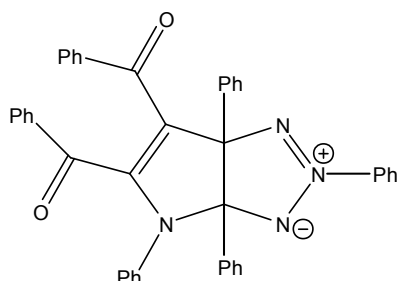
A solution of 1.4 g (3.54 mmol) of dibenzoyl-1,2-dibromoethane in 15 mLs of acetone and 0.75 g (7.4 mmol) of purified triethylamine was heated under reflux for 1 h. The precipitate

triethylammonium bromide was removed by filtration, and the solvent was evaporated under reduced pressure. The resulting orange-red residue was recrystallised from ethanol twice to give 0.66 g (**80% yield**) of a pale-yellow solid.

M.p. 109-110 °C

^1H NMR (CDCl_3) (ppm): 7.56 (6H, m), 8.21 (4H, d, $J=9.6$ Hz)

*Synthesis of 5,6-dibenzoyl-2,3a,4,6a-tetraphenyl-3,3a,4,6-tetrahydropyrrolo[2,3-d]-1,2,3-triazole **44(e)***



1.8 g (4 mmoles) of 1,2-bis(phenylazo)stilbene (**40**) were dissolved in 30 mLs of dry acetone and to this solution 1 g (4 mmoles) of dibenzoylacetylene were added. The solution was allowed to reflux for 3.5 h and after this time the solvent was removed by rotary evaporation, yielding 1.75 g (2.52 mmoles) of a bright yellow solid (**63% yield**).

M.p. 192-194°C

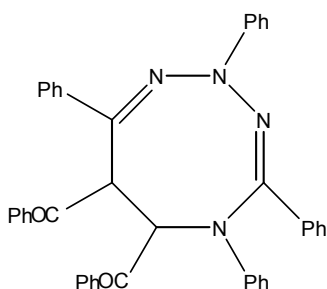
UV: λ_{max} =327nm

¹H NMR (CDCl₃) (ppm): 6.89 (3H, m), 6.91 (9H, m), 7.07 (2H, m), 7.21 (5H, m), 7.38 (1H, t, J=7.2Hz), 7.61 (4H, m), 7.64 (2H, m), 7.79 (2H, J=7.2Hz), 8.33 (2H, J=7.2Hz).

¹³C NMR (CDCl₃) (ppm): 92.92, 107.21, 117.23, 123.13, 125.90, 126.50, 127.09, 127.38, 127.44, 127.66, 127.82, 127.86, 128.10, 128.53, 128.60, 128.72, 128.77, 128.93, 128.97, 129.27, 130.71, 132.26, 132.49, 133.80, 135.55, 135.90, 136.45, 137.82, 140.31, 140.52, 161.78, 190.15, 190.48.

4.5.3 Synthesis of 1,2,3,5-tetrazocines

*Synthesis of 5,6-dibenzoyl-2,4,5,8-tetraphenyl-2,3,6,7-tetrahydro-1,2,3,5-tetrazocine **43(e)***



0.56 g (0.9 mmoles) of 5,6-dibenzoyl-2,3a,4,6a-tetraphenyl-3,3a,4,5,6,6a-hexahydropyrrolo[2,3-d]-1,2,3-triazole were dissolved in 150 mLs of dichloromethane and irradiated with 300 nm light for a period of 24 h. After this time the solvent was removed by reduced pressure, yielding an orange-red residue. This was recrystallised in a little warm diethyl

ether:cyclohexane mixture (1:1), yielding 0.32 g (0.5 mmol; **57% yield**) or an orange crystalline solid.

M.p. 112-114 °C

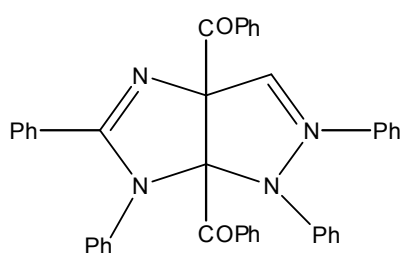
MS: M/z 624

^1H NMR (CDCl_3) (ppm): 6.56 (1H, m), 6.62 (2H, m), 6.97, (2H, t, $J=5.2$ Hz), 7.13 (3H, m), 7.17 (2H, m), 7.29 (2H, m), 7.30 (2H, m), 7.31 (2H, m), 7.32 (5H, m), 7.35 (1H, m), 7.48 (2H, d, $J=5.2$ Hz), 7.58 (2H, d, $J=5.2$ Hz), 7.63 (2H, d, $J=5.2$ Hz), 7.94 (2H, d, $J=5.2$ Hz), 8.11 (2H, d, $J=5.2$ Hz).

^{13}C NMR (CDCl_3) (ppm): 28.63 (C6) 67.54 (C7), 99.90, 101.80 114.07, 119.35, 126.78, 126.85, 126.87, 127.01, 127.11, 127.17, 127.26, 127.31, 127.44, 127.47, 128.34, 128.98, 129.32, 129.51, 129.88, 130.92, 132.26, 133.23, 134.76, 137.21, 141.29, 149.94, 164.93, 169.36, 192.32, (C=O), 194.18 (C=O).

4.5.4. Synthesis of imidazo-pyrazoles

Synthesis of 3a,6a-dibenzoyl-1,3,5,6-tetraphenyl-1,3a,6,6a-tetrahydroimidazo[4,5-c]pyrazole 47(e)



1.6 g (2.6 mmol) of 5,6-dibenzoyl-1,3,5,6-tetraphenyl-3,3a,4,6a-tetrahydropyrrolo[2,3-*d*]triazole **44(e)** were dissolved in 300 mLs of dichloromethane. The reaction mixture was placed in a Schlenk tube as in **Figure 4.3** and

subsequently illuminated with light of wavelength $\lambda=300\text{nm}$ for a duration of 3 h. After this time, the solvent was removed by reduced pressure and the residue was recrystallised in cyclohexane, yielding 1.31 g (2.13 mmol; **82% yield**) of a mustard-yellow solid.

M.p. 161-163 °C

^1H NMR (CDCl_3) (ppm): 6.52 (1H, t, $J=7.2$ Hz), 6.67 (2H, d, $J=8$ Hz), 6.78 (2H, t, $J=8.4$ Hz), 7.14 (3H, t, $J=7.6$ Hz), 7.22 (4H, m), 7.30 (3H, m), 7.41 (5H, m), 7.51

(2H, m), 7.62 (2H, d, J=7.2 Hz), 7.71 (2H, d, J=7.2 Hz), 7.76 (2H, d, J=7.2 Hz) 8.25 (2H, d, J=6.8 Hz) (all aromatic protons).

¹³C NMR (CDCl₃) (ppm): 100.95, 103.00 , 115.13 (C6a), 120.36 (C3a), 127.87, 127.94, 127.97, 128.10, 128.25, 128.42, 128.45, 128.89, 129.03, 129.44, 129.62, 130.02, 130.42, 130.54, 131.01, 132.05, 133.33, 133.75, 134.32, 135.86, 138.37, 142.42, 151.04, 165.97, 193.48, 195.27.

Chapter 5

***Ab initio* studies of 1,2,3,5-tetrazocines and related compounds**

5.1 Introduction

1,2,3,5-Tetrazocines are novel conformationally flexible eight-membered heterocycles. The aim of this chapter is to develop a better understanding of the energetics involved in the reactions leading to their formation, so as to better direct the future syntheses of these compounds. Dihydro-1,2,3,5-tetrazocines (**45**), as seen in *Scheme* 4.2, are not usually isolated following photochemical excitation of 5,6-dibenzoyl-1,3,5,6-tetraphenyl-3,3,4,6a-tetrahydropyrrolo-[2,3-*d*]triazole (**44**), but are thought to be an intermediate that rearranges to form the imidazo-[4,5-*c*]-pyrazole (**47**). To investigate the role of the tetrazocine in this reaction sequence we will examine the thermodynamic and kinetic barriers involved.

In order to accurately calculate reaction energy barriers, one needs to know all the conformations a molecule can adopt, in order to determine the lowest energy conformer. As this molecule is an eight-membered ring, it is desirable to review the literature on related cyclic systems. The structure for which the most physical data exists is cyclooctane, C₈H₁₈, which is not surprising given that it is the simplest eight-membered ring. Hendrickson's pioneering work on these medium-sized rings³⁴⁻³⁵ established nine conformations of cyclooctane and categorically subdivided these into three 'families'; crown, boat-boat and boat-chair. Further NMR work by Anet *et al*¹¹³ suggests that there are in fact four families of conformers, see *Figure 5.1*. The consensus that emerges from a large body of theoretical work performed on cyclooctane is that the boat-chair conformation is the most stable structure.¹¹³⁻¹¹⁸

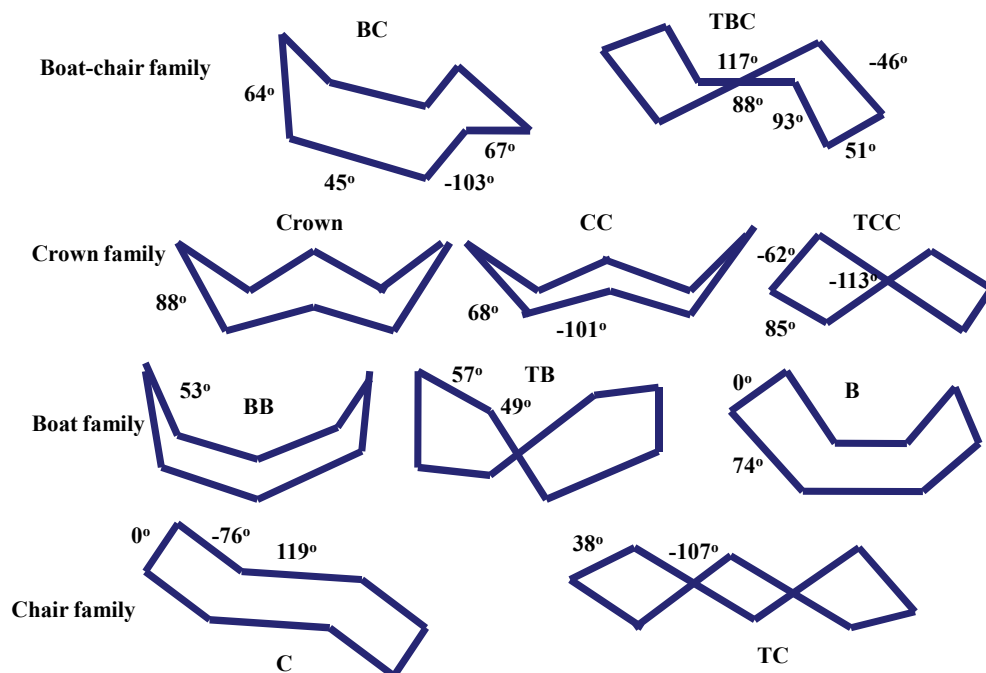


Figure 5.1 Conformations of cyclooctane as reported by Anet *et al.*,¹¹³ with the main torsional angles indicated.

The major conformational families located for cyclooctane by Anet *et al.*¹¹³ were:

- **Boat-chair family:** boat-chair, twist-boat-chair
- **Crown family:** crown, chair-chair, twist-chair-chair
- **Boat-family:** boat-boat, twist-boat, boat
- **Chair family:** chair, twist-chair

It is a challenging task to systematically search the PES of a cyclic molecule and successfully locate all possible configurations of that molecule. One method that has been developed to overcome this problem is that of torsional flexing.¹¹⁹ This is a stochastic/Monte Carlo procedure that involves a local torsional rotation about a ring bond, maintaining the original position of the majority of atoms in the ring. If the bonds between A–X and D–Y are cleaved, two fragments of the cyclic molecule remain. Subsequently atoms A, B and their substituents are rotated in one direction about the B–C bond, while D, C and its substituents are rotated in the opposite direction (see **Figure 5.2**). The ring is reformed accordingly, and the resulting

structure undergoes an energy minimisation. While this procedure primarily involves the perturbation of torsional space, both bond lengths and angles are also altered during the simulation. This search tool allows a large number of optimised structures to be located quickly for both cyclic and acyclic molecules.

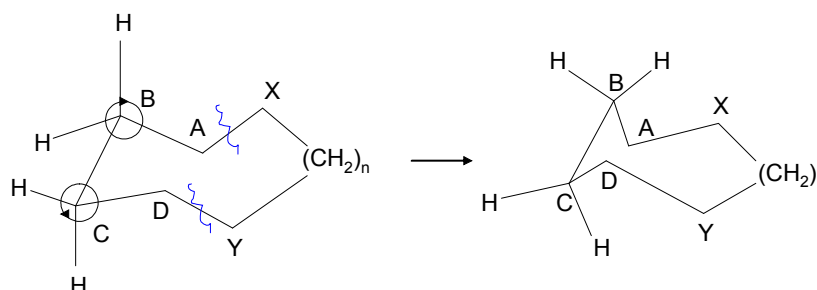
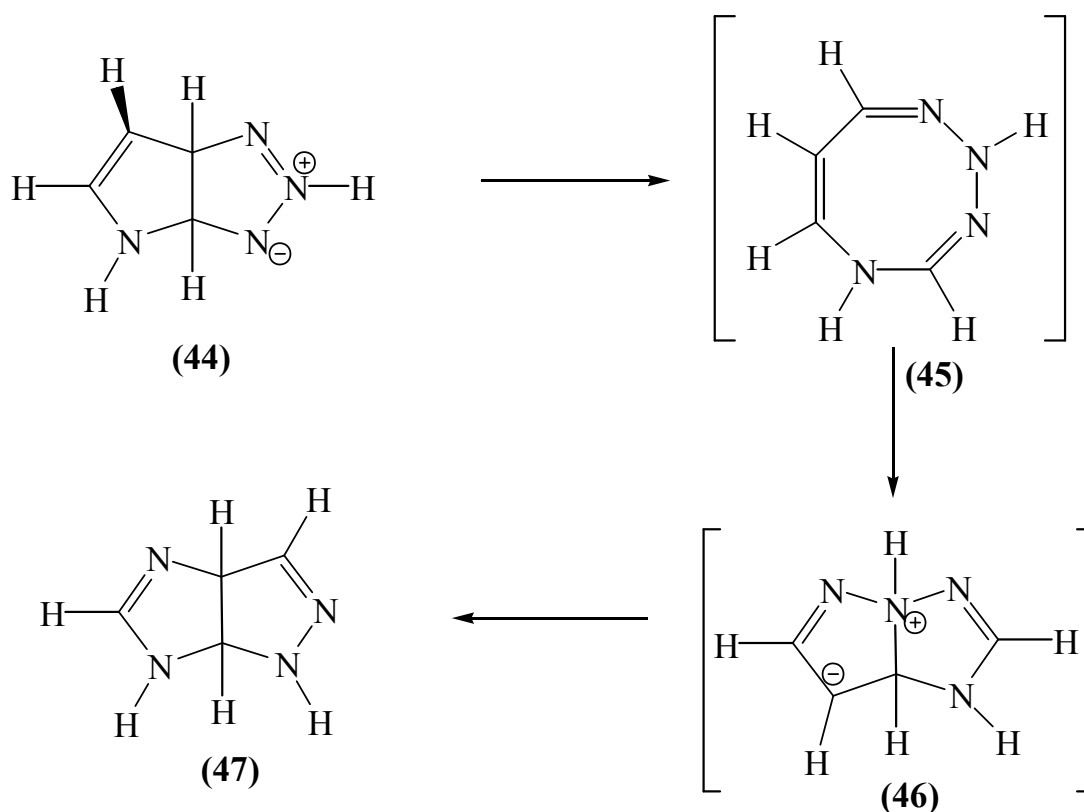


Figure 5.2 Torsional flexing procedure¹¹⁹

In an attempt to understand more about the physical properties of 1,2,3,5-tetrazocines and related molecules, the conformations, thermodynamic and kinetic driving forces of the sequence of reactions involving the dihydro-1,2,3,5-tetrazocine (**45**) as per *Scheme 4.2* were investigated. The species in this sequence of reactions with the largest number of conformers is dihydro-1,2,3,5-tetrazocine (**45**), an eight-membered ring. The computational effort that would be required for optimising a structure of this size, >52 atoms, is excessive. Consequently a set of hypothetical reactions for an underivatised 2,5-dihydro-1,2,3,5-tetrazocine were studied in detail, with the four phenyl groups and substituents X and Y in structures (**44**), (**45**), (**46**), (**47**) as per *Scheme 4.2* removed and replaced with hydrogens (see *Scheme 5.1*).



Scheme 5.1 Hypothetical synthesis of an underivatised imidazo-[4,5-*c*]pyrazole (**47**) from a pyrrolo-1,2,3-triazole (**44**) through a 1,2,3,5-tetrazocine intermediate (**45**)

Herein, we report molecular mechanics, ab initio and DFT calculations for the underivatised tetrazocine ring and investigate the conformations, thermodynamic and kinetic driving forces in these set of reactions and to investigate the role of 1,2,3,5-tetrazocines (**45**).

5.2 Computational methods

The conformations of the eight membered ring (**45**) were located using the ‘torsional flexing’¹¹⁹ algorithm at MM+ level within HyperChem V.7.1. The conformations that were located at this level were subsequently used as input geometries for calculations performed at ab initio (HF/3-21G) and DFT (B3LYP/6-31G(d)) level using the Gaussian ‘03 software package.⁷⁴ All stationary points were characterised by performing vibrational frequency analyses. Transition states were located using the QST3 method¹²⁰ in Gaussian ‘03 and IRC followings^{104,121} were performed to confirm that the transition states link the minima of interest on the PES.

5.3 Results and Discussion

5.3.1 Conformations of cyclooctane

The conformations of cyclooctane were explored using the torsional flexing procedure¹¹⁹ in Hyperchem V.7.1. Cyclooctane is a well-documented structure conformationally,¹¹³⁻¹¹⁸ so if the search procedure can locate the majority of the reported conformations for cyclooctane at a particular level of theory, it will validate the use of this method for investigating the conformations of dihydro-1,2,3,5-tetrazocine (**45**). **Figure 5.3** below shows the conformations for cyclooctane that were located at the MM+ level of theory using the torsional flexing procedure. As can be seen from this figure, the same four families for cyclooctane that were reported in the literature were identified for cyclooctane.¹¹³ Nine of the ten actual conformations were detected (the chair conformation was not detected at this level of theory). Most importantly, however, this method has detected the most stable conformations of cyclooctane (boat chair and crown). Optimising these structures at higher levels of theory has led to interesting results (*see Figure 5.4*).

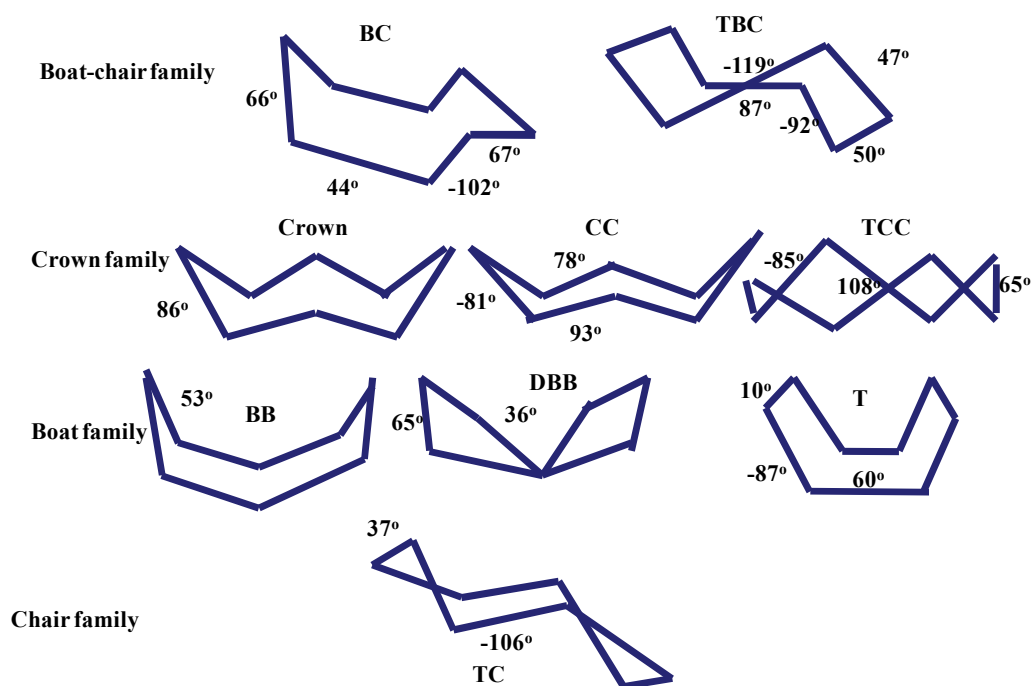


Figure 5.3 Conformations of cyclooctane located by the conformational search tool in Hyperchem (v.7.1) using the molecular mechanics force field. The main torsional angles are indicated.

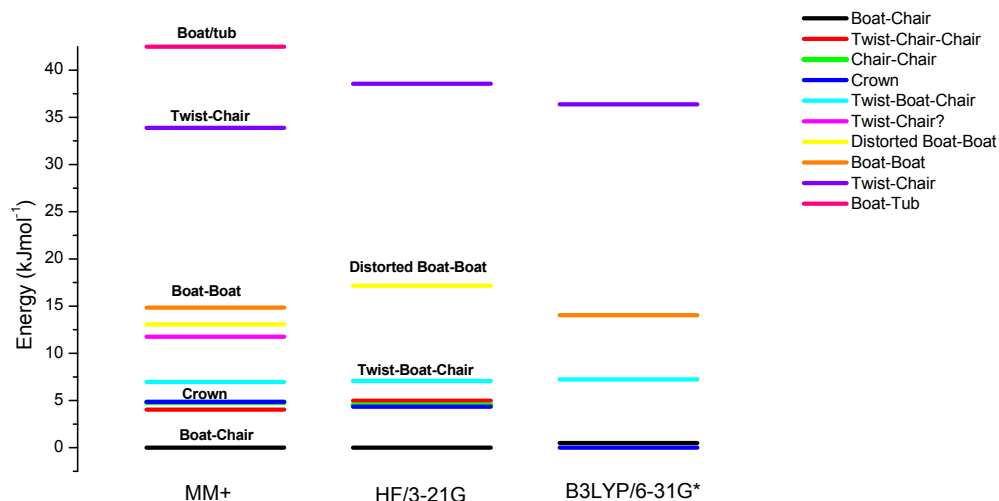


Figure 5.4 Conformations of cyclooctane calculated at three different levels of theory (MM+, HF/3-21G and B3LYP/6-31G(d)), including ZPE correction.

Fewer conformations were detected at higher levels of theory, but more notably, at the highest level of theory used (B3LYP/6-31G(d)), the crown conformation is found to be the global minimum for cyclooctane, albeit by a difference of 1 kJmol⁻¹ between the two conformers. As mentioned in the introduction, a large body of work has been performed on cyclooctane both experimentally and computationally.^{34,113-118,122-124} There is conflict in the literature as to the exact global minimum for cyclooctane (boat-chair/crown), presumably due to the fact that there are such small differences in energy between some conformations. Hence, a mixture of conformations may be observed at normal temperatures.¹¹⁷

As this torsional flexing procedure detected the majority of the conformations for cyclooctane, and most importantly detected the global minimum, this method was deemed a suitable procedure to locate minima for our eight-membered ring, dihydro-1,2,3,5-tetrazocine (**45**).

5.3.2 Conformations of dihydro-1,2,3,5-tetrazocine

The conformations of the eight-membered ring, dihydro-1,2,3,5-tetrazocine (**45**) were explored primarily using the molecular mechanics forcefield (MM+) using the conformational search procedure available within Hyperchem V.7.1. **Figure 5.5** illustrates the twenty stationary points located at this level of theory.

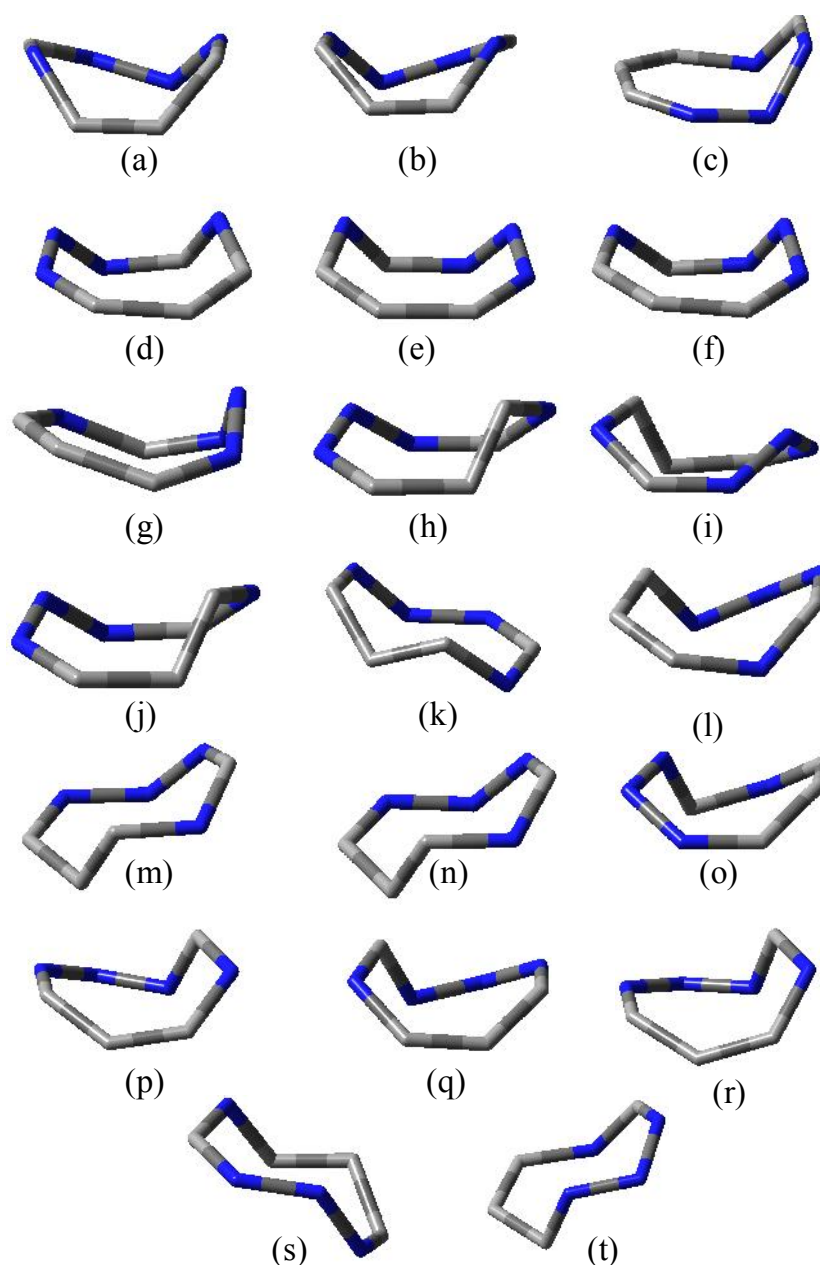


Figure 5.5 Conformations of dihydro-1,2,3,5-tetrazocines (**45**) located with molecular mechanics using the conformational search procedure, hydrogen atoms are omitted for clarity.

Although it may seem unusual that there are more stationary points for the 1,2,3,5-tetrazocine than for cyclooctane, in fact there are only six conformations for the tetrazocine. With the introduction of nitrogen atoms in the ring, slightly different phenomena are observed. Examining conformations **(d)**, **(e)** and **(f)**, it is apparent that the molecules possess the same general shape, although the nitrogen atoms are located at different vertices of the ring. This gives rise to different energies between the structures but we shall consider these to be of the same *conformational type*. *Nitrogen inversion* also gives rise to different, but closely related structures. Hence, structures **(m)** and **(n)** in **Figure 5.3** are not identical, due to the inversion of hydrogen atoms. Finally, this search procedure also located pairs of *enantiomers* on the potential energy surface. Structures **(p)** and **(q)** are mirror image representations of each other and is hence an enantiomeric pair on this potential energy surface. Hence the six conformational types are **(a,b)**, **(c,i,j,l)**, **(d,e,f,h)**, **(g)**, **(k,m,n,s,t)** and **(o,p,q,r)**.

The conformations located at MM+ were used as input geometries for calculations performed at the HF/3-21G and B3LYP/6-31G(d) levels. To ensure the potential energy surfaces at the ab initio and DFT levels were completely explored, the conformations that were located at HF/3-21G were optimised at B3LYP/6-31G* and vice-versa. Interestingly, the global minimum both at the HF/3-21G and B3LYP/6-31G(d) levels are the planar conformation (*see* conformation **(a)** in **Figure 5.6** and **Figure 5.7**), suggesting that it is a pseudo-aromatic species. Although there are three sets of double bonds (6π electrons), satisfying the Hückel number of electrons ($4n+2$, $n=1$), the double bonds are not conjugated throughout the ring, and therefore the molecule cannot be deemed ‘aromatic’ in character as the ‘ring current’ cannot circulate entirely around the ring. However, it is highly unlikely that the derivatised tetrazocine molecule is planar. The steric hindrance arising from forcing the four phenyl groups to be in close proximity would result instead in deformation of the central ring. **Figure 5.7** illustrates the conformations of the 1,2,3,5-tetrazocine optimised at B3LYP/6-31G(d) level.

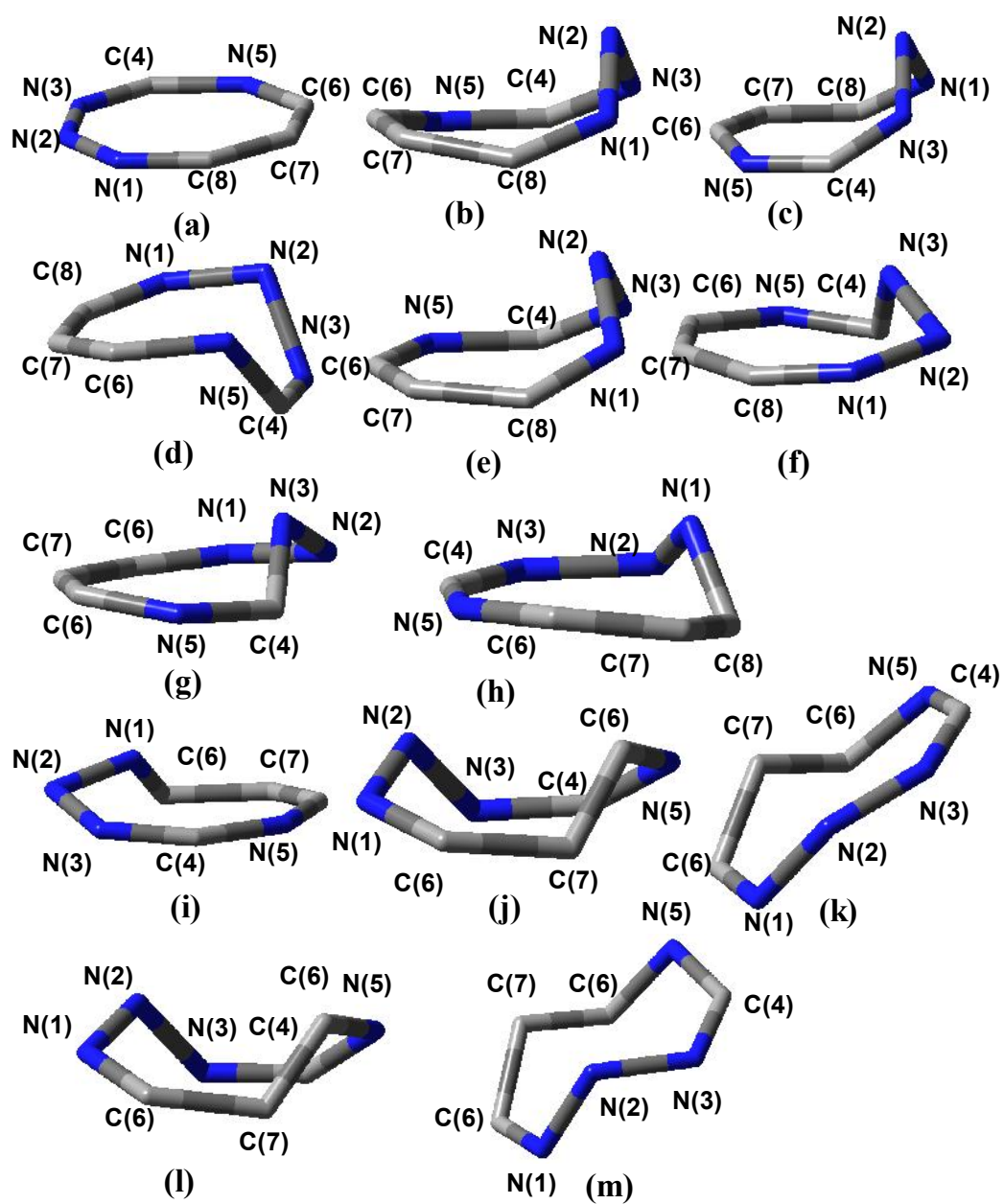


Figure 5.6 Conformations of the 1,2,3,5-tetrazocine (**45**) at the HF/3-21G level (hydrogens not shown for clarity)

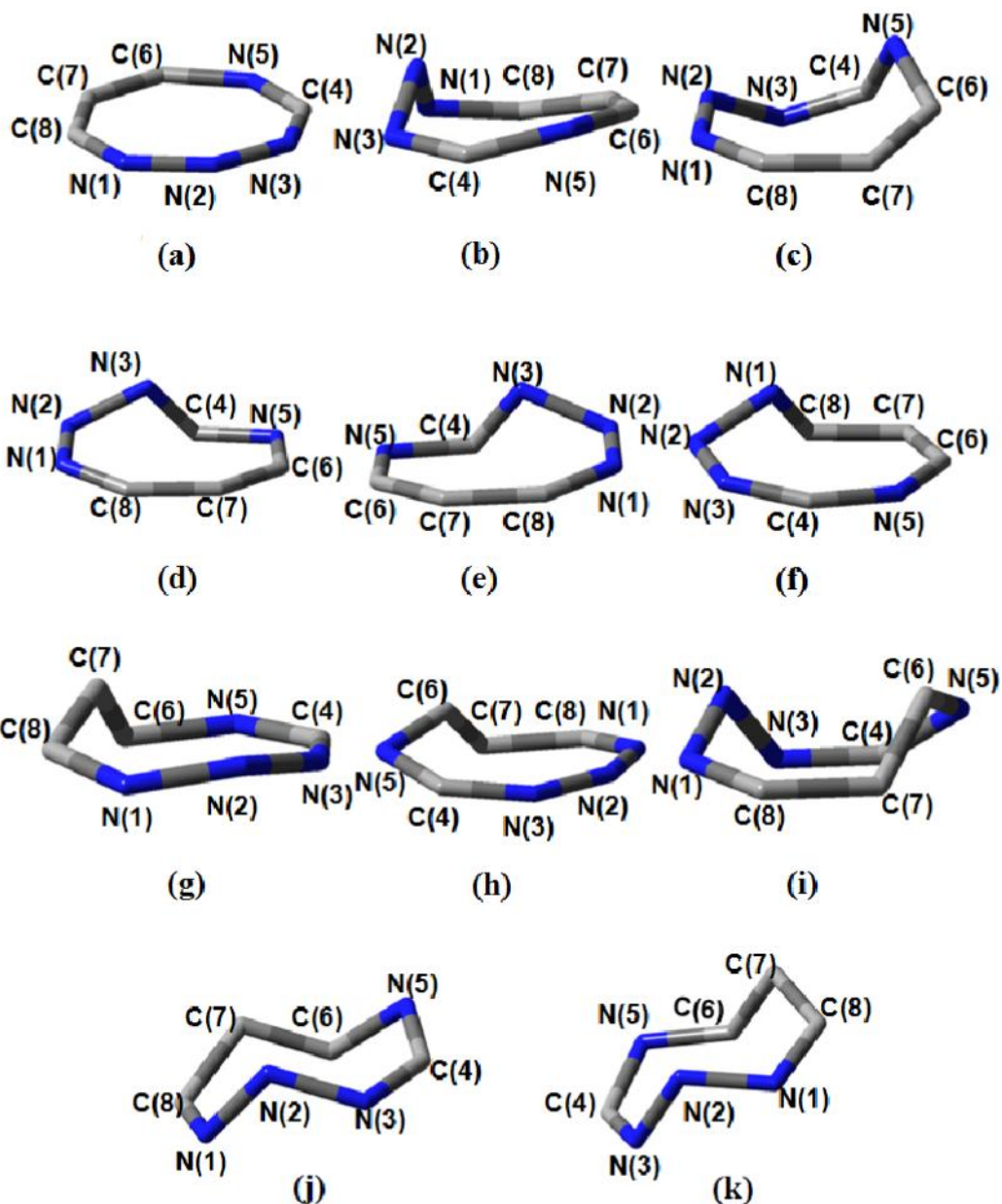


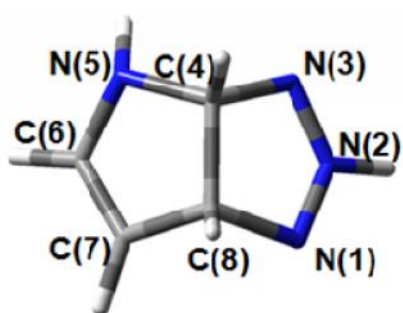
Figure 5.7 Conformations of the 1,2,3,5-tetrazocine (**45**) at B3LYP/6-31G(d) level (hydrogens not shown for clarity)

An eight-membered ring containing one nitrogen atom, azocane, $C_7H_{15}N$, has also been studied by NMR, with the boat-chair and crown being the most dominant forms of this molecule.¹²⁵ There are no boat-chair conformations for our dihydro-1,2,3,5-tetrazocine (**45**), although this is not an unusual result as this eight-membered ring possesses three double bonds throughout the ring, so it may not be capable of adopting some of the conformations observed for saturated eight-membered rings.

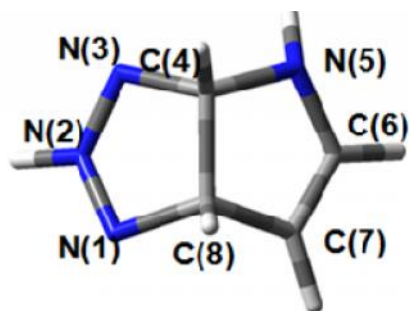
5.3.3 Conformations of bicyclic species (44),(46),(47)

In **Scheme 4.2**, the precursor to the dihydro-1,2,3,5-tetrazocine, the pyrrolo-triazole (**44**) and the subsequent intermediate (**46**) and imidazo-[4,5-*c*]-pyrazole (**47**) species are bicyclic structures and as such, are not as conformationally diverse as the dihydro-1,2,3,5-tetrazocine (**45**) due to the fused nature of these molecules. For completeness however, these structures were subjected to a conformational search at MM+ level, to thoroughly explore the potential energy surface. Six stationary points were located for the pyrrolo-[2,3-*d*]-1,2,3-triazole (**44**) at MM+ level, although some of these stationary points are simply variations of one of two conformations, a chair conformation and a more stable ‘bi-planar’ species. As can be seen from **Figure 5.8**, these six stationary points were also located at the B3LYP/6-31G(d) level. Structures **44(a)/(b)** and **(c)/(d)** are enantiomeric pairs, whereas **44(a)** and **(c)** are related to each other by *nitrogen inversion* at N(5). Furthermore, structures **44(e)** and **(f)** are of the same *conformational type*, with the nitrogen atoms occupying different vertices of the ‘chair’ conformation.

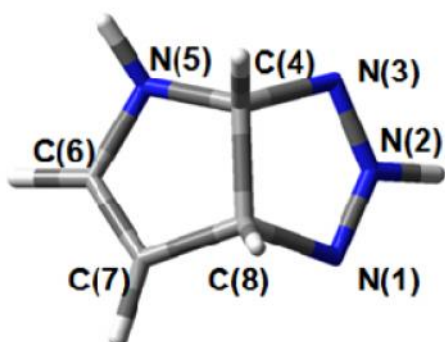
The same approach was applied to locate the conformations of other two bicyclic species involved in this reaction sequence, the intermediate (**46**) and the observed product of the reaction, the imidazo-[4,5-*c*]-pyrazole (**47**). These conformations were subsequently optimised at the HF/3-21G and B3LYP/6-31G(d) level. The same minima were located at each level, so only the structures for the B3LYP/6-31G(d) level are shown (*see Figure 5.9*).



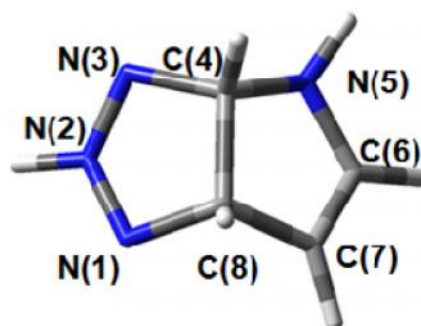
44(a)



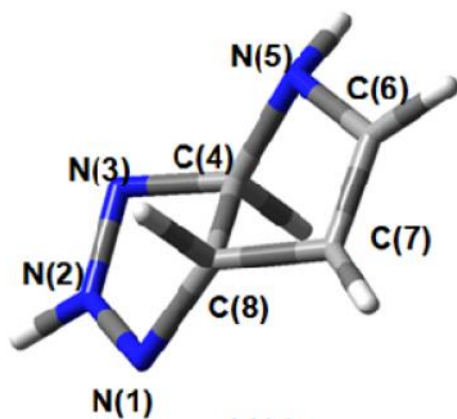
44(b)



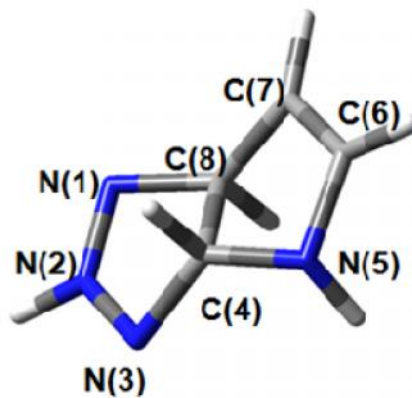
44(c)



44(d)



44(e)



44(f)

Figure 5.8 Conformations of the pyrrolo-triazole (**44**) optimised at B3LYP/6-31G(d) level

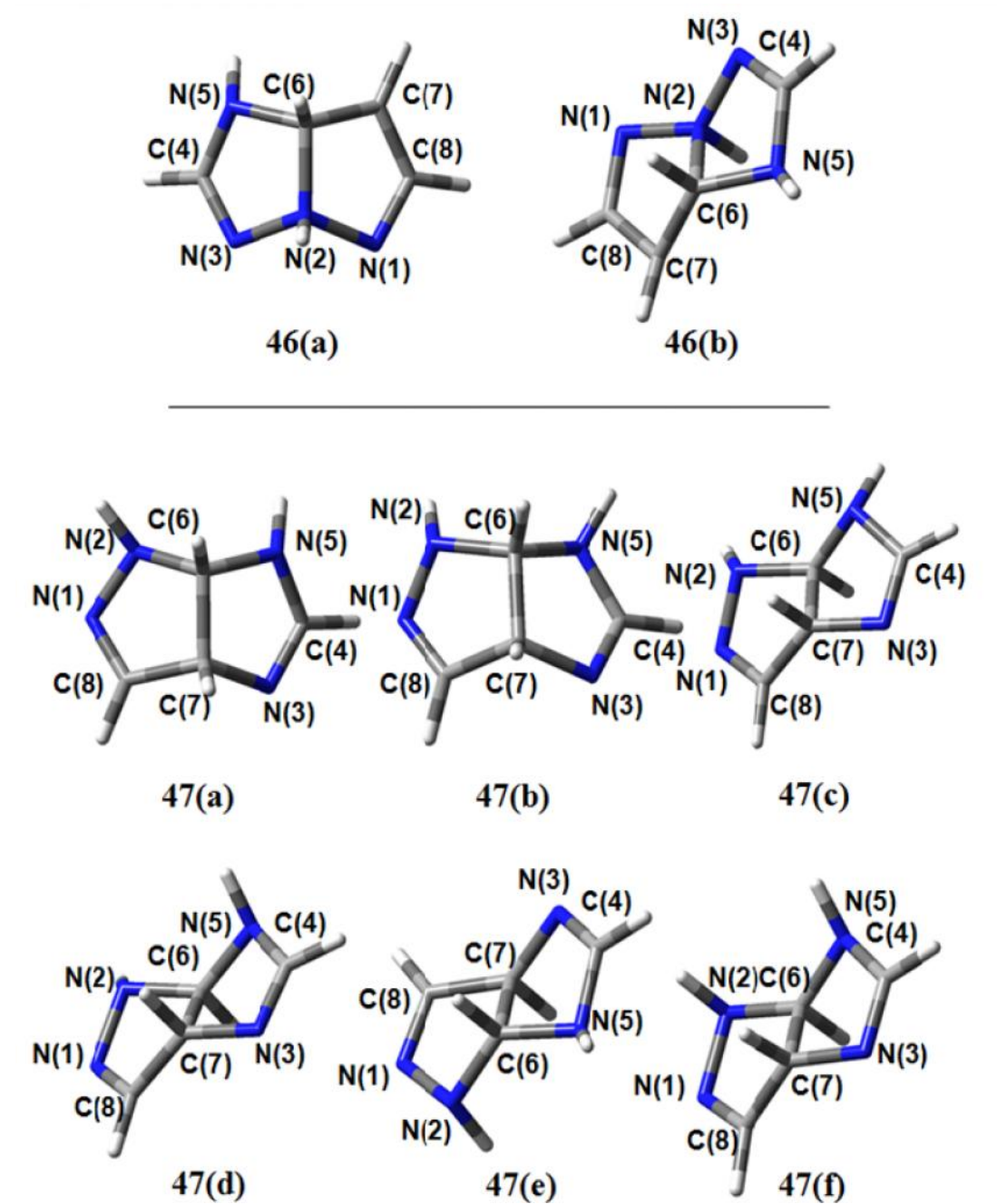


Figure 5.9 Conformations of the proposed intermediate (**46**) and the imidazopyrazole (**47**) at B3LYP/6-31G(d) level

5.3.4 Bond lengths of dihydro-1,2,3,5-tetrazocine (**45**)

The bond lengths for the conformations of the eight-membered ring optimised at the B3LYP/6-31G(d) level of theory are listed in *Table 5.1*. Comparing the average bond lengths of the underivatised 1,2,3,5-dihydro-1,2,3,5-tetrazocine (**45**) with that of the crystal structure for 2,5,6,7-tetrahydro-1,2,3,5-tetrazocine (**43**),⁶ the calculated N-N, C-C and C=N distances are reasonable (-0.05 Å, -0.04 Å and $+0.02$ Å, respectively). It should be noted however, that the crystal structure reported here is that of a tetrahydro-1,2,3,5-tetrazocine (**43**) and not a dihydro-1,2,3,5-tetrazocine (**45**). The C=C distances cannot be compared with that of the crystal structure therefore, as there is no carbon-carbon double bond in (**43**). The C-N distances vary more so, (± 0.07 Å) and in the crystal structure the C-N distances vary significantly from each another (1.37/1.47 Å) within the same ring (± 0.1 Å).

In addition, we compared the bond lengths of our B3LYP/6-31G(d) geometries of the dihydro-1,2,3,5-tetrazocines (**45**) to that of other reported eight-membered ring structures. The most cited eight-membered ring structure is 1,3,5,7-tetranitro-1,3,5,7-tetrazocine, also known as HMX. The interest in this particular molecule lies in its potential use as an explosive or as a rocket-propellant, since large amounts of energy are released upon the cleavage of a nitro group and the cascade of complex reactions which ensue.

1,3,5,7-tetra-nitro-1,3,5,7-tetrazocine(HMX) (see *Figure 5.10*) possesses a C-N-C-N framework and contains eight C-N bonds throughout the ring. The average C-N bond distance for the four polymorphs of HMX (α , β , γ and δ) is 1.45 Å. The average C-N bond distance is longest in δ -HMX (1.47 Å) and shortest in our eight-membered heterocycle, 7-ethoxycarbonyl-2,4,5,8-tetraphenyl-1,2,3,5-tetrazocine (**43**) (1.42 Å).⁶ These compare favourably with α -HMX for which there are four C-N bond lengths, varying from 1.445 to 1.471 Å.

Table 5.1 Bond lengths (Å) of 1,2,3,5-tetrazocines (**45**) for geometries optimised at B3LYP/6-31G(d) level

Bond Type	N-N	N-N	C=N	C-N	C-N	C=C	C-C	C=N
Conformation Label	N(1)-	N(2)-	N(3)-	C(4)-	N(5)-	C(6)-	C(7)-	C(8)-
	N(2)	N(3)	C(4)	N(5)	C(6)	C(7)	C(8)	N(1)
45(a)	1.33	1.33	1.29	1.38	1.37	1.36	1.42	1.31
45(b)	1.40	1.40	1.28	1.41	1.40	1.37	1.47	1.29
45(c)	1.37	1.43	1.28	1.41	1.44	1.34	1.48	1.29
45(d)	1.39	1.44	1.28	1.39	1.41	1.36	1.48	1.30
45(e)	1.39	1.44	1.28	1.39	1.39	1.36	1.48	1.30
45(f)	1.45	1.39	1.29	1.42	1.39	1.36	1.45	1.29
45(g)	1.40	1.38	1.29	1.41	1.39	1.35	1.46	1.29
45(h)	1.37	1.38	1.30	1.41	1.39	1.35	1.44	1.31
45(i)	1.48	1.43	1.29	1.42	1.40	1.36	1.48	1.29
45(j)	1.44	1.44	1.29	1.42	1.45	1.34	1.50	1.30
45(k)	1.44	1.44	1.30	1.44	1.41	1.35	1.50	1.30
Average bond length (Å)	1.41	1.41	1.29	1.41	1.40	1.35	1.47	1.30
tetra-hydro 1,2,3,5 tetrazocine (43) ⁶	1.46	1.44	1.29	1.37	1.47	1.55*	1.51	1.28

*This is the C-C bond distance

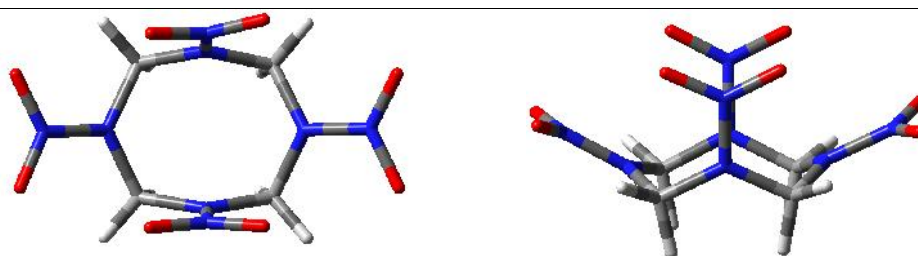


Figure 5.10 α -HMX (1,3,5,7-tetranitro-1,3,5,7-tetrazocine), the polymorph of HMX possessing the highest order of symmetry (four-fold axis). The representation on the left hand side is the top view and on the right is the side view of α -HMX.

5.3.5 Bond angles of dihydro-1,2,3,5-tetrazocine (**45**)

The bond angles for dihydro-1,2,3,5-tetrazocine (**45**) are listed in *Table 5.2*. The average bond angles appear to be significantly smaller in the crystal structure⁶ than for dihydro-1,2,3,5-tetrazocine, with the exception of the C-N-C bond length. The differences here may be attributed to the fact that there are crystal packing forces present for the crystal structure reported, whereas the calculations that were all performed at B3LYP/6-31G(d) are in vacuo. The average C-N-C bond angles in the form polymorphs of HMX (α , β , γ and δ) are 121.8, 124.8, 121.9 and 119.3 ° respectively. Note the largest C-N-C angle for the most symmetrical form of HMX.

The bond lengths and angles are reasonably well reproduced in the dihydro-1,2,3,5-tetrazocine (**45**), compared with that of the reported structure of 7-ethoxycarbonyl-2,4,5,8-tetraphenyl-2,5,6,7-tetrahydro-1,2,3,5-tetrazocine (**43**).⁶ Hence the conformations identified may be considered physically meaningful.

Table 5.2 Bond angles(°) of 1,2,3,5-tetrazocines (**45**) for minima located at the B3LYP/6-31G(d) level

Bond Angle	N-N-N	N-N=C	N=C-N	C-N-C	N-C=C	C=C-C	C-C-N	C-N-N
Label	N1-N2-	N2-N3-	N3-C4-	C4-N5-	N5-C6-	C6-C7-	C7-C8-	C8-N1-
	N3	C4	N5	C6	C7	C8	N1	N2
45(a)	141.4	132.9	136.7	135.5	131.2	135.2	137.8	129.3
45(b)	114.6	112.2	129.0	133.2	134.2	133.4	128.9	110.8
45(c)	127.5	115.7	126.0	112.4	128.9	139.3	141.5	123.8
45(d)	107.6	108.0	114.6	112.4	128.9	139.3	141.5	123.8
45(e)	107.7	108.0	114.6	112.3	128.9	139.3	141.6	123.8
45(f)	104.5	124.5	141.0	140.8	130.4	113.8	112.7	110.4
45(g)	140.4	138.5	135.4	117.9	113.9	123.0	115.4	120.2
45(h)	145.9	135.7	130.7	105.0	129.4	110.9	123.1	128.8
45(i)	113.1	119.5	129.0	114.8	115.4	122.6	120.0	117.2
45(j)	116.2	116.9	130.9	105.1	120.7	111.3	116.4	113.3
45(k)	118.6	115.6	127.6	105.8	135.6	107.1	118.9	114.0
Average	121.6	120.7	128.7	117.7	126.8	125.0	127.1	119.6
angle								
(43)⁶	108.3	112.5	128.4	128.4	115.8	111.6	123.2	110.0

5.3.6 Dihedral angles of dihydro-1,2,3,5-tetrazocine (45)

The dihedral angles for the different conformations of the dihydro-1,2,3,5-tetrazocine (**45**), located at the B3LYP/6-31G(d) level are presented in **Table 5.3**. The dihedral angles are a helpful way in labelling a particular ring conformation. The structure **45(a)** is the planar conformation as all torsional angles are 0°. Conformations **(d)** and **(e)** can be identified as an enantiomeric pair as the dihedral angles are the direct opposite of each other. Comparing the crystal structure of the tetrahydro-1,2,3,5-tetrazocine(**43**)⁶ to the conformations detected at the B3LYP/6-31G(d) level, the closest match is with conformation **45(i)**, see **Figure 5.11**. The two conformations are not a perfect match, but they are of the same *conformational type*; the four nitrogen atoms occupying different vertices of the ring. The central tetrazocine ring in the 7-ethoxycarbonyl-2,4,5,8-tetraphenyl-2,5,6,7-tetrahydro-1,2,3,5-tetrazocine as isolated by James *et al*⁶ is a tetrahydro-1,2,3,5-tetrazocine (**43**) that possesses two pairs of double bonds, whereas the central ring in the 2,5-dihydro-1,2,3,5-tetrazocine has three double bonds. This extra degree of unsaturation reduces the flexibility of the central 1,2,3,5-tetrazocine ring and this may also account for the fact that there are no comparable conformations between this structure and dihydro-1,2,3,5-tetrazocine (**45**).

Furthermore, there are a significant number of substituents attached to the tetrahydro-1,2,3,5-tetrazocine ring (**43**), see **Figure 5.11**, compared with the underivatized dihydro-1,2,3,5-tetrazocine (**45**) species that were optimised at the B3LYP/6-31G(d) level, **45(a)-(k)**. The additional bulky substituents may deform the ring slightly from a lower energy conformer that it may adopt if the ring were completely underivatized.

Table 5.3 Dihedral angles(^o) of 1,2,3,5-tetrazocines (**45**) for geometries optimised at B3LYP/6-31G(d) level

Label	N1-N2- N3-C4	N2-N3- C4-N5	N3-C4- N5-C6	C4-N5- C6-C7	N5-C6- C7-C8	C6-C7- C8-N1	C7-C8- N1-N2	C8-N1- N2-N3
45(a)	0.0	0.0	0.0	0.0	0.0	0.0	0.0	0.0
45(b)	108.1	-12.7	-25.6	7.9	-5.3	21.3	14.4	-107.0
45(c)	-66.1	-2.1	97.8	-77.4	-0.7	19.8	0.8	35.8
45(d)	98.8	-141.5	61.4	-4.3	-1.6	-8.2	4.0	-25.5
45(e)	-98.5	141.5	-61.8	4.5	1.6	8.1	-4.0	25.5
45(f)	-26.3	1.9	0.2	-11.1	3.3	49.4	-137.5	106.5
45(g)	25.5	-8.6	-4.1	44.5	-120.7	92.7	-2.0	-35.9
45(h)	-9.9	-2.7	-7.8	97.1	-127.3	36.2	4.5	-4.3
45(i)	-104.5	11.4	22.1	49.0	-113.5	49.5	-16.3	76.5
45(j)	101.7	-16.1	-40.3	95.6	-120.1	62.1	15.5	-104.7
45(k)	-107.5	26.9	24.2	-104.3	123.6	-47.2	-17.1	107.6
1,2,3,5- tetrazocine⁶	63.5	14.8	26.0	-89.3	14.8	55.3	1.6	-115.3

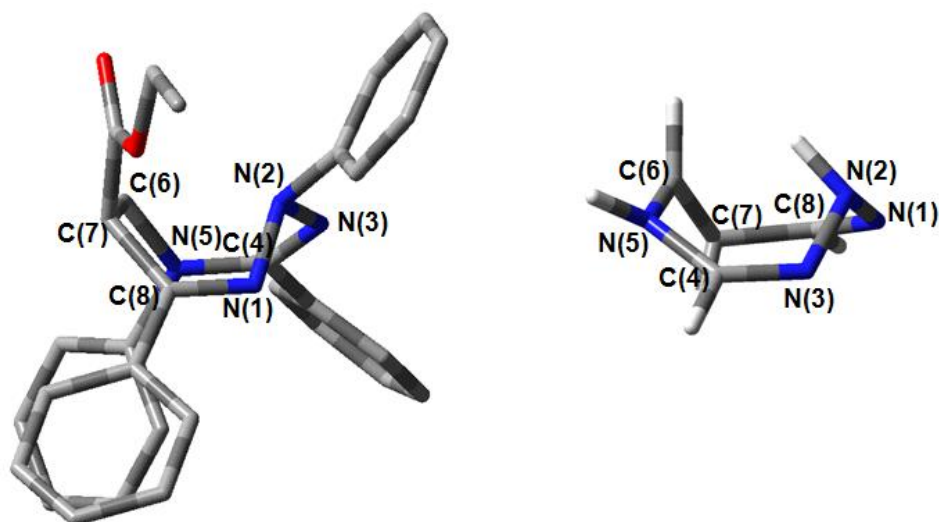


Figure 5.11 Molecular structure of 7-ethoxycarbonyl-2,4,5,8-tetraphenyl-2,5,6,7-tetrahydro-1,2,3,5-tetrazocine⁶ and the underivatised-1,2,3,5-tetrazocine **45(i)** optimised at B3LYP/6-31G(d)

Despite the absence of experimental data for the dihydro-1,2,3,5-tetrazocine (**45**) as it is an intermediate species, the bond lengths, angles and dihedral angles are in good agreement with well documented eight-membered ring species such as cyclooctane^{34,113-118,126} and HMX.¹²⁷⁻¹²⁸ Hence this validates our methods of locating the conformers of dihydro-1,2,3,5-tetrazocine (**45**) and related compounds at the B3LYP/6-31G(d) level, and the use of the global minima for determining thermodynamic driving forces, described in the next section.

5.3.7 Thermodynamics

The thermodynamic scheme for the underivatised molecules is shown in **Figure 5.12**, with all structures and energies calculated at the B3LYP/6-31G(d) level, including the Zero Point Correction. Since the energy values at DFT level are known to be more accurate, only these will be discussed. A first glance at **Figure 5.12**, suggests a definite thermodynamic driving force for the formation of the dihydro-1,2,3,5-tetrazocine structure (**45**) from the pyrrolo-[2,3-*d*]-1,2,3-triazole (**44**) and a further stabilisation in rearranging to the imidazo-[4,5-*c*]-pyrazole (**47**) via the higher-energy state intermediate (**46**). This is however, assuming that all species exist in the global minima conformations, and that the eight-membered ring (**45**) is capable of adopting the planar structure. If we consider the tetrazocine (**45**) to exist

in the conformation closest to that of the crystal structure, there would be a significant destabilisation (196 kJ/mol) of the eight-membered ring (conformation represented by the orange line for **(45)** in *Figure 5.12*) relative to the starting material, pyrrolo-[2,3-*d*]-1,2,3-triazole **(44)**. It is known however, that high energy UV light is required to form the eight-membered ring **(45)**, so this predicted energy pathway is not unreasonable. The cascade of reactions towards the imidazo-[4,5-*c*]pyrazole **(47)** would be thermodynamically downhill, with a possible stabilisation of as much as 333 kJ/mol. To prove that the imidazo-[4,5-*c*]-pyrazole **(47)** is accessible through a 1,2,3,5-tetrazocine intermediate **(45)**, one would need to look at the energy of the transition state structures linking both the 1,2,3,5-tetrazocine **(45)** to the intermediate **(46)** and a second transition state linking intermediate **(46)** to the imidazo-[4,5-*c*]-pyrazole **(47)**. Consequently we will turn our attention to the kinetics of the reaction sequence.

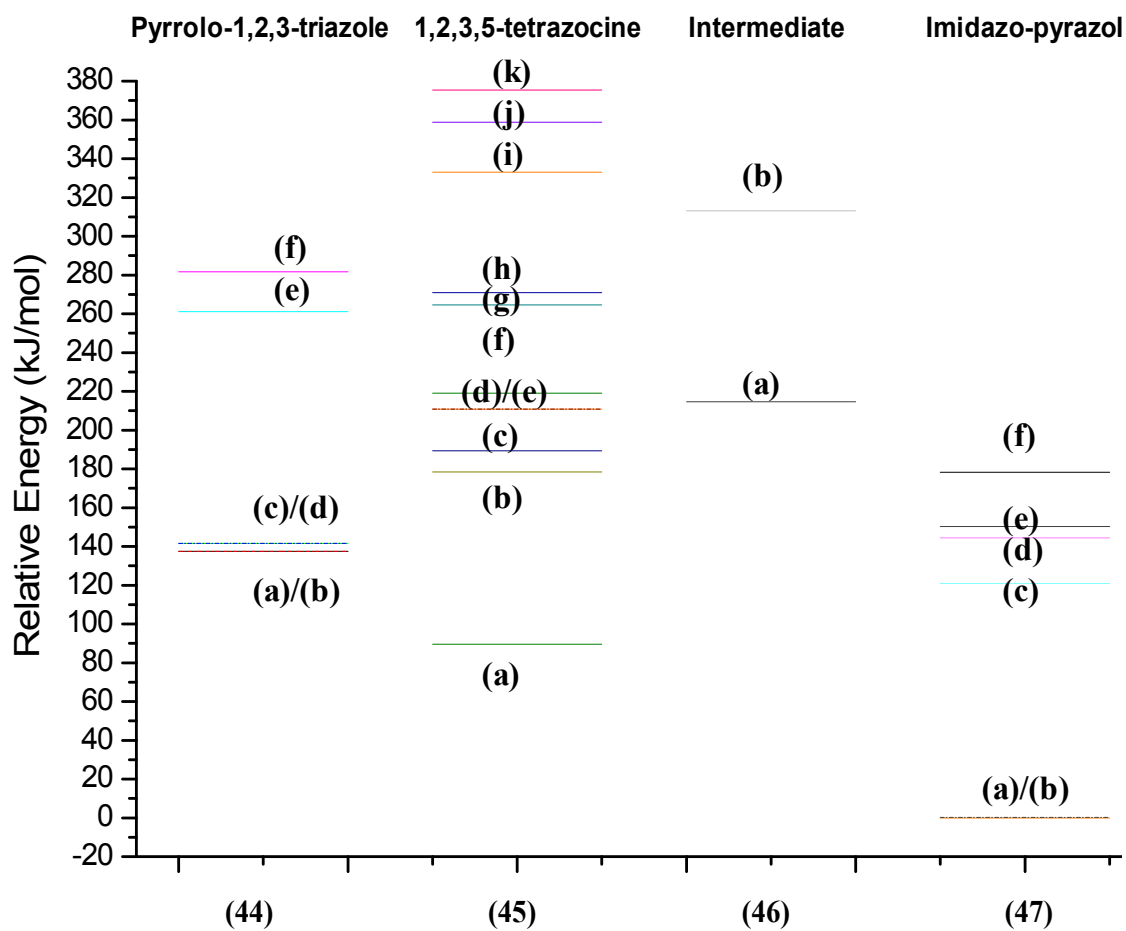


Figure 5.12 Energy level diagram of the underivatised 1,2,3,5-tetrazocine (**45**), its precursor (**44**), intermediate (**46**) and alternative products (**47**) at the B3LYP/6-31G(d) level, *see Scheme 4.2*. The labels refer to the geometries of the different species represented in *Figures 5.7-5.9*. All values include zero point energy corrections. The energies of the structures are all relative to the lowest energy conformer of the imidazo-[4,5-*c*]pyrazole.

Table 5.4 Relative Energies of 1,2,3,5-tetrazocines and its related compounds (all energies relative to the imidazo-pyrazole (**46**)); optimised at B3LYP/6-31G(d) level, *see Figure 5.12*. The lowest energy conformer of the imidazo-pyrazole (**46**) is considered the absolute zero.

Pyrrolo-triazole		1,2,3,5-tetrazocine		Intermediate		Imidazo-pyrazole	
Label	Relative Energy (kJ/mol)	Label	Relative Energy (kJ/mol)	Label	Relative Energy (kJ/mol)	Label	Relative Energy (kJ/mol)
44(a)	137.49	45(a)	89.52	46(a)	214.64	47(a)	0.00
44(b)	137.51	45(b)	178.46	46(b)	313.07	47(b)	0.25
44(c)	141.53	45(c)	189.37			47(c)	120.82
44(d)	141.53	45(d)	210.87			47(d)	144.40
44(e)	261.16	45(e)	210.88			47(e)	150.32
44(f)	281.71	45(f)	219.11			47(f)	178.30
		45(g)	264.60				
		45(h)	270.93				
		45(i)	332.97				
		45(j)	358.89				
		45(k)	375.37				

Table 5.5 Relative Energies for the conformations of pyrrolo-1,2,3-triazole (**44**)

Conformation Label	44(a)	44(b)	44(c)	44(d)	44(e)	44(f)
Total Energy (a.u.)	-374.9260100	-374.9260198	-374.9242601	-374.9242601	-374.8786601	-374.8702159
ZPE (a.u.)	0.112215	0.112212	0.119857	0.119857	0.1119506	0.111332
Total Energy (incl ZPE; a.u.)	-374.8138147	-374.8138079	-374.8134171	-374.8122744	-374.7667095	-374.7588838
Relative Energy (a.u.)	0	0.0000076	0.0015426	0.0015426	0.0471041	0.0549133
Relative Energy (kJ/mol)	0	0.02	4.05	4.05	123.67	144.22

Table 5.6 Relative energies for the conformations of 1,2,3,5-tetrazocine (**45**)

Conformation Label	45(a)	45(b)	45(c)	45(d)	45(e)	45(f)
Total Energy (a.u.)	-374.9443278	-374.9094254	-374.9039589	-374.8960201	-374.8960201	-374.8928500
ZPE (a.u.)	0.112241	0.111216	0.110285	0.110154	0.110159	0.110123
Total Energy (incl ZPE; a.u.)	-374.8320869	-374.7982091	-374.7940548	-374.7858653	-374.7858608	-374.7827272
Relative Energy (a.u.)	0	0.0338797	0.0380314	0.0462205	0.0462281	0.0493590
Relative Energy (kJ/mol)	0	88.95	99.85	121.35	121.37	129.59

Conformation Label	45(g)	45(h)	45(i)	45(j)	45(k)
Total Energy (a.u.)	-374.8747001	-374.8725199	-374.8476099	-374.8387902	-374.8320999
ZPE (a.u.)	0.109299	0.109532	0.108252	0.109305	0.108891
Total Energy (incl ZPE; a.u.)	-374.7654011	-374.7629886	-374.7393581	-374.7294847	-374.7232093
Relative Energy (a.u.)	0.0666850	0.0691003	0.0927304	0.1026030	0.1088762
Relative Energy (kJ/mol)	175.08	181.42	243.46	269.38	285.85

Table 5.7 Relative Energies for the conformations of the Intermediate **(46)** and the Imidazo-Pyrazole species **(47)**

Conformation Label	46(a)	46(b)
Total Energy (a.u.)	-374.894761	-374.858037
ZPE (a.u.)	0.110334	0.111101
Total Energy (incl ZPE; a.u.)	-374.784427	-374.746937
Relative Energy (a.u.)	0	0.0375
Relative Energy (kJ/mol)	0.00	98.43

Conformation Label	47(a)	47(b)	47(c)	47(d)	47(e)	47(f)
Total Energy (a.u.)	-374.97813	-374.978022	-374.932576	-374.922728	-374.920601	-374.9074833
ZPE (a.u.)	0.111957	0.111936	0.112411	0.111544	0.111673	0.109213
Total Energy (incl ZPE; a.u.)	-374.866182	-374.866086	-374.820165	-374.811184	-374.808927	-374.7982704
Relative Energy (a.u.)	0	0.0000952	0.0460186	0.0549999	0.0572547	0.0679119
Relative Energy (kJ/mol)	0.00	0.25	120.82	144.40	150.32	178.30

5.3.8 Kinetics

In *Section 5.3.7* we looked at the thermodynamics of the reaction sequence from the pyrrolo-[2,3-*d*]-1,2,3-triazole (**44**) to the imidazo-[4,5-*c*]-pyrazole (**47**) via a dihydro-1,2,3,5-tetrazocine (**45**) and a bicyclic intermediate (**46**), *Figure 5.12*. The calculations suggest that the formation of the imidazo-[4,5-*c*]-pyrazole (**47**) is thermodynamically favoured. To study the reaction we must also locate the transition states; one linking the 2,5-dihydro-1,2,3,5-tetrazocine (**45**) and the intermediate (**46**), TS1, and a second linking (**46**) and the imidazo-[4,5-*c*]-pyrazole species (**47**), TS2. It would however be too difficult to look at the kinetics of the photochemical transformation (**44**) to (**45**), as this may involve a number or range of excited states.

Locating transition states can be difficult computationally, one method which has become increasingly popular is that of the Quasi Synchronous Transit Method (QST3) method.¹²⁰ The reactant, product and ‘initial guess’ of the transition state geometry are required as input; this aids in the interpolation procedure to locate a stationary point on the PES with a single negative frequency. *Figure 5.13* shows the three structures that were used in the input file for the QST3 calculation along with the optimised geometry of the transition state structure itself. As can be seen from this figure, the inter-atomic distance between atoms N(2) and C(6) in the 1,2,3,5-tetrazocine (**45**) is 3.52 Å, whereas in the intermediate (**46**), this distance measures 1.56 Å. Consequently, the inter-atomic distance in the ‘initial guess’ structure was constructed at 2.54 Å, which is the average inter-atomic distance between structures (**45**) and (**46**). In the transition state structure (TS1) the final distance was 1.97 Å (see *Figure 5.14*). *Figure 5.15* displays snapshots of the animation of the single negative frequency of TS1, showing that the C-N distance in the eight-membered ring is contracting.

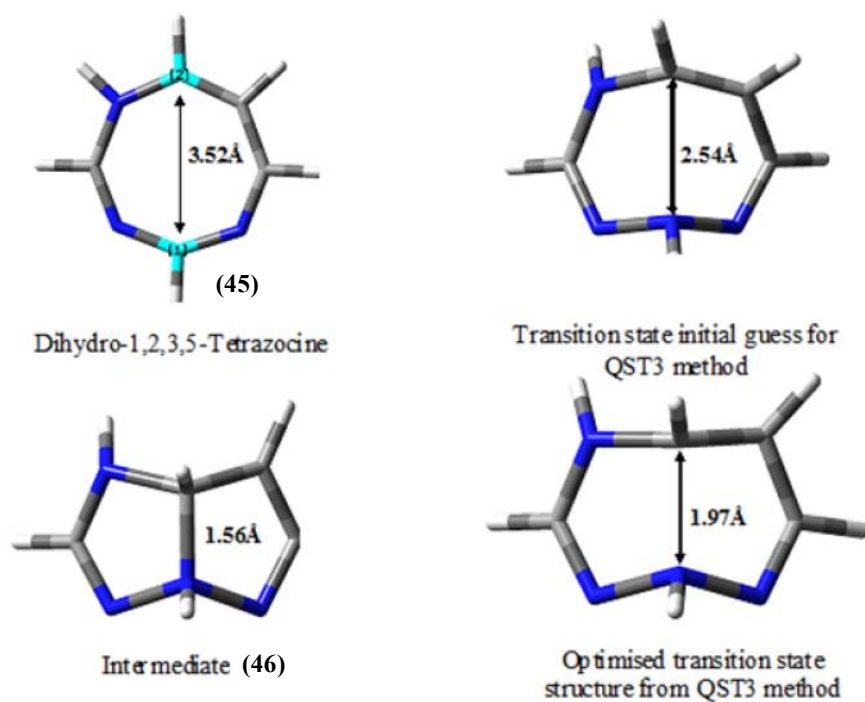


Figure 5.13 Structures used in the input file for locating the transition state using the QST3 method in Gaussian '03W and the optimised geometry at B3LYP/6-31G(d)

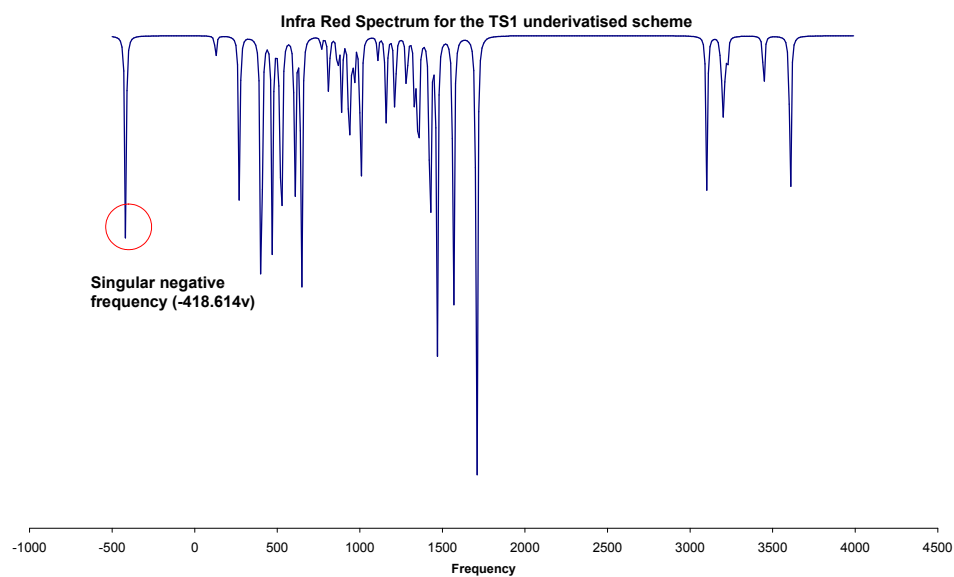


Figure 5.14 Predicted infra-red spectrum for the transition state (TS1) located between the dihydro-1,2,3,5-tetrazocine (45) and the intermediate (46).

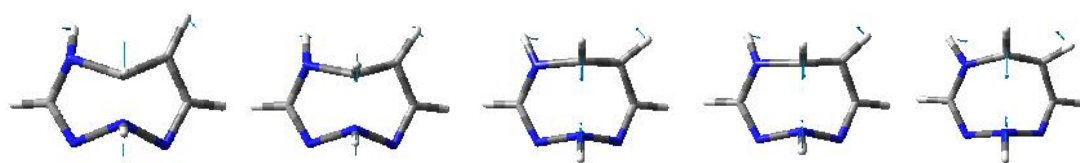


Figure 5.15 Snapshots from the animation of the negative frequency in the infra-red spectrum for the transition state TS1

The same approach was also taken in locating a transition state between the intermediate **(46)** and that of the imidazo-[4,5-*c*]-pyrazole **(47)**, with the presence of one negative mode confirming the identification.

The QST3 method proved successful in locating transition states on the potential energy surface of the underivatised dihydro-1,2,3,5-tetrazocine and its related compounds **(45)** and **(46)**. This method however, only locates a stationary point on the potential energy surface with one imaginary frequency, and does not necessarily prove that this transition state links the reactant and product together. To prove that the stationary point is a viable transition state, the reaction path must be followed by an eigenvector following or an intrinsic reaction coordinate (IRC) calculation.^{104,121} IRC calculations were performed by following the reaction pathway downhill from the transition state in both directions (the Hessian matrix from the transition state optimisation is required in order to define the direction of the minimum energy pathway). TS1 as seen in **Figure 5.13** and **Figure 5.15** was followed by an IRC in both directions downhill and the structure of the dihydro-1,2,3,5-tetrazocine **(45)** and the proposed intermediate **(46)** were successfully found at either end of the calculation. The results are illustrated in **Figure 5.16**. Similarly, TS2 was mapped by IRC methods to the proposed intermediate **(46)** and to the imidazo-[4,5-*c*]-pyrazole **(47)**, see **Figure 5.16**.

We can conclude that the conversion of the dihydro-1,2,3,5-tetrazocine **(45)** to the bicyclic intermediate **(46)** requires an activation energy of 187 kJ/mol (253.87-66.88 kJ/mol). Once the bicyclic intermediate is accessed, the activation energy to complete the transformation to the imidazo-[4,5-*c*]-pyrazole only requires an additional 36 kJ/mol. In **Table 5.8**, the bond lengths relating to the stationary points involved in the kinetics barrier of **Figure 5.16** are presented. The transformation of

the bicyclic intermediate **(46)** to the imidazo-[4,5-*c*]-pyrazole **(47)** involves the cleavage of the N(2)-N(3) bond and the formation of a new C-N bond between atoms N(3) and C(7). As can be seen from the input geometries relating to the QST3 optimisation of the transition state, TS2, the N-N bond length in the intermediate was 1.49 Å, where as the interatomic distance between these two atoms in the imidazo-[4,5-*c*]pyrazole is 3.27 Å. The ‘initial guess’ of the transition state geometry was set to 2.39 Å, which made for a good starting geometry as this helped interpolate the transition state structure, as confirmed by IRC followings.

Bond Type	N-N	N-N	C-N	C-N	C-N	C=C	C-C	C-N
Label	N(1)-N(2)	N(2)-N(3)	N(3)-C(4)	C(4)-N(5)	N(5)-C(6)	C(6)-C(7)	C(7)-C(8)	C(8)-N(1)
Intermediate	1.35	1.49	1.29	1.37	1.49	1.48	1.36	1.35
Initial TS2	1.39	2.39*	1.41	1.41	1.45	1.51	1.46	1.40
Final TS2	1.32	2.43*	1.25	1.43	1.44	1.50	1.37	1.36
(47)	1.41	3.27*	1.28	1.35	1.46	1.57	1.51	1.21

Bond type	C-N	N-H	C-H	N-H	C-H	C-H	C-H	C-N
Label	N(2)-C(6)	N(2)-H	C(4)-H	N(5)-H	C(6)-H	C(7)-H	C(8)-H	N(3)-C(7)
Intermediate	1.56	1.02	1.09	1.02	1.10	1.08	1.09	3.41*
Initial TS2	1.45	1.01	1.10	1.02	1.11	1.10	1.10	2.40*
Final TS2	1.47	1.01	1.10	1.02	1.11	1.08	1.08	2.86*
(47)	1.48	1.02	1.09	1.01	1.09	1.10	1.08	1.48

*Interatomic distances

Table 5.8 Bond lengths/interatomic distances for the stationary points involved in the formation of the imidazo[4,5-*c*]pyrazole **(47)** for *Figure 5.16*.

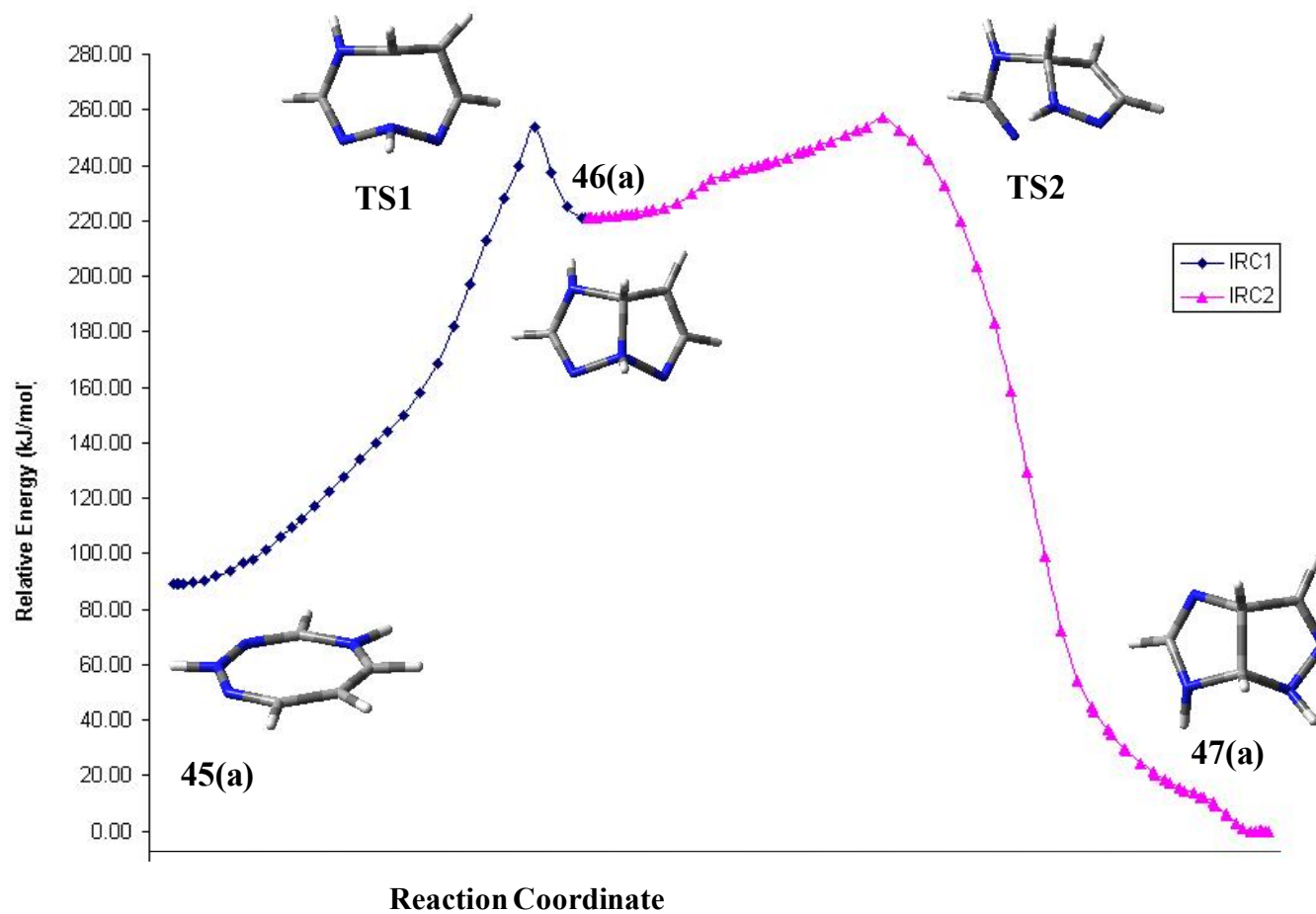


Figure 5.16 Two transition states (TS1 and TS2) located using the QST3 procedure and IRC method for the conversion of dihydro-1,2,3,5-tetrazocine (**45**) to a bicyclic intermediate as shown in *Scheme 5.1*.

5.4 Conclusions

Due to conformational mobility, a range of minima can exist for the 2,5-dihydro-1,2,3,5-tetrazocine(**45**). The most stable structure for the underivatised 2,5-dihydro-1,2,3,5-tetrazocine (**45**) is the planar, ‘pseudo-aromatic’ species. It is unlikely that the 7-ethoxycarbonyl-2,4,5,8-tetraphenyl-2,5,6,7-tetrahydro-1,2,3,5-tetrazocine (**43**) is likely to adopt this conformation however, due to the number of bulky substituents present and is likely to deform from such a planar geometry. Furthermore it has only two double bonds compared with the dihydro-1,2,3,5-tetrazocine (**45**), so does not possess a Hückel number of π electrons. Therefore the 7-ethoxycarbonyl-2,4,5,8-tetraphenyl-2,5,6,7-tetrahydro-1,2,3,5-tetrazocine (**43**) is not capable of inducing an aromatic stabilisation of the ring.

The calculations suggest that there is a thermodynamic driving force for the formation of an imidazo-[4,5-*c*]-pyrazole (**47**) from the photochemical excitation of pyrrolo-[2,3-*d*]-1,2,3-triazole (**44**). We have also shown that there is a viable route to access the imidazo-[4,5-*c*]-pyrazole (**47**) with the dihydro-1,2,3,5-tetrazocine (**45**) acting as an intermediate along this reaction pathway, with a total activation energy of 187 kJmol⁻¹. This is consistent with observed reactivity of a range of related molecules. We suggest that this is the reason why dihydro-1,2,3,5-tetrazocine (**45**) is not isolated when pyrrolo-[2,3-*d*]-1,2,3-triazole (**44**) is irradiated. On the other hand, when pyrrolo-[2,3-*d*]-1,2,3-triazole of the type (**42**) is irradiated, the tetrahydro-1,2,3,5-tetrazocine (**43**) is isolated.

Chapter 6

Conclusions and Future Work

6.1 Thesis Conclusions

In *Chapter 2*, we demonstrated that it was not possible to synthesise 1,2-bis(phenylhydrazone) propane **14(c)** from the reaction of phenylhydrazine with the diketone **12(c)**, as the reaction consistently faltered at the monohydrazone stage **13(c)**. Wolfe *et al* claimed to have synthesised 1,2-bis(4'-nitro-phenylhydrazone) propane **14c(ii)** from an oxidation product of 1-phenyl-prop-1-yne (**30**), which the workers believed to be the diketone **12(c)**,²⁹ see *Scheme 1.11*. We have shown however, that the dihydrazone **14c(ii)** was more likely to have been formed from the brominated product (**31**) as we have synthesised **14c(ii)** from α -bromo-propiophenone, a related compound. To this end, we have developed a high yield synthetic route to 1,2-bis(phenylhydrazone) propane **14c(ii)** from the reaction of α -bromo-propiophenone with three molecular equivalents of 4'-nitro-phenylhydrazine hydrochloride, *Scheme 2.10*. In addition, we have synthesised a novel azo compound, 1-phenyl-1,2-bis-(phenylazo)propene **40(c)**, by oxidation of **14c(ii)**, using lead tetraacetate as the oxidising agent (*Scheme 2.1*). Through this work, we also determined the isomeric form of the keto-monohydrazone **13(c)** formed, by reaction of phenylhydrazine with the diketone **12(c)**, and found that the hydrazone functional group is adjacent to the methyl group. The actual configuration was not previously known. Details of the crystal structure are provided in *Appendix A.1*.

In *Chapter 3* a detailed computational study on the reactivity and non-reactivity of monohydrazones (**13**) was presented. This showed that there is no thermodynamic explanation for the non-reactivity of 1-phenyl-2-phenylhydrazone propan-1-one **13(c)** with phenylhydrazine. Distributed multipole analyses suggest that the problem may be kinetic in origin. Our findings suggest in situations where the reactivity is kinetically determined, multipole analyses of the ground state and nearby soft modes may have predictive value.

Due to the difficulties in preparing 1,2,3,5-tetrazocines with three phenyl and one methyl group attached to the ring in *Chapter 4* we refocused on the previously established routes to tetraphenyl-1,2,3,5-tetrazocines (**43**) and related bicyclic compounds (**47**).⁶ We have synthesised a few examples of these tetra-phenyl compounds, **43(e)** and **47(e)** as per *Scheme 4.2*, where for these derivatives X and Y=COPh.

A conformational, thermodynamic and kinetic study on dihydro-1,2,3,5-tetrazocines (**45**) was presented in *Chapter 5*. We also examined the possibility of dihydro-1,2,3,5-tetrazocine (**45**) acting as an intermediate in the photochemical rearrangement of pyrrolo-[2,3-*d*]triazole (**44**) to imidazo-[4,5-*c*]pyrazole (**47**). The calculations suggest that there is a thermodynamic driving force for the formation the imidazo-[4,5-*c*]pyrazole (**47**) from the pyrrolo-[2,3-*d*]triazole (**44**), with the 1,2,3,5-tetrazocine acting as an intermediate. This reaction pathway has an activation energy barrier of ~187 kJ/mol. We suggest that this is the reason why the dihydro-1,2,3,5-tetrazocine (**45**) is not isolated when the pyrrolo-[2,3-*d*]-1,2,3-triazole (**44**) is irradiated.

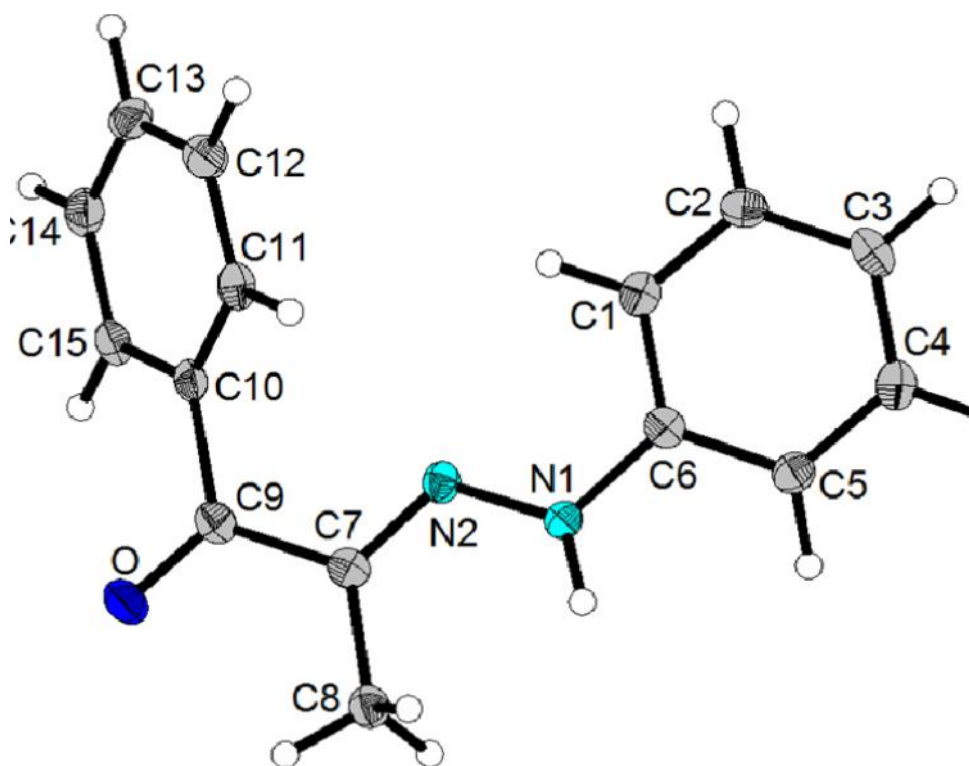
6.2 Future Work

To direct the future synthesis of 1,2,3,5-tetrazocines, it would be desirable to perform multipole analyses on both an underivatised tetrahydro-1,2,3,5-tetrazocine (**43**) and an underivatised dihydro-1,2,3,5-tetrazocine (**45**), as in *Scheme 4.2*. It has been established in this thesis and elsewhere,⁶ that it is possible to isolate the tetrahydro-1,2,3,5-tetrazocine (**43**), but that it is more difficult to isolate a dihydro-1,2,3,5-tetrazocine (**45**). If one could generate a representative picture of the distributed electronic charge about the ‘stable’ (**43**) and ‘non-stable’ (**45**) tetrazocines, it may be possible to ascertain the character of an appropriate electronic charge distribution. By altering the substituents at positions X and Y on C(6) and C(7) in the dihydro-1,2,3,5-tetrazocine (**45**) one could possibly apply DMA to drive the synthetic efforts in pursuit of these compounds.

An obvious question that arises is the value of a combined QM/synthetic approach. With computational methods currently available it seems that detailed simulations of reaction pathways for molecular systems, containing ~ 30 heavy atoms and one or two rings are at the edge of what can be achieved. The challenge in *ab initio* prediction of reactivity, which is required to develop ‘greener’ and more rapidly advancing heterocyclic chemistry, remains a substantial one. While further advancement in computational models and computing capacity may make such work routine in coming years; the present study suggests some possible strategies for elucidating the detailed reactivity of heterocyclic systems.

Appendix A.1

Molecular structure for **13(c)**: 1-phenyl-2-(phenylhydrazone)propan-1-one



brg01, molecule; thermal ellipsoids are drawn on the 50% probability level

Table A1 Crystal data and structure refinement for brg01.

Identification code	brg01	
Empirical formula	C ₁₅ H ₁₄ N ₂ O	
Formula weight	238.28	
Temperature	100(2) K	
Wavelength	0.71073 Å	
Crystal system	Monoclinic	
Space group	P2 ₁ /c (#14)	
Unit cell dimensions	a = 3.8675(4) Å	α = 90°.
	b = 11.5524(11) Å	β = 90.217(3)°.

	$c = 26.558(3) \text{ \AA}$	$\gamma = 90^\circ$.
Volume	1186.6(2) \AA^3	
Z	4	
Density (calculated)	1.334 Mg/m^3	
Absorption coefficient	0.085 mm^{-1}	
F(000)	504	
Crystal size	0.63 x 0.20 x 0.07 mm^3	
Theta range for data collection	1.53 to 26.42°.	
Index ranges	$-4 \leq h \leq 4$, $-14 \leq k \leq 14$, $-33 \leq l \leq 32$	
Reflections collected	10324	
Independent reflections	2437 [R(int) = 0.0337]	
Completeness to theta = 26.42°	99.7 %	
Absorption correction	Semi-empirical from equivalents	
Max. and min. transmission	0.9941 and 0.8419	
Refinement method	Full-matrix least-squares on F^2	
Data / restraints / parameters	2437 / 0 / 219	
Goodness-of-fit on F^2	1.069	
Final R indices [$I > 2\sigma(I)$]	R1 = 0.0473, wR2 = 0.1070	
R indices (all data)	R1 = 0.0563, wR2 = 0.1114	
Largest diff. peak and hole	0.283 and -0.179 e.\AA^{-3}	

Table A2 Atomic coordinates ($\times 10^4$) and equivalent isotropic displacement parameters ($\text{\AA}^2 \times 10^3$)

for brg01. $U(\text{eq})$ is defined as one third of the trace of the orthogonalized U^{ij} tensor.

Atom	x	y	z	U(eq)
C(1)	6121(4)	7236(1)	925(1)	19(1)
C(2)	4884(4)	6486(1)	562(1)	20(1)
C(3)	3387(4)	5440(2)	694(1)	22(1)
C(4)	3108(4)	5151(1)	1198(1)	22(1)
C(5)	4304(4)	5894(1)	1565(1)	19(1)
C(6)	5854(4)	6934(1)	1430(1)	17(1)
N(1)	7171(3)	7638(1)	1815(1)	18(1)
N(2)	8168(3)	8711(1)	1711(1)	17(1)
C(7)	9646(4)	9305(1)	2066(1)	17(1)
C(8)	10366(4)	8859(1)	2582(1)	19(1)
C(9)	10572(4)	10505(1)	1936(1)	18(1)
O	11507(3)	11175(1)	2269(1)	26(1)
C(10)	10346(4)	10907(1)	1404(1)	18(1)
C(11)	11722(4)	10261(1)	1011(1)	20(1)
C(12)	11626(4)	10691(2)	528(1)	23(1)
C(13)	10107(4)	11753(2)	428(1)	23(1)
C(14)	8739(4)	12399(2)	817(1)	23(1)
C(15)	8892(4)	11984(1)	1304(1)	20(1)

Table A3 Bond lengths [\AA] and angles [$^\circ$] for brg01.

C(1)–C(2)	1.381(2)
C(1)–C(6)	1.390(2)
C(2)–C(3)	1.386(2)
C(3)–C(4)	1.381(2)
C(4)–C(5)	1.378(2)
C(5)–C(6)	1.391(2)
C(6)–N(1)	1.399(2)
N(1)–N(2)	1.3274(18)
N(2)–C(7)	1.296(2)
C(7)–C(9)	1.473(2)
C(7)–C(8)	1.489(2)
C(9)–O	1.2281(19)
C(9)–C(10)	1.489(2)
C(10)–C(15)	1.390(2)
C(10)–C(11)	1.392(2)
C(11)–C(12)	1.377(2)
C(12)–C(13)	1.386(2)
C(13)–C(14)	1.381(2)
C(14)–C(15)	1.381(2)
C(2)–C(1)–C(6)	119.28(15)
C(1)–C(2)–C(3)	120.99(15)
C(4)–C(3)–C(2)	119.28(15)

C(5)–C(4)–C(3)	120.53(15)
C(4)–C(5)–C(6)	119.95(15)
C(1)–C(6)–C(5)	119.95(14)
C(1)–C(6)–N(1)	121.98(14)
C(5)–C(6)–N(1)	118.06(14)
N(2)–N(1)–C(6)	119.78(13)
C(7)–N(2)–N(1)	118.10(13)
N(2)–C(7)–C(9)	115.79(14)
N(2)–C(7)–C(8)	124.48(14)
C(9)–C(7)–C(8)	119.72(13)
O–C(9)–C(7)	119.75(14)
O–C(9)–C(10)	120.12(14)
C(7)–C(9)–C(10)	120.13(13)
C(15)–C(10)–C(11)	119.43(15)
C(15)–C(10)–C(9)	118.95(14)
C(11)–C(10)–C(9)	121.52(14)
C(12)–C(11)–C(10)	119.78(16)
C(11)–C(12)–C(13)	120.55(16)
C(14)–C(13)–C(12)	119.93(15)
C(15)–C(14)–C(13)	119.80(16)
C(14)–C(15)–C(10)	120.48(15)

Symmetry transformations used to generate equivalent atoms:

Table A4 Anisotropic displacement parameters ($\text{\AA}^2 \times 10^3$) for brg01. The anisotropic displacement factor exponent takes the form: $-2\pi^2 [h^2 a^{*2} U^{11} + \dots + 2 h k a^* b^* U^{12}]$

Atom	U^{11}	U^{22}	U^{33}	U^{23}	U^{13}	U^{12}
C(1)	17(1)	17(1)	22(1)	0(1)	2(1)	1(1)
C(2)	20(1)	24(1)	17(1)	-1(1)	1(1)	3(1)
C(3)	19(1)	22(1)	24(1)	-8(1)	-4(1)	1(1)
C(4)	19(1)	19(1)	28(1)	0(1)	1(1)	-1(1)
C(5)	18(1)	19(1)	19(1)	2(1)	1(1)	1(1)
C(6)	15(1)	17(1)	18(1)	-1(1)	0(1)	3(1)
N(1)	22(1)	15(1)	16(1)	2(1)	-2(1)	-1(1)
N(2)	18(1)	15(1)	19(1)	0(1)	1(1)	0(1)
C(7)	16(1)	18(1)	18(1)	-2(1)	1(1)	3(1)
C(8)	21(1)	18(1)	20(1)	-1(1)	-1(1)	0(1)
C(9)	18(1)	18(1)	19(1)	-3(1)	-2(1)	2(1)
O	38(1)	19(1)	22(1)	-3(1)	-8(1)	-1(1)
C(10)	17(1)	16(1)	20(1)	-1(1)	-3(1)	-5(1)
C(11)	17(1)	19(1)	24(1)	-2(1)	-1(1)	-2(1)
C(12)	19(1)	28(1)	21(1)	-3(1)	2(1)	-4(1)
C(13)	22(1)	28(1)	20(1)	6(1)	-3(1)	-8(1)
C(14)	22(1)	18(1)	27(1)	3(1)	-6(1)	-4(1)
C(15)	21(1)	16(1)	22(1)	-4(1)	-3(1)	-3(1)

Table A5 Hydrogen coordinates ($\times 10^4$) and isotropic displacement parameters ($\text{\AA}^2 \times 10^{-3}$)

for brg01.

Atom	x	y	z	U(eq)
H(1)	7220(50)	7962(17)	837(7)	27(5)
H(2)	5030(40)	6713(15)	212(7)	18(4)
H(3)	2570(50)	4932(15)	438(7)	19(4)
H(4)	1980(50)	4439(17)	1292(7)	27(5)
H(5)	4060(40)	5714(15)	1917(7)	18(4)
H(1N1)	7600(50)	7304(16)	2117(7)	25(5)
H(8A)	11880(50)	8182(17)	2560(7)	25(5)
H(8B)	8260(50)	8605(16)	2757(7)	26(5)
H(8C)	11490(50)	9457(17)	2789(7)	30(5)
H(11)	12780(40)	9510(15)	1079(6)	12(4)
H(12)	12590(50)	10250(16)	254(7)	25(5)
H(13)	10030(50)	12034(16)	86(7)	24(5)
H(14)	7710(50)	13143(16)	748(6)	21(4)
H(15)	8000(40)	12427(15)	1574(7)	17(4)

Table A6 Torsion angles [°] for brg01.

C(6)–C(1)–C(2)–C(3)	0.0(2)
C(1)–C(2)–C(3)–C(4)	0.5(2)
C(2)–C(3)–C(4)–C(5)	0.0(2)
C(3)–C(4)–C(5)–C(6)	–1.0(2)
C(2)–C(1)–C(6)–C(5)	–1.0(2)
C(2)–C(1)–C(6)–N(1)	177.64(14)
C(4)–C(5)–C(6)–C(1)	1.6(2)
C(4)–C(5)–C(6)–N(1)	–177.17(14)
C(1)–C(6)–N(1)–N(2)	12.0(2)
C(5)–C(6)–N(1)–N(2)	–169.35(14)
C(6)–N(1)–N(2)–C(7)	–174.21(14)
N(1)–N(2)–C(7)–C(9)	–177.65(13)
N(1)–N(2)–C(7)–C(8)	1.1(2)
N(2)–C(7)–C(9)–O	169.34(14)
C(8)–C(7)–C(9)–O	–9.5(2)
N(2)–C(7)–C(9)–C(10)	–10.1(2)
C(8)–C(7)–C(9)–C(10)	171.04(14)
O–C(9)–C(10)–C(15)	–43.4(2)
C(7)–C(9)–C(10)–C(15)	136.10(15)
O–C(9)–C(10)–C(11)	133.08(17)
C(7)–C(9)–C(10)–C(11)	–47.5(2)
C(15)–C(10)–C(11)–C(12)	–0.1(2)

C(9)–C(10)–C(11)–C(12)	–176.51(14)
C(10)–C(11)–C(12)–C(13)	–1.3(2)
C(11)–C(12)–C(13)–C(14)	1.4(2)
C(12)–C(13)–C(14)–C(15)	0.0(2)
C(13)–C(14)–C(15)–C(10)	–1.4(2)
C(11)–C(10)–C(15)–C(14)	1.5(2)
C(9)–C(10)–C(15)–C(14)	177.98(14)

Symmetry transformations used to generate equivalent atoms:

Table A7 Hydrogen bonds for brg01[Å and °].

D–H...A	d(D–H)	d(H...A)	d(D...A)	<(DHA)
N(1)–H(1N1)...O#1	0.90(2)	2.12(2)	3.0051(18)	167.1(17)

Symmetry transformations used to generate equivalent atoms:

#1 $-x+2, y-1/2, -z+1/2$

References

- (1) Gompper, R.; Schwarzensteiner, M. L. *Angew. Chem.-Int. Edit. Engl.* **1983**, 22, 543.
- (2) Butler, R. N.; Colleran, D. M.; Oshea, D. F.; Cunningham, D.; McArdle, P.; Gillan, A. M. *J.Chem. Soc. Perkin Trans I* **1993**, 2757.
- (3) Vicentini, C. B.; Veronese, A. C.; Giori, P.; Guarneri, M. *Tet. Lett.* **1988**, 29, 6171.
- (4) Giori, P.; Veronese, A. C.; Poli, T.; Vicentini, C. B.; Manfrini, M.; Guarneri, M. *J.Het. Chem.* **1986**, 23, 585.
- (5) Vicentini, C. B.; Veronese, A. C.; Giori, P.; Lumachi, B.; Guarneri, M. *Tet.* **1990**, 46, 5777.
- (6) Byrne, C.; Draper, S. M.; James, J. P.; Long, C. *J. Chem. Res.-S* **1995**, 438.
- (7) Fischer, E. *Chem. Ber.* **1884**, 17, 579.
- (8) Garard, I. D.; Sherman, H. C. *J. Am. Chem. Soc.* **1918**, 40, 1918.
- (9) Weygand, F. *Chem. Ber.* **1940**, 1284.
- (10) Theilacker, W.; Troster, P. *J. Liebig* **1951**, 572, 144.
- (11) Ruggli, P.; Zeller, P. *Helv. Chim. Acta* **1945**, 28, 747.
- (12) Shemyaki.Mm; Maimind, V. I.; Ermolaev, K. M.; Bamdas, E. M. *Tetrahedron* **1965**, 21, 2771.
- (13) Weygand, F.; Simon, H.; Klebe, J. F. *Chem. Ber.* **1958**, 91, 1567.
- (14) Simon, H.; Keil, K. D.; Weygand, F. *Chem. Ber.* **1962**, 95, 17.
- (15) Muller, H.; von Pechmann, H. *Chem. Ber.* **1889**, 22, 2129.
- (16) Allen, C. F. H. *J. Am. Chem. Soc.* **1951**, 73, 5850.
- (17) Maerky, M. *Helv. Chim. Acta* **1978**, 61, 1477.
- (18) Al-Mousawi, S. M.; El-Asasery, M. A.; Al-Kandery, N.; Elnagdi, M. H. *J. Het. Chem.* **2008**, 45, 359.
- (19) Jensen, K. A. *J. Prak. Chem.* **1938**, 151, 167.
- (20) Woodward, R. B.; Wintner, C. *Tet.Lett.* **1969**, 2697.
- (21) Kano, H.; Makizumi, Y. *Y. Zasshi* **1955**, 75, 465.
- (22) Friedlina, R. K. *I. Akad. Nauk SSSR, S. Khim.* **1965**, 10, 1788.
- (23) Hess, K. *Ber.* **1917**, 50, 365.
- (24) Ried, W.; Sommer, K. *J Lieb.* **1958**, 611, 108.
- (25) Mester, L. *Angew. Chem.-Int. Edit.* **1965**, 4, 574.
- (26) Neugebauer, F. A.; Kuchler, B. *Liebigs Ann. Chem.* **1967**, 104.
- (27) Caglioti, L.; Rosini, G.; Rossi, F. *J. Am. Chem. Soc.* **1966**, 88, 3865.
- (28) Stickler, W. C.; Hoffman, W. C. *Angew. Chem.-Int. Edit.* **1970**, 9, 242.
- (29) Wolfe, S.; Pilgrim, W. R.; Garrard, T. F.; Chamberl.P *Can. J. Chem.* **1971**, 49, 1099.
- (30) Schantl, J. G.; Karpellus, P.; Prean, M. *Tet.* **1982**, 38, 2643.
- (31) Tita, T. T.; Kornet, M. J. *J.Het.Chem.* **1988**, 25, 265.
- (32) Moore, G. E. *Elec.* **1965**, 38.
- (33) Westheimer, F. H.; Mayer, J. E. *J. Chem. Phys.* **1946**, 14, 733.
- (34) Hendrickson, J. B. *J. Am. Chem. Soc.* **1964**, 86, 4854.
- (35) Hendrickson, J. B. *J. Am. Chem. Soc.* **1967**, 89, 7047.
- (36) Wiberg, K. B. *J. Am. Chem. Soc.* **1965**, 87, 1070.
- (37) Allinger, N. L.; Hirsch, J. A.; Miller, M. A.; Tyminski, I. J.; Vancatle.Fa *J. Am. Chem. Soc.* **1968**, 90, 1199.
- (38) Allinger, N. L.; Sprague, J. T. *J. Am. Chem. Soc.* **1973**, 95, 3893.

- (39) Allinger, N. L.; Tribble, M. T.; Miller, M. A. *Tet.* **1972**, 28, 1173.
- (40) Allinger, N. L.; Sprague, J. T. *J. Am. Chem. Soc.* **1972**, 94, 5734.
- (41) Allinger, N. L. *J. Am. Chem. Soc.* **1977**, 99, 8127.
- (42) Allinger, N. L.; Rahman, M.; Lii, J. H. *J. Am. Chem. Soc.* **1990**, 112, 8293.
- (43) Allinger, N. L.; Chen, K. S.; Lii, J. H. *J. Comp. Chem.* **1996**, 17, 642.
- (44) Moller, C.; Plesset, M. S. *Phys. Rev.* **1934**, 46, 618.
- (45) Pople, J. A.; Binkley, J. S.; Seeger, R. *Int. J. Quant. Chem.* **1976**, 1.
- (46) Krishnan, R.; Pople, J. A. *Int. J. Quant. Chem.* **1978**, 14, 91.
- (47) Krishnan, R.; Frisch, M. J.; Pople, J. A. *J. Chem. Phys.* **1980**, 72, 4244.
- (48) Bartlett, R. J.; Shavitt, I. *Chem. Phys. Lett.* **1977**, 50, 190.
- (49) Kucharski, S. A.; Bartlett, R. J. *Adv. in Quant. Chem.* **1986**, 18, 281.
- (50) Knowles, P. J.; Somasundram, K.; Handy, N. C.; Hirao, K. *Chem. Phys. Lett.* **1985**, 113, 8.
- (51) Raghavachari, K.; Pople, J. A.; Replogle, E. S.; Headgordon, M. *J. of Phys. Chem.* **1990**, 94, 5579.
- (52) Shavitt, I. *Mod. Theor. Chem.*; Plenum Press: New York, 1977; Vol. 3.
- (53) Pople, J. A.; Seeger, R.; Krishnan, R. *Int. J. Quant. Chem.* **1977**, 149.
- (54) Langhoff, S. R.; Davidson, E. R. *Int. J. Quant. Chem.* **1974**, 8, 61.
- (55) Cizek, J. *J. Chem. Phys.* **1966**, 45, 4256.
- (56) Paldus, J.; Shavitt, I.; Cizek, J. *Phys. Rev. A* **1972**, 5, 50.
- (57) Hohenberg, P.; Kohn, W. *Phys. Rev. B* **1964**, 136, B864.
- (58) Parr, R. G.; Yang, W. T. *Density Functional Theory*; Oxford University Press, 1989.
- (59) Thomas, L. H. *Proc. Cambridge Phil. Soc.* **1927**, 23, 542.
- (60) Fermi, E. *Z. Physik* **1928**, 48, 73.
- (61) Block, F. *Z. Physik* **1929**, 57, 545.
- (62) Dirac, P. A. M. *Proc. Camb. Phil. Soc.* **1930**, 26, 376.
- (63) Kohn, W.; Sham, L. J. *Phys. Rev.* **1965**, 140, 1133.
- (64) Becke, A. D. *Phys. Rev. A* **1988**, 38, 3098.
- (65) Lee, C. T.; Yang, W. T.; Parr, R. G. *Phys. Rev. B* **1988**, 37, 785.
- (66) Becke, A. D. *J. Chem. Phys.* **1993**, 98, 5648.
- (67) Riley, K. E.; Op't Holt, B. T.; Merz, K. M. *J. Chem. Theory and Comp.* **2007**, 3, 407.
- (68) Sousa, S. F.; Fernandes, P. A.; Ramos, M. J. *J. Phys. Chem. A* **2007**, 111, 10439.
- (69) Butler, R. N.; Morris, G. J. *J. Chem. Soc.-Perkin Trans. I* **1980**, 2218.
- (70) von Auwers, K. *Chem. Ber.* **1917**, 50, 1177.
- (71) Hassner, A.; Catsoula, P. *Chem. Comm.* **1967**, 121.
- (72) Sukumara.Kb; Satish, S.; George, M. V. *Tet.* **1974**, 30, 445.
- (73) Sukumara.Kb; Angadiya.Cs; George, M. V. *Tet.* **1972**, 28, 3987.
- (74) Frisch, M. J. T., G. W.; Schlegel, H. B.; Scuseria, G. E.; Robb, M. A.; Cheeseman, J. R.; Montgomery, Jr., J. A.; Vreven, T.; Kudin, K. N.; Burant, J. C.; Millam, J. M.; Iyengar, S. S.; Tomasi, J.; Barone, V.; Mennucci, B.; Cossi, M.; Scalmani, G.; Rega, N.; Petersson, G. A.; Nakatsuji, H.; Hada, M.; Ehara, M.; Toyota, K.; Fukuda, R.; Hasegawa, J.; Ishida, M.; Nakajima, T.; Honda, Y.; Kitao, O.; Nakai, H.; Klene, M.; Li, X.; Knox, J. E.; Hratchian, H. P.; Cross, J. B.; Bakken, V.; Adamo, C.; Jaramillo, J.; Gomperts, R.; Stratmann, R. E.; Yazyev, O.; Austin, A. J.; Cammi, R.; Pomelli, C.; Ochterski, J. W.; Ayala, P. Y.; Morokuma, K.; Voth, G. A.; Salvador, P.; Dannenberg, J. J.; Zakrzewski, V. G.; Dapprich, S.; Daniels, A. D.; Strain,

- M. C.; Farkas, O.; Malick, D. K.; Rabuck, A. D.; Raghavachari, K.; Foresman, J. B.; Ortiz, J. V.; Cui, Q.; Baboul, A. G.; Clifford, S.; Cioslowski, J.; Stefanov, B. B.; Liu, G.; Liashenko, A.; Piskorz, P.; Komaromi, I.; Martin, R. L.; Fox, D. J.; Keith, T.; Al-Laham, M. A.; Peng, C. Y.; Nanayakkara, A.; Challacombe, M.; Gill, P. M. W.; Johnson, B.; Chen, W.; Wong, M. W.; Gonzalez, C.; and Pople, J. A.; B03 ed.; Gaussian Inc.: Wallingford, CT, 2003.
- (75) Mulliken, R. S. *J. Chem. Phys.* **1955**, *23*, 1833.
 - (76) Reed, A. E.; Weinhold, F. *J. Am. Chem. Soc.* **1986**, *108*, 3586.
 - (77) Luthi, H. P.; Ammeter, J. H.; Almlöf, J.; Faegri, K. *J. Chem. Phys.* **1982**, *77*, 2002.
 - (78) Collins, J. B.; Streitwieser, A. *J. Comput. Chem.* **1980**, *1*, 81.
 - (79) Lowdin, P. O. *Physical Review* **1955**, *97*, 1474.
 - (80) Reed, A. E.; Weinstock, R. B.; Weinhold, F. *J. Chem. Phys.* **1985**, *83*, 735.
 - (81) Singh, U. C.; Kollman, P. A. *J. Comput. Chem.* **1984**, *5*, 129.
 - (82) Breneman, C. M.; Wiberg, K. B. *J. Comput. Chem.* **1990**, *11*, 361.
 - (83) Darley, M. G.; Handley, C. M.; Popelier, P. L. A. *J Chem Theory and Comp.* **2008**, *4*, 1435.
 - (84) Stone, A. J. *Chem. Phys. Lett.* **1981**, *83*, 233.
 - (85) Stone, A. J.; Misquitta, A. J. *Int. Rev. Phys. Chem.* **2007**, *26*, 193.
 - (86) Stone, A. J. *J Chem Theory and Comp.* **2005**, *1*, 1128.
 - (87) Walter, W.; Meese, C. O.; Schroder, B. *J. Liebig* **1975**, 1455.
 - (88) Cunningham, I. D.; Hegarty, A. F. *J. Chem. Soc.-Perkin Trans. 2* **1986**, 537.
 - (89) Idoux, J. P.; Sikorski, J. A. *J. Chem. Soc.-Perkin Trans. 2* **1972**, 921.
 - (90) Jennings, W. B.; Alshowiman, S.; Tolley, M. S.; Boyd, D. R. *J. Chem. Soc.-Perkin Trans. 2* **1975**, 1535.
 - (91) Conlon, P. R.; Sayer, J. M. *J. Org. Chem.* **1979**, *44*, 262.
 - (92) Satterth.A.; Jencks, W. P. *J. Am. Chem. Soc.* **1974**, *96*, 7045.
 - (93) Pankratz, M.; Childs, R. F. *J. Org. Chem.* **1985**, *50*, 4553.
 - (94) Holloway, C. E.; Vuik, C. P. J. *Tet.Lett.* **1979**, 1017.
 - (95) Dignam, K. J.; Hegarty, A. F. *J. Chem. Soc.-Perkin Trans. 2* **1979**, 1437.
 - (96) Childs, R. F.; Dickie, B. D. *J. Am. Chem. Soc.* **1983**, *105*, 5041.
 - (97) Childs, R. F.; Shaw, G. S.; Lock, C. J. L. *J. Am. Chem. Soc.* **1989**, *111*, 5424.
 - (98) Johnson, J. E.; Silk, N. M.; Nalley, E. A.; Arfan, M. *J. Org. Chem.* **1981**, *46*, 546.
 - (99) Johnson, J. E.; Silk, N. M.; Arfan, M. *J. Org. Chem.* **1982**, *47*, 1958.
 - (100) Hegarty, A. F.; Scott, F. L. *J. Org. Chem.* **1968**, *33*, 753.
 - (101) Kessler, H. *Tet.* **1974**, *30*, 1861.
 - (102) Johnson, J. E.; Morales, N. M.; Gorczyca, A. M.; Dolliver, D. D.; McAllister, M. A. *J. Org. Chem.* **2001**, *66*, 7979.
 - (103) Stone, A. J.; Dullweber, A.; Engkvist, O.; Fraschini, E.; Hodges, M. P.; Meredith, A. W.; Nutt, D. R.; Popelier, P. L. A.; Wales, D. J.; 4.5 ed.; University of Cambridge: 2002.
 - (104) Gonzalez, C.; Schlegel, H. B. *J.Phys. Chem.* **1990**, *94*, 5523.
 - (105) Ochterski, J. W. *White Paper* **2000**,
http://www.gaussian.com/g_whitepap/thermo.htm.
 - (106) Marenich, A. V.; Cramer, C. J.; Truhlar, D. G. *J Phys Chem B.* **2009**, *113*, 6378.
 - (107) Miertus, S.; Scrocco, E.; Tomasi, J. *Chem. Phys.* **1981**, *55*, 117.
 - (108) Steiner, T. *Angew. Chem.-Int. Ed.* **2002**, *41*, 48.

- (109) Mirifico, M. V.; Caram, J. A.; Vasini, E. J. *Tet. Lett.* **2006**, 47, 6919.
- (110) Willey, G. R.; Drew, M. G. B. *Acta Cryst.(C)-Cryst. Str. Comm.* **1983**, 39, 403.
- (111) Woodward, R. B.; Hoffmann, R. *V Chem, Weinheim* **1970**.
- (112) Ramaiah, D.; Rath, N. P.; George, M. V. *Acta Cryst (C)- Cryst. Str. Comm.* **1998**, 54, 872.
- (113) Anet, F. A. L.; Krane, J. *Tet.Lett.* **1973**, 5029.
- (114) Anet, F. A. L.; Basus, V. J. *J. Am. Chem. Soc.* **1973**, 95, 4424.
- (115) Pakes, P. W.; Rounds, T. C.; Strauss, H. L. *J. Phys. Chem.* **1981**, 85, 2469.
- (116) Pakes, P. W.; Rounds, T. C.; Strauss, H. L. *J. Phys. Chem.* **1981**, 85, 2476.
- (117) Dorofeeva, O. V.; Gurvich, L. V.; Mastryukov, V. S. *J. Mol. Str.* **1985**, 129, 165.
- (118) Rocha, W. R.; Pliego, J. R.; Resende, S. M.; dos Santos, H. F.; de Oliveira, M. A.; de Almeida, W. B. *J. Comput. Chem.* **1998**, 19, 524.
- (119) Kolossvary, I.; Guida, W. C. *J. Comput. Chem.* **1993**, 14, 691.
- (120) Peng, C. Y.; Ayala, P. Y.; Schlegel, H. B.; Frisch, M. J. *J. Comput. Chem.* **1996**, 17, 49.
- (121) Gonzalez, C.; Schlegel, H. B. *J. Chem. Phys.* **1989**, 90, 2154.
- (122) Meiboom, S.; Hewitt, R. C.; Luz, Z. *J. Chem. Phys.* **1977**, 66, 4041.
- (123) Almennin.A; Bastians.O; Jensen, H. *Acta Chem.Scan.* **1966**, 20, 2689.
- (124) Bharadwaj, R. K. *Mol. Phys.* **2000**, 98, 211.
- (125) Anet, F. A. L.; Degen, P. J.; Yavari, I. *J. Org. Chem.* **1978**, 43, 3021.
- (126) Hendrickson, J. B. *J. Am. Chem. Soc.* **1967**, 89, 7047.
- (127) Cady, H. H.; Cromer, D. T.; Larson, A. C. *Acta Cryst.* **1963**, 16, 617.
- (128) Main, P.; Cobbledick, R. E.; Small, R. W. H. *Acta Cryst.(C)- Cryst. Str. Comm.* **1985**, 41, 1351.